Temperature and cosolvent effects of polymer conformations in solution

Abdulhakim Ali Jangher

ProQuest LLC
789 East Eisenhower Parkway
P.O. Box 1346
Ann Arbor, MI 48106-1346

DECLARATION

This work has not previously been accepted in substance for any degree and is not concurrently submitted in candidature for any degree.

Signed .....Abdul..... (Candidate) Date ..02/09/2011.....

STATEMENT 1

This thesis is the results of my own independent work/investigation, except where otherwise stated. Other sources are acknowledged by explicit references.

Signed. ....Abdul.....(Candidate) Date ..02/09/2011.....

STATEMENT 2

I hereby give consent for my thesis, if accepted, to be available for phptocopying and for inter-library loan, and for the title and summary to be made available to outside organisation.

Signed .....Abdul..... (Candidate) Date ...02/09/2011.....

Abstract

Formulation is a complex science. Many functional molecules require formulation to enhance their aqueous solubility or to promote and protect their function. Understanding the interaction between the formulation components is a necessary first step in that process. This project focuses predominantly on quantifying the interactions (synergistic and antagonistic) that arise when a triblock copolymer Pluronic (P123) is mixed with the anionic surfactant sodium dodecyl sulfate (SDS), in the presence of the cosolvent, ethanol. The interaction between P123 and SDS is synergistic, and leads to the formation of mixed micelles at low P123 concentrations and liquid crystalline phases at high P123 concentrations. Ethanol is shown to weaken that interaction, introducing antagonistic interactions at low P123 concentrations.

Moreover, we also study the physicochemical characteristics of some new biocompatible responsive polymers with potential biomedical applications. Here, the "formulation" is inherently built into the structure of the polymer-protein construct. These constructs possess a thermo-responsive character, and pulsed-gradient spin-echo NMR (PGSE-NMR) and small-angle neutron scattering (SANS) have been used to examine the solution conformation of these polymers as a function of temperature.

Acknowledgements

First I would like to thank my supervisor Dr Pete Griffiths for his help, guidance, support and total patience during my PhD studies leading to the completion my thesis; also I would like to thank Dr Alison Paul and Cardiff University for supporting my PhD studies.

In addition I would like to give heart-felt big thanks to my family (especially my mum and my wife), my sons, my brothers, my sisters for their love and great support during this study. It has been invaluable.

During my study I have met the most amazing people, all had to listen to me moan, so a huge thank you to Craig James , Nilmini, Gemma, Paola, Mari, and I would like to thank all my friends and colleagues, former and current, who helped in many way both directly and indirectly. I wish them all best in the future.

Also, thanks to everyone else in and out the department for the past few years that has helped in their own way since this all began.

Finally also thanks for financial support, the Libyan Ministry of Higher Education and Scientific Research and Al-Fathe University, Tripoli.

Table of Contents

List of Figures

Chapter 1: General introduction

Chapter 2: Material and equipments

Chapter 3: Experimental approaches

Chapter 4: Cosolvent effects on polymer-surfactant systems

Chapter 5: Phase behaviour of concentrated Pluronic

Chapter 6: Physiochemical characterization of responsive polymers

List of Tables

List of Abbreviation

Np	Degree of polymerization
PEO	Poly(ethylene oxide)
PPO	Poly(propylene oxide)
CMC	Critical micellization concentration
CMT	Critical micellization temperature
LLC	Lyotropic liquid crystalline
NaCl	Sodium chloride
NaF	Sodium fluoride
NaI	Sodium iodide
NaSCN	Sodium thiocyanate
KCl	Potassium chloride
KCl	Potassium chloride
KI	Potassium iodide
KF	Potassium fluoride
KSCN	Potassium thiocyanate
CP	Cloud point
CST	Critical solution temperature
UCST	Upper critical solution temperature
LCST	Lower critical solution temperature
PNIPAAM	Poly(N- iso-propylacrylamide)
NIPAAM	N- iso-propylacrylamide
AAM	acrylamide
N-tBAAm	N-tert-butylacrylamide
SDS	Sodium dodecyl sulfate
HLB	Hydrophilic-lipophilic balance

T	Absolute temperature
Nagg	Aggregation number
CAC	Critical aggregation concentration
DLS	Dynamic light scattering
SLS	Static light scattering
SAS	Small angle scattering
SANS	Small angle neutron scattering
SAXS	Small angle X-ray scattering
SALS	Small angle light scattering
CTAC	Cetyltrimethylammonium chloride
EO	Ethylene oxide
PO	Propylene oxide
LC	Liquid crystalline
D_2O	Deuterium oxide
NMR	Nuclear magnetic resonance
PGSE-NMR	Pulsed-gradient spin-echo-NMR
PEGMA-EE	Poly (ethylene glycol ethyl ether methacrylate)
PEGMA-ME	Poly (ethylene glycol methyl ether methacrylate)
Na_2SO_4	Sodium sulphate
PBS	Phosphate buffer solution
ANS	8-anilino-1-napththalene sulfonic acid
n_D	Rrfractive index
Mw	Weight average molecular weight
Mn	Number average molecular weight
GPC	Gel permeation chromatography
THF	Tetrahydrofuran
σ	Surface tension

P_{max}	Maximum pressure
P_0	Hydrostatic pressure
R	Maximum bubble radius
Ds	Self-diffusion coefficient
A	Peak integral
δ	Field gradient duration
σ	Ramp time
G	Gradient intensity
Δ	Separation
γ	Magnetogyric ratio of the nucleus
I	Current
Q	Scattering vector
λ	Neutron wavelength
θ	Scattering angle
I(Q)	Scattering intensity
P(Q)	Form factor
B_{inc}	Background
n_p	Number of scattering
V_p	Volume of scattering bodies
Δ_p	Contrast
S(Q)	Structure factor
η	Absolute viscosity
η_0	Solvent viscosity
η_{rel}	Relative viscosity
η_{sp}	Specific viscosity
η_{red}	Reduced viscosity
η_{inh}	Inherent viscosity

$[\eta]$	Intrinsic viscosity
C	Concentration
M	Molecular weight
κ_B	Boltzmann constant
f	Friction coefficient
R_h	Hydrodynamic radius
SLD	Scatting length density
b	Coherent neutron scattering length
M	Molar mass
k_i	Incidents neutron
k_s	Scattered neutron
B(r)	Effective field
$\partial\Sigma/\partial\Omega$	Differential cross-section

Chapter 1: General Introduction

1.1. Introduction

Waterborne mixtures play a major role in modern technologies. Key examples include foods, paints, cosmetics, herbicides, drug delivery, medical imaging etc. In general these systems contain-besides water–a multitude of different components, such as polymers, surfactants, proteins, and small ions such as salts [1]. The reasons of these components to industrial products are varied; paints contain polymers to obtain a suitable viscosity so that the paint will stick to the wall [2], cosmetics contain surfactants to ease the mixing of the hydrophilic and hydrophobic components, herbicide formulations contain surfactants to ensure that the product covers the whole leaf after application, and in the biomedical applications surfactants are used as carrier to deliver drugs [3, 4]. However, in such a complex mixture, these components may influence the behaviour of others. It is possible that component A can only fulfill its technological role in the presence of component B, or the other way around, that component A can not fulfill its role because it is hindered by component B.

Two important materials are considered in this study, polymers and surfactants and in particular their properties in aqueous solution. As solutes, both types have unique properties and it is not surprising that mixed polymer-surfactant solution can display unusual properties due to the interactions between the two materials. Polymers and surfactants are often used together in industrial formulations to take advantage of these different properties. When present together, they can interact to provide useful properties. In industrial systems, such interactions have significant effects on the processing conditions. For instance, in biological systems the interactions between natural polymers (proteins) and biological membrane surfactants control the structure of biological membranes and processes such as trans-membrane transport. Therefore, polymer-surfactant interactions are not only of interests to various industrial applications, but also of fundamental importance and therefore stimulate academic research. The following sections will discuss background to polymers, surfactants and their mixtures and the effects of solvency on these interactions. The stimuli-responsive polymers and phase behaviour of polymer-surfactant systems will be also discussed.

1.2. Polymers

A polymer is a substance in which one or more constitutional units known as monomers is repeated many times. There are linked to each other by covalent bonds to form large chains or macromolecules, as first established by Hermann Staudinger, who received the Nobel Prize in 1953. In 1932, polyethylene was accidentally discovered by ICI co-workers, R.O. Gibson and J. Swallow. In 1934 W. H. Carothers, working for DuPont, made nylon. Carothers consequently produced an excellent series of publications on condensation polymerization. By the late 1930s Hill and Crawford from ICI had developed poly(methyl methacrylate), "Perspex" and both polystyrene and poly(vinyl chloride) were in commercial production [5]. In the 1950s, Ziegler and Natta developed a family of stereo-specific transition metal catalysts that lead to the commercialization of polypropylene. The 1960s-1970s witnessed the development of a number of high performance polymers that could compete favourably with more traditional materials, such as metals, for automotive and aerospace applications. Nowadays, polymers are used in almost all areas of daily life and are one of the most significant products of the major global industries. A useful division of the science of polymers is that deals with natural and synthetic macromolecules. Natural polymers are, for example, proteins and polysaccharides while synthetic polymers are, for example, the common plastics and adhesives. Natural polymers usually have more complex structures than synthetic polymer

1.2.1. Classification of polymers

The polymers can be divided into main groups according to their nature: *e.g.* cationic polymers such as poly(ethylene imine), and anionic polymers such as poly(acrylic acid). On the other hand, in colloid science, one often defines polymers using several different sets of nomenclature as below [6].

1. Homopolymers consist of only one monomer that is repeated Np times, where Np is called the degree of polymerization.

2. Heteropolymers, in which two or more different monomer units are joined in a nonregular pattern, and often found in biopolymers *e.g.* (proteins, and nucleic acids).

3. Block copolymers in which the polymer chains consist of blocks of one repeating monomer unit followed by one or more blocks of other repeating units.

4. Polyelectrolyte in which the monomer units are charged and can refereed to a homo -----, hetero -----, or block copolymers.

1.2.2. Block copolymers

Polymers consisting of various types of monomers, are called block copolymers, and include a series of polymeric structures in which there are at least two distinct regions that possess different solvent affinities to one another. Two general methods were used in the synthesis of block copolymers which involve step and chain polymerization [7]. Block copolymers can act as amphiphiles, like surfactants. This means that they are able to self-assemble, in a similar way to surfactants. Block copolymers emerged as an alternative way of combining properties of different macromolecules by building a macromolecule containing additional monomers, depending on the polymerization procedure, these copolymers may present a variety of molecular architectures, as represented in Figure 1-1 [8].

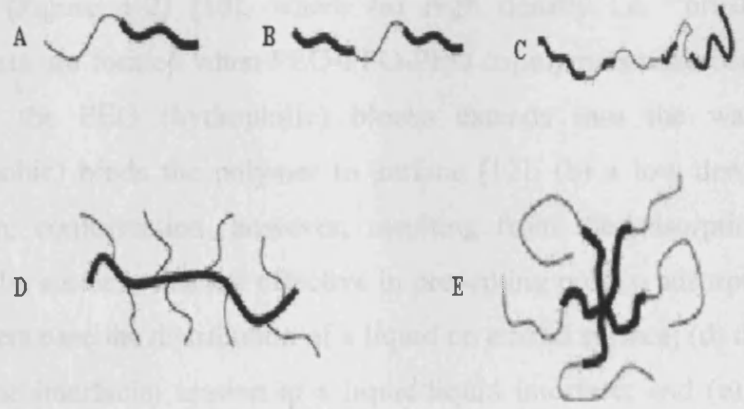

Figure 1-1: *Different block copolymer architectures: (a) diblock copolymer, (b) triblock copolymer, (c) random copolymer, (d) graft copolymer, and (e) star copolymer. Figure adapted from Watson et al. Ref. [8].*

1.2.2.1. Properties of block copolymers

The following section will highlight the self-assembly of block copolymers in the presence of different solvents, at surfaces or interfaces, in dilute and concentrated solutions.

1.2.2.1.1. Block copolymers at surfaces and interfaces

The adsorption of copolymers from solution to surface and interface is an important area of research in colloidal science. The process is accompanied by decrease in the conformation entropy of the copolymer chains, which opposes the attraction between the chains and the surface. Therefore, the adsorption energy per copolymer segment much reach some critical value before any adsorption occurs, usually comparable to the thermal energy, KT, where K is the Boltzmann constant and T is the temperature. As this value exceeds KT copolymer adsorption increases sharply as the individual energy for each of the segment accumulates to give large net adsorption energy per copolymer chain [9].

Amphiphilic copolymers are interracially active and adsorb at surfaces which interacts favourably with one of the blocks, whereas the other block extends into the solution (Figure 1-2) [10], where (a) high density i.e. "brush" formation [11] monolayers are formed when PEO-PPO-PEO copolymers adsorbed into hydrophobic surfaces; the PEO (hydrophilic) blocks extends into the water and the PPO (hydrophobic) binds the polymer to surface [12]; (b) a low density i.e. "Pancake" formation, conformation, however, resulting from the adsorption PEO blocks at hydrophilic surface, was not effective in preventing protein adsorption [13]; (c) block copolymers ease the distribution of a liquid on a solid surface; (d) diblock copolymers reduce the interfacial tension at a liquid/liquid interface; and (e) block copolymers sarcastically stabilize colloidal particles.

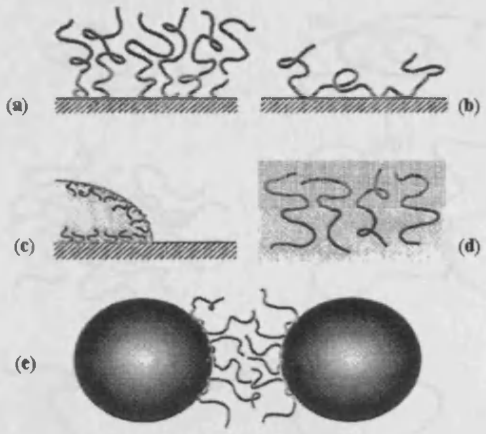

Figure 1-2: *Amphiphilic copolymers at surfaces and interfaces. Figure adapted from Alexandridis et al. Ref. [10].*

1.2.2.1.2. Block copolymers in dilute aqueous solutions

The tendency of amphiphilic copolymers in dilute aqueous solutions spontaneously to associate emanates from the minimization of the contact between their hydrophobic parts and the aqueous polar environment [14]. Typically, most diblock and triblock copolymers with insoluble middle blocks assemble into spherical micelles having a "core" consisting of the water-insoluble hydrophobic blocks and a "corona" composed of solvated segments of the water-soluble blocks [15, 16]. Different types of association structures are possible depending on the molecular architecture (Figure 1-3).

The various states of association depicted in Figure 1-3 are thermodynamically stable and attained spontaneously by the amphiphilic copolymers under suitable conditions, where (a) diblock copolymers adopt a Gaussian chain conformation in solution "unimer state"; (b) "monomolecular micelle" formed by a collapsed hydrophobically grafted polymer; (c) block copolymers assembled into a spherical micelle having a "core" consisting of the insoluble (hydrophobic) blocks and a "corona" composed of solvented segments of the water-soluble (hydrophilic) blocks, (d) "chrysanthemum" type micelle formed by loosely associated polymers with hydrophobic end-caps; (e) network formed by the association of the hydrophobic parts of end-capped triblock copolymers.

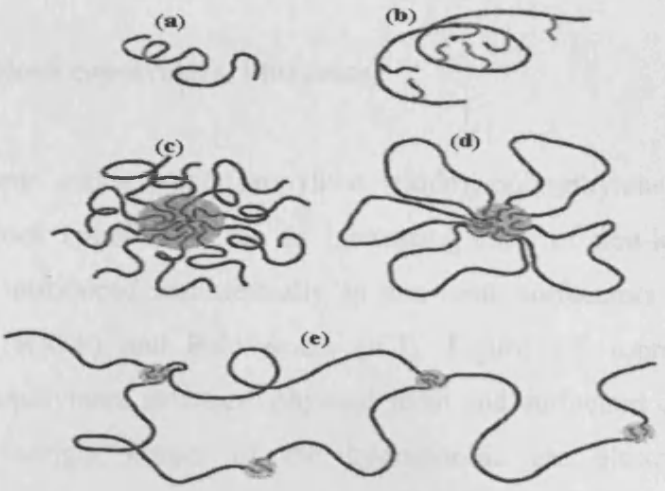

Figure 1-3: *Amphiphilic copolymers in dilute aqueous solutions. Figure adapted from Alexandridis et al. Ref. [10].*

1.2.2.1.3. Block copolymers in concentrated solutions

Amphiphilic triblock copolymers PEO-PPO-PEO at high concentrations (>30%) in water have been known to associate [15] and form various Lyotropic Liquid Crystalline (LLC) phases [17], depending on the polymer characteristics. Figure 1-4 represents: (a) block copolymer spherical micelles crystallized into a cubic 3D lattice; (b) block copolymer cylindrical micelles crystallized into a hexagonal 2D lattice; and (c) block copolymer bilayers (lamellar arrangement). Triblock copolymers play an important role in colloidal chemistry and have been used in various applications. Therefore, more details about triblock copolymers (phase behaviour) will be discussed in details in section 1.5.

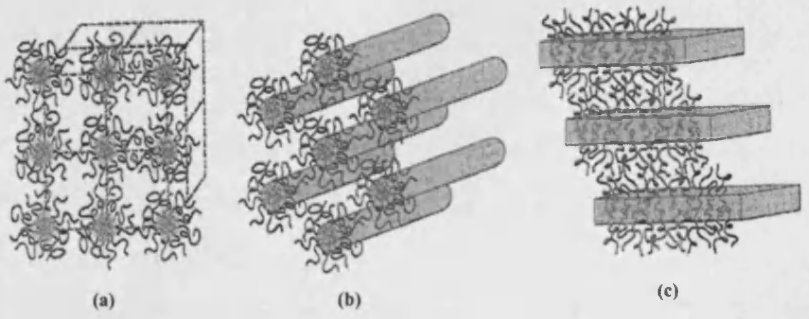

Figure 1-4: *Structures formed by amphiphilic copolymers in concentrated solutions. Figure adapted from Alexandridis et al. Ref. [10].*

1.2.3. Triblock copolymers, Pluronics

Poly(ethylene oxide)$_m$-poly(propylene oxide)$_n$-poly(ethylene oxide)$_m$, (PEO-PPO-PEO) triblock copolymers are an interesting class of non-ionic surfactants. These were first introduced commercially as non-ionic surfactants under the trade names Pluronics (BASF) and Poloxamers (ICI). Figure 1-5 represents the relationship between copolymers structure, physical form and surfactant characteristics in which molecular weight ranges of the hydrophobic are plotted against percent of hydrophobic in the final polymer [18]. They contain various (PEO/PPO) ratios or different chain length of the two components. The molecular weights range from 2,000 - 20,000 with 20 - 80 wt% PEO content [19-29]. Therefore, such polymeric materials with hydrophilic-lipophilic properties meet the diverse requirements for a range of applications, such as detergency, dispersion, stabilization, foaming, emulsification, lubrication, as well as in cosmetics, bioprocessing and pharmaceutical applications [15, 30, 31]. Moreover, due to of their amphiphilic nature and apparent low toxicity [32], they have generated considerable interest for both drug delivery and disuse engineering applications [33]. Recently, Pluronics have been proposed for pharmaceutical use and as components in different drug delivery systems for sparingly soluble drugs [34] as formulations to obtain controlled release from "gelled" states at body temperature, as injectable [35] solutions for subcutaneous administration or as gel formers in nasal administration, as components in the formation of treatments for thermal burns and in topical formulation to increase bioavailability etc. [10, 34]. Coding of Pluronic starts a litter to define it physical state at room temperature, L (liquid), P (paste) and F (flake or solid).

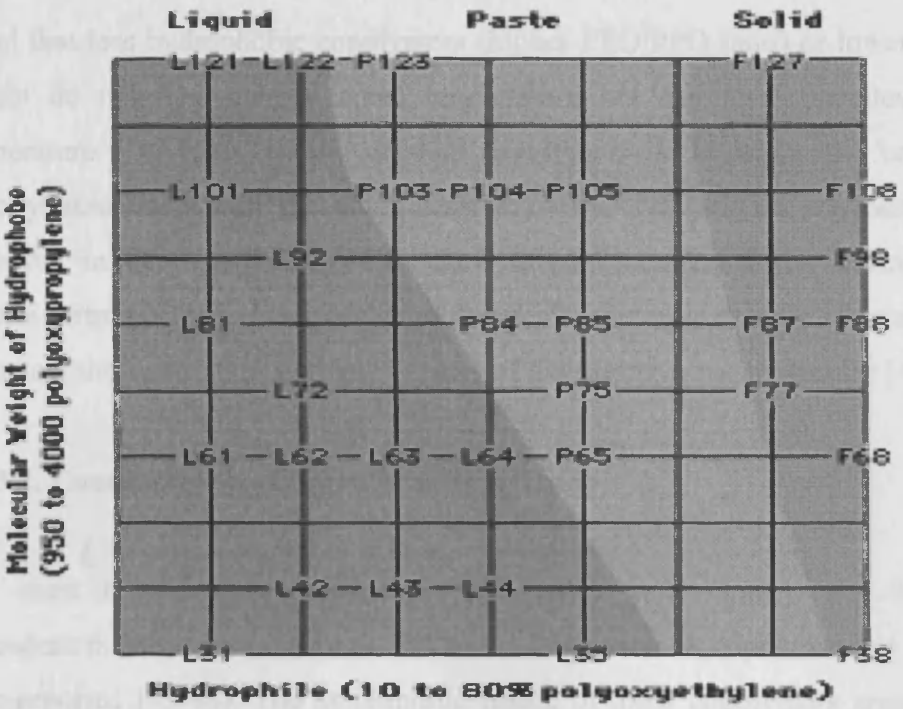

Figure 1-5: *Pluronic grid of molecular weight of hydrophobe (PPO) vs. hydrophile (PEO). Figure adapted from BASF website Ref. [17].*

1.2.3.1. Aggregation properties of Pluronic in aqueous solution

Micellization of PEO-PPO block copolymer in water depends on compositional parameters. Three parameters affect the process. *Firstly*, the composition (PEO/PPO) ratio and molecular weight. The higher the content of (PEO/PPO) and lower (PEO/PPO) ratio, and the lower the molecular weight of the copolymer, the higher the critical micellization temperature CMT. Early studies showed that Pluronics F68 [36] $(PEO)_{76}$-$(PPO)_{30}$-$(PEO)_{76}$, L64 [37] $(PEO)_{13}$-$(PPO)_{30}$-$(PEO)_{13}$, and P85 [38] $(PEO)_{26}$-$(PPO)_{40}$-$(PEO)_{26}$ exhibited different aggregation behaviour in aqueous solution, dependent on (PEO/PPO) ratio. Both critical micellization concentration (CMC) and CMT values decrease with increasing molecular weight for copolymers displaying similar (PEO/PPO) ratios. *Secondly*, the concentration of the copolymer is another characteristic of consideration. In general, the higher of concentration of the copolymer, the lower temperature required to attain micellization[39, 40]. *Finally,* the effect of temperature on the micellization of PEO-PPO-PEO has been reported by several researchers [41-43]. For example, P85 formed micelles at 15°C and L64 formed micelles above 30°C, whereas, F68 does not form micelles below 40°C. It was

found that less hydrophobic copolymers (higher PEO/PPO ratio) or lower molecular weight do not aggregate at room temperature but can form micelles at higher temperature. The micellization of such copolymers is driven by the unfavourable entropy associated with the solubilization of the additives in aqueous solutions. However, in water the entropy-induced hydrophobic effect is the driving force for micelle formation, which arises due to the smaller entropic penalty of assembling the surfactant molecules than entropic penalty of the caging water molecules [44].

1.2.3.2. Concentration-temperature dependence

The most characteristic properties of strongly concentration and temperature dependent micellar behaviours of PEO-PPO-PEO triblock copolymers in water have been reported [45-48]. The amphiphilic nature of these copolymers arises from the temperature-dependent solubility of PPO in water. Below 15°C, PPO is soluble in water (remains hydrated), but it turns hydrophobic at elevated temperature because of diminishing hydrogen bonding with water. In contrast, PEO is predominantly hydrophilic within the temperature range of 0-100°C [49]. As a consequence, these copolymers form aggregates above the CMC and CMT with a core consisting of predominantly PPO and a corona made up of hydrated PEO blocks [21, 30, 31, 47, 50, 51]. On the other hand, the CMTs of these copolymers are concentration-dependent and decrease with increasing copolymer concentration [21, 30, 52, 53]. Above the CMT, an increase in temperature weakens the hydrogen bonding between the PEO chains and water and leads to a progressive dehydration of the PEO chains. As a result, the micellar size generally increases due to the phase separation at the cloud point [29], and the PEO chains becoming insoluble.

1.2.3.3. Pluronic in selective solvents

Similar to small molecules, copolymers may or may not be soluble in a solvent. Polymers that are soluble in a given solvent are called hydrophilic in the case of water, hydrophilic or lipophilic in the case non-aqueous environments. The solvent quality is therefore, a strong factor in the determining CMC, CMT, and structure of micelles [53, 54]. The addition of a polar cosolvent to water provides an extra degree of freedom in tailoring of solution properties for specific application. For example, in

formulation of aqueous preparations of non-water soluble drugs and cosmetics, and as templates in mesoporous silica formation [55, 56]. Differences in solubilities of the PEO and the PPO blocks in polar and non-polar solvents gives the copolymer an "amphiphilic character" which leads to formation of micelles in aqueous solution with hydrophobic PPO blocks and hydrated PEO blocks hydrophilic. The copolymers aggregate in selective solvents (a good solvent for one block but poor for the other). This situation represents what is called "a selective solvent", being selective to the block whose solvation is stronger. This situation, consequently, leads to an amphiphilic behaviour and, therefore, to a tendency to the copolymer self-assembly similar to surfactant solutions. This self-assembling produces structures of the same type as those established in normal surfactant solutions, generally called micelles and mesophases [8], as depicted in Figure 1-6.

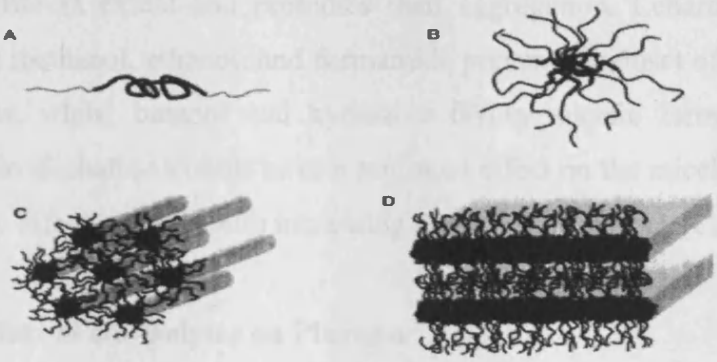

Figure 1-6: *Structures of block copolymers in solution: (a) copolymer unimer; (b) spherical micelle; (c) hexagonal arrangement of cylindrical micelles; and (d) lamellar. Figure adapted from Watson et al. Ref. [8].*

1.2.3.4. Additives effect on micellization of Pluronic

The sensitive nature of Pluronic micellization means that the addition of other compounds is likely to alter the aggregation characteristics. Indeed, it has been found that the addition of cosolvent or solutes to an aqueous Pluronic solution can influence properties, such as the CMC and CMT. Therefore, the influences of cosolvent and cosolutes on the micellar behaviour of PEO-PPO-PEO base block copolymer aqueous solutions are diverse in nature [22, 54, 55, 57]. Moreover, the aggregation of triblock copolymers in water is sensitive to the presence of many additives, and a series of

investigations showed that the presence of salting-out electrolytes such as NaCl, NaF, which decrease in the solubility of the copolymers, therefore, would decrease both CMC and CMT values. Whereas, salting-in electrolytes like NaI, NaSCN and non-electrolytes such as small chain alcohols, urea, have an opposite affects because increases the solubility of particular copolymers [53, 58-60]. The effect of both cosolvent and electrolytes on Pluronic is given more details in the following sections.

1.2.3.4.1. Effect of cosolvents on Pluronic

Relatively limited numbers of studies on the effect of addition of cosolvents such as alcohols and highly polar solvents such as glycols on the phase behaviour Pluronics have been reported [22, 54, 55, 57, 61]. The glycol interacts with PEO and PPO blocks to different extent and promotes their aggregation. Leharne et al. [54, 61] reported that methanol, ethanol, and formamide prevent the onset of micellization for F87 in water, while, butanol and hydrazine favour micelle formation. Moreover, medium-chain aliphatic alcohols have a profound effect on the micellization of F85 in water and the effect increase with increasing alcohol chain length (C_4-C_6) [61].

1.2.3.4.2. Effect of electrolytes on Pluronic

Addition of electrolytes having anions and cations of different sizes and polarizabilities may lead to "salting-out" and stabilizing effect or "salting-in" and destabilizing effect [15, 62]. In general, a gradual decrease in the CMC and CMT was observed with the increase of neutral salts concentration [39]. It should be stressed that studies with the same cation showed that the properties of the counter-anion are also relevant. For potassium halides, the effect on micellization follows the sequence KCl > KBr > KI [63]. In another work, it was shown that while NaCl (salting-out), had a stabilizing effect, NaSCN (salting-in) displayed the opposite influence [63]. Pandit and Kisaka reported that salts with multivalent anions, at characteristic concentrations, prevent Pluronic F127 solutions from forming gels, being an indication of a destabilizing effect [58]. Moreover, inorganic salts such as KCl, NaCl and KF dehydrate the chain of PEO and PPO blocks, reduce CMC, CMT, CP and enhance the aggregation, whereas, salt such as KSCN have exactly the opposite effects. In this study, we have used Pluronic [P123: $(PEO)_{20}$-$(PPO)_{70}$-$(PEO)_{20}$] which

is a difunctional block copolymer surfactant terminated by primary hydroxyl groups. It is non-ionic surfactant with an average molecular weight of 5800 and consists of a centre segment of hydrophobic part PPO (with 70 monomer units) flanked by two hydrophilic part PEO segment each containing 20 monomers units.

1.2.4. Stimuli-responsive polymers

Polymers that exhibit large changes, in their physical state or properties as respond to small changes in environmental stimuli are often called "smart polymers" and also known as "stimuli-responsive polymers". They are defined as polymers that undergo relatively large and sudden physical or chemical changes in response to small external changes in the environmental conditions. Names coined such as "stimuli-responsive" polymers have been given as stimuli-sensitive, intelligent [64], smart [65, 66] or environmentally sensitive polymers [67]. These polymeric systems might distinguish a stimulus as a signal, evaluate the magnitude of this signal, and then change their chain conformation in a direct response. There are many different stimuli to modulate the response of the polymeric systems. These stimuli could be classified as either physical or chemical stimuli. Physical stimuli, such as temperature, electric or magnetic fields, and mechanical stress and affect the level of various energy sources and alter molecular interactions at critical onset points. The chemical stimuli, such as pH, ionic factors and chemical agents change the interactions between polymer chains or between polymer chains and solvents at the molecular level. These responses of polymeric systems are very useful in bio-related applications such as drug delivery [68-74], bio-technology [75-77], and chromatography [78-80]. Some systems have been developed to combine two or more stimuli-responsive mechanisms into one polymeric system. For instance, temperature-sensitive polymers may also act in response to pH changes [81-84]. In this thesis, we focused on the temperature responsive polymers, because they have been the most intensively investigated in various laboratories and industries due to their relatively effective control *in vivo* as well as *in vitro* and their versatile application range [81]. Therefore we a brief survey of the most important thermosensitive are given in the following section.

1.2.4.1. Temperature responsive polymers

Temperature is the most widely used stimulus in environmentally responsive polymer systems as they have potential applications in the biomedical field [85]. This type of polymeric system exhibit a critical solution temperature CST, usually in water at which the phase of polymer and solution is changed in accordance with their composition. Those systems exhibiting one phase above this defined temperature and phase separation below it, i.e. they possess an upper critical solution temperature UCST. On the other hand, polymer solutions that appear as monophasic below a specific temperature and biphasic above it, normally exhibit the so-called lower critical solution temperature LCST. These represent the types of polymers with the vast number of applications [86].

The classic example of temperature responsive polymers is *poly(N-iso-propylacrylamide)* (PNIPAAm) that presents a LCST at 32°C in water [87]. Below that temperature the polymer is soluble as the hydrophilic interactions driven hydrogen bonding predominant, whereas a phase separation occurs above the LCST due to the onset of hydrophobic interactions. Other types of temperature sensitivity are based on intermolecular associations as in the case of Pluronics or Poloxamers (PEO-PPO-PEO) [88], where the hydrophobic associations of PPO blocks lead to the formation of micelle structures above the CMT.

1.2.4.1.1. Polymers with LCST

The LCST can be defined as the critical temperature at which in which polymer solutions undergo phase separation from one phase to two phases the concentration of polymer is different [89]. Below the LCST the enthalpy term, related to the hydrogen bonding between the polymer chains and water molecules, is responsible for the polymer dissolution. When the temperature rises above the LCST, the entropy term (hydrophobic interactions) dominates, leading to polymer precipitation. The LCST of polymers in aqueous solutions can be modulated by incorporating hydrophilic or hydrophobic moieties. For example, when *N-iso-propylacrylamide (NIPAAm)* is copolymerized with hydrophilic monomers such as *acrylamide (AAm),* the LCST increases up to about 45°C when 18% of *AAm* is incorporated to the polymer, and in

contrast the LCST deceases to about 10°C when 40% of hydrophobic *N-tert-butylacrylamide (N-tBAAm)* is added to the polymer [90].

1.2.4.1.2. Coil -to-globule transition

Thermosensitive polymer exhibits a coil-to-globule transition and has been used in a large number of applications that require switching of a material property with temperature. Such polymers have various applications and can be used in drug delivery, bio-separation and microfluidics. Polymer chains in solution exhibit different conformations depending on the nature of the polymer and the solvent conditions. In a good solvent, where segment-solvent contacts are favoured, the polymer has an extended coil conformation. Whereas, in a poor solvent, where segment-segment contacts are favoured, the polymer is collapsed. The transition between the extended and collapsed states in which temperature or solvent was varied has been the focus of many theoretical studies [91]. The coil and globule are two different and distinct (in theory) thermodynamically stable states for a linear flexible homopolymers, chain in solution. The transition from a coil to a globule has long been predicted if the solvent quality changes from good to poor [92]. Experimentally, the coil-to-globule transition has been widely studied in the last twenty years [91], because not only it is a fundamental problem, but drives many useful phenomena, such as the collapse of gel network [14], and the complexation between two polymeric chains [93]. Some water-soluble polymers undergo a sharp coil-to-globule transition in water upon heating and change from an expanded coil below their LCST to a collapsed globule above the LCST. For instance, most applications that make use of this phenomenon aqueous solution of PNIPAM as it exhibits a LCST near body temperature, 32°C. As the temperature is changed during the LCST, the polymer chains are known to undergo a reversible "coil-to-globule" transition (Figure 1-7) [94].

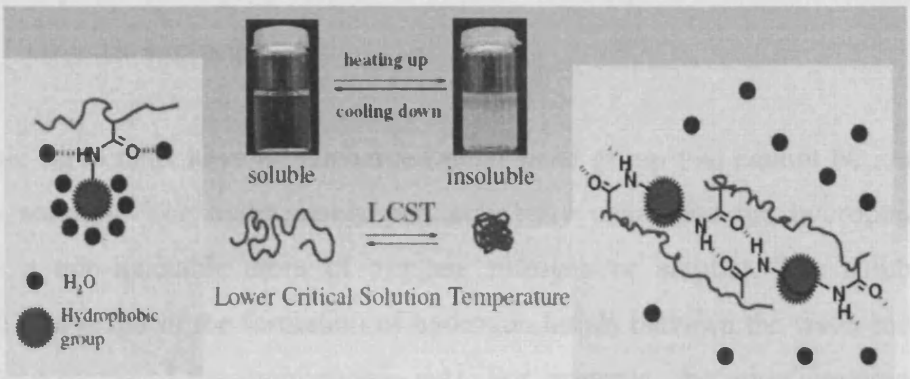

Figure 1-7: Temperature induced coil-to-globule transition of PNIPAM chain in aqueous solution. Figure adapted from Tanford et al. Ref. [93].

1.3. Surfactants

Surfactants or amphiphiles are relatively small molecules that are hydrophilic and hydrophobic moieties in one molecule. It is general practice to refer to the hydrophilic moiety as the head, and the hydrophobic moiety as the tail. The name surfactant comes from the term ***surf***ace ***act***ive ***a***g***ent***, which immediately refers to the distinctive property that a surfactant molecule has an affinity to virtually all types of surfaces. For instance, at an air-water interface, a surfactant will absorb with its hydrophobic moiety such that the contact area between the hydrophobic segments and the water will decrease [91]. On a hydrophilic surface, such as silica, it will be adsorbed via its head groups which triggers the adsorption of a secondary layer to form bilayers [92].

1.3.1. Classification of surfactants

A surfactant molecule consists of hydrophilic part (soluble in water) and hydrophobic one (insoluble in water). These molecules are highly active in the interfaces between air and water or oil and water. They have various names including surface active agents, detergents, surfactants or amphiphiles. The surfactant can be classified by the presence of formally charged groups in its head. A *non-ionic* surfactant has no charge groups in its head. The head of an ionic surfactant carries a net charge. If the charge is negative, the surfactant is more specifically called *anionic*; if the charge is positive, it is called *cationic*. If a surfactant contains a head with two oppositely charged groups, it is termed *amphoteric or zwitterionic*.

1.3.1.1. Non-ionic surfactants

Non-ionic surfactants have an uncharged polar head group that cannot be ionized in aqueous solution. The hydrophobic part is a fatty chain and the hydrophilic part contains a non-ionizable atom of oxygen, nitrogen or sulphur. The solubility is obtained as a result of the formation of hydrogen bonds between the water molecules and certain atoms of the hydrophobic part. For example, the ether function of the poly(ethylene oxide), PEO or poly(propylene oxide), PPO, but sugar esters and alkanolamides can also be included.

1.3.1.2. Anionic surfactants

Anionic surfactants constitute the largest group of available surfactants. When the polar group, which is linked in a covalent manner with the hydrophobic part of the surfactant, carries a negative charge ($-COO^-$, $-SO_3^-$, and $-SO^{2-}_4$) the surfactant is anionic. Common examples includes: soaps, alkyl benzene sulfonates, fatty alcohol sulfates. Anionic surfactants are used in greater volume than any other type, the main reasons for this being the ease and low cost of manufacture. Anionic surfactants are used in most detergent formulations and best detergency is obtained when the alkyl chains are in the C_{12}-C_{15} range. Most anionic surfactants are moncovalent but there are also important examples of divalent anionic ampholyte. For anionic surfactants the choice of counter-ion plays a role in the physicochemical properties. Most anionic surfactants have sodium as a counter-ion but other cations, such as lithium, potassium, calcium and protonated amines, are used as surfactant counter-ions for specific purposes. Sodium Dodecyl Sulfate (SDS) has been used in this work, as the interaction of polymer with such anionic surfactant is grater than with other surfactants.

1.3.1.3. Cationic surfactants

Cationic surfactants are frequently based on amine-containing polar groups ($-NR_1R_2R_3^+$). Due to their charged nature, the properties of cationic surfactant, e.g., surface activity and self-assembly, are generally strongly dependent on the nature and

concentration of any salt present as well as the pH of the solution. Cationic surfactant is frequently used as antibacterial agents.

1.3.1.4. Amphoteric (Zwitterionic) surfactants

Amphoteric surfactants are generally less commonly encountered than non-ionic, anionic, and cationic ones. In an amphoteric surfactant, the polar head group frequently consists of a quaternary amine group and either a sulfonate or carboxylate group. Due to the amphoteric nature of the polar head group, the surfactant can become charged such that it is cationic at low pH and anionic at high pH, although when permanent cationic are present in the head group (such as in a phosphocholine head group), the surfactant will always contain a positive charge regardless of pH.

The properties and applications of surfactants are determined by the balance between the hydrophilic and hydrophobic groups in the molecule. Some of the fundamental characteristics that must be evaluated for a surfactant proposed for some specific applications are given in Table 1.1.

Table 1-1: *Some characteristics of surfactants evaluated for various applications.*

Application	Characteristic
Detergency	Low CMC, good salt and pH stability and biodegradability, desirable foaming properties.
Emulsification	Hydrophilic balance, environmental and biological impact (safety) in application.
Lubrication	Chemical stability and adsorption at surfaces.
Mineral flotation	Adsorption characteristics on the ore(s) of interest and low cost.
Pharmaceuticals	Biocompatibility, low toxicity and emulsifying properties.

1.3.2. Surface activity

Surfactants possess a characteristic chemical structure that consists of molecular components that have little attraction for the solvent, normally called hydrophobic part often referred to as a tail, and a chemical component that has a strong attraction

for solvent or bulk phase, called the hydrophilic group often known as a head. Although, in principle, surface activity and related concepts are applicable to any system composed of at least one condensed phase. However, the majority of the scientific and technological literatures are concerned with aqueous solvents and their interaction with a second phase usually air or oil [95]. The hydrophobic group is normally hydrocarbon (alkyl or alkyl aryl), typically with at least eight-carbon atoms. It therefore has very low solubility in polar solvents, but dissolves in non-polar ones. Furthermore, the surface activity of a particular surfactant depends on the balance between its hydrophilic and hydrophobic properties, for simplest case of a homologous series of surfactants, an increase in the length of the hydrocarbon chain as the series is ascended results in increased surface activity.

1.3.3. Hydrophilic – lipophilic balance (HLB)

The hydrophilic-lipophilic balance of a surfactant is a measure of the degree to which it is hydrophilic or lipophilic, determined by calculation values for the different regions of the molecules, as described by Griffin in 1949 [96] and in 1954 [97]. Other methods have been suggested, notably in 1957 by Davies [98]. Moreover, the hydrophilic-hydrophobic balance can be adjusted by introducing two side chains that have hydrophilic and hydrophobic properties respectively. Therefore, when surfactants dissolve in a solvent, solvation of the hydrophilic group increases the free energy of the system. Accordingly, molecules adsorbed at surfaces have higher potential energies than those in the bulk. The difference being the work required to bring a surfactant molecule from the core to the surface which will be lower than for a water molecule and as result the surfactant concentration becomes higher at the surface.

1.3.4. Formation of micelles

The process of micelle formation is known as micellization. Micelles, and indeed other aggregates, only form when the temperature of the system is greater than the CMT, and the concentration of surfactant is greater than the CMC of the surfactant. Therefore, when surfactant molecules are dissolved in water at concentrations above the CMC, they form micelles. In a micelle, the hydrophobic tail flock to the interior in

order to minimize their contact with water, and the hydrophilic heads remain on the outer surface in order to maximize their contact with water (Figure 1-8) [94, 99]. The spontaneous formation of micelles (i.e. aggregation) can be understood by considering the thermodynamics of the systems: micelle can form spontaneously because of a balance between the entropy and enthalpy of the system. In water, the hydrophobic effect is driving force for micelle formation, despite the fact that assembling of the surfactant molecules together reduces their individual entropy. This is because, above the CMC, the entropic penalty of this aggregation of the surfactant molecules is less than the entropic penalty of the hydrophobic portion of the surfactant monomers by the water molecules. Also important are enthalpic considerations, such as the electrostatic interactions that occur between the charged surfactants head groups (ionic surfactant) and hydration forces (non-ionic surfactants).

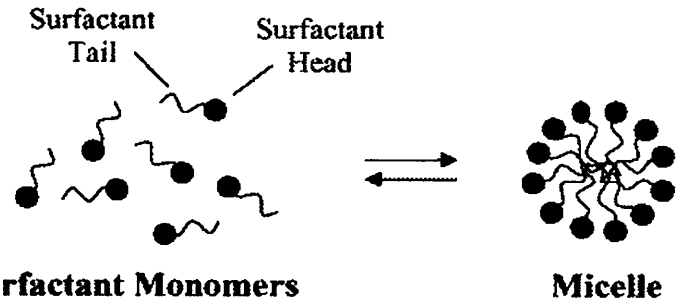

Figure 1-8: *Scheme illustration of the reversible monomer-micelle thermodynamic equilibrium. Figure adapted from Tanford et al. Ref. [93].*

1.3.5. Micellization measurement of surfactant

Measuring different physicochemical properties of aqueous surfactant solution as a function of concentration, one finds many peculiarities [100]. For anionic surfactants, at low concentrations the properties should be similar to those of a strong electrolyte. There are many of the physical properties of surfactant solutions undergo an abrupt change at the CMC, as illustrated in Figure 1-9. Apparently, very simple surface tension measurements probably constitute the most frequently employed method for determining the CMC of a surfactant system. The determination of a surfactant CMC experimentally is usually by plotting some physical properties, such as surface tension, conductivity, osmotic pressure, *etc.* as a function of surfactant concentration and extrapolating the results at low and high concentrations to an intersection point.

For instance, in the case of the surface tension a sharp break was observed in the curves indicating the formation of micelles at that point [101].

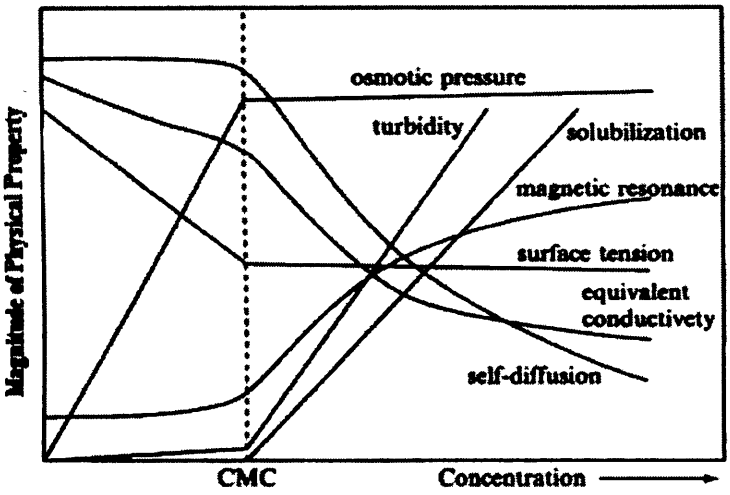

Figure 1-9: *Schematic representation of the effect of surfactant concentration on various physical properties. Figure adapted from Lindman and Wennerstrom et al. Ref. [99].*

1.3.6. Aggregation number (N_{agg})

Other important parameter that characterizes micelles is the aggregation number that corresponds to the average number of surfactant monomers in each micelle of a micellar solution. Usually, in a micellar solution the aggregation number is approximately constant for a broad total concentration range (up to about 100 times the CMC), with the number of micelles varying [102]. However, at certain conditions micelles can grow and as a result the aggregation number varying with the surfactant concentration [103].

1.4. Polymer- surfactant mixtures

Polymer and surfactant mixtures in solution may interact strongly, weakly or not at all. In systems that do not interact in the bulk phase there seems generally also to be no interaction at the air/water interface. The adsorption behaviour of a polymer-surfactant system at the air/water interface is dependent on a number of factors including the surface activity of the polymer, and whether or not the surfactant and polymer interact with each other at the surface. Understanding the nature of the interactions between polymers (both biological and synthetic) and surfactants in bulk aqueous solutions is of fundamental important of industrial products. These including cosmetics, detergents, coatings, paints, adhesives and glues, lubricants and food and pharmaceutical products. In general, many of these products are based on dispersion of polymers and surfactant, where the polymers impart colloidal stability and special rheological features, whereas surfactants provided emulsification ability, interfacial tension control, and colloidal stability [104]. The interaction is generally referred to as binding of the surfactant to the polymer and represented as a "binding isotherm". At *C*ritical *A*ggregation *C*oncentration (CAC), the interaction between surfactant micelles and polymer chains began. CAC is thus an equivalence of the CMC of polymer-free surfactant solution.

1.4.1. Polymer- surfactant interactions

Generally, there are three main types of polymer-surfactant interaction at the air/water interface, "weak interactions" with the surfactant head groups, "strong hydrophobic interactions" with the surfactant chains and "strong electrostatic interactions" between oppositely charged polyelectrolyte and surfactant head groups. These can be divided into two main areas according to the type of polymer, non-ionic polymers, where the interactions with surfactant are driven by hydrophobic forces and polyelectrolyte, where the interactions tend to be dominated by strong electrostatic interactions with the surfactant head groups, although hydrophobic interactions sometimes seem to play a significant role. The polymer acts as a nucleation core for the surfactant unimers. Such concentration where the first aggregate start to form the CAC. When the

surfactant concentration is increased further, more aggregates on the polymer will form, and the unimer concentration will essentially be constant.

1.4.1.1. Non-ionic polymers

The most widely studied polymer-surfactant solution has been poly(ethylene oxide) with sodium dodecyl sulfate PEO-SDS. The variation of surface tension with surfactant concentration at a fixed concentration of polymer shows break points at two concentrations, the first at the CAC, which corresponds to the beginning of the formation of micelles on the polymer, and the second at the CMC, which corresponds to normal micellization of the surfactant [105]. Experimental binding studies of mixed polymer-surfactant solutions can be summarized as shown in Figure 1-10, [106]. The figure is schematic but gives a good description for aqueous mixtures of a non-ionic homopolymers and an ionic surfactant.

1. At low surfactant concentrations there is no significant association at any polymer concentration, *i.e.* CMC is only very weakly dependent on polymer concentration over wide ranges.

2. Above the CAC, association increases up to a surfactant concentration which increases linearly with the polymer concentration (CAC/CMC) is to a good approximation of polymer molecular weight down to low values. For very low molecular weight the interaction is weakened.

3. Association is saturated and the surfactant unimer concentration increases (the plateau binding increases linearly with the polymer concentration).

4. There is a coexistence of surfactant aggregates at polymer chains and micelles (anionic surfactants show a marked interaction with most homopolymers while cationic surfactants show a weaker but still significant interaction).

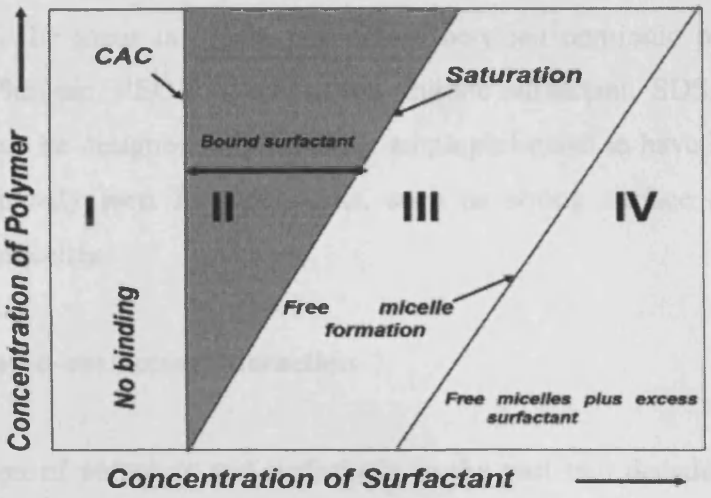

Figure 1-10: *Association between a homopolymers and a surfactant in different concentration domains. Figure adapted from La Mesa Ref. [105].*

1.4.1.2. Polyelectrolytes

The interaction between polyelectrolytes and surfactants has been studied extensively due to various applications of these systems ranging from personal care products, pharmaceuticals to industrial usages. It has been known that the properties of these systems such as viscosity and solubility of polymers can be altered upon interacting with surfactants. Moreover, It has been found that the systems of polyelectrolytes and surfactants of opposite charges generally show strong interactions and often leads to the formation of three-dimension networks (gels) (Figure 1-11) which offer novel rheological properties, not available in the pure systems. Whereas, the systems of uncharged polymers and ionic surfactants of the same charges show relatively weak or no interaction [107].

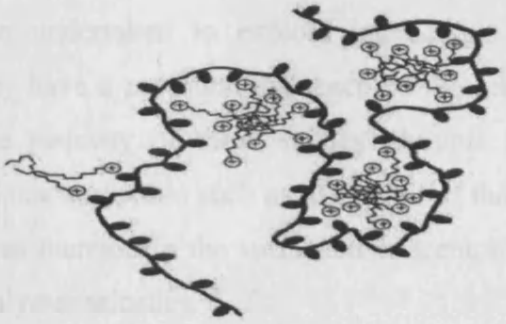

Figure 1-11: *Illustration of the interaction of the surfactant molecules with the polyelectrolyte. Figure adapted from Abuin and Scaiano Ref. [106].*

In this study, the focus is on the interaction between non-ionic polymer, triblock copolymer, Pluronic, PEO-PPO-PEO, and anionic surfactant, SDS, which triblock copolymers can be designed to be strongly amphiphilic and to have bulk and surface properties typically seen for surfactants, such as strong surface activity and the formation of micelles.

1.4.1.3. Pluronic–surfactant interaction

The interaction of polymers and surfactants in the past two decades, have received significant attention [108] and the studies of the interaction in Pluronic-surfactant systems are mostly limited to the dilute concentrations regions of the triblock copolymer and surfactant [20, 109, 110]. Surfactants are expected to bind strongly with the polymer if they are more hydrophobic than PPO block and will interface with polymer aggregation at low concentrations. Studies of Pluronic PEO-PPO-PEO micellization in the presence of SDS with self-association of SDS in the presence of triblock copolymers monomers up to the saturation of the polymer by surfactant. Hecht et al. [111] have studied the interaction between the SDS Pluronic F127 $(PEO)_{97}$-$(PPO)_{69}$-$(PEO)_{97}$ using many techniques including differential scanning calorimetry DSC, static light and small angle neutron scattering (SLS and SANS), they found that SDS suppresses the micellization of F127. Almgren et al. have been also studied the interaction between SDS and two Pluronics F68 [$(PEO)_{78}$-$(PPO)_{30}$-$(PEO)_{78}$] and L64 [$(PEO)_{13}$-$(PPO)_{30}$-$(PEO)_{13}$] using fluorescence quenching and ^{13}C NMR measurements showed that SDS binds strongly to both Pluronics [20]. Hecht et al.[110, 111] have reported that very small amount of SDS interfered with the micelle formation of F127 and when the concentration of added SDS was sufficiently high the micellization of F127 was completely suppressed. In recent times, many studies [41] [112-121] have been undertaken to explore interactions between Pluronics and surfactants, since they have a profound influence on the self-assembly behaviour of the Pluronics. In the majority of these studies Pluronic have been employed in combination with anionic surfactant such as SDS. One of the important findings from these studies is that an increase in the surfactant concentration gradually suppresses the formation of copolymer micelles.

1.4.1.3.1. P123-SDS interaction

The Interaction of P123 [$(PEO)_{20}$-$(PPO)_{70}$-$(PEO)_{20}$] with SDS has been studied using NMR [20], DLS [122], and SANS [111], where in a P123-SDS aggregate, SDS goes into the core hydrophobic of the P123 micelle (Figure 1.12) because of favourable interaction between the hydrophobic PPO blocks and SDS. According to Jansson et al. [123]have been investigated with copolymer P123 in the presence of SDS reveal that at low surfactant to copolymer mole ratio, a few anionic surfactant molecules associate with copolymer micelles and form a large complex. Whereas, in contrast, at high surfactant to copolymer mole ratio, the copolymer micelles are broken up and small surfactant micelles are formed with attachment of a few copolymer molecules.

Furthermore, Ganguly et al. [27] later have been also characterized the P123-SDS systems using SANS and viscosity measurements, according to their findings, in the region of 1:5 mole ratio of SDS to P123, the copolymer forms mixed micelles with SDS, and the aggregation number of these mixed micelles decreases with an increase in the mole ratio. However, when presence of SDS the volume fraction of the micelles is achieved by stretching of the PEO blocks in the corona region in the presence of SDS. In these mixed micelles, it has been assumed that the SDS molecules are dissolved in the core of P123 micelles and their head groups are in the corona region (Figure 1-12). This assumption has been made on the basis that the interaction between PPO units and SDS is significant stronger than that between PEO units and SDS [20].

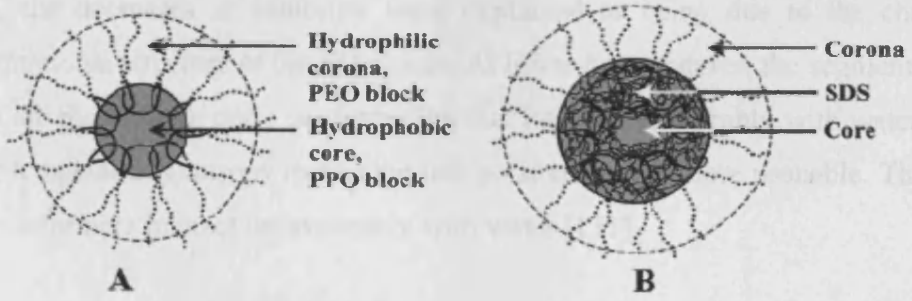

Figure 1-12: *Schematic representation of (A) P123 Micelle and (B) P123-SDS self-assembly. Figure adapted from Ganguly et al. Ref. [26].*

1.5. Phase behaviour of polymer-surfactant systems

Polymer-surfactant solutions have been extremely studied during last decade, [124-126] mainly with respect to rheological properties and aggregation phenomena in relatively dilute systems. Phase diagrams are simple to prepare and can convey a large amount of information on the phase behaviour of a system, provide fundamental information on the solute-solute interactions and have been obtained for a number of cases. It was suggested that the phase behaviour for polymer-polymer and surfactant-surfactant systems should provide an appropriate starting point for analysing the complex patterns observed for polymer-surfactant systems [127]. In this section some of findings for polymer-surfactant systems will be reviewed. Also, the behaviour of such findings will be compared those of analogous systems. The problems of phase separation in solutions containing two types of molecules or self-assemblies of colloidal dimensions will be also discussed.

There are three different mechanisms behind this behaviour that were suggested. *The oldest* of these models was reported by Kjellander and Florin [128]. It was suggested that water forms an ordered structure around the EO chain at low temperatures to produce a highly ordered structure, which is entropically unfavourable, and destroyed at higher temperatures. *The second* model [129] was an adaption of the early work of Hirschfelder et al. [130] to the systems containing EO groups. In this model the decrease in solubility was explained by a hydrogen-bonding between the EO groups and water and the hydrogen bonds were destroyed at higher temperature. In the *last model,* the decreases in solubility were explained as being due to the change in conformational structure of the EO chains. At lower temperatures, the segments of EO chains are mainly in a polar conformation that interacts favourably with water, but at higher temperatures entropy makes the less polar structures more probable. These less polar conformers interact unfavourably with water [131].

1.5.1. Liquid crystals (LCs)

Liquid crystals LCs are states of matter intermediate between that of a crystalline and an isotropic liquid. For instance, an LC may flow like a liquid, but its molecules may

be oriented in a crystal-like way. LCs possess many of the mechanical properties of liquid e.g., high fluidity, formation and coalescence of droplets. Liquid crystals can be divided into thermotropic, loytropic and metallotropic phases. Thermotropic and loytropic LCs consist of organic molecules. Whereas, metallotropic LCs are composed of both organic and inorganic molecules. Therefore, the thermotropic LCs exhibit a phase transition into the LC phase as temperature is changed. Loytropic LCs exhibits a phase transitions as a function of both temperature and concentration of the LC molecules in a solvent (typically water). Whereas, metallotropic LCs their LC transition depends not only on concentration and temperature, but also on the inorganic-organic composition ratio. In this study we focus on the loytropic LCs type owing to our system (triblock copolymers) at concentration high and/or temperature are formed LLC phases.

1.5.1.1. Lyotropic liquid crystal (LLC)

A liquid crystalline material is called "Lyotropic" if phases having long-ranged orientational order are induced by the addition of solvent. Historically the term was used to describe materials composed of amphiphilic molecules. Such molecules comprise a water-loving "hydrophilic" head-group (which may be ionic or non-ionic) attached to a water-hating "hydrophobic" group. Typical hydrophobic groups are saturated or unsaturated hydrocarbon chains. The LLC were actually discovered long before their thermotropic counterparts were known. In 1850, their texture was noticed in a mixture of myelin and water. At the time of discovery, however, the significance of LCs was not understood, so most research has been done on thermotropic. Only justly recently have LLCs begun to catch up. The molecules that make up LLCs are surfactants consisting of two distinct parts: a polar, often ionic, head and a non-polar, often hydrocarbon tail, not all surfactants, however, form LLC Figure 1-13.

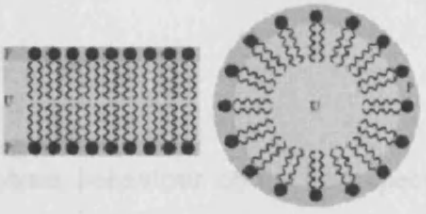

Figure 1-13: *Structure of LLC. Red heads of surfactant molecules are in contact with water, whereas blue tails are immersed in oil either in bilayer(left) or micelle (right).*

1.5.1.2. Lyotropic liquid crystal of Pluronic

Amphiphilic triblock copolymers of the PEO-PPO-PEO type at a higher polymer concentration normally produced LLC phases [132-134]. Since the effective volume of the systems is much larger than the real volume, where it is normally not expected for hydrocarbon surfactants. It was shown for the first time by SANS measurements that the gelation process, which is observed in some moderately concentrated block copolymer solutions with increasing temperature is actually due to the formation of a cubic phase [135]. Since then Mortensen et al. [136] have obtained detailed information by SANS on the cubic phase. They showed in particular that these phases can be aligned by shear. Beside the cubic phases, other LC phases like hexagonal and lamellar phases have also been observed [137].

1.5.2. Phase behaviour of surfactant

Low molecular weight non-ionic surfactant associate into micelles above the CMC in water and form different LC phases "cubic, hexagonal, and lamellar mesophases" at higher concentrations. In addition, the aqueous solution of PEO non-ionic surfactants shows a "cloud point" where the one-phase solution is separated into a dilute surfactant solution and a concentrated solution containing micelles. Phase behaviour of non-ionic hydrocarbon surfactants, particularly of the PEO alkyl ether type $C_m(EO)_n$, has been extensively investigated. In general, the phase equilibria examined showed some common features independent of the detailed chemical structure of the polar groups. The phase equilibria are governed not only by the balance between the energetically favourable hydration of the polar groups and the energetically unfavourable contact between hydrocarbon and water, but also by the solubility behaviour of the PEO portion in water as a function of temperature which leads to the occurrence of a LCST.

1.5.3. Phase behaviour of Pluronic

In principle, similar phase behaviour could be expected for Pluronic copolymers, namely; the self-assembly of the copolymer chains to form associated structures of different shapes (spheres, rods, etc.), the growth and interactions of micelles to form

order structures (e.g., LCs) and the occurrence of the cloud point for the solution phases and the melting point for the LC phases. On the other hand, the phase behaviour of aqueous solution of non-ionic polymers and surfactants containing the EO segment is a problem that has both theoretical and experimentally received much attention in recent years, perhaps mainly due to the phase separation occurring in such systems at elevated temperatures [138-140]. The obvious explanation to this decrease in solubility at higher temperatures is a rapid increase in the effective attraction between different solute molecules with temperature. Pluronic can display with water and cosolvent and/or surfactant binary ternary phase behaviour, therefore, we focus these behaviour of Pluronic P123 in the following sections.

1.5.3.1. Binary phase behaviour

The block copolymer displays a rich morphology in water where the binary polymer/water phase diagram is presented [133]. The binary phase diagram of P123 with water has been reported by Wanka et al. [132]. It presents below 60°C and with increasing concentration P123, the solution and LLC phases appear in the following: isotropic solution → cubic phase → hexagonal phase. Two phases region exists between the adjacent phases in the above sequence of phases. All the LLC phases melt below 90°C, but the cubic phase at 50°C as indicated in Figure 1-14.

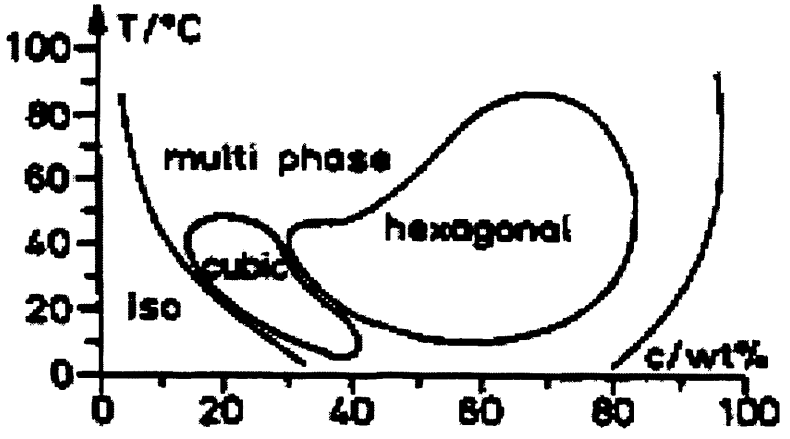

Figure 1-14: Binary Phase diagram of P123/H_2O system with concentration and temperature. Figure adapted from Wanka et al. Ref. [131].

Recently, Zhao et al. [141] have studies the phase behaviour of binary system of P123/water, using dynamic density functional method, the mesoscopic dynamics which simulates the microphase separation of P123/water binary mixtures. Obtained results shows that with the increase of P123 concentration, different aggregation such as micelle (M), hexagonal (H), and lamellar (L) phases are formed, Figure 1-15. Therefore, it can be conclude that the mesoscopic simulation method is a valuable tool for the description of mesoscopic morphology formation and gives an insight into process of aggregation formation.

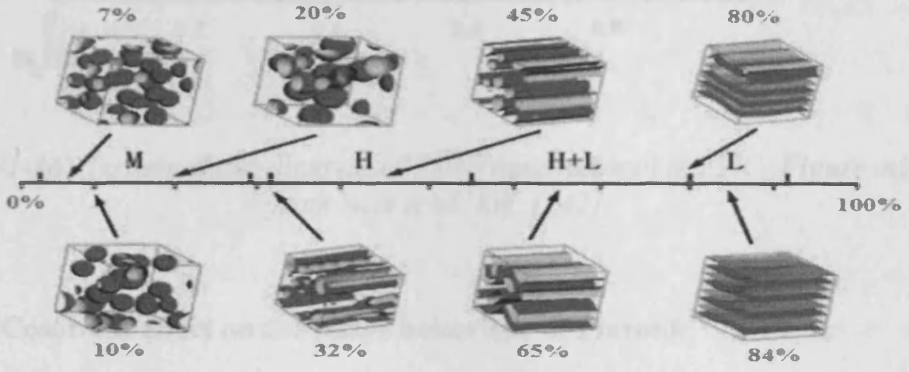

Figure 1-15: *Simulated phase evolution of Pluronic P123 with its concentration in aqueous solution at 25°C. Figure adapted from Yurong et al. Ref. [140].*

1.5.3.2. Ternary phase behaviour

Nowadays, it is more common to plot phase behaviour of simple microemulsions comprising surfactant or Pluronic with water and cosolvent on a ternary phase diagram in which each apex of the triangle represents 100% of that particular component [22, 55, 142, 143]. The concentration and temperature ranges over which the different phases formed depend on the block copolymer molecular weight, the block (EO/PO) ratio, and the solvent quantity and quality. Soni et al. [144] have studied the phase behaviour of ternary system of P123/ethanol/water by small-angle X-ray scattering SAXS. The microstructure resulting from the self-assembly of the block copolymer varies from micelles in solution to various types of LC phases such as L_1 denotes region with isotropic solution, I_1 denoted the clear isotropic gels and mixture of cubic and hexagonal close packed sphere (HCPS) lattice, H_1 denotes cylindrical micelles arranged in a D_2 hexagonal lattice, and L_α denotes the lamellae-

planner micelles Figure 1-16. The boundaries of one-phase regions are drawn with solid lines. Points indicate the compositions of P123/water/ethanol in ternary mixture.

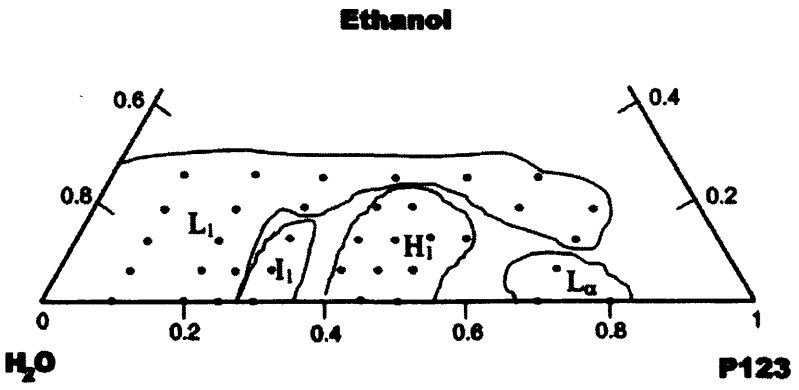

Figure 1-16: Ternary phase diagram of P123/water/ethanol at 23°C. *Figure adapted from Soni et al. Ref. [142].*

1.5.3.3. Cosolvent effect on the phase behaviour of Pluronic

The addition of cosolvents can modulate the swelling behaviour of the different blocks of the polymer and hence alter the phase behaviour to a great extent. The rich phase behaviour observed in ternary mixture of block copolymer, water and additives provide new pathways for morphological control that suits specific applications. The cosolvent effects on the self-assembled microstructure are related to changes in the mean interfacial area occupied by PEO blocks, its preference to locate in different microdomains and ability to modify the interfacial curvature by swelling different block of the copolymer to different extents [55, 57].

The phase behaviour of block copolymers is affected by various organic solvents, [55, 145] therefore, the block copolymer-solvent interactions can lead to either suppressing or facilitating the formation on micelles in solution and of LLC having long-range order. Organic solvents depending on their relative polarities locate either in the PEO-rich or PPO-rich domains of the microstructure. Where some solvents, however, independent on their polarities (*e.g.* ethanol and glycerol triacetate) may show amphiphilic behaviour and act as cosurfactant locating at the interface between the PEO-rich and the PPO-rich domains [57]. Latterly, Ganguly et al. [146] reported the effect of the addition of ethanol on the structure of P123/water system in the

diluted isotropic phase by using SANS, DLS and viscosity at 23°C. The studies show in the presence of a small amount of ethanol (5-10%) induces a sphere to rod shape transition of micelles at high temperature.

1.5.3.4. Surfactant effect on the phase behaviour of Pluronic

Mixed aqueous mixtures of Pluronics and classical surfactants have been studied mostly in diluted solutions of both components. Since the studies of Pluronic block copolymer micellization in presence of SDS revealed that with increasing the SDS concentration, the micelle association number decreases until pure SDS micelles and individual Pluronic macromolecules saturated with SDS are presents, surfactants are believed to bind the PPO block of the block copolymer amphiphilicity. At saturation of the Pluronics with surfactant, the block copolymer micellization is completely suppressed [20, 111] and this leads to the destruction of the LC phases formed by the block copolymer [108]. Hecht and Hoffmann [110] has greatly contributed to a better understanding of the association in dilute solutions of a Pluronic and SDS.

Zhang et al. [108] one of three authors of a new contribution analyzed the phase behaviour of Pluronic with surfactant of ternary system of (L64/SDS/water), and stressed the effect of SDS on the LLC Phases of L64. Pluronic L64 is a commercial copolymer with a normal composition of $(PEO)_{13}$-$(PPO)_{30}$-$(PEO)_{13}$, which alone displays a rich polymorphism in water (micellar solution→ hexagonal → cubic → lamellar LC phases upon increasing the copolymer concentration). The interaction between L64 and SDS was mainly studied at 25°C by NMR quadruple splitting (of ^{23}Na and ^{2}H of D_2O) and ^{1}H-NMR self-diffusion coefficients. At moderately high copolymer concentrations the LC phases of L64, consisting of infinite aggregates, melted upon the addition of SDS in a large isotropic liquid region. The solution microstructure of this region was not well defined and hence remains structurally uncharacterized [108].

Ivanova and his workers [142] have explored the interaction of Pluronic F127 with anionic surfactant, SDS by studying the ternary phase diagrams of the F127/SDS/water system, their interest was in the part of the phase diagram where the block copolymer forms LC structures and also shows that SDS do not maintain the

stability of the block copolymer assemblies. In this case, the micellar cubic structure can accommodate less than 6 wt% surfactant. The presence of one-phase hexagonal structure (H_1) in the ternary system has not been detected within the resolution of their concentration grid, they believe, however (on the basis of two-phase samples), that H_1 is stable at less than 2 wt% surfactant. The extent of the micellar cubic structure in the case of SDS as obtained here is in very good agreement with the data of 30 wt% F127 at 25°C and identical conditions reported in [111].

1.6. Objective of the studies in this thesis

The chief goal of this PhD project dissertation was to study the effect of cosolvents such as ethanol on the competitive interaction between the anionic surfactant sodium dodecyl sulfate (SDS) and a non-ionic triblock copolymer Pluronic P123, $(PEO)_{20}$-$(PPO)_{70}$-$(PEO)_{20}$. Both SDS and P123 form micelles in aqueous solutions whose structure may change as a function of ethanol content. Our additional goal was to investigate the phase behaviour of Pluronic copolymer (P123) in water as a function of its concentration to ethanol and sodium dodecyl sulfate concentration. Finally, was explored the physico-chemical properties of stimuli-polymers as a function of temperature for polyethylene glycol ethyl ether methacrylate (PEGMA-EE, Mn 246) and polyethylene glycol methyl ether methacrylate (PEGMA-ME, Mn 475) in the absent and in the presence of protein (trypsin).

1.7. Outline of this thesis

The work represented in this thesis described the interaction between copolymer and surfactant. We have selected the P123-SDS model system to carry out this research. Chapter one deals with the background for the research involved. Chapter two describes the most important features of the surface tension, fluorescence, viscosity, Pulsed-Gradient Spin-Echo NMR, PGSE-NMR and Small Angle Neutron Scattering (SANS) and the materials used in this research. Chapter three deals with the basic experiments and theory of techniques that have been used. Chapter four describes the results of a systematic set of experiments performed with polymer-surfactant interaction. Chapter five deals with how the P123 and SDS concentrations range

effect of phase behaviour of the LLC structures attained by the PEO-PPO-PEO block copolymers is modulated by the interactions of the PEO and PPO blocks with surfactant, SDS, in cosolvent ethanol. Finally, Chapter six describes the temperature effect on some responsive-polymers, "Hybrid" block copolymers, named P6 and P7, composed of statistical sequences of PEGMA-EE246 with PEGMA-ME475, from which were grown an outer block of PEGMA-ME475 (PEGMA-EE, Mn=246), (PEGMA-ME, M_n= 475) and their conjugates with trypsin which conjugate P6-trypsin (Hybrid A) and conjugate P6-trypsin (Hybrid B).

1.8. References

[1] B. Jonsson, B. Lindman, K. Holmberg, B. Kronberg, Surfactants and Polymers in aqueous solution, John Wiley & Chichester (1998).
[2] R. Lambourne, T. A. Strivens, Paint and Surface Coatings - theory and practice, Woodhead Publishing, Norwich (1999).
[3] S. M. Moghimi, A. C. Hunter, Poloxamers and Poloxamines in nanoparticle engineering and experimental medicine, Trends in Biotechnology 18 (2000) 412-420.
[4] R.M.Ottenbrite, E.Chiellini, Frontiers in biomedical polymer applications. CRC Press, London (1997).
[5] J.M.G. Cowie, Polymer : Chemistry and Physics of Modern Materials, Blackie Academic and Professional (1991).
[6] D. Evons, H. Wennerstron, The Colloidal Domain, where Physics, Chemistry, Biology, and Technology Meet, 2nd Ed., John Wiley & Sons: New York, 1999.
[7] G. Riess, G. Hurtrez, P. Bahadur, in Encyclopaedia of Polymer Science Engineering, Wiley, NY, vol. 2 (1985) pp. 324-434.
[8] L. Watson, Encyclopaedia of Surface and Colloid Science, 2nd Ed. (2006).
[9] T. Radeva, Encylopaedia of Surface and Colloid Science (2002) 547-557.
[10] P. Alexandridis, Amphiphilic copolymers and their applications, Current Opinion in Colloid & Interface Science 1 (1996) 490-501.
[11] G. Fleer, M. Cohen Stuart, J. Scheutjens, T. Cosgrove, B. Vincent, Polymers at Interfaces, London: Chapman & Hall, 1993.
[12] D. Gingell, N. Owens, Journal of Biomedical Materials Research 28 (1994) 491-503.
[13] C. Schroen, M.A.C. Stuart, K.V. Maarschalk, A. Vanderpadt, K. Vantriet, I, Langmuir 11 (1995) 3068-3074.
[14] M.J. Rosen, Surfactants and Interfacial Phenomena, 2nd Ed., John Wiley & Sons; New York, 1989.
[15] P. Alexandridis, T.A. Hatton, Colloids and Surfaces 96 (1995) 1- 46.
[16] M. Moffitt, K. Khougaz, A. Eisenberg, Accounts of Chemical Research 29 (1996) 95-102.
[17] R. G. Laughlin, The Aqueous Phase Behaviour of Surfactants, Academic Press, London, 1994.
[18] http:www2.basf.us/performancechemical/bcperpluronic_grid.html., 2010.
[19] P. Alexandridis, Current Opinion in Colloid & Interface Science 2 (1997) 478-489.
[20] M. Almgren, J. Vanstam, C. Lindblad, P.Y. Li, P. Stilbs, P. Bahadur, Journal of Physical Chemistry 95 (1991) 5677- 5684.
[21] P. Alexandridis, J.F. Holzwarth, T.A. Hatton, Macromolecules 27 (1994) 2414-2425.
[22] R. Ivanova, B. Lindman, P. Alexandridis, Advances in Colloid and Interface Science 89 (2001) 351-382.
[23] Y.L. Su, X.F. Wei, H.Z. Liu, Langmuir 19 (2003) 2995-3000.
[24] Y.H. Ding, Y. Wang, R. Guo, Journal of Dispersion Science and Technology 24 (2003) 673-681.
[25] J. Mata, T. Joshi, D. Varade, G. Ghosh, P. Bahadur, Colloids and Surfaces 247 (2004) 1-7.
[26] J. Ma, C. Guo, Y. Tang, J. Wang, L. Zheng, X. Liang, S. Chen, H. Liu, Journal of Colloid and Interface Science 299 (2006) 953-961.

[27] R. Ganguly, V. K. Aswal, P. A. Hassan, I. K. Gopalakrishnan, S. K. Kulshreshtha, Journal of Physical Chemistry B 110 (2006) 9843-9849.
[28] J.H. Ma, C. Guo, Y.L. Tang, J.F. Xiang, S. Chen, J. Wang, H.Z. Liu, Journal of Colloid and Interface Science 312 (2007) 390-396.
[29] J.P. Mata, P.R. Majhi, O. Kubota, A. Khanal, K. Nakashima, P. Bahadur, Journal of Colloid and Interface Science 320 (2008) 275-282.
[30] P. Alexandridis, V. Athanassiou, S. Fukuda, T.A. Hatton, Langmuir 10 (1994) 2604- 2612.
[31] P. Alexandridis, T. Nivaggioli, T.A. Hatton, Langmuir 11 (1995) 1468-1476.
[32] I.R. Schmolka, Journal of Biomedical Materials Research 6 (1972) 571-582.
[33] P.K. Sharma, M.J. Reilly, S.K. Bhatia, N. Sakhitab, J.D. Archambault, S.R. Bhatia, Colloids and Surfaces B-Biointerfaces 63 (2008) 229-235.
[34] M. Youssry, F. Asaro, L. Coppola, L. Gentile, I. Nicotera, Journal of Colloid and Interface Science 342 (2010) 348-353.
[35] Y. Liu, W.L. Lu, H.C. Wang, X. Zhang, H. Zhang, X.Q. Wang, T.Y. Zhou, Q. Zhang, Journal of Controlled Release 117 (2007) 387-395.
[36] P. Bahadur, P.Y. Li, M. Almgren, W. Brown, Langmuir 8 (1992) 1903-1907.
[37] M. Almgren, P. Bahadur, M. Jansson, P.Y. Li, W. Brown, A. Bahadur, Journal of Colloid and Interface Science 151 (1992) 157-165.
[38] W. Brown, K. Schillen, M. Almgren, S. Hvidt, P. Bahadur, Journal of Physical Chemistry 95 (1991) 1850-1858.
[39] N.J. Jain, V.K. Aswal, P.S. Goyal, P. Bahadur, Journal of Physical Chemistry B 102 (1998) 8452-8458.
[40] J.P. Mata, P.R. Majhi, C. Guo, H.Z. Liu, P. Bahadur, Journal of Colloid and Interface Science 292 (2005) 548-556.
[41] J. P. Mata, P. R. Majhi, M. Yamashita, A. Khanal, K. Nakashima, P. Bahadur, Journal of Dispersion Science and Technology 29 (2008) 1248-1256.
[42] Y. Kadam, U. Yerramilli, A. Bahadur, Colloids and Surfaces B-Biointerfaces 72 (2009) 141-147.
[43] L.X. Fan, M. Degen, N. Grupido, S. Bendle, P. Pennartz, Materials Science and Engineering 528 (2010) 127-136.
[44] V.K. Aswal, J. Kohlbrecher, Chemical Physics Letters 425 (2006) 118-122.
[45] P.N. Hurter, T.A. Hatton, Langmuir 8 (1992) 1291-1299.
[46] L. Yang, P. Alexandridis, D.C. Steytler, M.J. Kositza, J.F. Holzwarth, Langmuir 16 (2000) 8555-8561.
[47] C. Guo, J. Wang, H.Z. Liu, J.Y. Chen, Langmuir 15 (1999) 2703-2708.
[48] Y.L. Su, J. Wang, H.Z. Liu, Macromolecules 35 (2002) 6426-6431.
[49] K. Mortensen, J.S. Pedersen, Macromolecules 26 (1993) 805-812.
[50] M. Almgren, W. Brown, S. Hvidt, Colloid and Polymer Science 273 (1995) 2-15.
[51] A.V. Kabanov, E.V. Batrakova, V.Y. Alakhov, Journal of Controlled Release 82 (2002) 189-212.
[52] S. Hvidt, E.B. Jorgensen, W. Brown, K. Schillen, Journal of Physical Chemistry 98 (1994) 12320-12328.
[53] P. Alexandridis, J.F. Holzwarth, Langmuir 13 (1997) 6074-6082.
[54] J. Armstrong, B. Chowdhry, J. Mitchell, A. Beezer, S. Leharne, Journal of Physical Chemistry 100 (1996) 1738-1745.
[55] R. Ivanova, B. Lindman, P. Alexandridis, Langmuir 16 (2000) 3660-3675.
[56] P. Kipkemboi, A. Fogden, V. Alfredsson, K. Flodstrom, Langmuir 17 (2001) 5398-5402.
[57] P. Alexandridis, R. Ivanova, B. Lindman, Langmuir 16 (2000) 3676-3689.

[58] N.K. Pandit, J. Kisaka, International Journal of Pharmaceutics 145 (1996) 129-136.
[59] N. Pandit, T. Trygstad, S. Croy, M. Bohorquez, C. Koch, Journal of Colloid and Interface Science 222 (2000) 213-220.
[60] Y.L. Su, H.Z. Liu, J. Wang, J.Y. Chen, Langmuir 18 (2002) 865-871.
[61] A. Caragheorgheopol, H. Caldararu, I. Dragutan, H. Joela, W. Brown, Langmuir 13 (1997) 6912-6921.
[62] D.A. Chiappetta, A. Sosnik, European Journal of Pharmaceutics and Biopharmaceutics 66 (2007) 303-317.
[63] M. Malmsten, B. Lindman, Macromolecules 25 (1992) 5440-5445.
[64] A. Kikuchi , T. Okano Progress in Polymer Science 27 (2002) 1165 - 1193.
[65] A.S. Hoffman , e. al., Journal of Biomedical Materials Research A 52 (2000) 577 -586.
[66] L.Y. Galaev , B. Mattiasson Trends in Biotechnology 17 (2000) 335 - 340.
[67] Y. Qiu , K. Park Advanced Drug Delivery Reviews 53 (2001) 321 - 339.
[68] L. E. Bromberg, E.S. Ron, Advanced Drug Delivery Reviews 31 (1998) 197 - 221.
[69] A. Chikoti , M. R. Dreher, D. E. Meyer, D. Raucher, Advanced Drug Delivery Reviews 54 (2002) 613 - 630.
[70] P. Gupta, K. Vermani, S. Garg, Drug Discovery Today 7 (2002) 569 - 579.
[71] S. Sershen, J. West, Advanced Drug Delivery Reviews 54 (2002) 1225 - 1235.
[72] J. Weidner, Drug Discovery Today 6 (2001) 1239 - 1248.
[73] M. Yokoyama, Drug Discovery Today 7 (2002) 426 -432.
[74] S. Sharma, P. Kaur, A. Jain, M. R. Rajeswari, M. N. Gupta, Biomacromolecules 4 (2003) 330 - 336.
[75] S. Anastase-Ravion, Z. Ding, A. Pelle, A. S. Hoffman, D. Letourneur, Journal of Chromatogragraphy B 761 (2001) 247 - 254.
[76] J. Kobayashi, A. Kikuchi, K. Sakai, T. Okano, Journal of Chromatography A 2002 (2002) 109-119.
[77] F. Bignotti, M. Penco, L. Sartore, I. Peroni I, R. Mendichi , M. Caslaro , A. D' Amore Polymer 41 (2000) 8247- 8256.
[78] L. H. Gan, Y. Y. Gan, G. R. Deen, Macromolecules 33 (2000) 7893-7897.
[79] T. Peng, Y. L. Cheng, Polymer 41 (2001) 2091- 2100.
[80] V. T. Pinkrah, M. J. Snowden, J. C. Mitchell, J. Seidel J, B. Z. Chowdhry, G. R. Fern Langmuir 19 (2003) 585-590.
[81] E. S. Gil, E. M. Hudson, Progress Polymer. Science, 29 (2004) 1173 -1222.
[82] S. Fujishige, K. Ando, Journal of Physical Chemistry A 93 (1989) 3311- 3313.
[83] X. Zhang, R. Zhuo, Y. Yang, Biomaterials 26 (2002) 1313-1318.
[84] W. Brown, K. Schillen, S. Hvidt, Journal of Physical Chemistry A 96 (1992) 6038-6044.
[85] S. Shao-Tang, N. Lzumi, S. Gerald, T. Toyoichi, Journal of Chemical Physics 73 (1980) 5971-5975.
[86] T. Birshtein, V. Pryamitsyn, Macromolecules 24 (1991) 1554-1560.
[87] M. Nakata, Physical Chemistry Review 51 (1995) 5770-5775.
[88] Y. Hirokawa, T. Tanaka, Journal of Chemical Physics 81 (1984) 6379-6380.
[89] M. Xiang, M. Jiang, Y. Zhang, C. Wu, L. Feng, Macromolecules 30 (1997) 2313-2319.
[90] G. Graziano, International Journal of Biological Macromolecule 27 (2000) 89-97.

[91] J. Lu, R. Thomas, J. Penfold, Advanced Colloid Interface Science 84 (2000) 143-304.
[92] S. Paria, K. Khilar, Advanced Colloid Interface Science 110 (2004) 75-95.
[93] Y. Chevalier, T. Zemb, Reports on Progress in Physcis 53 (1990) 279-371.
[94] C. Tanford, The hydrophobic effect: formation of micelles and biological membranes; Wiley, New York,1980.
[95] D. Myers, Surfactant Science and Technology, 2nd Ed., VCH Publishers , UK, 1992.
[96] W. C. Griffin, "Classification of Surface-Active Agents by HLB", , Journal of the Society of Cosmetic Chemists, 1(1949):311.
[97] W. C. Griffin, "Calculation of HLB Values of Non-Ionic Surfactants", Journal of the Society of Cosmetic Chemists, 5(1954):259.
[98] J.T. Davies, Proceedings of the International Congress of Surface Activity, 1957, p 426-438.
[99] J.N. Israelachvili, Intermolecular and Surfaces Forces, 2nd Ed., Academic Press, London, 1991.
[100] B. Lindman, H. Wennerstrom, Topic in Current Chemistry, Springer-Verlag, Berlin, 1980, vol. 87, p 6-13.
[101] M. N. Jones, D. Chapman, Micelles, monolayers and biomembranes, Wiley - Liss, New York, 1995, p 252.
[102] S. Puvvada, D. Blankschtein, Journal of Chemical Physics. 92 (1990) 3710-3724.
[103] J. W. McBain, Trans Faraday Society 9 (1913) 99-100.
[104] E.D. Goddard, K.P. Ananthpaadmanabhan, Interactions of Surfactants with Polymers and proteins, CRC, Press: Boca Raton, FL,1993, p 395.
[105] M. N. Jones, Journal of Colloid and Interface Science, 23 (1967) 36.
[106] C. La Mesa, Colloids and Surfaces 160 (1999) 37-46.
[107] E. B. Abuin, Journal of American Chemical Society 106 (1984) 6274-6283.
[108] K. Zhang, B. Lindman, L.Coppola, Langmuir 11 (1995) 538-542.
[109] R. C. da Silva, G. Olofsson, K. Schillen, W. Loh, Journal of Physical Chemistry B 106 (2002) 1239-1246.
[110] E. Hecht, H. Hoffmann, Langmuir 10 (1994) 86-91.
[111] E. Hecht, K. Mortensen, M. Gradzielski, H. Hoffmann, Journal of Physical Chemistry 99 (1995) 4866-4874.
[112] M. J. Kositza, G. D. Rees, A. Holzwarth, F. Holzwarth, Langmuir 16 (2000) 9035-9041.
[113] Y. Li, R. Xu, S. Couderc, D. M. Bloor, E. Wyn-Jones, J. F. Holzwarth, Langmuir 17 (2001) 183-188.
[114] S. Dai, C. K. Tam, L. Li, Macromolecules 34 (2001) 7049-7055.
[115] T. Thurn, S. Couderc, J. Sidhu, D. M. Bloor, J. Penfold, J. F. Holzwarth, E. Wyn-Jones, Langmuir 18 (2002) 9267-9275.
[116] R. De Lisi, S. Milioto, M. Munafo, N. Muratore, Journal of Physical Chemistry B 107 (2003) 819-825.
[117] R. De Lisi, G. Lazzara, S. Milioto, N. Muratore, Journal of Physical Chemistry B 108 (2004) 1189-1196.
[118] A. Kelarakis, C. Chaibundit, M. J. Krysmann, V. Havredaki, K. Viras, I. W. Hamley, Journal of Colloid and Interface Science 330 (2009) 67-72.
[119] R. K. Mahajan, A. Shaheen, S. Sachar, Journal of Dispersion Science and Technology 30 (2009) 1020-1026.

[120] B. Bharatiya, G. Ghosh, P. Bahadur, J. Mata, Journal of Dispersion Science and Technology 29 (2008) 696-701.
[121] Y. Kadam, Journal of Dispersion Science and Technology 31 (2009) 870-876.
[122] J. Jansson, K. Schillen, G. Olofsson, R. C. da Silva, W. Loh, Journal of Physical Chemistry B 108 (2004) 82-92.
[123] J. Jansson, K. Schillen, M. Nilsson, O. Soderman, G. Fritz, A. Bergmann, O. Glatter, Journal of Physical Chemistry B 109 (2005) 7073-7083.
[124] B. Cabance, R. Duplessix, Colloids and Surfaces A 13 (1985) 19-33.
[125] E. D. Goddard, Colloids and Surfaces A 19 (1986) 255.
[126] P. G. de Gennes, Journal of Physical Chemistry 94 (1990) 8407-8413.
[127] L. Piculell, B. Lindman, Advances in Colloids and Interface Sciences 245 (1989) 1371.
[128] R. Kjellander, E. Florin, Journal of Chemical Society Faraday Trans 177 (1981) 2053.
[129] R. E. Golgstein, Journal of Physical Chemistry 80 (1984) 5340.
[130] J. Hirschfelder, D. Stevenson, H. Eyring, Journal of Chemical Physics 5 (1937) 896.
[131] G. Karlstrom, Journal of Chemical Physics 89 (1985) 4962.
[132] G. Wanka, H. Haffmann, W. Ulbricht, Marcromolecules 27 (1994) 4145.
[133] K. Zhang, A. Khan, Marcromolecules 28 (1995) 3807.
[134] P. Alexandridis, D. Zhou, A. Khan, Langmuir 12 (1996) 2690.
[135] G. Wanka, H. Hoffmann, W. Ulbricht, Colloid and Poymer Science 268 (1990) 101.
[136] K. Almdal, F. S. Bates, K. Mortensen, Journal of Chemical Physics 96 (1992) 9122.
[137] Q. Yang, G. Yu, Y. Deng, C. Price, C. Booth, European Polymer Journal 29 (1993) 665.
[138] B. Lindman, G. Karlstrom, Journal of Physical Chemistry 155 (1987) 199.
[139] S. Saeki, N. Kuwahara, M. Kaneko, Polymer 17 (1976) 685.
[140] T. Warnheim, J. Bokstrom, Y. Williams, Colloid and Polymer Science 266 (1988) 2053.
[141] Zhao Yurong, Chen Xiao, Yang Chunjie, Zhang Guodong, Journal of Physical Chemistry B 111 (2007) 13937.
[142] R. Ivanova, P. Alexandridis, B. Lindman, Colloids and Surfaces A 183 (2001) 41-53.
[143] M. Youssry, F. Asaro, L. Coppola, L. Gentile, I. Nicotera, J Colloid Interface Science 342 (2010) 348-353.
[144] S. S. Soni, G. Brotons, M. Bellour, T. Narayanan, A. Gibaud, Journal of Physical Chemistry B 110 (2006) 15157-15165.
[145] P. Alexandridis, U. Olsson, B. Lindman, Langmuir 14 (1998) 2627-2638.
[146] R. Ganguly, V. k. Aswal, P. A. Hassan, I. K. Gopalakrishnan, J. V. Yakhmi, Journal of Chemical Physics B 109 (2005) 5653.

Chapter 2: Materials and Equipment

2. Introduction

In this chapter we will briefly describe about the materials used and how they were purified and the preparation of these materials. Techniques used in this study were surface tension, fluorescence and viscosity. Further work involved the use of pulsed–gradient spin-echo NMR (PGSE-NMR) and small-angle neutron scattering (SANS), these techniques are discussed in Chapter 3.

2.1. Materials

2.1.1. General materials

8-anilino-1-naphthalene sulfonic acid (ANS), ethanol, (Fisher Scientific, 99.99%), deuterium oxide (D_2O), (Fluorochem, 99.9%), trypsin, sodium sulphate (Na_2SO_4), (Fisher scientific) and phosphate buffer solution (PBS) at pH 7.2, (Sigma diagnostics, USA) were all used as received.

2.1.2. Surfactants

Sodium dodecyl sulfate (SDS) (Aldrich, purity 98%) was purified by repeated recrystallization from ethanol (see section 2.1.5). Deuterated sodium dodecyl sulfate (d-SDS) for use on SANS experiments (Chapter 4) was obtained from Aldrich (99.9%) and used as received.

2.1.3. Pluronic studies

Poly(ethylene glycol)$_{20}$-block-poly(propylene glycol)$_{70}$-block-poly(ethylene glycol)$_{20}$ as known Pluronic P123 copolymer, average molecular weight M_n~5800 gmol^{-1}, n_D(20°C) =1.4650, (Aldrich), was used as received. The ^{1}H-NMR spectrum of this copolymer (Figure 2-1), show the intensities of the signals attributed to water (HDO),

polymer (EO-CH_2-), (PO-CH_2-) and (PO-CH_3), respectively and found to be in agreement with the literature reports [1-3].

A value of the ratio of the weight-average to number-average molar mass, (Mw/Mn) =1.4, was determined by Gel Permeation Chromatography (GPC) using tetrahydrofuran (THF) as solvent, at 25°C, is depicted in Figures 2-2.

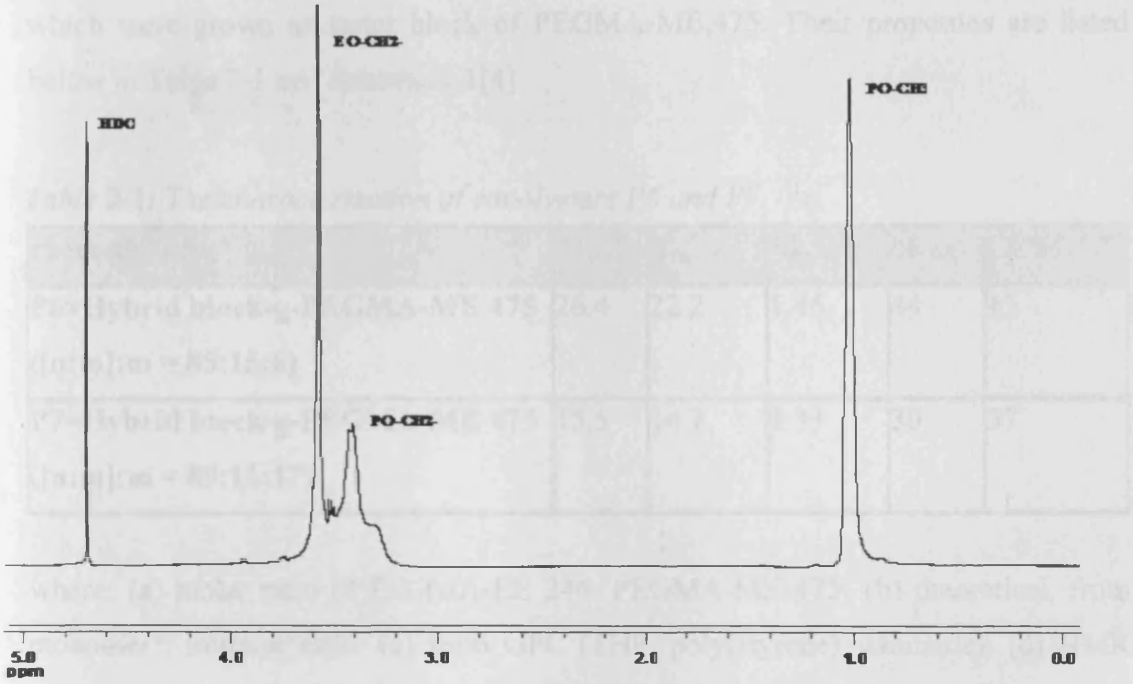

Figure 2-1: ^{1}H-NMR spectrum for 1.0 wt% P123 in D_2O at 25°C.

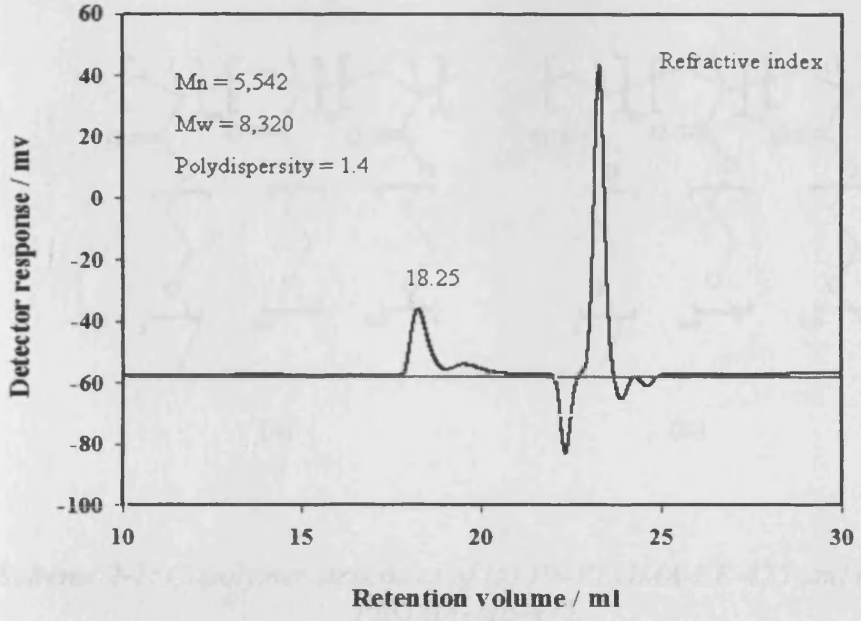

Figure 2-2: Gel Permeation Chromatography (GPC) data for 1.0 wt% P123 in THF.

2.1.4. Stimuli responsive copolymers

Hybrids block copolymers namely P6, P7, conjugates P6 and P7 with trypsin (hybrid A and hybrid B) were supplied by Prof. Cameron Alexander, School of Pharmacy Nottingham University. The hybrid block copolymers, P6 and P7, composed of statistical sequences of poly(ethylene glycol) ethyl ether methacrylate (PEGMA-EE, 246) with poly(ethylene glycol) methyl ether methacrylate (PEGMA-ME, 475) from which were grown an outer block of PEGMA-ME,475. Their properties are listed below in Table 2-1 and Scheme 2-1[4].

Table 2-1: *The characterization of copolymers P6 and P7.*

Polymer- n:m[a]	M_{nth}[b]	M_n[c]	M_w/M_n[c]	% m[d]	LCST,°C[e]
P6=Hybrid block-g-PEGMA-ME 475 ([n:m]:m = 85:15:6)	26.4	22.2	1.46	44	45
P7=Hybrid block-g-PEGMA-ME 475 ([n:m]:m = 89:11:17)	15.5	14.7	1.33	30	37

where: (a) molar ratio of PEGMA-EE 246: PEGMA-ME 475; (b) theoretical, from monomer : initiator ratio; (c) from GPC (THF, poly(styrene) standards); (d) NMR integral; (e) from sharp increase in UV adsorption of solution in water at 550nm [4].

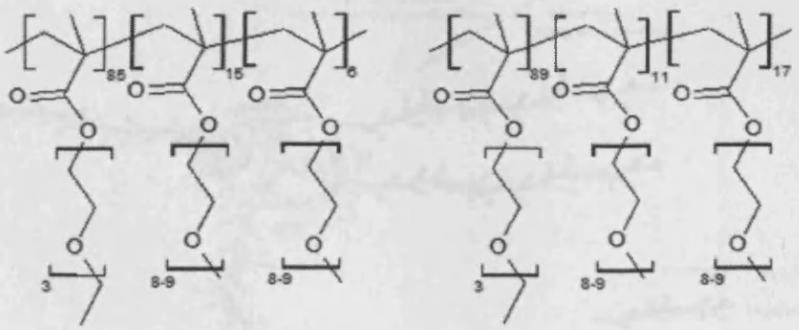

(a) (b)

Scheme 2-1: *Copolymer structures of (a) P6-PEGMA-EE-475 and (b) P7-PEGMA-ME-475.*

For Hybrids A and B, the polymerization from trypsin was carried out by adopting a previous polymerization method of "smart" PEGMA previously reported by Magnusson et al. [4], Scheme 2-2 and Table 2.2. A polymer with a targeted LCST of 37°C was initially grown from the functionalized trypsin protein to create a smart trypsin Hybrid A. The purified polymer conjugate was then used to initiate a second polymerization with PEGMA (Mn 475) to create the triblock trypsin Hybrid B [5].

Table 2-2: *The characterization of hybrid A and hybrid B.*

Conjugate	M_n[a]	M_w/M_n[a]	% BCA[b]	LCST,°C[c]
Hybrid A = conjugate trypsin-P6	28,300	1.19	14.82	36
Hybrid B = conjugate trypsin-P7	45,606	1.53	9.14	36

where: (a) from GPC; (b) Protein content and assay (BCA); and (c) UV absorption of 3mg/ml solutions in 1 x PBS at 550 nm.

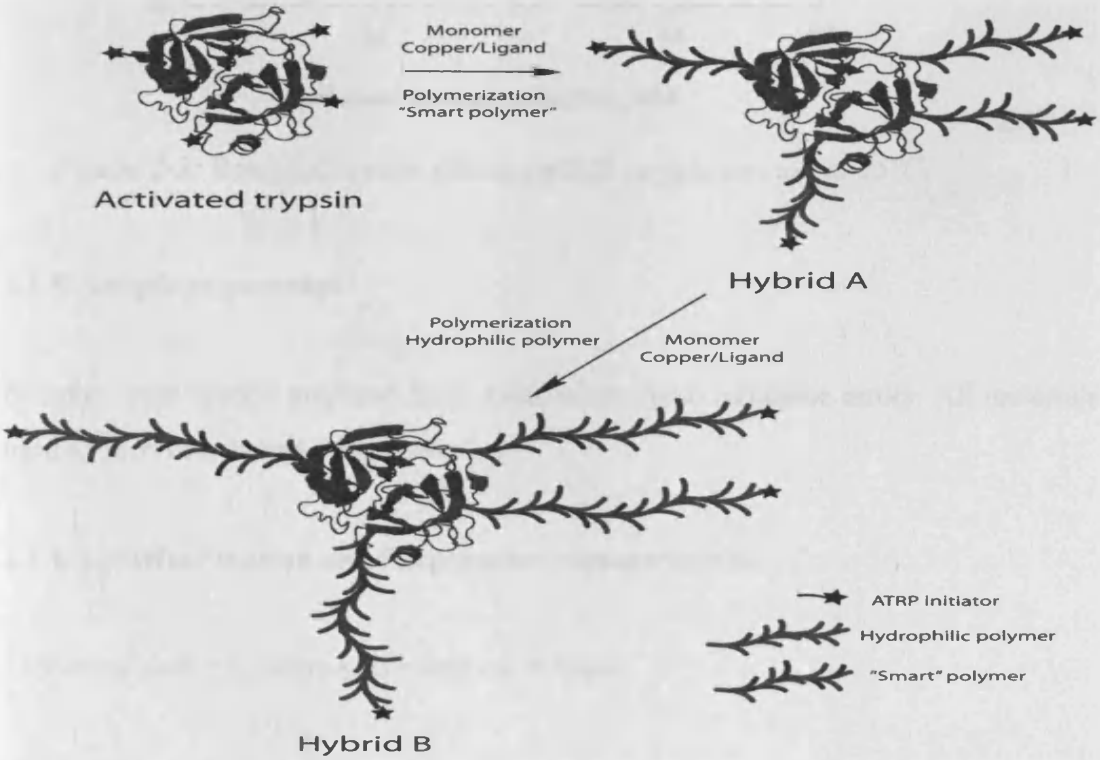

Scheme 2-2: *Polymerization and schematic of trypsin conjugate to synthesize a statistical "smart" hybrid (trypsin-hybrid A) a triblock (trypsin-hybrid B). Scheme adapted from Yasayan et al. Ref. [5]*

2.1.5. Purification of sodium dodecyl sulfate (SDS)

Sodium dodecyl sulfate was purified by four times recrystallization in absolute ethanol to remove the impurities present, as these can noticeably affect the surface tension data obtained (Figure 2-3). (N.B. black lines added to this data to highlight the change in surface tension.

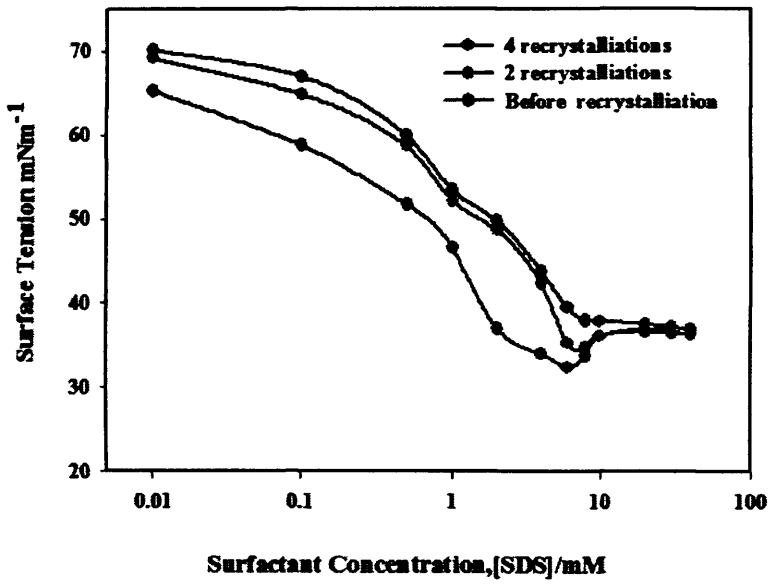

Figure 2-3: Recrystallization *effects on SDS surface tension at 25°C.*

2.1.6. Sample preparation

Samples were always prepared from stock solutions to minimise errors. All materials used as received, except where stated.

2.1.6.1. Surface tension and fluorescence measurements

1) Sodium dodecyl sulfate SDS solutions (Chapter 4)

First, stock sodium dodecyl sulfate SDS solutions were prepared by dissolving the appropriate mass of SDS in distilled water or ethanol mixtures, to produce a total SDS concentration of 50mM. Serial dilutions were prepared to obtain different SDS concentrations ranging from 0.01mM to 40mM, on a 3.0mL a scale.

2) Pluronic P123 solutions (Chapter 4)

Pluronic P123 stock solutions were prepared by dissolving the appropriate mass of P123 in distilled water or ethanol mixtures, to produce a total P123 concentration of 2.0wt%. Serial dilutions were prepared to obtain different P123 concentration ranging from $5.0e^{-5}$ to 1wt %, on a 3.0mL a scale.

3) Pluronic P123 with SDS solutions (Chapter 4)

P123/SDS solutions were prepared by dissolving the appropriate masses of P123 and SDS in distilled water or ethanol mixtures to produce a total P123 and SDS concentrations of 0.2wt % (fixed) and 50mM of SDS respectively. Serial sample dilutions were prepared to obtain 0.2wt % P123 with different SDS concentration ranging from 0.01mM to 40mM on a 3.0mL a scale.

For fluorescence measurements, 8-anilino-1-naphthalene sulfonic acid (ANS) was used as a probe. This was prepared by dissolving 5.98mg (20μm) in 1mL acetone and transferring this to a 1000 ml volumetric flask, removing the acetone and adding water and covered by aluminium foil. This stock solution was then used to prepare the appropriate concentrations of SDS, P123 and P123 with SDS, following the procedure employed to prepare the surface tension measurement samples.

2.1.6.2. Viscosity measurements

1) Pluronic P123 solutions (Chapter 4)

First, a stock P123 solution was prepared by dissolving the appropriate mass of P123 in distilled water or ethanol mixtures, to produce a total P123 concentration of 10wt% P123. Serial dilutions were made to obtain different P123 concentrations, ranging from 0.5 to 10wt %, on a 15mL a scale.

2) Pluronic P123 with SDS solutions (Chapter 4)

P123/SDS solutions were prepared by dissolving the appropriate masses of P123 and SDS in distilled water or ethanol mixtures to produce a total P123 concentration of 1.0wt % (fixed). Serial dilutions were made with a 1.0wt % P123/SDS solution to obtain a fixed 1.0wt % P123 concentration with different SDS concentration ranging from 0.01mM to 100mM, on a 15mL a scale.

2.1.6.3. PGSE-NMR measurements

1) Pluronic P123 (Chapter 4)

First, a stock P123 solution was prepared by dissolving the appropriate mass of P123 in deuterium oxide or ethanol mixtures, to produce a total P123 concentration of 10wt % P123 in 10mL (1.0g/10ml). Serial dilutions were made to obtain different P123 concentrations, ranging from 0.05 to 5.0wt %, on a 1.0mL a scale.

2) Pluronic P123 with SDS solutions (Chapter 4)

P123/SDS solutions were prepared by dissolving the appropriate mass of P123/SDS in deuterium oxide or ethanol mixtures to produce a total P123 and SDS concentrations. Serial sample dilutions were made with 5.0wt % a P123/SDS solution to obtain a fixed 5.0wt % P123 concentration with different SDS concentration ranging from 10 to 100mM, on a 1.0mL a scale.

3) Pluronic P123 solutions (Chapter 5)

15 samples comparing 1.0, 5.0, 10, 15 and 20(w/w) % P123 in 0, 8 and 15(w/w) % ethanol/D_2O mixtures respectively and in d_6-ethanol were prepared on a 4.0g scale. Vials were placed on a roller mixed for 24 hours in order for the P123 to dissolve and the samples to equilibrate.

4) Hybrid polymers and their conjugated with trypsin (Chapter 6)

a) Trypsin in phosphate buffer solution, PBS (8.3mmol/l, pH 7.2). 10ml of PBS was prepared in D_2O, into which was dissolved of 10mg trypsin.

b) Copolymer P6 was prepared at a concentration of 10mg/ml P6 in D_2O and P6 with salt (Na_2SO_4) prepared 0.3M Na_2SO_4 (42.6mg/mL),10mg of P6 dissolved in 1.0ml 0.3M Na_2SO_4/D_2O in NMR tube.

c) Copolymer P7 was prepared at a concentration of 5mg/0.5ml P7 in D_2O and P7 with salt (Na_2SO_4) prepared 0.3M Na_2SO_4 (42.6mg/mL),5mg of P7 dissolved in 0.5ml 0.3M Na_2SO_4/D_2O in NMR tube.

d) Conjugate P6-trypsin was prepared at a concentration of 10mg/1.0ml in PBS/D_2O in a NMR tube.

2.1.6.4. SANS measurements

1) Pluronic P123 solutions (Chapter 4)

a) Prepared 0.2 wt% P123 in D_2O.

b) Prepared four samples of 0.2 wt% P123 with 0.5 and 5.0mM hydrogenation and deuterated respectively in D_2O.

c) Prepared 5.0 wt% P123 in D_2O (0.25g in 5ml), 5.0 wt% P123 in 15 wt% d-ethanol/D_2O (0.25g in 5.0ml) and 5.0 wt% P123 in 0, 8 and 15 wt% d-ethanol/D_2O (0.25g in 5.0ml).

d) Prepared four samples of 5.0 wt% P123 in 15 wt% h-ethanol, in 15 wt% d-ethanol, in (10 wt% h-ethanol + 5.0 wt% d-ethanol) and in (5.0 wt% h-ethanol + 10 wt% d-ethanol) in D_2O.

e) Prepared 5.0 wt% P123 with 50mM d-SDS (0.25g P123, 72.1mg SDS in 5.0ml) in 0, 8 and 15 wt% ethanol in D_2O.

2) Pluronic P123 solutions (Chapter 5)

a) Prepared 12 samples comparing 10, 20, and 30 wt% P123 in 0, 8 and 15 wt% ethanol/D_2O mixtures, respectively and in d6-ethanol were prepared on a 1.0g scale. Vials were placed on a roller mixed for 24 hour in order for the P123 to dissolve and the samples to equilibrate.

b) Prepared 12 samples of 30 wt% P123 comparing with 5.0, 10, 20, and 25 wt% SDS in 0, 8, and 15 wt% ethanol/D_2O mixtures, respectively were prepared on a 2.0g scale. Vials were placed on a roller mixed for 24 hour in order for the P123/SDS to dissolve and the samples to equilibrate.

3) Hybrid polymers (P6 and P7) and their conjugated with trypsin (Chapter 6)

a) Trypsin was prepared at a concentration of 10mg/1.0ml in D_2O in a glass vial.

b) P6 was prepared at a concentration of 10mg/1.0ml P6 in D_2O and P6 with salt (Na_2SO_4) prepared 0.3M Na_2SO_4 (42.6mg/mL),10mg of P6 dissolved in 1ml 0.3M Na_2SO_4/D_2O in a glass vial.

c) P7 was prepared at a concentration of 10mg/1.0ml P7 in D_2O and P7 with salt (Na_2SO_4) prepared 0.3M Na_2SO_4 (42.6mg/mL), 10mg of P7 dissolved in 1.0ml 0.3M Na_2SO_4 in a glass vial.

d) Conjugate P6-trypsin (hybrid A) was prepared at a concentration of 10mg/1.0ml in D_2O in a NMR tube.

e) Conjugate P7-trypsin (hybrid B) was prepared at a concentration of 10mg/1.0ml in D_2O in a NMR tube.

2.2. Analytical instruments

2.2.1. Surface tension

There are many methods for measuring surface tension; in this study we will use a maximum bubble pressure method.

2.2.1.1. Maximum bubble pressure method

The maximum bubble pressure method is a convenient approach to measure the dynamic surface tension. In this method gas bubbles are produced in the sample liquid at an exactly defined bubble generation rate. The gas bubbles enter the liquid through a capillary whose radius is known. During this process, (Figure 2-4) the pressure rises to a maximum pressure. Here the bubble has smallest radius equal to the radius of capillary and forms hemisphere. Beyond this point, the size of the bubble increases exponentially with time and the pressure inside the bubble decreases. Finally the bubble is removed from the capillary and movements to the surface and the cycle begins again with the formation of the next bubble.

The maximum pressure reached is proportional to the surface tension; the pressure is converted into surface tension by Laplace's relation [6]:

$$\sigma = \left(\frac{P_{max} - P_0}{2} \right) R \qquad (2.1)$$

where σ is the surface tension, P_{max} is the maximum pressure reached, P_0 is the hydrostatic pressure at the tip of the capillary and R is the maximum bubble radius.

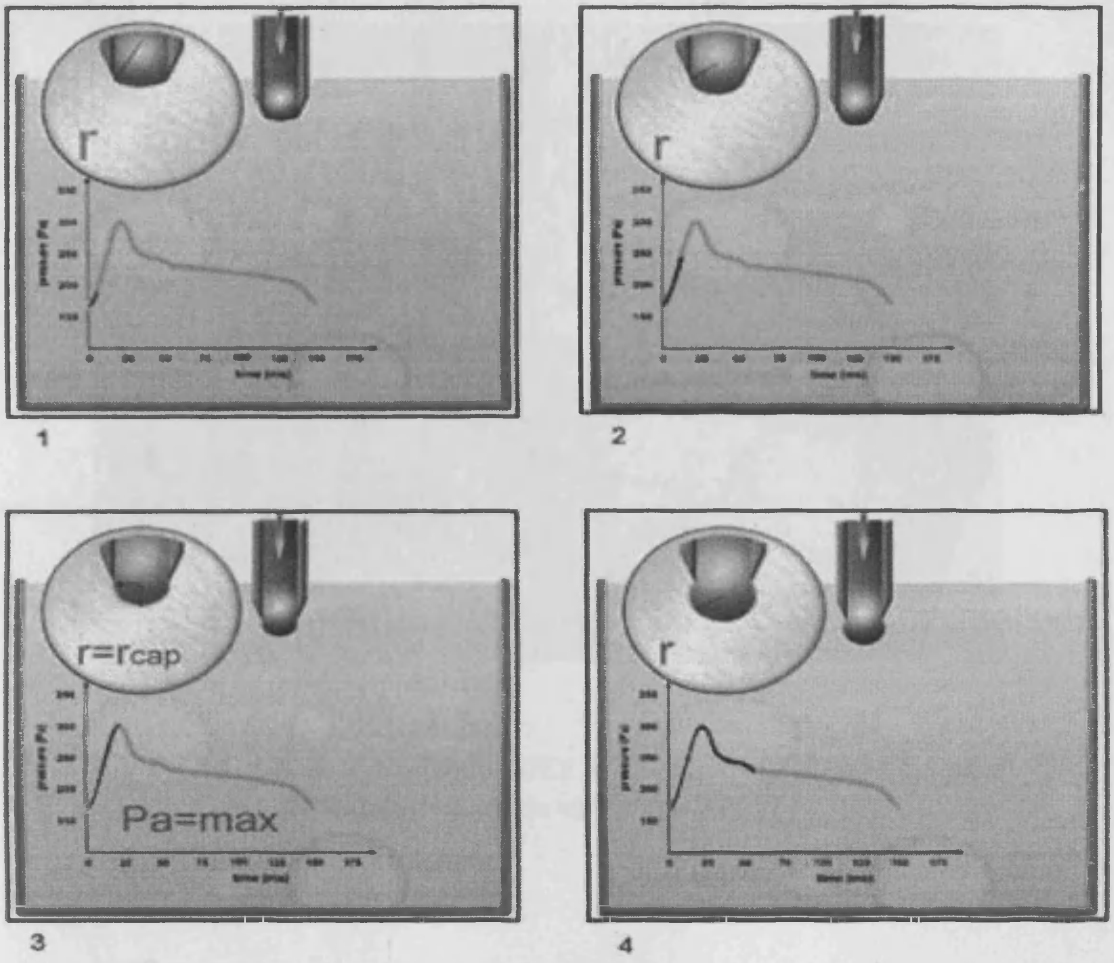

Figure 2-4: *Bubble pressure method. Figure adapted from Ref. [6].*

In this study, we used a simple tensiometer known the SITA science line t60 (SITA, Messtechnik GmbH, Germany). This tensiometer has been used to measure the dynamic surface tension, which measured in the range from10 to 100 mN/m, bubble lifetime: controlled range from 30 ms to 60s, measuring temperature range: from 0 to 100°C. (Figure 2-5) [7]. This tensiometer works by measuring the bubble pressure, and it is done by pumping air through a capillary into the liquid to be analysed. The surface tensions (γ) for all samples were recorded as a function of bubble lifetime, to the maximum value accessible on this instrument, 30s. It was found that γ was within experimental error, constant for bubble lifetime longer than 10s, for all bar the lowest [SDS] systems, all values recorded at 10s in this study (Figure 2-6).

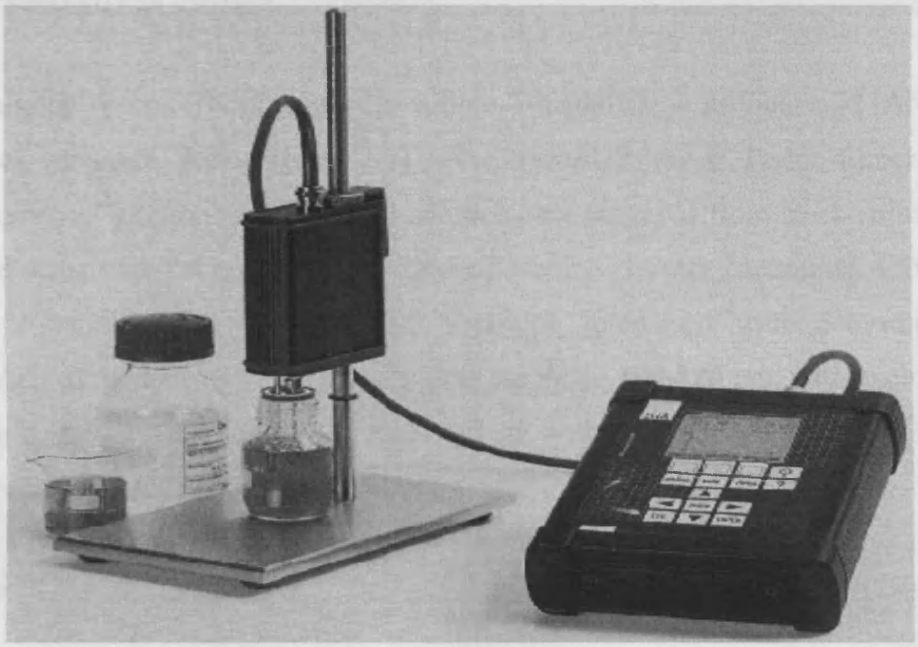

Figure 2-5: *Online Tensiometer SITA Science line t60. Figure adapted from online-tensiometer website Ref. [6].*

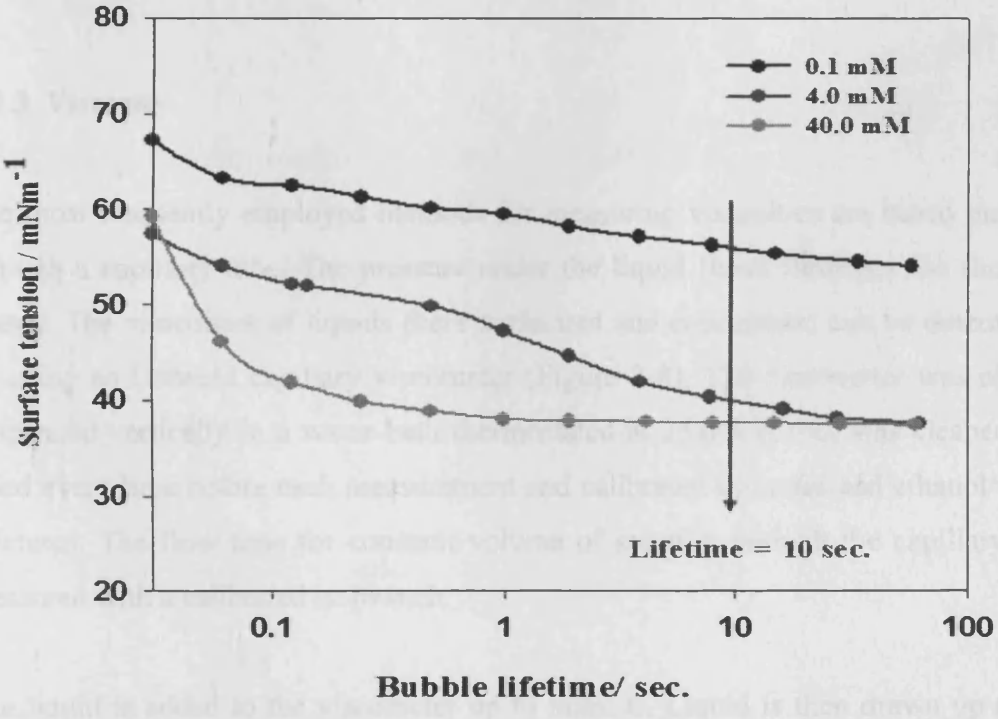

Figure 2-6: *Surface tension vs. bubble lifetime of sodium dodecyl sulfate in H_2O at 25°C.*

2.2.2. Fluorescence Spectra

All emission spectra from the probe 8-anilino-1-naphthalene sulfonic acid (ANS) and chemical structure see (Figure 2-7) were recorded on a Perkin-Elmer LB50 Luminescence spectrophotometer. All solutions are prepared from stock solutions of distilled water with the appropriate volume of acetone (1.0ml), containing ANS probe at the a concentration of $2x10^{-5}$ M. Emission intensities were determined by integration of the fluorescence intensity over the range 490-520 nm, with excitation at 320 nm using a scan speed of 240 nm/s and slit widths of 5.0 nm, were obtained on samples equilibrated at room temperature.

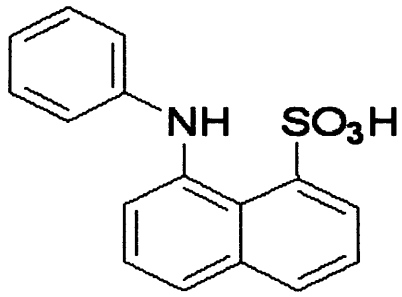

Figure 2-7: *Structure of the fluorescent probe, ANS.*

2.2.3. Viscosity

The most frequently employed methods for measuring viscosities are based on flow through a capillary tube. The pressure under the liquid flows furnishes the shearing stress. The viscosities of liquids (here surfactant and copolymer) can be determined by using an Ostwald capillary viscometer (Figure 2-8). The viscometer was always suspended vertically in a water bath thermostated at 25.0 ± 0.1°C, was cleaned and dried every time before each measurement and calibrated by water and ethanol/water mixtures. The flow time for constant volume of solution through the capillary was measured with a calibrated stopwatch.

The liquid is added to the viscometer up to mark ***C***. Liquid is then drawn up (from right hand side) until the liquid levels are above ***A***. The liquid is then released and the time to pass between the marks ***A*** and ***B*** is measured, (***L*** is the length of the capillary section).

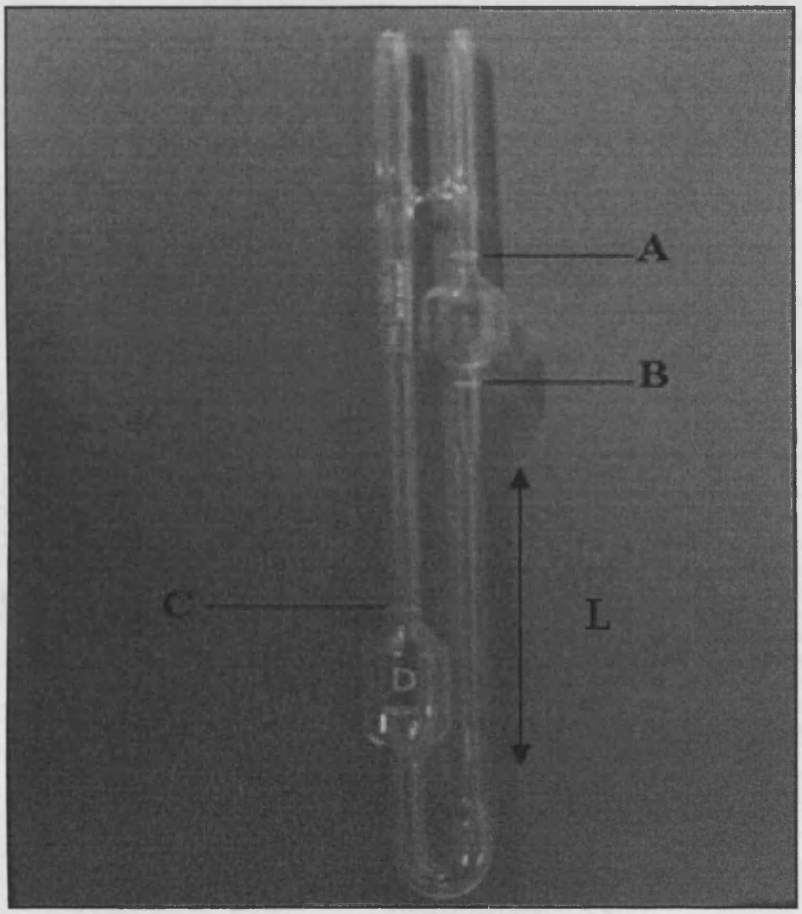

Figure 2-8: The Ostwald viscometer.

2.2.4. Pulsed-Gradient Spin-Echo NMR (PGSE-NMR)

PGSE-NMR measurements were conducted on a Bruker AMX360 NMR spectrometer using a stimulated echo sequence [8]. The self-diffusion coefficient, D_s is extracted by fitting to equation (2.2), the measured peak integral, $A\ (G, \delta)$, as a function of field gradient duration δ and ramp time σ, intensity G, and separation Δ,

$$A(G,\delta) = A_0 \exp\left[-\gamma^2 G^2 \left(\frac{30\Delta(\delta+\sigma)^2 - (10\delta^3 + 30\sigma\delta^2 + 35\sigma^2\delta + 14\sigma^3}{30}\right) D_s\right] \quad (2.2)$$

This simplifies to:

$$A(G,\delta) = A_0 \exp\left[-\kappa D_s\right] \quad (2.3)$$

where γ is the magnetogyric ratio of the nucleus under observation, in this case, protons. The A_0 term is determined by the number of protons in the sample and the exponential term is the attenuation from spin-spin relaxation during the duration of the experiments. Typically values of δ, Δ and σ for the polymer systems studied here are ***d4*** ***(δ)*** = 500μsec, ***d2*** ***(Δ)*** = 400msec and ***G*** = 2 Amps (20%). The gradient intensity ***G*** that is obtained when a current ***(I)*** is passed though the gradient coils is obtained from calibration using a H_2O/D_2O standard with a known diffusion coefficient (Figure 2-9).

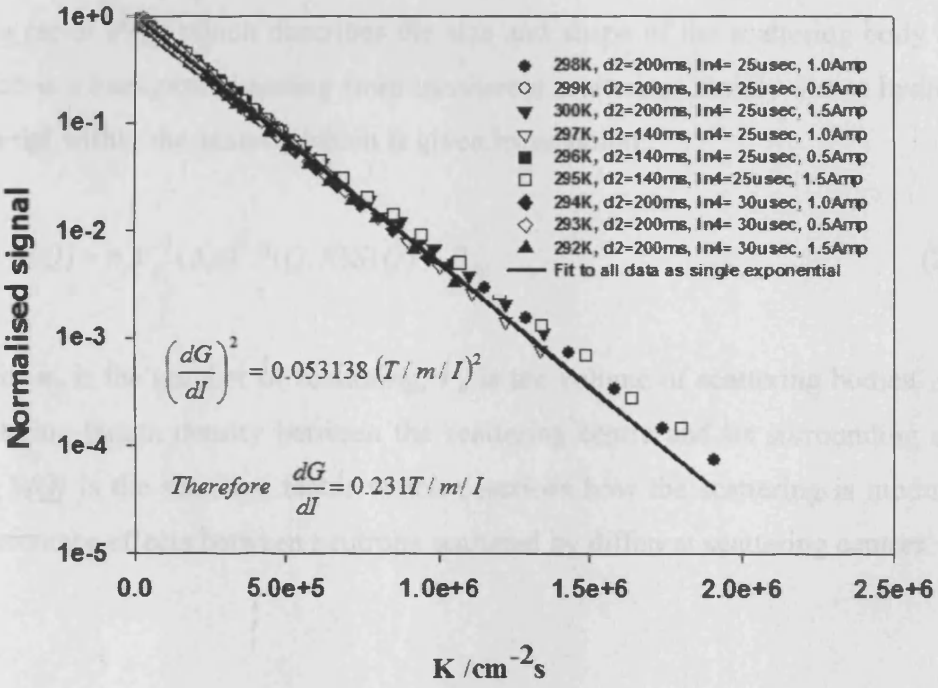

Figure 2-9: *Calibration of gradient coils, H_2O/D_2O at different temperatures.*

2.2.5. Small-angle neutron scattering (SANS)

SANS experiments were performed on the LOQ time-of-flight diffractometer at ISIS (Rutherford Appleton Laboratories, Oxford). Pluronic solutions were prepared in D_2O to achieve the essential contrast and were located in 2-mm pathlength quartz cells, mounted in a motorised thermostated sample changer. Collected data were corrected for the scattering and transmission of the solvent and cell and transformed into an absolute intensity scale with reference to a well-characterized calibrant. Neutron

wavelengths (between 2 and 10 Å) were used to span a Q-range of approximately 0.008-0.3 $Å^{-1}$, where $\boldsymbol{Q}$ is the scattering vector, is given by:

$$Q = \frac{4\pi}{\lambda}\sin(\frac{\theta}{2}) \tag{2.4}$$

where $\boldsymbol{\lambda}$ is the neutron wavelength and $\boldsymbol{\theta}$ is the scattering angle.

The scattering intensity $\boldsymbol{I(Q)}$ is described in terms of the relative contributions of the form factor $\boldsymbol{P(Q)}$ which describes the size and shape of the scattering body and $\boldsymbol{B_{inc}}$ which is a background arising from incoherent scattering, mainly due to hydrogenous material within the sample, which is given by equation:

$$I(Q) = n_p V_p^{\,2} (\Delta\rho)^2 P(Q,R) S(Q) + B_{inc} \tag{2.5}$$

where $\boldsymbol{n_p}$ is the number of scattering, $\boldsymbol{V_p}$ is the volume of scattering bodies, $\boldsymbol{\Delta_\rho}$ is the scattering length density between the scattering centre and its surrounding medium, and $\boldsymbol{S(Q)}$ is the structure factor which describes how the scattering is modulated by interference effects between neutrons scattered by different scattering centres.

2.3. References

[1] L. Zheng, C. Guo, J. Wang, X. F. Liang, S. Chen, J. H. Ma, B. Yang, Y. Y. Jiang, H. Z. Liu, Journal of Physical Chemistry B 111 (2007) 1327-1333.
[2] K. M. Park, J. W. Bae, Y. K. Joung, J. W. Shin, K. D. Park, Colloids and Surfaces B-Biointerfaces 63 (2008) 1-6.
[3] M. Youssry, F. Asaro, L. Coppola, L. Gentile, I. Nicotera, Journal of Colloid and Interface Science 342 (2010) 348-353.
[4] J. P. Magnusson, A. Khan, G. Pasparakis, A. O. Saeed, W. X. Wang, C. Alexander, Journal of the American Chemical Society 130 (2008) 10852-10853.
[5] G. Yasayan, A. O. Saeed, F. Fernandez-Trillo, S. Allen, M. C. Davies, A. Jangher, A. Paul, K. J. Thurecht, S. M. King, R. Schweins, P. C. Griffiths, J. P. Magnusson, C. Alexander., Polymer Chemistry 7 (2011) 1567-1578.
[6] www.Kruss.de/.../bubble.pressure.method.html, 2010.
[7] www.online-tensiometer.com/produkte/t60/science, 2010.
[8] J. A. Davies, P. C. Griffiths, Macromolecules 36 (2003) 950-952.

Chapter 3: Experimental Approaches

3. Introduction

Several techniques have been employed in this study to characterise certain facets of the systems. Therefore, in this chapter these techniques will be described in detail; for example, surface tension measurement of CMC, fluorescence to measure changes in the structure of the palisade layer by using the probe 8-anilino-1-napthalene sulfonic acid (ANS), viscosity measurements to investigate the macroscopic changes in the polymer conformation, pulsed-gradient spin-echo NMR (PGSE-NMR) to quantify the binding of polymer to surfactant and small-angle neutron scattering (SANS) to probe the radii of gyration of polymer, the size and shape of the polymer-bound micelles. Moreover, we have used the last two techniques (PGSE-NMR and SANS) to measure polymer conformation too.

3.1. Surface Tension

A wide range of tensiometer has been developed to determine surface tension; these instruments can determine both static and dynamic surface tension. Static surface measurements are generally defined as those made a long time after the formation of the surface, when the system has attained an equilibrium state. Dynamic tension measurements determine how the surface tension changes over time periods of a fraction of a second to tens of seconds and such systems may be far from the equilibrium state.

Basically, the molecules at the surface of a liquid do not behave in a similar way to the molecules within the bulk of the solution. The molecules which are located in bulk of a liquid are balanced by to equal forces of attraction in all directions, whereas those located at a liquid/air interface are lacking in one direction due to the unbalanced attractive forces [1] (Figure 3-1).

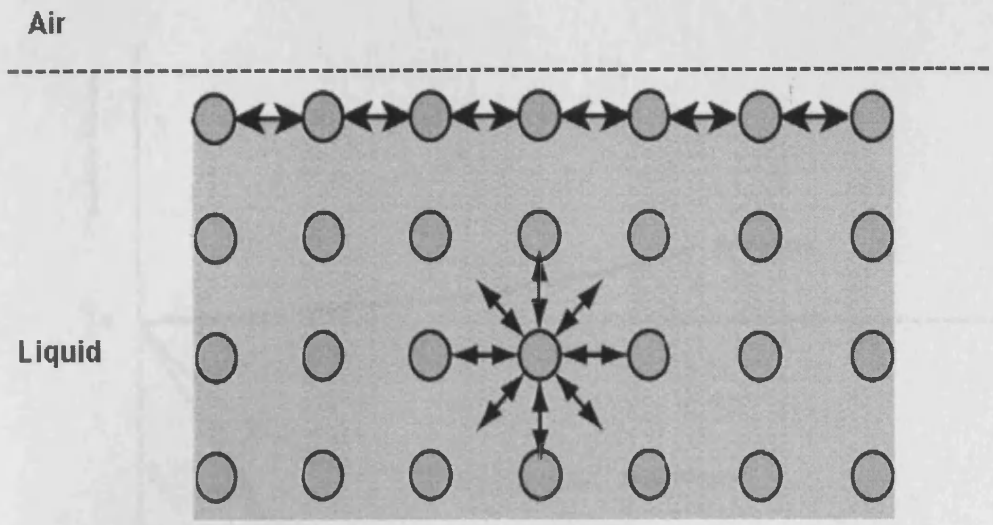

Figure 3-1: Attractive forces on a molecule in bulk and the surface at an liquid/air interface . *Figure adapted from Ref. [1].*

The surface tension depends on the nature of the two substances between which the surface is formed. Polar liquids, such as water, have strong intermolecular interactions and thus high surface tension (72.2 mNm^{-1}). Any factor which decreases the strength of this interaction will lower surface tension. Therefore, an increase in the temperature and concentration of this system will lower the surface tension.

3.1.1. Solutes affect surface tension

Solutes affect the surface tension in three broad ways (Figure 3-2), Electrolytes that dissolve and completely dissociate can raise the surface tension by modest amounts, because they have strong attractions with the solvent. Simple organic water-soluble materials, such as ethanol, normally decrease the surface tension with increasing concentration. This is due to a special adsorption of the organic molecules at the liquid/air interface. Surfactants show a very large reduction in surface tension at very law concentrations. Upon increasing the concentration of a pure surfactant, the surface tension decreases rapidly until a point at which it levels off and becomes almost independent of concentration due to saturation of the surfactant in the surface.

This point is known critical micelle concentration (CMC). At concentration higher than the CMC all additional surfactant will form new micelles, hence, the surface tension will not change with surfactant concentration above the CMC [2].

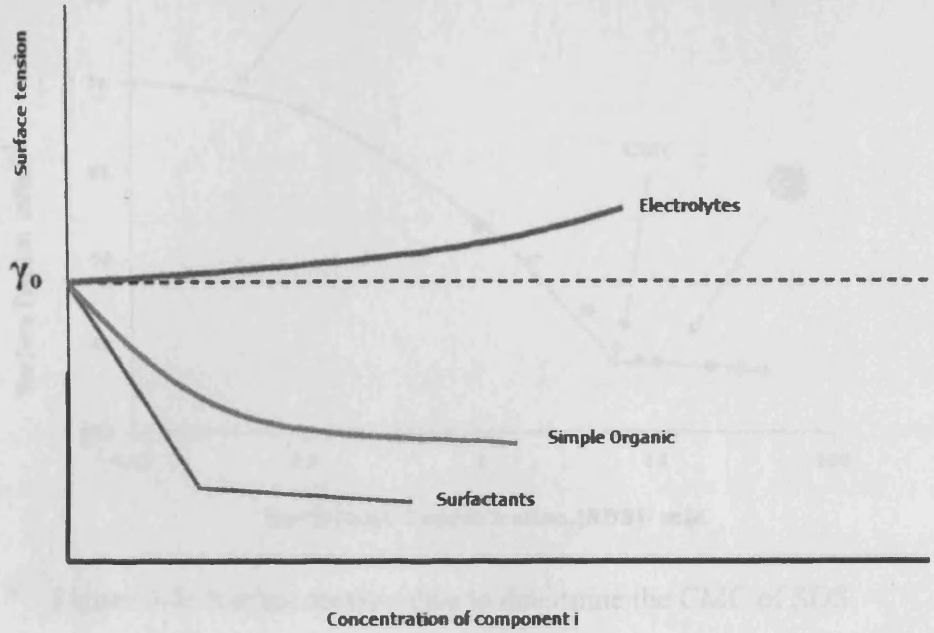

Figure 3-2: *Variation of surface tension in aqueous systems with added component. Figure adapted from Jonsson et al. Ref. [2].*

3.1.2. Surface tension measurement on micellar systems

Surfactants or polymers when dissolved in a liquid, can achieve a separation of nonpolar segments from the solvent if it is hydrophilic or a separation of polar segments if the solvent is hydrophobic. The process of self-aggregation is called micellization, micelles are any solvent soluble aggregates formed spontaneously from amphiphilic molecules. The concentration of the surfactants or polymers at which molecules aggregate is called the CMC. Increasing the concentration further than the CMC of the surfactant may result in other structures which known as Lyotropic Liquid Crystalline, LLC, such as cubic or hexagonal phases. Surface tension techniques can be used to characterize micellar systems, especially CMC of surfactants. Equilibrium surface tension-concentration such as in Figure 3-3 can be analysed using polynomial and straight-line equations, corresponding, respectively, to descending and the horizontal part of the curve [3].

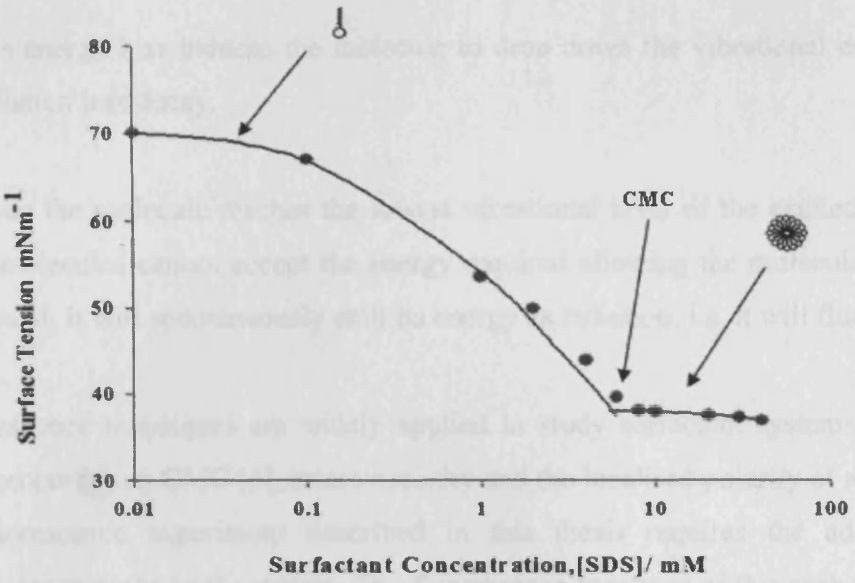

Figure 3-3: Surface tension data to determine the CMC of SDS.

3.2. Fluorescence

Fluorescence is the emission of light by a substance that has absorbed light or other electromagnetic radiation of a different wavelength. In most cases, emitted light has a longer wavelength, and therefore lower energy, than the absorbed radiation. However, when the absorbed electromagnetic radiation is intense, it is possible for one electron to absorb two photons; this two-photon absorption can lead to emission of radiation having a shorter wavelength than the absorbed radiation [4].

3.2.1. Theory of fluorescence spectroscopy

Spectroscopic methods use the characteristic absorption or emission frequencies of molecules to gain extract information on molecular states or environment of irradiated molecules that are used as probes. Therefore, there are four basic steps involved in fluorescence:

1. Initial absorption of radiation, which promotes the molecule to an excited state.

2. The exited molecule then undergoes collisions with other neighbouring molecules and thus loses energy.

3. This energy loss induces the molecule to drop down the vibrational energy levels by radiation less decay.

4. When the molecule reaches the lowest vibrational level of the excited state if the other molecules cannot accept the energy required allowing the molecule to re-enter its ground, it will spontaneously emit its energy as radiation, i.e. it will fluoresce.

Fluorescence techniques are widely applied to study surfactant systems, to analyse such properties as CMC [5], microviscosity and the localised polarity of a system [6]. A fluorescence experiment described in this thesis requires the addition of a fluorescence probe to the system. The fluorescence spectrum of this probe is analysed to give information about the particular characteristic of interest and accordingly specific probes are used for specific experiments e.g. 8-anilino-1-naphthalene sulphonic acid (ANS) is used mainly to investigate surfactant CMC value.

3.2.2. Fluorescent probes and π- π^* transitions

There are some fluorescent probes such as naphthalene and pyrene, that consist mainly conjugated molecules, in which the absorption of radiation by a carbon-carbon double bond causes an electron to be excited from a π orbital to a π^* antibonding orbital. Therefore, it is the carbon-carbon double bond that is performing as the chromophore. A chromophore is a broad term used to explain any chemical group, which gives specific optical absorptions, and hence colour. Unconjugated double bond absorption lies in the UV region. However, if the double bond is in a conjugated environment the π electrons are free to move around the whole molecule and are said to be delocalised. The molecular orbital in a conjugated molecule are closer together than they would be in an un-conjugated molecule and therefore require less energy to complete the transition (Figure 3- 4).

Conjugated chain Unconjugated chain

Figure 3-4: A simple example of a conjugated and an unconjugated system.

3.2.3. ANS (8-anilino-1-naphthalene sulphonic acid)

One such probe employed in this study is ANS (Figure 3-5). This probe is used when studying surfactant systems as its gives information regarding the environment surrounding the probe, hence, the functionality of the probe determines in part its location within the micelle.

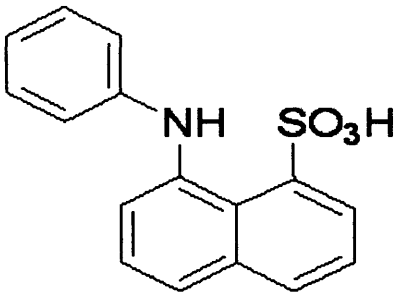

Figure 3-5: Chemical structure of the fluorescent probe, ANS.

ANS is frequently used as a probe in polymer-surfactant systems [7-9], and is known to bind to the region of the micelle occupied by the hydrated head group, the palisade layer. The equilibrated sample is excited at 320nm and the fluorescence emission intensity monitored as a function of surfactant concentration by integration of the intensity between 490-520nm. The spectra obtained display a gradual reduction in the intensity between these values, as the concentration decreases, until a plateau is reached, indicating the CMC of the surfactant, as shown in Figure 3-6.

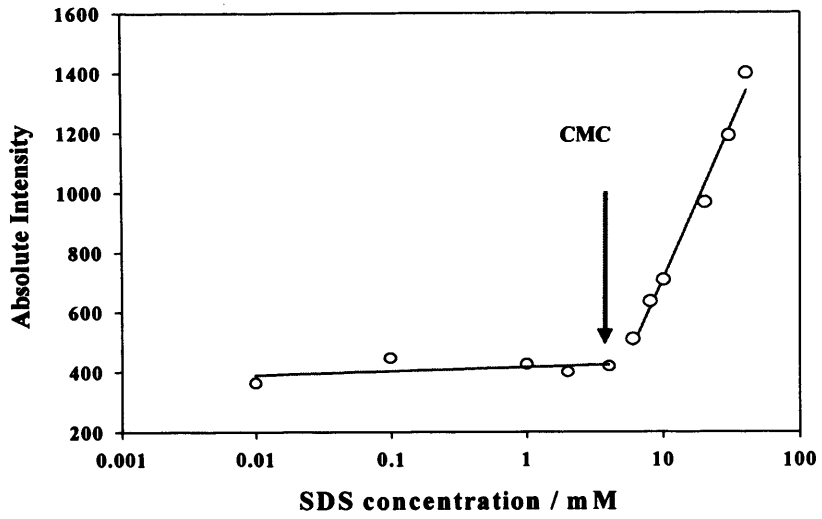

Figure 3-6: *ANS intensity detects the CMC through changes in both ANS partitioning and environment.*

3.2.3.1. ANS in surfactant-polymer systems as a probe

There are a number of studies using fluorescence techniques to probe the polymer-surfactant system, using ANS, as probe [7-9]. The ANS provides a qualitative indication of the polarity in the surrounding environment. Such probes find use in the determination of CAC or CMC by detecting changes in polarity. The fluorescence intensity of ANS increases with increasing hydrophobicity, and thus, the measured fluorescence is an average of the intensity within the polar shell and in the aqueous pseudo phase.

3.3. Viscosity

The viscosity of a liquid is a measure of the internal resistance offered to the relative motion of different parts of the liquid. Polymer dissolved in a liquid, the solvent and solute are very different in size. Therefore, the frictional properties of the solvent in the solution are significantly changed, and an increase in viscosity occurs, reflecting the size and shape of the dissolved solute, even in dilute solution. This was observed in 1930 by Staudinger who found that an empirical relationship existed between the relative magnitude of the increase in viscosity and the molar mass of polymer [10].

There are various measures of viscosity. The list below gives the common nomenclature used in solution viscosity;

1) Relative viscosity:

$$\eta_{rel} = \frac{\eta}{\eta_0} = \frac{t}{t_0} \tag{3.1}$$

where; η_0 is the solvent viscosity and t_0 is the time of flow of the solvent.

2) Specific viscosity:

$$\eta_{sp} = \frac{\eta - \eta_0}{\eta_0} = \frac{t - t_0}{t_0} = \eta_{rel} - 1 \tag{3.2}$$

3) Reduced viscosity:

$$\eta_{red} = \frac{\eta_{sp}}{c} \tag{3.3}$$

4) Inherent viscosity:

$$\eta_{inh} = \ln\left(\frac{\eta_{rel}}{c}\right) \tag{3.4}$$

5) Intrinsic viscosity:

$$[\eta] = \ln\left(\frac{\eta_{sp}}{c}\right)_{c=0} = \left(\frac{\eta_{rel}}{c}\right)_{c=0} \tag{3.5}$$

In dilute solution, molecular interference is expected to occur and η_{sp} is extrapolated to zero concentration to obtain a measure of the influence of an isolated polymer coil. This is carried out in one of two ways: (i) η_{sp} can be expressed as a reduced quantity (η_{sp}/c) and extrapolated to $c = 0$ according to the relation:

$$(\eta_{sp}/c) = [\eta] + \kappa'[\eta]^2 c \tag{3.6}$$

where; the intercept is the limiting viscosity number ***[η]***, a characteristic parameter for the polymer in a particular solvent and κ' is a shape dependent factor called the Huggins constant or (ii) extrapolating the inherent viscosity as:

$$(\log \eta_{rel} / c) = [\eta] + \kappa''[\eta]^2 c \qquad (3.7)$$

where; κ'' is another shape dependent factor.

For a given polymer-solvent system at a specified temperature, ***[η]*** can be related to molecular weight ***M*** through the Mark-Houwink equation [2]:

$$[\eta] = K_v M^v \qquad (3.8)$$

where K_v and v can be established by calibrating with polymer fractions of narrow known molar mass and once this has been quantified for a system, ***[η]*** alone will give ***M*** for an unknown fraction.

3.4. Pulsed-gradient spin-echo NMR (PGSE-NMR)

3.4.1. Introduction

Nuclear magnetic resonance, NMR is a technique which has been used throughout this study, in confirming chemical structures and observing interactions between molecules. NMR is a valuable technique which has found a huge range of applications in chemistry, physics, biology and medicine. The common encountered elements possessing a magnetic moment used for NMR spectroscopy are ^{1}H and ^{13}C nuclei which are found in the most surfactant molecules; in addition ^{2}H is present in selectively deuterated surfactant and ^{19}F found in fluorocarbon surfactant.

Pulsed-gradient spin-echo NMR, PGSE-NMR is an example of one of many NMR techniques; owing to its non-invasive nature and wide applicability, it has become the method of choice for measuring self-diffusion coefficients in solution state. Like all nuclear magnetic resonance techniques, it possesses a numbers of advantages when applied to multi-component systems; it is non-invasive, non-destructive but most importantly, the chemical specificity of NMR enables the behaviour of each

component within the mixture to be identified and analysed in a single experiment. PGSE-NMR [11, 12] sometimes referred as Pulsed Field-Gradient Spin-Echo, (PFGSE-NMR) has been reviewed previously in the context of polymer solutions [13], self-associating and supramolecular systems [14].

3.4.2. Self-diffusion coefficient

Self-diffusion is the random translational diffusive motion of molecules driven by internal kinetic energy. Translational diffusion also known as self-diffusion coefficients is the most fundamental from of transport [15] and is responsible for all chemical reactions, since the reacting species must collide before they can react. Therefore, the self-diffusion coefficient is one of the most fundamental and important physicochemical quantities and provides information on dynamic aspects of the liquid state.

The measurement of self-diffusion coefficients is extremely valuable in the study of multi-component systems, as correlation between diffusion rates is a good indicator that two molecules are interacting in solution.

The self-diffusion coefficient, D_s, of a particle in solution is described by the Stokes-Einstein equation [16, 17] :

$$D_s = \frac{\kappa_B T}{f} \qquad (3.9)$$

where; κ_B is the Boltzmann constant, T the absolute temperature, and f is the friction coefficient. For the simple case of a spherical particle with an effective hydrodynamic radius (Stokes radius) R_h in a solution of viscosity η the friction factor is given below.

$$f = 6\pi\eta R_h \qquad (3.10)$$

Then we can rewrite equation (3.9);

$$D_s = \frac{\kappa_B T}{6\pi\eta R_h} \qquad (3.11)$$

3.4.3. The nuclear spin-echo method

The simplest pulsed-gradient spin-echo sequence, which is based upon the Stejskal and Tanner sequence in 1965 [18] (Figure 3-7). Basically, in PGSE-NMR experiment the attenuation of a spin-echo signal after two pluses have been applied. The first $\pi/2$ (90°) pulse is applied to the sample along x-axis and the net magnetization is tipped into x-y plane [17, 19]. A second pulse π (180°) is then applied after τ, if the spins have not diffused they will be refocused by the 180° pulse and attenuation of the signal which is proportional to the displacement of the nuclei [20].

For a single diffusing species the normalized signal attenuation, E, is related to experimental parameters and the self-diffusion coefficient, D_s as below.

$$E = \frac{S(g)}{S(0)} \exp[-\gamma^2 g^2 \delta^2 (\Delta - \delta/3)] \qquad (3.12)$$

where; $S(0)$ is the signal in the absence of the gradient pulses, γ is the gyromagnetic ratio, g is the magnitude, δ is the duration of the gradient pulses, and Δ is the separation between the leading edges of the gradient pulse.

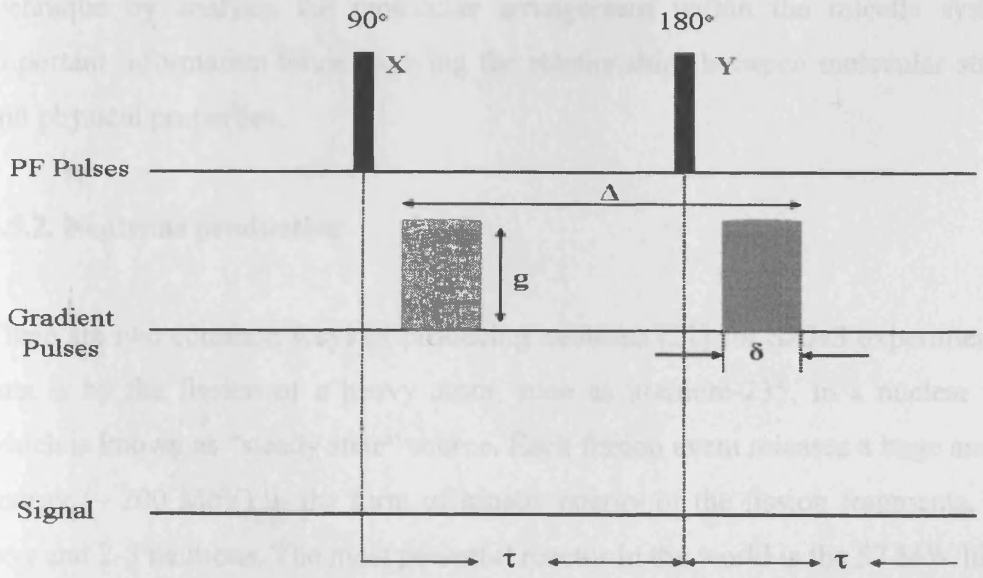

Figure 3-7: The basic Stejskal-Tanner PGSE experiment. Figure adapted from Price et al. Ref. [19].

3.5. Small-angle neutron scattering (SANS)

3.5.1. Introduction

The techniques of small-angle neutron scattering SANS, small-angle X-ray scattering SAXS and small-angle light scattering (SALS) are together given the name small angle scattering "SAS". In the above techniques, the radiation is scattered elastically by a sample and the scattering pattern thus attained is analysed to provide information about the size, shape and orientation of the components of the sample. The main difference between these three techniques is that light and X-ray are both scattered by the electrons surrounding the nucleus of an atom, whereas the neutrons are scattered by the nucleus itself. An electron which is charged is unable to travel a long distance inside a material without being attracted by the nucleus or repelled by the electrons present in the materials. Neutrons, being electrically neutral particles, are capable of penetrating substance to charged particles. However, this technique suffers from weak scattering and low intensities greater degree due to the interaction of neutrons with nucleus.

Owing to neutrons properties above, small-angle neutron scattering is a very powerful technique by analysis the molecular arrangement within the micelle systems is important information when studying the relationships between molecular structures and physical properties.

3.5.2. Neutrons production

There are two common ways of producing neutrons [21] for SANS experiments. The first is by the fission of a heavy atom, such as uranium-235, in a nuclear reactor, which is known as "steady state" source. Each fission event releases a huge amount of energy (~ 200 MeV) in the form of kinetic energy of the fission fragments, gamma rays and 2-3 neutrons. The most powerful reactor in the world is the 57 MW high-flux reactors at the Institute Laue Langevin (ILL) in Grenoble, France [22] (Figure 3-8).

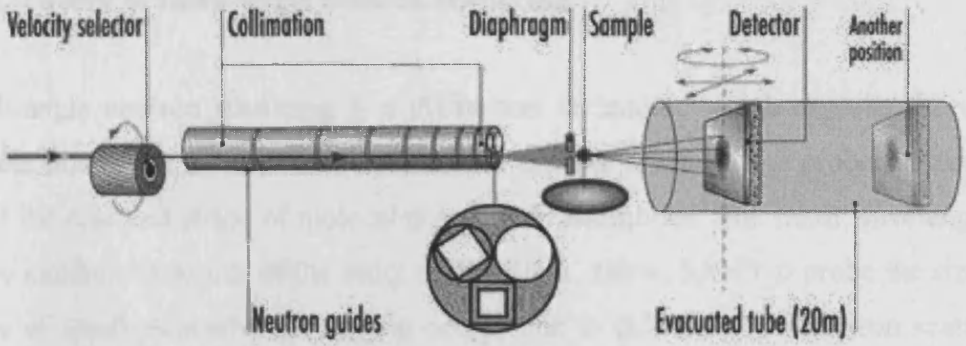

Figure 3-8: Schematic Layout of the D_{22} instrument, ILL reactor source, Grenoble, France. Figure adapted from ILL website Ref [22].

The second way to produce neutrons is by "spallation" and 5 of the 37 sources worldwide use this method [21]. Here, the neutrons are produced by particle accelerators and the extracted proton beam breaks off pieces of a heavy target nucleus resulting in the production of protons and neutrons approximately 15 neutrons per occurrence proton. The most powerful spallation neutron source is ISIS, Didcot, UK [23, 24] Figure 3-9).

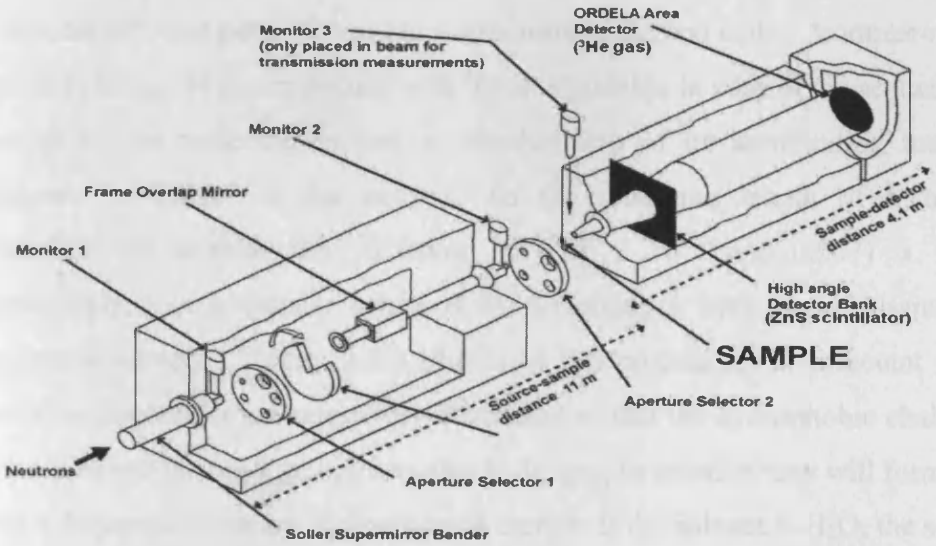

Figure 3-9: Schematic diagram representation the instrument LOQ, ISIS, Didcot, UK. Figure adapted from ISIS website Ref. [24].

3.5.3. Theory of small-angle neutron scattering

Small-angle neutron scattering is a diffraction technique, which exploits the wave-particle duality of a neutron and its unique nuclear properties to probe information about the size and shape of molecules and their assemblies. The small wavelength, λ, of the incident neutrons, of the order of 1 to 10 Å, allow, SANS to probe the size and shape of small structures. Scattering occurs due to differences in neutron scattering length density (***SLD/ ρ***) within the sample, which can readily be calculated from the sample composition and density:

$$\rho = N\sum_i b_i = \frac{\delta N_A}{M}\sum_i b_i \qquad (3.13)$$

where; δ is the bulk density of the molecule ($g.cm^{-3}$), N_A is Avogadro's number ($6.023x10^{-23}$ mol^{-1}), b_i is the coherent neutron scattering length of nucleus i, and M is the molar mass of the sample. ρ has dimensions of $(length)^{-2}$ and units of 10^{-10} cm^{-2} or 10^{-6} $Å^{-2}$.

3.5.4. Contrast matching

One very powerful characteristic of neutron scattering is that it is possible to underline different parts of the systems by using a method called "contrast-matching". By substituting ^1H in a molecule with ^2D, it is possible to control the scattering length density of the molecule so that it matches that of its surrounding medium and becomes "invisible" to the neutron. As the scattering length of hydrogen and deuterium are considerably different, -0.3741 x 10^{-10} and 0.6671 x 10^{-10} cm^{-2} respectively, this is usually achieved by dissolving a hydrogenated sample into a deuterated solvent. Figure (3.10) illustrated this process for a surfactant micelle. If surfactant molecules are selectively deuterated so that the hydrophobic chains contain deuterium and the head groups contains hydrogen, in solution they will form a micelle with a deuterated core and hydrogenated corona. If the solvent is H_2O, the solvent and corona are said to be contrast matched and scattering will be highlighted form the deuterated core (Figure 3.10: a), when dissolved in H_2O the solvent and core are contrast matched and scattering from the corona is highlighted Figure (3.10: b). The

non-deuterated surfactant in D_2O is the "standard" system and scattering from the whole particle is seen (Figure 3.10: c).

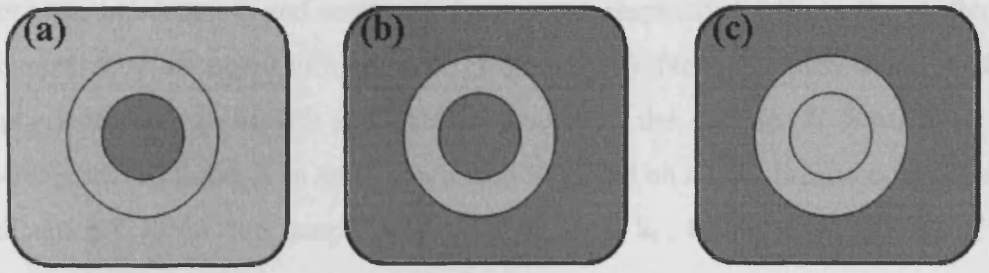

Figure 3-10: *Diagram of a contrast matching experiment for a surfactant micelle :(a) in H_2O scattering from the core is observed,(b) in D_2O the corona is highlighted and (c) The non-deuterated micelle in D_2O shows scattering from the whole particle.*

The contrast term is very useful to the experimentalist as different isotopes have different scattering length densities (ρ). Fortunately, for polymer chemists, the scattering length densities of hydrogen and deuterium exhibit a large difference in their ρ values. The difference is scattering length densities for several common solvents and polymers in their fully hydrogenated and perpetuated forms can be seen in Table 3.1 [25].

Table 3-1: *Various scattering length densities of some common solvents and polymers.*

Solvent	ρ(h-form) ($x10^{10}$ cm^{-2})	ρ(d-form) ($x10^{10}$ cm^{-2})	Polymer	ρ(h-form) ($x10^{10}$ cm^{-2})	ρ(d-form) ($x10^{10}$ cm^{-2})
Water	- 0.56	+ 6.38	**PE**	- 0.33	+ 8.24
Octane	- 0.53	+ 6.43	**PS**	+ 1.42	+ 6.42
Toluene	+ 0.94	+ 5.66	**PEO**	+ 0.64	+ 6.46
Chloroform	+ 2.39	+ 3.16	**PMMA**	+ 1.10	+ 7.22

3.5.5. Scattering vector, Q

The scattering vector, $\boldsymbol{Q}$, also known the wave vector, describes the relationship between the incidents, $\boldsymbol{k_i}$ and scattered, $\boldsymbol{k_s}$ neutrons respectively. Since the scattering is coherent, they are equal in magnitude (Figure 3.10). Neutrons with wavelength, λ are spherically symmetrically scattered by nuclei in the sample. A fraction of the neutrons scattered through an angle θ are then recorded on a two-dimensional detector at a distance $\boldsymbol{L_{sd}}$ from the sample at a radial $\boldsymbol{r_{det}}$, and $\mathbf{k_i}$, $\mathbf{k_s}$ are wave vectors of the incident and scattered neutrons respectively.

The scattering vector, $\boldsymbol{Q}$, described as the change in direction of the neutrons, has the dimensions of inverse length and is normally quoted for neutron scattering in terms of cm^{-1} or $Å^{-1}$, $\boldsymbol{Q}$ is defined as:

$$Q = |\mathrm{Q}| = |k_s - k_i| = \frac{4\pi n}{\lambda}\sin(\frac{\theta}{2}) \approx \frac{4\pi n}{\lambda}\frac{r_{\det}}{L_{sd}} \tag{3.14}$$

where; $\boldsymbol{n}$ is the neutron refractive index may be taken as unity, and θ is the scattering angle. By substituting equation 3.14 into to the Bragg law of diffraction.

$$\lambda = 2d\sin(\frac{\theta}{2}) \tag{3.15}$$

One obtains the very useful expression

$$d = \frac{2\pi}{Q} \tag{3.16}$$

where; $\boldsymbol{d}$ is a molecular-level length scale by virtue of the Q-range accessible in a SANS experiment. In essence, $\boldsymbol{d}$ and $\boldsymbol{Q}$ are inversely related, thus small $\boldsymbol{Q}$ values are requires do investigate the large–scale structure in a sample.

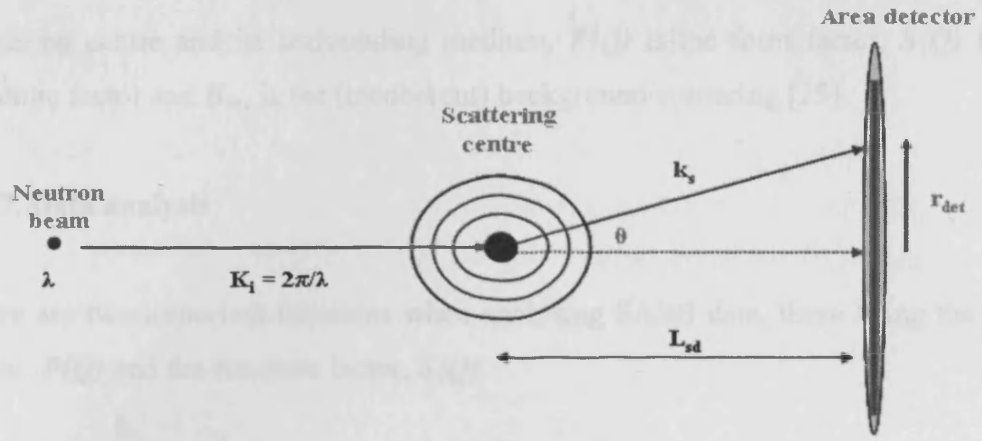

Figure 3-11: Schematic of the scattering vector of the incident and scattered neutrons.

3.5.6. Neutron scattering measurement

In a SANS experiment the scattering intensity, I, is measured as a function of the scattering vector Q. this scattering intensity, I(Q), is not just dependent upon the value of the differential cross section of the particle, but also the neutron flux, I_0; the solid angle element defined by the size of a detector pixel, Ω_0; the detector efficiency, ε; the area of the beam, A; the sample thickness, d_s; the transmission of neutron through the sample, t_s; and the differential cross section, $d\sigma/d\Omega$ [26].

$$I(Q) = I_0 \Omega_0 \varepsilon A d_s t_s \left(\frac{d\sigma}{d\Omega}\right)(Q) \qquad (3.17)$$

It is the differential cross-section that contains characteristic such as particle size, shape, and the position of the scattering bodies within the system. The differential cross-section is given below.

$$\frac{\partial \Sigma}{\partial \Omega}(Q) = N_p V_p^{\,2} (\Delta\rho)^2 P(Q) S(Q) + B_{inc} \qquad (3.18)$$

where N_p is the number concentration of scattering centres, V_p is the volume of one the scattering centre, $(\Delta\rho)$ is the contrast in scattering length density between the

scattering centre and its surrounding medium, ***P(Q)*** is the form factor, ***S(Q)*** is the structure factor and B_{inc} is the (incoherent) background scattering [25].

3.5.7. Data analysis

There are two important functions when analysing SANS data, these being the form factor, ***P(Q)*** and the structure factor, ***S(Q)***.

3.5.7.1. Form factor, P(Q)

The form factor or shape factor is a mathematical function from which information on the size and shape of the particles can be obtained. Expressions for the form factor are known for a range of different shapes including homogeneous spheres, spherical shells, polyelectrolytes, Gaussian coils and cylinders or rods. In this study, a number of P(Q) were used, and each discussed in the relevant chapter e.g. Chapters 4 and 5 Pedersen and Chapter 6 Gaussian coil [27].

Therefore, its value is highly dependent upon the size and shape of the scattering centre and expression exist describing for factors common shapes, some of which are shown in Table 3.2.

Table 3-2: *Form factor expressions for spheres, discs and a Gaussian coil.*

Description	**Analytical expression**
Sphere of radius R	$P(Q) = \left[\frac{3\{Sin\ (QR) - QRCos\ (QR)^2\}}{(QR)^3}\right]^2$
Disc of negligible thickness and radius R	$P(Q) = \frac{2}{(QR)^2}\left[1 - \frac{j_1(2QR)}{QR}\right]$
Gaussian coil with radius of gyration Rg	$P(Q) = \frac{2(\exp(-Q^2Rg^2) + Q^2Rg^2 - 1}{(Q^2Rg^2)^2}$

3.5.7.2. Structure factor, S(Q)

The structure factor is a dimensionless function, which describes how the scattering is modulated by inference effects between neutrons scattered from scattering centres. Consequently it is dependent on the degree of local order in the sample and the interaction potential between adjacent scattering centres. The interparticle structure factor is given below.

$$S(Q) = 1 + \frac{4\pi N_p}{QV_s} \int_0^\infty [g(r) - 1] r \sin(Q_r) d_r \qquad (3.19)$$

where; ***r*** is the distance between each nearest-neighbour coordination shell and ***g(r)*** is the radial density distribution function.

3.6. References

[1] http:www.ksvinc.com/surface_tension1.htm, Surface and Interfacial Tension, Langmuir-Blodgett Instruments, Retrieved 2007.
[2] B. Jonsson, B. Lindman, K. Holmberg, B. Kronberg, John Wiley and Sons, Inc., New York, 1998.
[3] G.G. Jayson, G. Thompson, M. Hull, A.L. Smith, R.H. Ottewill, C.H. Rochester, Eds; Academic Press: Paris, 1st Ed, (1983), 129 - 138.
[4] F. James Holler, Douglas A. Skoog, S.R. Crouch, Principles of Instrumental Analysis, 2006.
[5] R. Zana, Surfactant Solution: New Methods of Investigation, M. Dekker, Inc., Chapter 5, 1987.
[6] A. Ito, K. Kamogawa, H. Sakai, K. Hamano, Y. Kondo, N. Yoshino, M. Abe, Langmuir 13 (1997) 2935-2942.
[7] P. C. Griffiths, J. A. Roe, B. L. Bales, A. R. Pitt, A. M. Howe, Langmuir 16 (2000) 8248-8254.
[8] P. C. Griffiths, N. Hirst, A. Paul, S. M. King, R. K. Heenan, R. Farley, Langmuir 20 (2004) 6904-6913.
[9] P. C. Griffiths, P. Stilbs, A. M. Howe, T. H. Whitesides, Langmuir 12 (1996) 5302-5306.
[10] J. M. G. Cowie, Polymer : Chemistry and Physical of Modern Materials, Blackie Academic and Professional, 3 rd Ed., CRC Press, Taylor & Francis Group, 1991.
[11] W. S. Price, Concepts in Magnetic Resonance 9 (1997) 299-336.
[12] W. S. Price, Concepts in Magnetic Resonance 10 (1998) 197-237.
[13] P. Griffiths, P. Stilbs, Current Opinion in Colloid & Interface Science 7 (2002) 249-252.
[14] O. Soderman, U. Olsson, Current Opinion in Colloid & Interface Science 2 (1997) 131-136.
[15] E. Hawlicka, Chemical Society Reviews 24 (1995) 367-&.
[16] H. J. V. Tyrrell, Diffusion in Liquid: A Theoretical and Experimental Study, Butterworths, London, 1984.
[17] P. Stilbs, Progress in Nuclear Magnetic Resonance Spectroscopy 19 (1987) 1-45.
[18] E.O. Stejskal, J.E. Tanner, Journal of Chemical Physics 42 (1965) 288 - 293.
[19] W.S. Price, F. Elwinger, C. Vigouroux, P. Stilbs, Magnetic Resonance in Chemistry 40 (2002) 391-395.
[20] E.O. Stejskal, Journal of Chemical Physics 43 (1965) 3597- 3603.
[21] R.K. Heenan, J. Penfold, S.M. King, Journal of Applied Crystallography 30 (1997) 1140-1147.
[22] ILL world wide web page: www.ill.fr, 2010.
[23] J. Eastoe, Small-Angle Neutron Scattering and Neutron Reflection, Chapter 12, University of Bristol, UK, 2000.
[24] ISIS web site, www.isis.rl.ac.UK, 2010.
[25] S. M. King, Small Angle Neutron Scattering. ISIS Report, Large-Scale Structure Group, 1995.
[26] C. E. Williams, in X-ray Characterisation of Materials, ed. E. Lifshin, Wiley-VCH, Toronto, 1999, p 212-254.
[27] R. K. Heenan, Fish, Rutherford Appleton Laboratory, Didcot, UK.

Chapter 4: Cosolvent effects on Polymer and Surfactant Systems

4. Context

The association of Pluronic triblock copolymers PEO-PPO-PEO and the anionic surfactant sodium dodecyl sulfate (SDS) has been examined using several methods, such as fluorescence spectroscopy, nuclear magnetic resonance, dynamic light scattering and isothermal titration calorimetry. One of the important findings from these studies shows that, depending on their concentration and temperature, interactions between these materials lead to formation of mixed micelles [1, 2].

In this current study, we have studied the effect of the cosolvent ethanol on the competitive interaction between SDS and the Pluronic P123 $(PEO)_{20}$-$(PPO)_{70}$-$(PEO)_{20}$, using surface tension, fluorescence, viscosity, PGSE-NMR and SANS. In this chapter, the experimental data for each experimental method will be first presented, this significance highlighted, and collectively discussed at the end of the chapter. Inherently, a different Pluronic concentration had to be used for the various techniques, typically; surface tension and fluorescence (0.2 wt%), viscosity (1.0 wt%), PGSE-NMR and SANS (0.2 wt% and 5.0 wt%), and the implications of this are discussed.

4.1. Determination of the CMC by surface tension and ANS fluorescence data

Surface tension is one of the techniques commonly used for the determination of the CMC in micellar solutions. In combination with tensiometry, fluorescence probes such as 8-anilino-1-naphththalene sulfonic acid (ANS) provide a qualitative indication of the polarity of the probe environment and therefore a complimentary measure of the CMC.

4.1.1. An ionic surfactant SDS in ethanol/water mixtures

Figures 4-1 and 4-2 show the combined surface tension and normalised ANS fluorescence intensity behaviour for aqueous solution of SDS as a function of the concentration of added ethanol. In both figures there is clearly only one break in each curve yielding the CMC SDS "(CMC (SDS)". For pure water, the CMC = 8.0mM, in excellent agreement with the literature value [3, 4]. In the presence of 5.0 wt% ethanol the break in surface tension occurs at a lower SDS concentration, CMC = 5.0mM, compared with the water case, confirming that micellization is promoted (the CMC decreases) by this amount of ethanol. The CMC for 10 wt% ethanol was found be 3.5mM. These estimates are in excellent agreement with Griffiths et al. [4] and Safarpour et al. [5]. The reduction in CMC is called the co-surfactant effect.

The measured fluorescence intensity ($I_{measured}$) from ANS in solution may be simply interpreted as a concentration weighted summation of the intensity arising from that fraction of ANS dissolved into the solution phase ($p_{solution}$) and that fraction of ANS solubilised into micelle ($p_{micelle}$), modulated by the environment-specific intensity associated with those two phases, $I_{solution}$ and $I_{micelle}$ respectively:

$$I_{measured} = p_{solution} I_{solution} + p_{micelle} I_{micell\ e} \qquad (4.1)$$

For ease, the intensities stated here have been normalised to account for subtle changes in ANS solubility by:

$$I_{normal}^{ANS} = \frac{I^{ANS}}{I^{ANS}(SDS = 0.01mM)} \qquad (4.2)$$

It is clear that on passing through the CMC for both systems, there is an increase in the intensity, and we may conclude that $p_{solution} I_{solution} < p_{micelle} I_{micelle}$. Further, it is well-known that $I_{micelle} >> I_{solution}$ due to the more hydrophobic and less fluid environment the ANS experiences.

The normalised intensity of ANS in SDS solution in both the absence and presence of ethanol increases significantly above the CMC, but the increase in pure water is much more rapid than the 5.0 wt% ethanol case, reflecting the fact that either the ANS is

reporting a more hydrophobic environment in the water ($I_{solution}$) compared to an ethanol solution or that fewer ANS molecules are solubilised into the micellar phase ($p_{micelle}$) once ethanol is present or their intensity is that phase is reduced ($I_{micelle}$) compared with the micelle in the pure water case, consistent with a smaller aggregation number. However, when compared with the surface tension data, the correspondence between the two CMC estimates is clear.

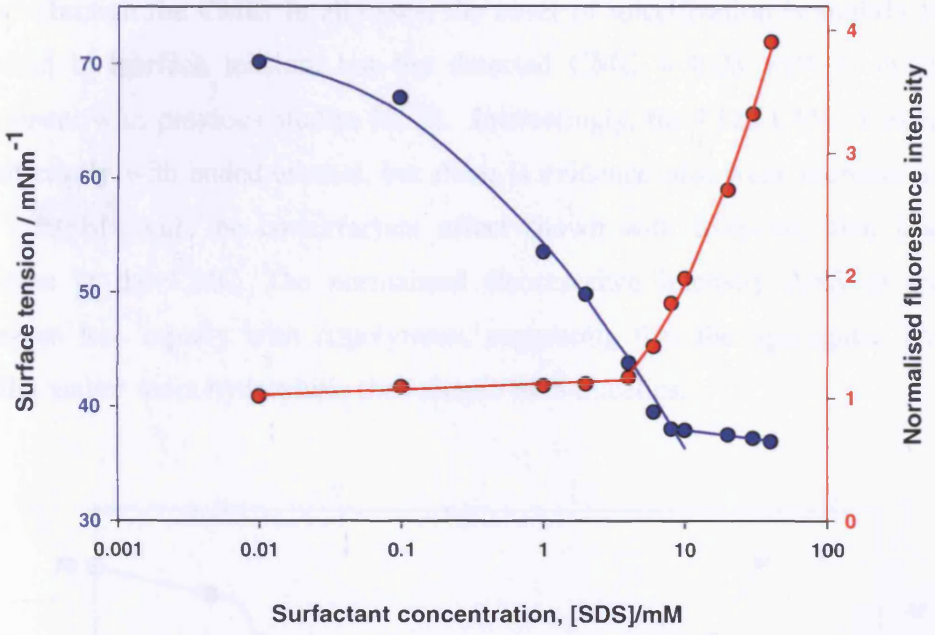

Figure 4-1: Surface tension (blue circles) and fluoresence intensity of ANS (red circles) as a function of SDS concentration in SDS in H_2O.

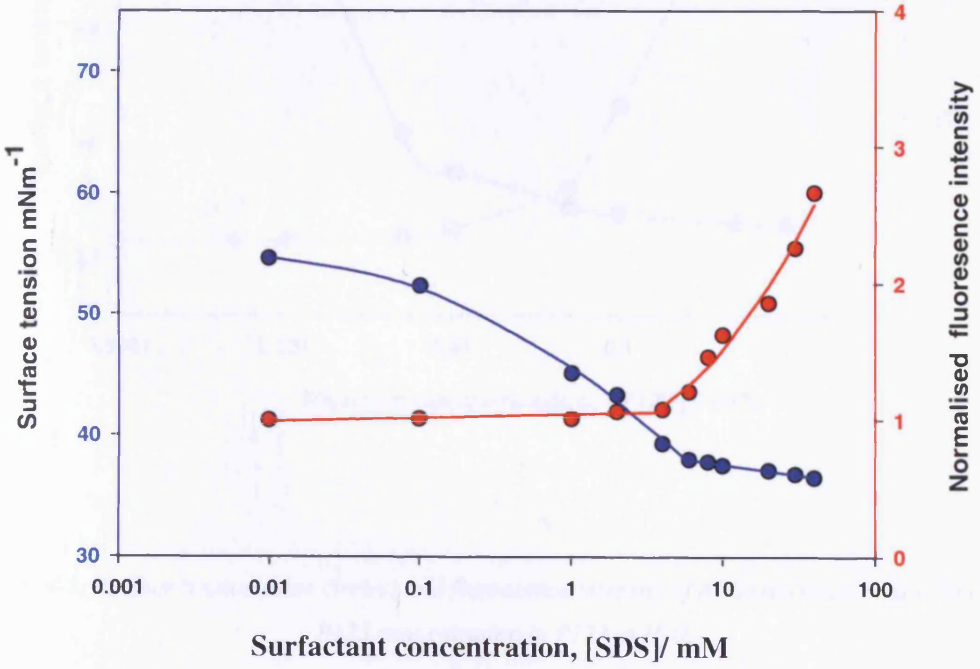

Figure 4-2: Surface tension (blue circles) and fluoresence intensity of ANS (red circles) as a function of SDS concentration in SDS in 5.0 wt% EtOH/H_2O.

4.1.2. Pluronic P123 in ethanol/water mixtures

Figures 4-3 to 4-5, show the combined surface tension and fluorescence intensity approach also detects the CMC of the P123 copolymer. The surface tension decreases with increasing P123 concentration, reaching a constant value above the CMC, whilst the ANS fluorescence intensity increases above the CMC as the P123 concentration passes through the CMC. In all cases, the onset of micellization is slightly lower as detected by surface tension, but the detected CMC = 0.03 wt% is in excellent agreement with previous studies [6, 7]. Interestingly, the P123 CMC does not vary **significantly** with added ethanol, but these is evidence of a weak increase in CMC, and contrasts with the co-surfactant effect shown with SDS-only that leads to a decrease in the CMC. The normalised fluorescence intensity ANS of the P123 increases less rapidly with copolymers, suggesting that the aggregates are either smaller and/or more hydrophilic than simple SDS micelles.

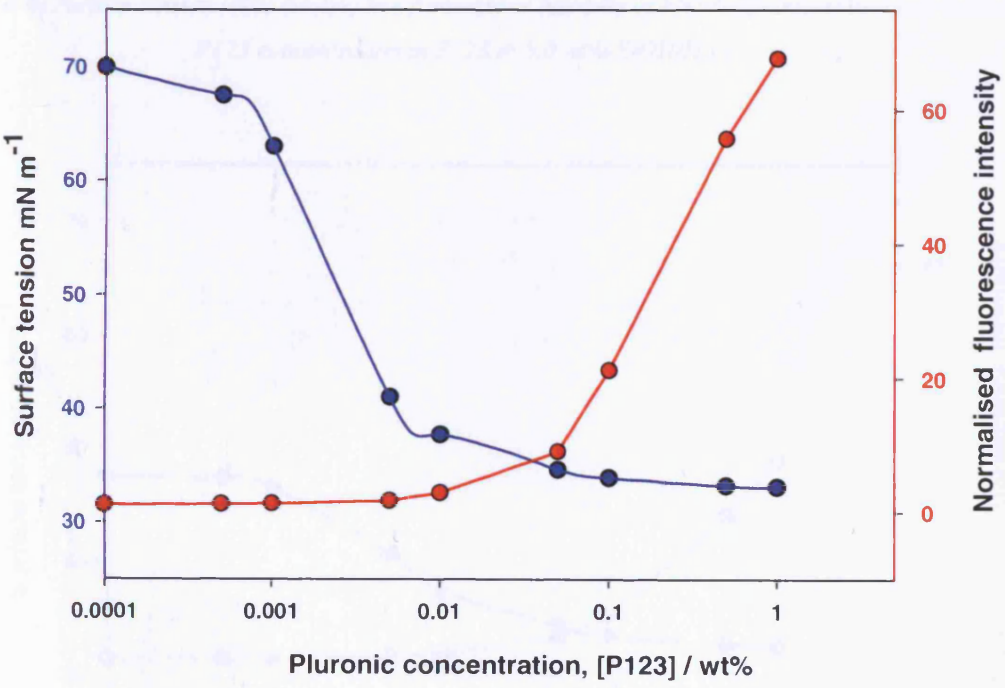

Figure 4-3: Surface tension (blue circles) and fluoresence intensity of ANS (red circles) as a function of P123 concentration in P123 in H_2O.

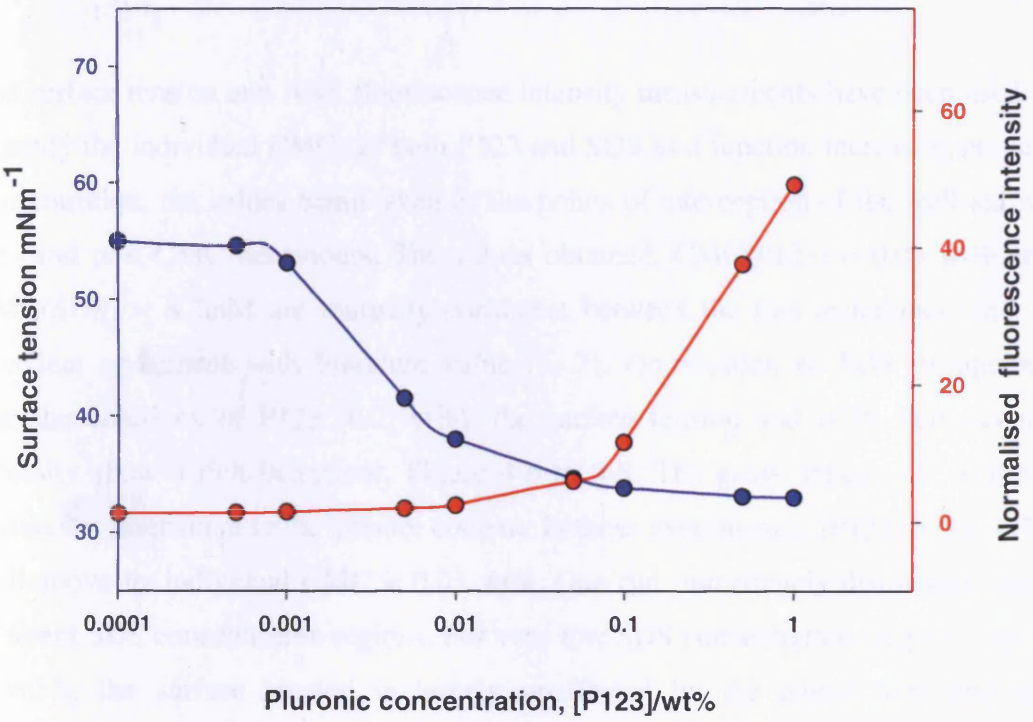

Figure 4-4: Surface tension (blue circles) and fluoresence intensity of ANS (red circles) as a function of P123 concentration in P123 in 5.0 wt% EtOH/H_2O.

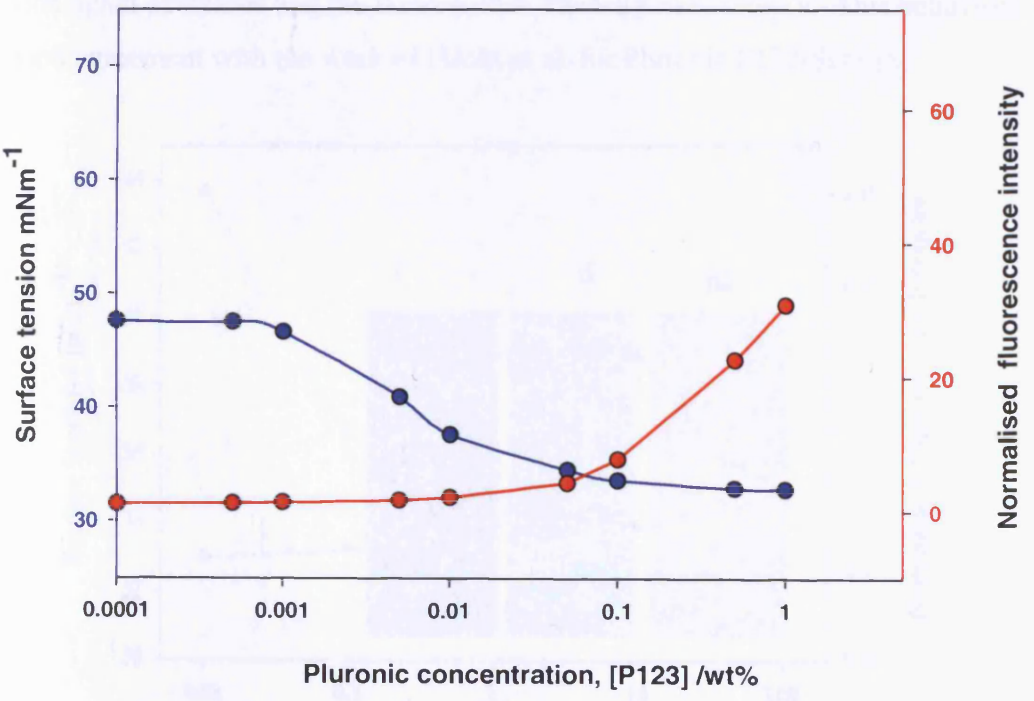

Figure 4-5: Surface tension (blue circles) and fluoresence intensity of ANS (red circles) as a function of P123 concentration in P123 in 10 wt% EtOH/H_2O.

4.1.3. P123 with SDS in ethanol/water mixtures

The surface tension and ANS fluorescence intensity measurements have been used to quantify the individual CMCs of both P123 and SDS as a function increasing ethanol concentration, the values being taken as the points of interception of the well-known ore- and post-CMC behaviours. The values obtained, CMC(P123) = 0.03 wt% and CMC(SDS) = 8.2mM are mutually consistent between the two techniques, and in excellent agreement with literature value [4, 7]. On addition of SDS to aqueous micellar solutions of P123 (0.2 wt%), the surface tension and ANS fluorescence intensity show a rich behaviour, Figure 4-6 to 4-8. The gross appearance of these features is insensitive to the ethanol content. In these experiments, [P123] = 0.2 wt%, well above its individual CMC = 0.03 wt%. One can immediately distinguish three different SDS concentration regions. For very low SDS concentration (region i, up to 1.0mM), the surface tension is largely unaffected by the added SDS and the fluorescence intensity drops significantly. Over the intermediated surfactant concentration range, (1.0mM < [SDS] < 10mM, region ii), the surface tension increases sharply to a plateau whereas the fluorescence intensity attain a minimum value. On increasing the [SDS] further, ([SDS] > 10mM, region iii), the surface tension again decreases and the fluorescence intensity rises steeply. This behaviour is in good agreement with the work of Hecht et al. for Pluronic F127/SDS [8].

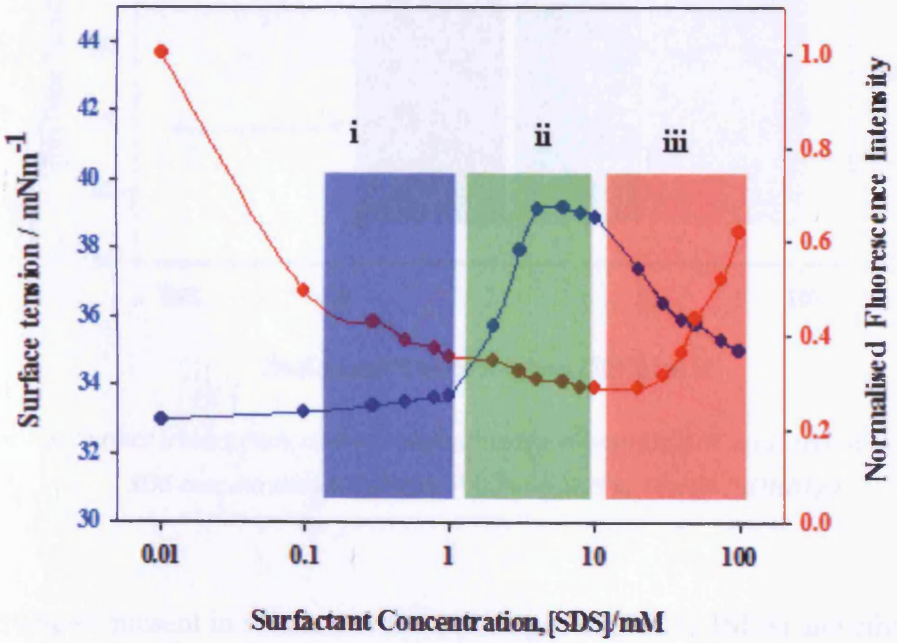

Figure 4.6: Surface tension (bule circles) and fluoresence intensity of ANS (red circles) as a function of SDS concentration in 0.2 wt% P123 with SDS in H_2O.

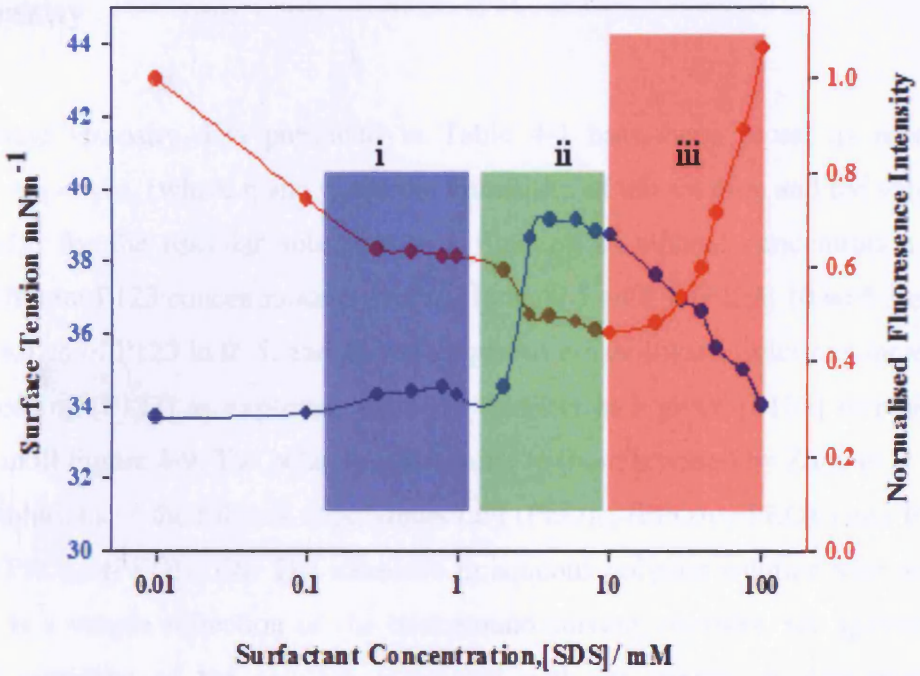

Figure 4-7: Surface tension (bule circles) and fluoresence intensity of ANS (red circles) as a function of SDS concentration in 0.2 wt% P123 with SDS in 5.0 wt%EtOH/H_2O.

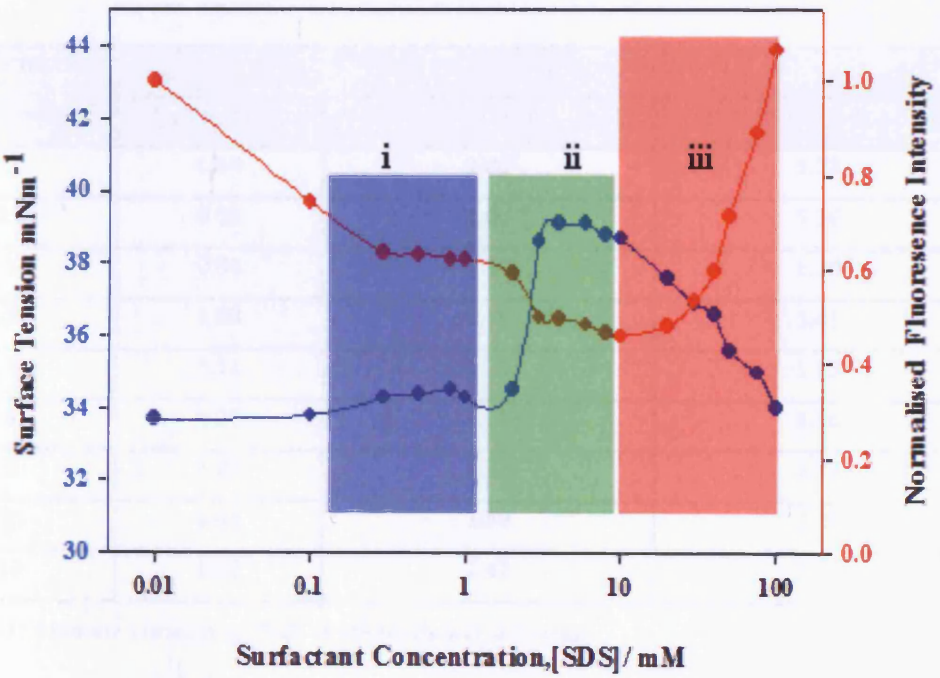

Figure 4-8: Surface tension (bule circles) and fluoresence intensity of ANS (red circles) as a function of SDS concentration in 0.2 wt% P123 with SDS in 10 wt% EtOH/H_2O.

The structures present in solution over these ranges of [P123], [SDS] and ethanol have been examined using viscosity, PGSE-NMR and SANS in the next section.

4.2. Viscosity

The absolute viscosity data presented in Table 4-1 have been recast as relative viscosity, $\eta_{rel} = \eta / \eta_o$ (where η and η_o are the viscosities of the solution and the solvent respectively) for the micellar solutions as a function of ethanol concentration for several different P123 concentrations, over the range 0.5 wt% < [P123] 10 wt% range. The viscosities of P123 in 0, 5, and 10 wt% aqueous ethanol/water solutions increase with increasing [P123] as expected, with the viscosity at a given [P123] increasing with [ethanol] Figure 4-9. The behaviour is similar to those reported by Zhou et al. for aqueous solutions of the triblock copolymers L64 $(PEO)_{13}$-$(PPO)_{30}$-$(PEO)_{13}$ and P105 $(PEO)_{37}$-$(PPO)_{58}$-$(PEO)_{37}$ [9]. The increases in aqueous polymer solution viscosities for P123 is a simple reflection of the background solvent viscosity, set against an increased crowding of the solution associated with the greater micelle number concentration on account of the reducing aggregation number [3, 10].

Concentration, P123/ wt%	Absolute viscosity/ Centipoise (cP)		
	H_2O (± 1.0%)	5.0 wt% EtOH (± 1.0%)	10 wt% EtOH (± 1.0%)
0	0.89	1.02	1.21
0.5	0.93	1.07	1.26
1	0.96	1.10	1.30
2	1.03	1.19	1.41
3	1.11	1.28	1.53
4	1.20	1.39	1.66
5	1.29	1.52	1.83
7.5	1.63	1.88	2.30
10	1.98	2.42	2.93

Table 4-1: *Absolute viscosity of P123 in ethanol/water mixtures.*

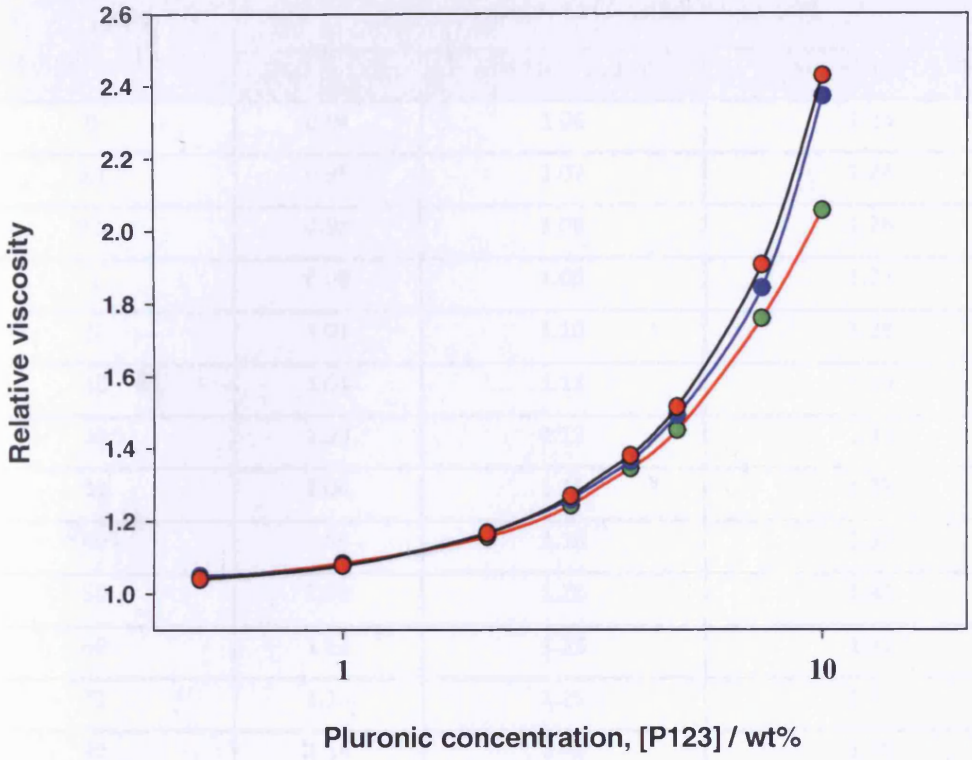

Figure 4-9: *Relative viscosity of P123 as a function of P123 concentration, (green circles) in H_2O, (bule circles) in 5.0 wt% EtOH/H_2O and (red circles) in 10 wt% EtOH/H_2O. Errors are comparable to the size of the symbol.*

Additional viscosity data have been presented again in terms of relative viscosity for solutions of a constant [P123] (1.0 wt%) as a function of SDS concentration in the same (0, 5 and 10 wt%) water/ethanol mixtures at 25°C. The absolute viscosities obtained under different solution conditions are recorded in Table 4-2. The relative viscosity of P123/SDS/ethanol solutions show pronounced dependencies on [P123], [SDS] and ethanol content, and the exemplar data presented here is in a good agreement with that previously published by Ganguly et al. [10]. Therefore, an increase in relative viscosity was observed in 0.5mM SDS concentration which is followed by gradual viscosity with concentration.

The binding of the surfactant to the Pluronic is a key factor in determining the viscosity, and this has been studied by PGSE-NMR.

Concentration,SDS/mM	Absolute viscosity/ Centipoise (cP)		
	H_2O (± 1.0)	5 wt% EtOH (± 1.0%)	10 wt% EtOH (± 1.0%)
0	0.94	1.06	1.24
0.1	0.95	1.07	1.24
0.5	0.98	1.08	1.26
1	0.99	1.09	1.27
5	1.01	1.10	1.28
10	1.01	1.11	1.29
20	1.03	1.13	1.31
30	1.04	1.15	1.33
40	1.06	1.18	1.37
50	1.09	1.20	1.40
60	1.12	1.23	1.42
70	1.13	1.25	1.47
80	1.15	1.28	1.49
90	1.18	1.31	1.51
100	1.20	1.33	1.54

Table 4-2: *Absolute viscosity of 1.0 wt% P123 with SDS in ethanol/water mixtures.*

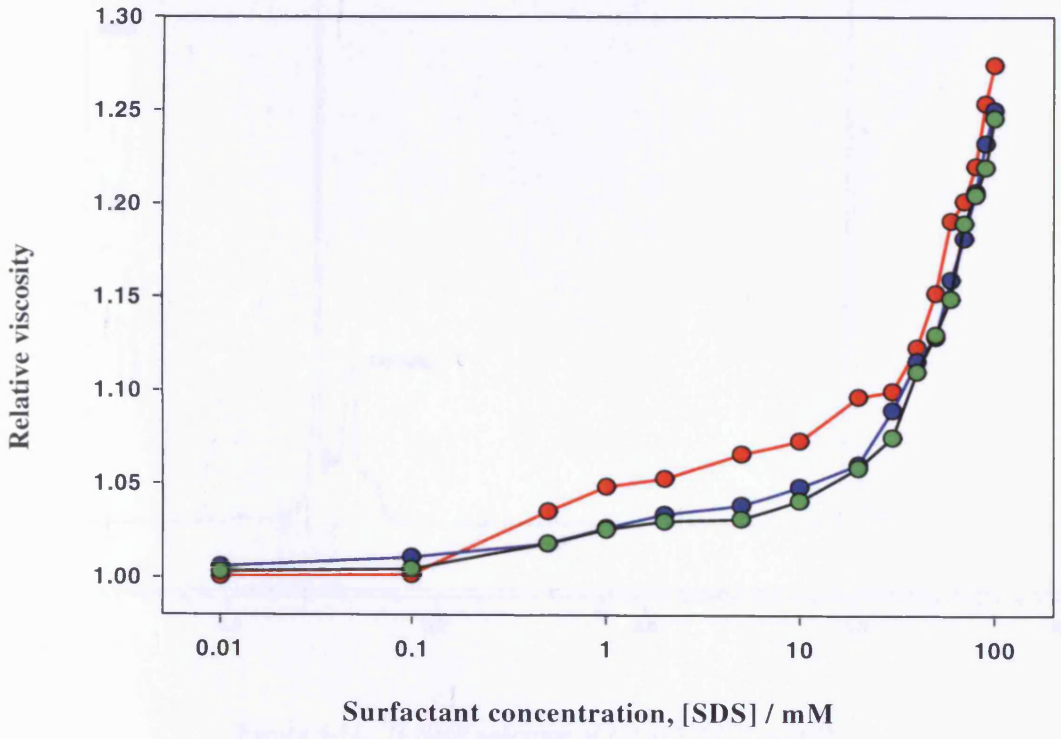

Figure 4-10: *Relative viscosity of 1.0 wt% P123 as a function of SDS concentration, (red circles) in H_2O, (bule ciricles) 5.0 wt% EtOH/H_2O and (green circles) 10 wt% EtOH/H_2O. Errors are comparable to the size of the symbol.*

4.3. Pulsed-gradient spin-echo NMR (PGSE-NMR) study

PGSE-NMR measurements were conducted on a Bruker AMX360 NMR spectrometer using a stimulated echo sequence, (see chapter two and three for more detail). The chemically selective PGSE-NMR experiment was carried out to quantify the diffusive rates of each component within the mixture, and to interpret those rates in terms of the interaction between the Pluronic (P123) and SDS in water/ethanol mixtures aqueous solution.

4.3.1. Self-diffusion coefficient of P123 in ethanol/water mixtures

A typical ^{1}H-NMR spectrum (1.0 wt% P123 in D_2O) is reported in Figure 4-11, along with the assignments of some resonance peaks. The intensities of the signal attributed to water (HDO), polymer (EO-CH_2-), (PO-CH_2-), (PO-CH_3) and agreement with the literature reports [11-13].

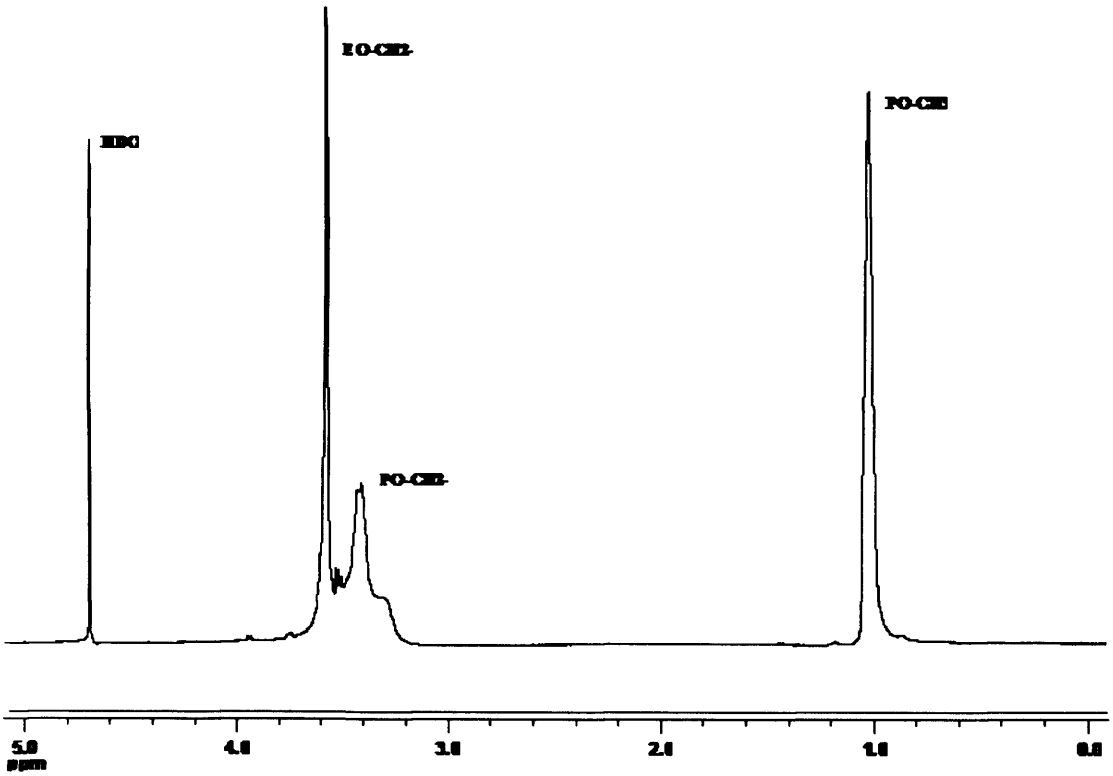

Figure 4-11: ^{1}H-NMR spectrum of 1.0 wt% P123 in D_2O.

Figure 4-12 shows the attenuation behaviour plus associated fits to stretched exponential of 1.0 wt% P123 in D_2O and in 5.0 wt% ethanol respectively. The signal decays fastest for the 1.0 wt% P123 in D_2O indicating that the polymer in this solution has a larger self-diffusion coefficient, commensurate with a smaller size. Similarly, the signal from 1.0 wt% P123 in 5.0 wt% ethanol decays slowest, indicating its larger size. The nonlinearity of the PGSE-NMR attenuation function indicates this polymer is slightly polydispere. The stretched exponential is a convenient method to quantify this polydispersity via the parameter β. Typically, (β = 0.6 - 0.8) the impact of the solvent composition on the Pluronic micellization is shown by the ratio of 1.0 wt% P123 in 0 and 5.0 wt% ethanol solutions is ($\frac{\eta_{H_2O}}{\eta_{5\%\ EtOH}} / \frac{Ds_{H_2O}}{Ds_{5\%\ EtOH}} = 2:1$), the absolute viscosity compared with the self-diffusion coefficient.

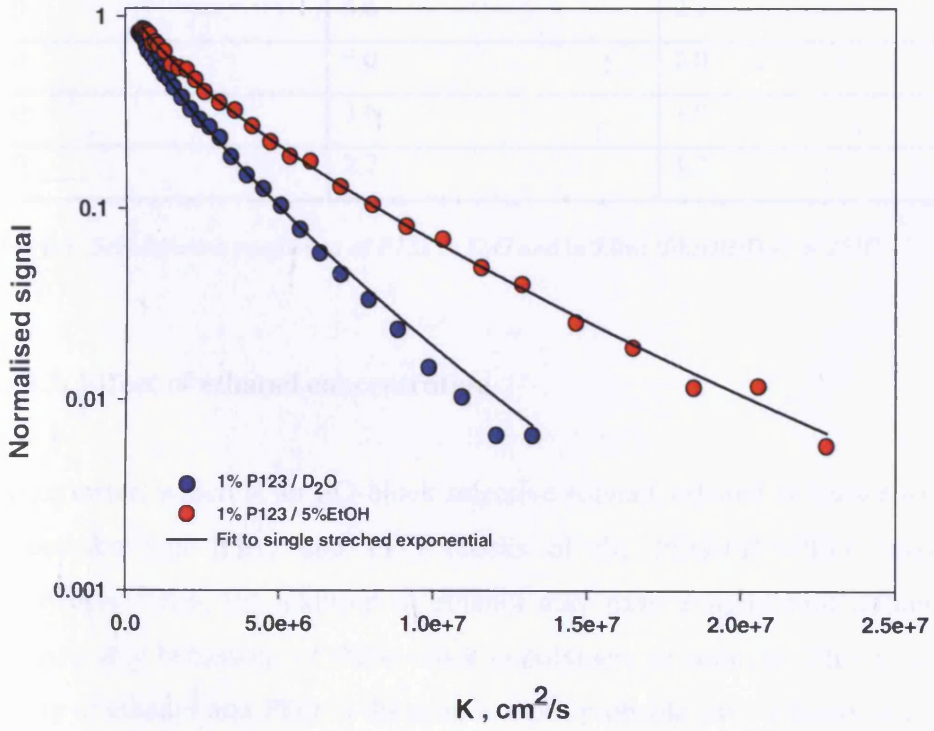

Figure 4-12: Attenuation functions of 1.0 wt% P123 in D_2O and in 5.0 wt% EtOH/D_2O.

4.3.1.1. Effect of P123 concentration

The self-diffusion coefficient versus concentration behaviour of P123 in D_2O and 5.0 wt% ethanol is presented in Table 4-3 and Figure 4-13. Both samples exhibited a similar pattern in that the diffusion coefficient decreased with increasing concentration of P123. Note that the range studied (0.2-5.0 wt%), is well above the CMC (0.03 wt%) of this Pluronic at 25°C, and also above the CMT = 16°C [6, 14], i.e. it is to be expected that most of the P123 exist in spherical micelles [15].

Concentration, P123/wt%	Self-diffusion coefficient / (10^{-11} ± 5%) / m^2s^{-1}	
	in D_2O	in 5.0 wt% EtOH/D_2O
0.2	10.0	3.0
0.5	9.0	2.4
1.0	5.6	2.1
2.0	5.0	2.0
3.0	3.6	1.9
5.0	2.7	1.7

Table 4-3: *Self-diffusion coefficient of P123 in D_2O and in 5.0wt %EtOH/D_2O at 25°C.*

4.3.1.2. Effect of ethanol concentration

Unlike water, which is an EO-block selective solvent, ethanol is known to be a good solvent for both PEO and PPO blocks of the PEO-PPO-PEO based triblock copolymers. Thus, the addition of ethanol may have a significant influence on the self-assembly behaviour of these block copolymers in solution. This means that the mixing of ethanol and PPO in the core is more probable since ethanol is known to be a good solvent for both PEO and PPO [16]. Therefore, we see in Figure 4-13 and Table 4-3, the self-diffusion coefficient decreases with increase concentration P123 and the self-diffusion coefficient values in water case bigger than in ethanol case, consistent with an increase in the bulk solution viscosity, Table 4-1.

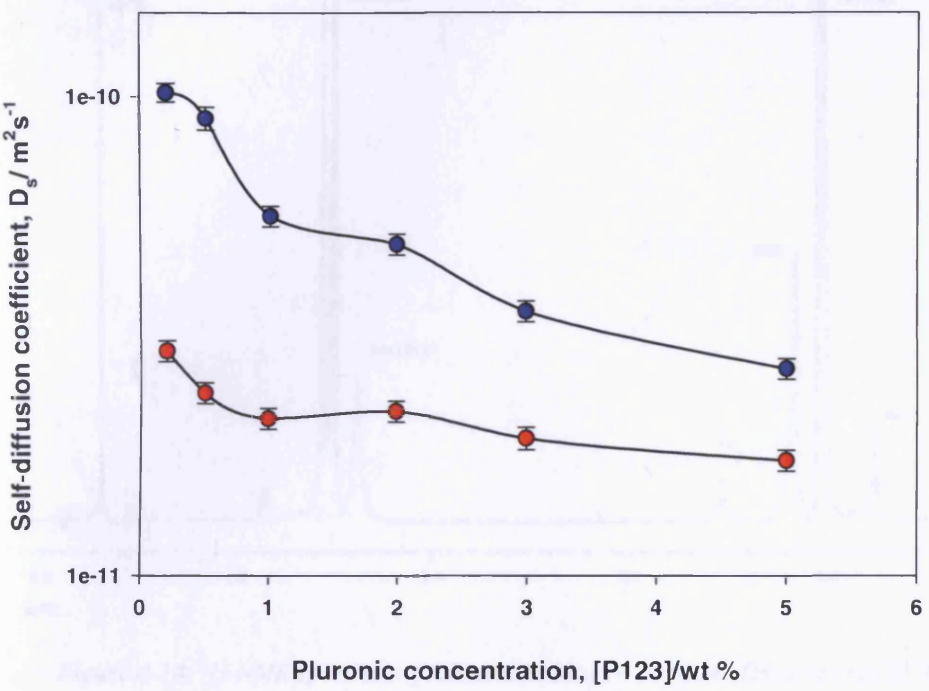

Figure 4-13: *Self-diffusion coefficient of P123 as a function of P123 concentration, where ,Ds values in D_2O (blue circles) and in 5.0 wt% EtOH (red circles).*

4.3.2. Self-diffusion coefficient for P123/SDS in ethanol/water mixtures

The interaction between the triblock copolymer P123 and sodium dodecyl sulfate SDS has been studied at fixed concentration of P123 (5.0 wt%) and the SDS concentration is varied (10, 30, 50, 70 and 100mM). The ^{1}H-NMR spectrum of a selected sample on 5.0 wt% P123 with 100mM SDS in D_2O is reported in Figure 4-14, along with the assignments of some resonance peaks. The intensities of the echo signal attributed to water (HDO), polymer (EO-CH_2-), (PO-CH_2-), (PO-CH_3), surfactant (SDS) has been confirmed by reference to Youssry et al. [13].

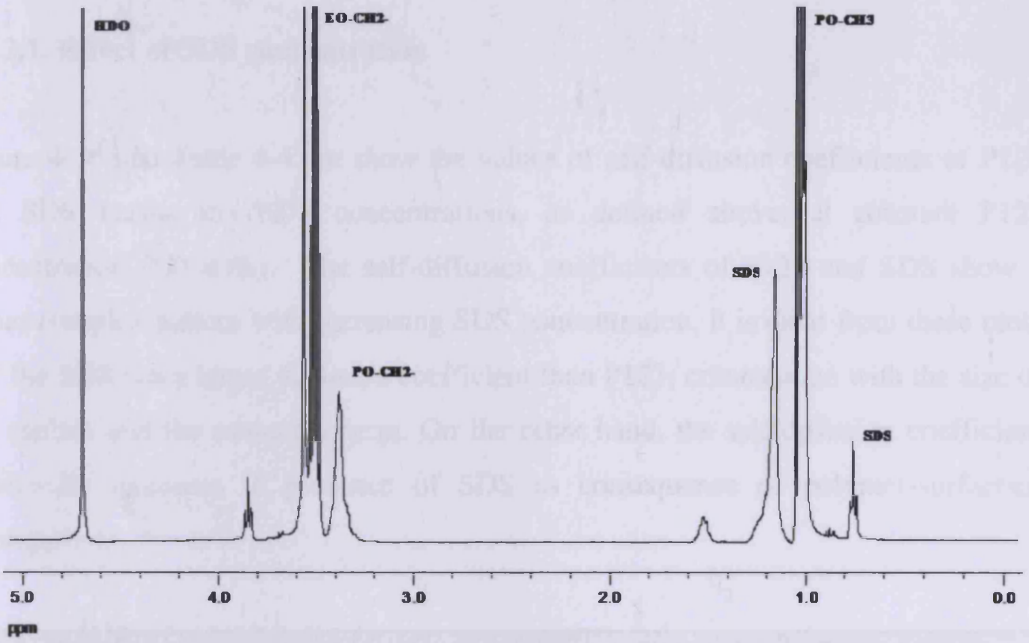

Figure 4-14: ^{1}*H-NMR spectrum of 5.0 wt% P123 with 100 mM SDS in* D_2O *at 25°C.*

Figure 4-15 shows the attenuation functions of 5.0 wt% P123 with 10 and 100 mM SDS in D_2O and in 5.0 wt% ethanol respectively. The linearity of PGSE-NMR attenuation data indicates that these systems still show a small but constant degree of polydispersity. Again, the stretched exponential analysis has been employed a convenient method to quantify this slight polydispersity.

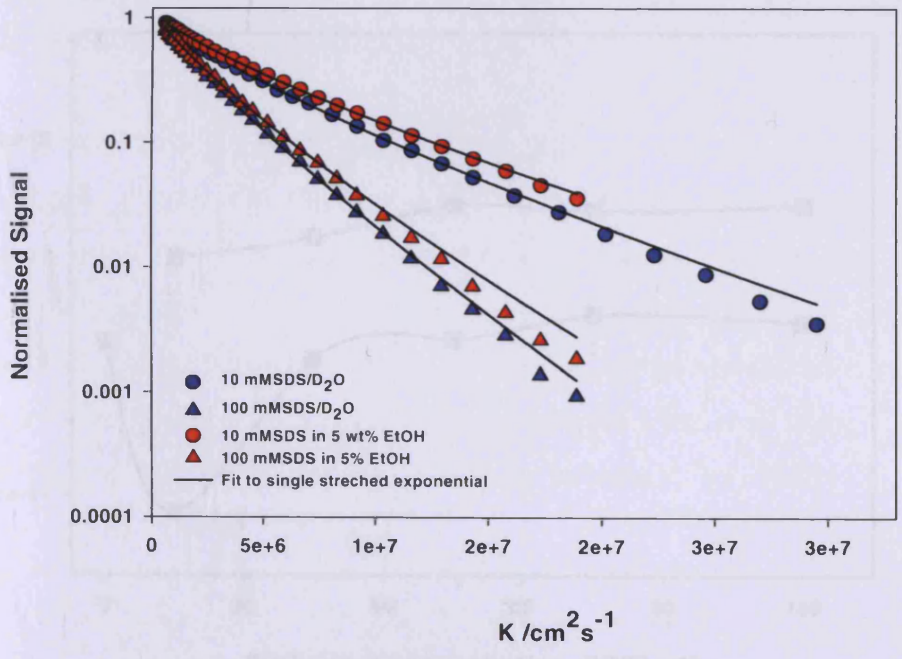

Figure 4-15: Attenuation functions for the polymer peak 3.5ppm for 5.0 wt% P123 with SDS in D_2O *and 5.0 wt% EtOH/*D_2O *at 25°C.*

4.3.2.1. Effect of SDS concentration

Figure 4-16 and Table 4-4 are show the values of self-diffusion coefficients of P123 and SDS versus the SDS concentrations, as defined above, at constant P123 concentration (5.0 wt%). The self-diffusion coefficients of P123 and SDS show a rather complex pattern with increasing SDS concentration, it is clear from these plots that the SDS has a larger diffusion coefficient than P123; commentate with the size of the species and the monomer term. On the other hand, the self-diffusion coefficient expectedly increases in presence of SDS as consequence of polymer-surfactant aggregation.

Concentration, SDS/mM	Self-diffusion coefficient/ (10^{-11} ± 5%) / m^2s^{-1}	
	SDS	P123
0	---	2.7
10	4.7	1.0
30	5.3	2.4
50	5.5	2.7
70	6.3	3.2
100	6.5	3.1

Table 4-4: *Self-diffusion coefficient values of 5.0 wt% P123/SDS in D_2O at 25°C.*

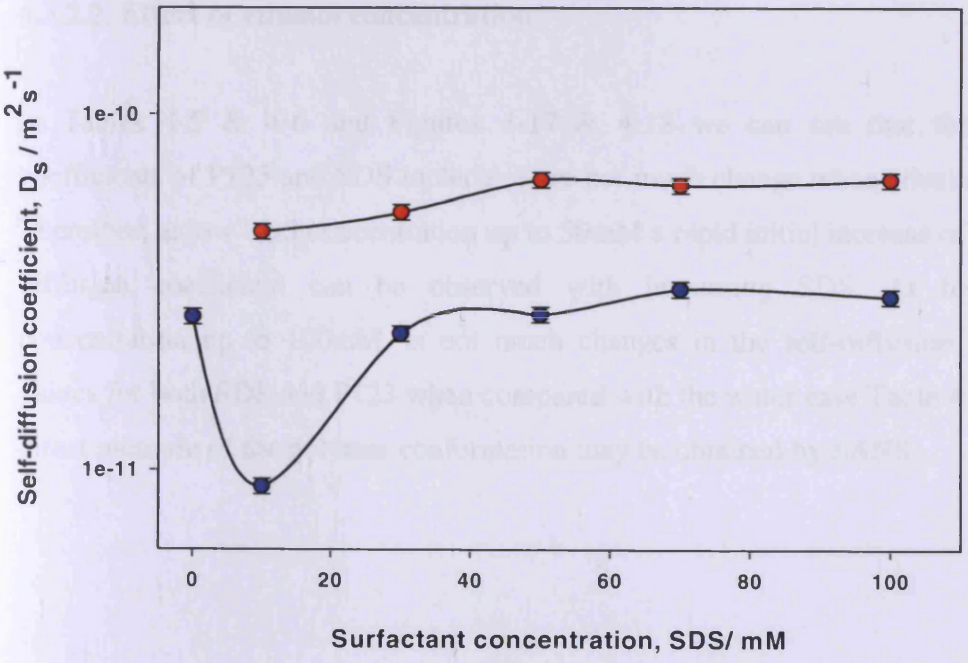

Figure 4-16: *Self-diffusion coefficient of 5.0 wt% P123 as a function of SDS concentration in D_2O, where ,Ds values of SDS (red circles) and P123 (blue circles).*

The measured diffusion coefficient of the P123 and SDS will each be weighted averages of those fractions in monomer and micellar forms, with each component being described by a two-state mobility model,

$$\overline{D}^{P123} = p_{micelle}^{P123} D_{micelle}^{P123} + (1 - p_{micelle}^{P123}) D_{monomer}^{P123} \quad (4.3)$$

$$\overline{D}^{SDS} = p_{micelle}^{SDS} D_{micelle}^{SDS} + (1 - p_{micelle}^{SDS}) D_{monomer}^{SDS} \quad (4.4)$$

and one would assume that

$$D_{micelle}^{P123} = D_{micelle}^{SDS}$$

Given that the CMC of the P123 is low, it is valid to assume that

$p_{micelle}^{P123} \approx 1$, and thus,

$$\overline{D}^{SDS} = p_{micelle}^{SDS} D^{P123} + (1 - p_{micelle}^{SDS}) D_{monomer}^{SDS} \quad (4.5)$$

where; D^{P123} is the measured diffusion coefficient of P123.

4.3.2.2. Effect of ethanol concentration

In Tables 4-5 & 4-6 and Figures 4-17 & 4-18 we can see that the diffusion coefficients of P123 and SDS molecules are not much change when ethanol is added. Therefore, at low SDS concentration up to 50mM a rapid initial increase of P123 self-diffusion coefficient can be observed with increasing SDS. At higher SDS concentration up to 100mM, is not much changes in the self-diffusion coefficient values for both SDS and P123 when compared with the water case Table 4-3. A more direct measure of the polymer conformation may be obtained by SANS.

Concentration, SDS/mM	Self-diffusion coefficient/(10^{-11} ± 5%)/ m^2s^{-1}	
	SDS	P123
0	--	1.7
10	5.8	1.4
30	5.1	1.6
50	5.9	2.5
70	6.3	2.8
100	7.2	2.8

Table 4-5: Self-diffusion coefficients of 5.0 wt% P123/SDS in 5.0 wt% EtOH/D_2O at 25°C.

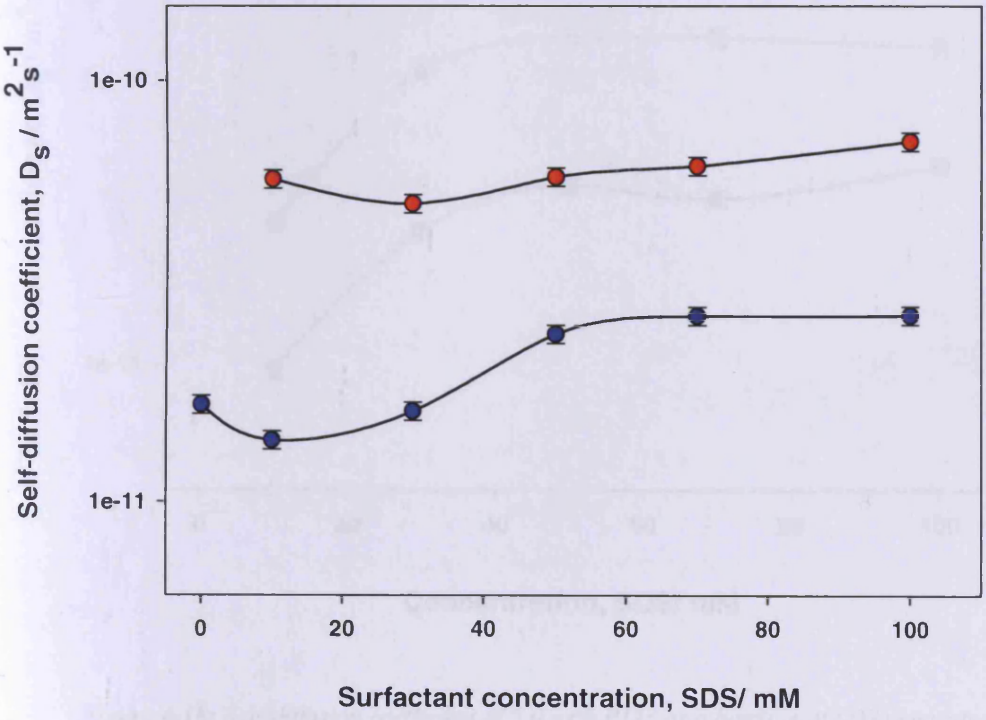

Figure 4-17: Self-diffusion coefficient of 5.0 wt%P123 as a function of SDS concentration in 5.0 w% EtOH/D_2, where ,Ds values of SDS (red circles) and P123 (blue circles).

Concentration, SDS/mM	Self-diffusion coefficient/(10^{-11} ± 5%)/ m^2s^{-1}	
	SDS	P123
10	2.2	1.0
30	5.1	2.1
50	6.1	2.5
70	6.7	2.7
100	5.8	3.0

Table 4-6: *Self-diffusion coefficients of 5.0 wt% P123/SDS in 10 wt% EtOH/D_2O at 25°C.*

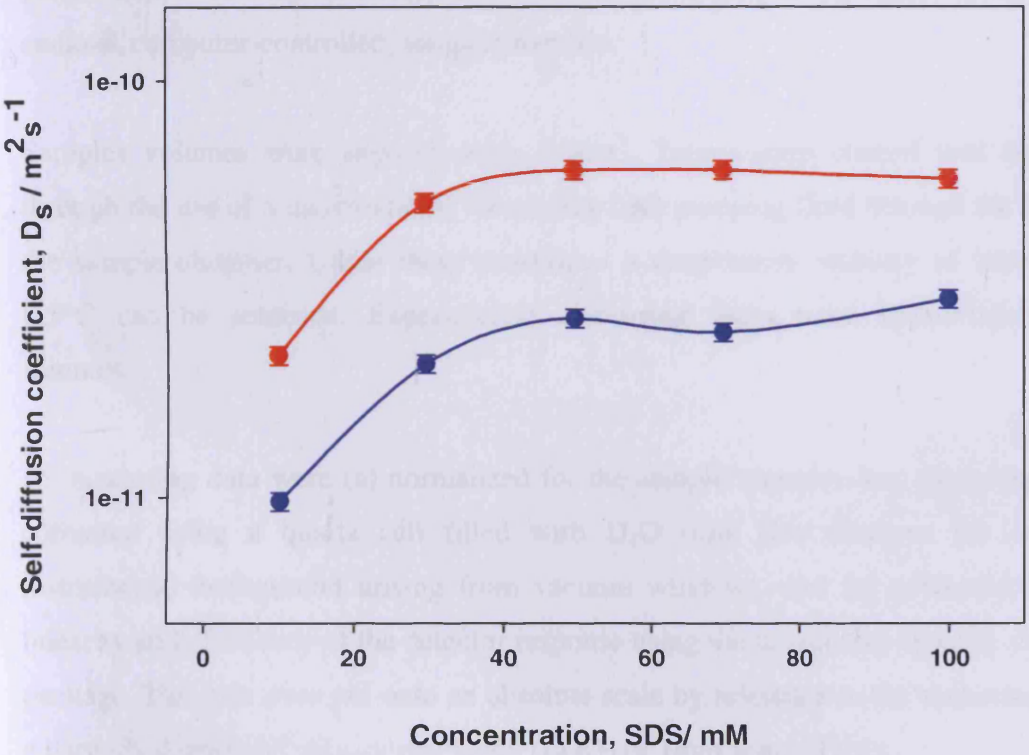

Figure 4-18: *Self-diffusion coefficient of 5.0 wt% P123 as a function of SDS concentration in 10 w% EtOH/D_2, where ,Ds values of SDS (red circles) and P123 (blue circles).*

4.4. Small-angle neutron scattering (SANS) study

Small-angle neutron scattering (SANS) measurements were performed on two instruments – the fixed-geometry, time of flight LOQ diffractometer (ISIS Spallation Neutron Source, Oxfordshire UK) and the fixed-wavelength D11 diffractometer (ILL, Grenoble, France). On LOQ neutron wavelengths spanning 2.2 to 10 Å were used to access a Q range {$Q = 4\pi \sin(\theta/2/\lambda)$} of approximately 0.008 to 0.25 $Å^{-1}$ (25Hz), with a fixed sample- detector distance of 4.1. On D11, the wavelength was set at 8 Å, and three sample-detector distances were employed to span a comparable Q range. On both cameras, the samples were contained in 2mm path length, uv-spectrophotometer grade, quartz cuvettes (Hellma) and mounted in aluminium holders on top of an enclose, computer-controlled, sample chamber.

Samples volumes were approximately $0.4cm^3$. Temperature control was achieved through the use of a thermostatted circulating bath pumping fluid through the base of the sample chamber. Under these conditions a temperature stability of better than 0.5°C can be achieved. Experimental measuring times were approximately 40 minutes.

All scattering data were (a) normalized for the sample transmission; (b) background corrected using a quartz cell filled with D_2O (this also removes the inherent instrumental background arising from vacuum windows, etc) (c) corrected for the linearity and efficiency of the detector response using the instrument-specific software package. The data were put onto an absolute scale by reference to the scattering from a partially deuterated polystyrene blend (LOQ) or 1mm water (D11).

4.4.1. SANS data analysis

Pluronic micelles are generally thought to consist of a spherical core containing the hydrophobic part of the copolymer (PPO), with this core surrounded by a shell of dissolved polymer chains consisting of the hydrophilic part of the copolymer (PEO). Data were fitted using the Pedersen model for Pluronics in solution [17, 18], which uses a form factor based on a spherical core surrounded by polymer chains, with the

latter adopting Gaussian statistics. This model allows unimers and micelles to coexist, accounting for the gradual aggregation characteristics of Pluronic, and has previously been used to successfully describe scattering data from Pluronics [18, 19].

The form factor, F_{mic}, given in Equation 4.1, combines four different terms: self-correlation of the sphere $[F_s(Q, R_c)]$, the self-correlation of the chains $[F_c(Q, L, b)]$, the cross-term between the sphere and the chains $[S_{sc}(Q)]$ and the cross-term between chains $[S_{cc}(Q)]$. These parameters have previously been described fully by Pedersen and Gerstenberg [17]:

$$\begin{aligned} F_{mic}(Q) = {} & N_{agg}{}^2 \beta_s^2 F_s(Q,R_c) \\ & + N_{agg} \beta_c{}^2 F_c(Q,L,b) \\ & + N_{agg}(N_{agg}-1)\beta_c{}^2 S_{cc}(Q) \\ & + 2(N_{agg})^2 \beta_s \beta_c S_{sc}(Q) \end{aligned} \qquad (4.6)$$

where; N_{agg} is the aggregation number of the micelle, β_s and β_c are the excess scattering lengths of the polymer blocks in the spherical core (PPO) and the chain (PEO), respectively, R_c is the radius of the core; L and b represent the contour length and Kuhn segment length of the chain PEO block of the polymer.

A structure factor S (Q) has been included in the fitting routine, as provided by the Leckner formulism [20]. In this, the polymeric micelles are modelled as hard-spheres, with N Particles of radius R_{HS} per unit volume:

$$S(Q) = [1\text{-}N(2Q R_{HS})]^{-1} \qquad (4.7)$$

where; RHS is the sum of the core radius R_C and the thickness of the hydrated EO chain, t, ($R_{HS} = R_C + t$).

Scattering data can also be fitted to models which described combinations of the relevant form and structure facture for different systems. For the SANS data fitting in this chapter, the fitting program "Insanity" was used, which was written by Prof. Terence Cosgrove (Bristol University). The program uses a least-square fitting

procedure to minimise the $\chi 2$ closeness-of-fit parameter, and outputs estimated values for the parameters, along with error margins (representing one standard deviation).

4.4.2. Pluronic scattering

Small-angle neutron scattering has been used to explore the structures present within these three regions, and exemplar data – that for simple aqueous solutions was presented in Figure 4.6 - 4.8. As may be seen, there is appreciable scattering even at [P123] = 0.2 wt%, with a noticeable "bump" around Q = 0.09 $Å^{-1}$, Figure 4-19. Parameters describing the fit of the Pederson model to these data are given in Table 4-7, the aggregation number N_{agg} being around 145 (± 1.6).

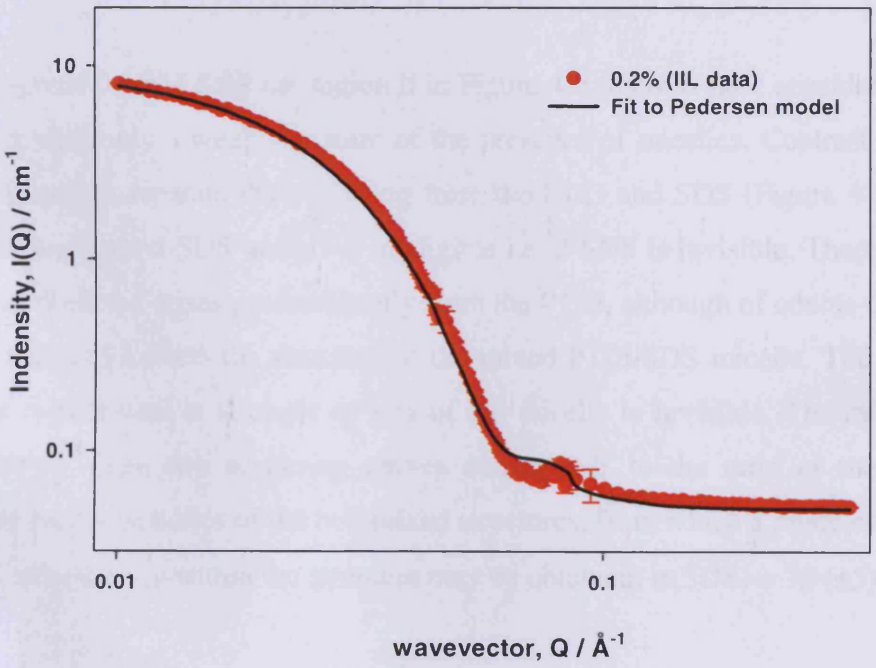

Figure 4-19: Small-angle neutron scattering data for Pluronic 0.2 wt% P123 in D2O.

Parameter	value
Aggregation number N_{agg} ± 1.6	145
Volume fraction of solvent in the core Φ_{sol} ± 0.002	0.01
Radius of gyration of PEO in the corona $Rg/Å$ ± 5.0	59
Incoherent background scattering B/cm^{-1} ± 0.001	0.05
Volume fraction of hard spheres Φ_{HS} ± 0.003	0.04
interaction radius $R_{int}/Å$ ± 1.1	37
Polydispersity σ_{core} ± 0.03	0.66
The radius of gyration of the unimer chain $Rg/Å$ ± 3.1	68
Core radius of the core $R_{core}/Å$	87

Table.4-7: Fit parameters from Pederson model used to fit 0.2 wt% P123/D_2O at 25°C.

4.4.2.1. 0.2 wt% / SDS scattering

On addition of 0.5mM SDS i.e. region ii in Figure 4-6, there is now considerably less scattering with only a weak signature of the presence of micelles. Contrast variation has been used to separate the scattering from the P123 and SDS (Figure 4-20) since the scattering from d-SDS in D_2O is negligible i.e. d-SDS is invisible. Therefore, any scattering observed arises predominantly from the P123, although of course the nature of the scattering reflects the structure of the mixed P123/SDS micelle. The intensity from the h-SDS case is stronger as less of the micelle is invisible. The ratio of the intensities of these two scattering curves corresponds to the ratio of the average scattering length densities of the two mixed structures, from which a crude estimate of the SDS composition within the structure may be obtained, α(SDS) = 35 (±5)%.

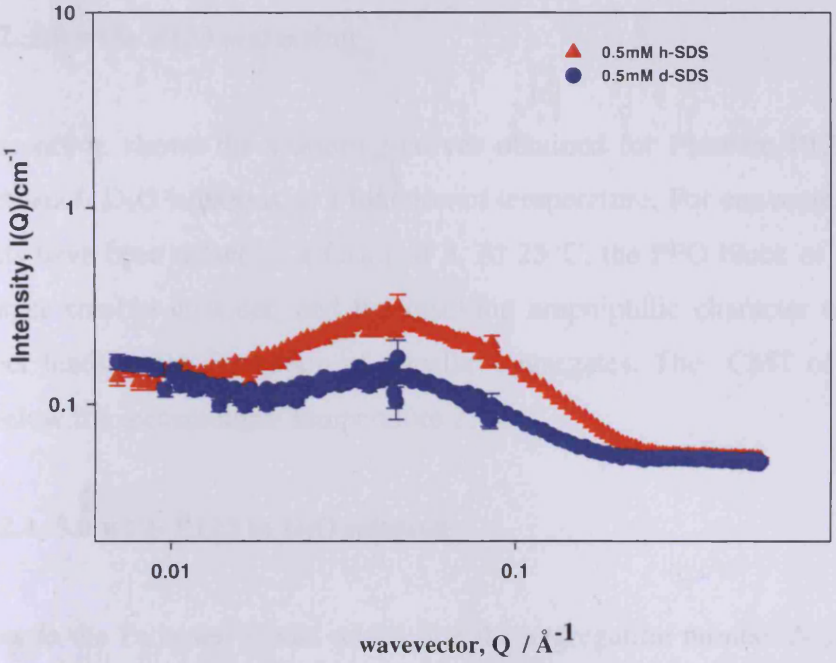

Figure 4-20: SANS data of 0.2 wt% P123 with 0.5(h- and d-SDS) in D_2O at 25°C.

On further addition of SDS e.g. [SDS] = 5mM, region iii in Figure 4.6, the scattering intensity is recovered, Figure 4-21, but the form of the scattering is subtly different at low Q in that now the data decrease, indicating the presence of an electrostatic repulsion between the micellar structures, i.e. the mixed micelles have acquired some ionic character due to the solubilised SDS. The ratio of the scattering intensities suggests that α(SDS) = 5 (± 0.5) %.

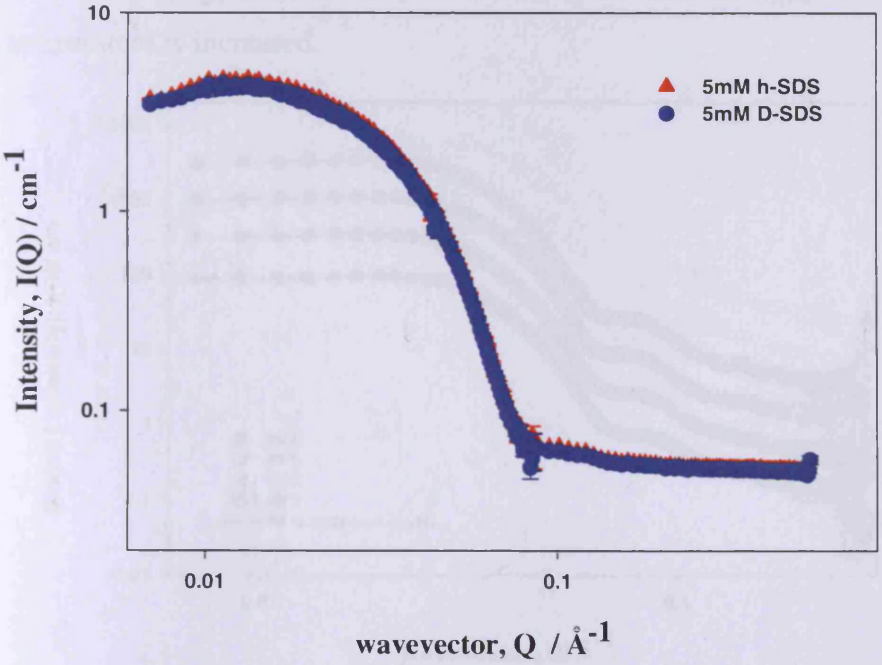

Figure 4-21: SANS data of 0.2 wt% P123 with 5.0 (h- and d-SDS) in D_2O at 25°C.

4.4.2.2. 5.0 wt% P123 scattering

In this section shows the scattering curves obtained for Pluronic P123 in 0 and 15 wt% ethanol/ D_2O solutions as a function of temperature. For convenience successive datasets have been offset by a factor of 3. At 25°C, the PPO block of the polymer is no longer soluble in water, and the resulting amphiphilic character of the Pluronic polymer leads to the formation of micellar aggregates. The CMT of P123 is 16°C [14] below the measurement temperature 25°C.

4.4.2.2.1. 5.0 wt% P123 in D_2O solution

Our fits to the Pedersen model reveal that the aggregation number N_{agg} of P123/D_2O solution under goes a significant increase from (87-121±1.3), upon increasing the temperature from 25 to 37°C Figure 4.22 and Table 4.8. This is driven by a decrease in polarity of both PEO and PPO segments and by the entropy gain in water caused by micellization (hydrophobic effect) [21]. The volume fraction of solvent in the core of the micelles Φ_{sol} was found to decrease slightly, since the Φ_{sol} reflects the combined water in the micellar core for these measurements because the solvent are contrast matched. The radii of the core of the micelles R_{core} as well as the polydispersity σ_{core} were found to decrease with increasing temperature. From the fitting it is also found that the radius of gyration of the PEO chains in the micelles Rg_{PEO} decreases slightly as temperature is increased.

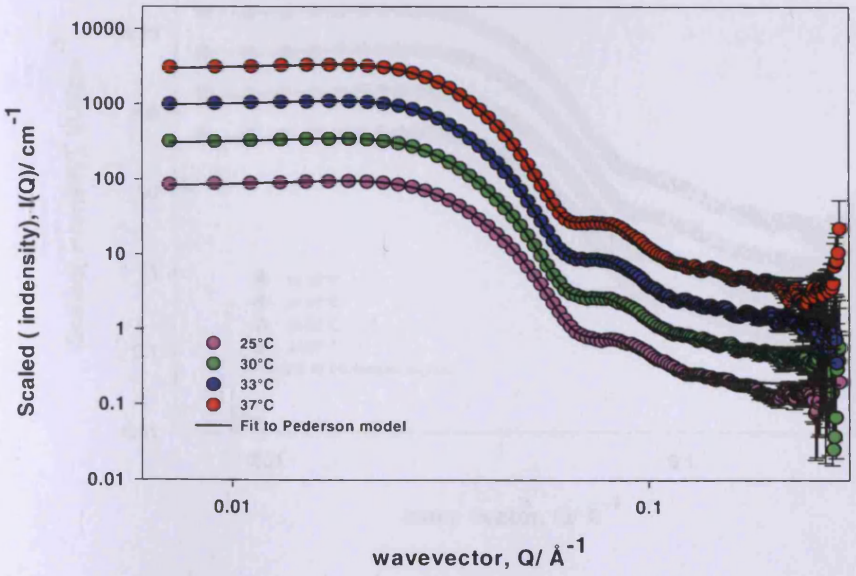

Figure 4-22: SANS data (symbols) and data fits (solid curves) of 5.0 w % P123/D_2O. Data have been offset by a factor of 3.

Temperature / °C	25	30	33	37
Aggregation number N_{agg} ±1.3	87	109	118	122
Volume fraction of solvent in the core Φ_{sol} ±0.004	0.23	0.19	0.17	0.16
Radius of gyration of PEO in the corona *Rg/Å* ±0.3	8.3	8.3	7.8	7.1
Incoherent background scattering B/cm^{-1} ± 0.03	0.17	0.17	0.16	0.15
Volume fraction of hard spheres Φ_{HS} ± 0.004	0.10	0.10	0.10	0.09
interaction radius R_{int}/Å ± 0.84	35.8	37.3	35.4	35.5
Polydispersity σ_{core} ± 0.02	0.54	0.51	0.48	0.46
The radius of gyration of the unimer chain *Rg/Å*	11	11	11	11
Core radius of the core R_{core}/Å	77	80	81	81

Table.4-8: Fit parameters from Pederson model used to fit 5.0 wt% P123/D_2O at difference temperature.

4.4.2.2.2. 5.0 wt% P123 in d-ethanol $_{(15\ wt\%)}$ and D_2O $_{(85\ wt\%)}$ solution

Figure 4-23 and Table 4-9 shows the scattering curves and data respectively, obtained for Pluronic 5.0 wt% P123 in d-ethanol $_{(15\ wt\%)}$ and D_2O $_{(85\ wt\%)}$ solutions as a function of temperature. The results are compared with 5.0 wt% P123 in D_2O solution at the same range of temperatures. It is seen that the effect of temperature in both cases is similar. Furthermore, when the temperature increases, the aggregation number also increases and there is a decrease in the monodisperse of the micelles are more. Additionally, the PPO core becomes more hydrophobic.

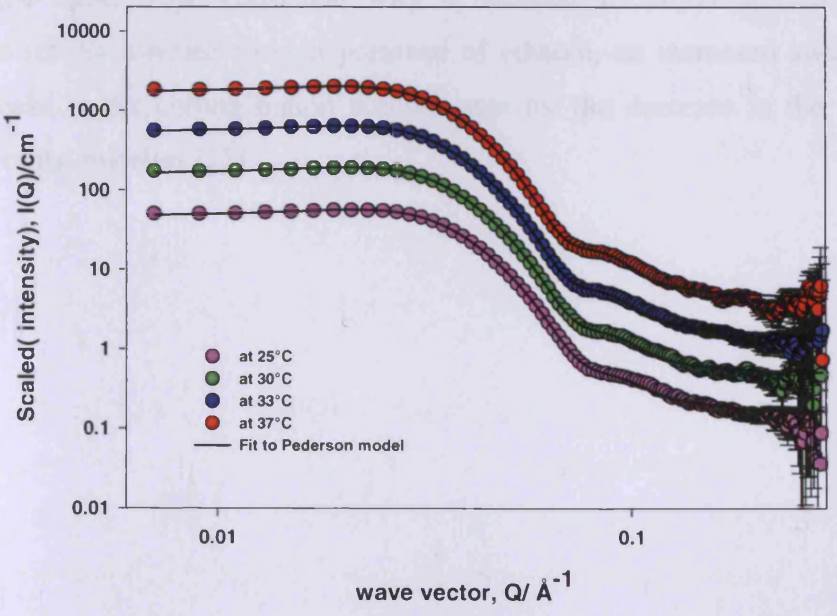

Figure 4-23: *SANS data (symbols) and data fits (solid curves) of 5.0 wt% P123 d-ethanol$_{(15\ wt\%)}$ and $D_2O_{(85\ wt\%)}$. Data have been offset by a factor of 3.*

Temperature / °C	25	30	33	37
Aggregation number N_{agg} ± 1.7	43	52	58	61
Volume fraction of solvent in the core Φ_{sol} ± 0.005	0.31	0.30	0.29	0.29
Radius of gyration of PEO in the corona $Rg/Å$ ± 0.05	10.3	9.6	9.0	8.4
Incoherent background scattering B/cm^{-1} ± 0.03	0.15	0.15	0.15	0.15
Volume fraction of hard spheres in solution Φ_{HS} ± 0.001	0.10	0.10	0.10	0.10
interaction radius $R_{int}/Å$ ± 0.7	32.3	33.3	34.6	34.3
Polydispersity σ_{core}± 0.05	0.87	0.77	0.73	0.71
The radius of gyration of the unimer chain $Rg/Å$	11	11	11	11
Core radius of the core $R_{core}/Å$	70	72	74	75

Table 4-9: *Fit parameters from Pederson model used to 5.0 wt% P123/$D_2O_{(85\ wt\%)}$ /d-$EtOH_{(15\ wt\%)}$ at difference temperature.*

4.4.3. Effect of ethanol content

Figure 4-24 shows the evolution of the SANS spectra of 5.0 wt% P123 at different ethanol concentration (0, 8 and 15 wt% d-ethanol). Datasets have been offset by a factor of 3, analysis of these data shows that the core radius and subsequently the aggregation number of the micelles decrease steadily with an increase in the ethanol concentration but their volume fraction of hard spheres in solution remains almost unchanged Table 4.10, consistent with a decrease in diffusion coefficient. The observed results indicate that, in presence of ethanol, an increased swelling of the PEO blocks in the corona region compensates for the decrease in the aggregation number of the micelles [22].

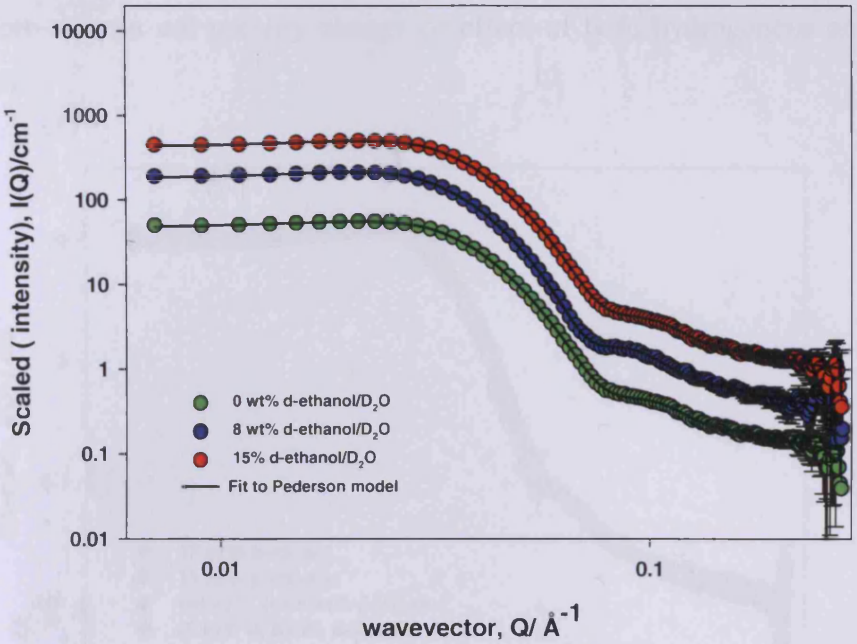

Figure 4-24: *SANS data (symbols) and data fits (solid curves) of 5.0 wt % P123 in (0, 8, and 15 wt%) of d-EtOH at 25°C. Data have been offset by a factor of 3.*

Deuterated ethanol concentration, wt%	0	8	15
Aggregation number N_{agg} ± 1.3	87.3	62.6	43.0
Volume fraction of solvent in the core Φ_{sol} ± 0.006	0.23	0.27	0.30
Radius of gyration of PEO in the corona *Rg* /Å ± 0.05	8.4	9.2	11.5
Incoherent background scattering B/cm^{-1} ± 0.007	0.17	0.16	0.16
Volume fraction of hard spheres in solution Φ_{HS} ± 0.001	0.097	0.10	0.11
interaction radius R_{int}/Å ± 0.8	35.6	34.6	31.3
Polydispersity σ_{core} ±0.04	0.55	0.64	0.90
The radius of gyration of the unimer chain *Rg*/Å	11.2	10.9	11.1
Core radius of the core R_{core} /Å	77.0	72.8	69.9

Table.4-10*: Fit parameters from Pederson model used to 5.0 wt% P123 in (0, 8, and 15 wt%) of d-EtOH at 25°C.*

4.4.3.1. Effect of h- and d-ethanol mixtures on Pluronic scattering

Figure 4-25 presented the scattering data of 5.0 wt% P123 in 15 wt% hydrogenous and deuterated ethanol either separated (15 wt% h-ethanol and 15 wt% d-ethanol) or mixture (10 wt% h-ethanol + 5.0 wt% d-ethanol and (5.0 wt% h-ethanol +10 wt% d-ethanol. We can find from this figure the same scattering intensity for four cases;

therefore we can not see any change or effect of both hydrogenous and deuterated ethanol.

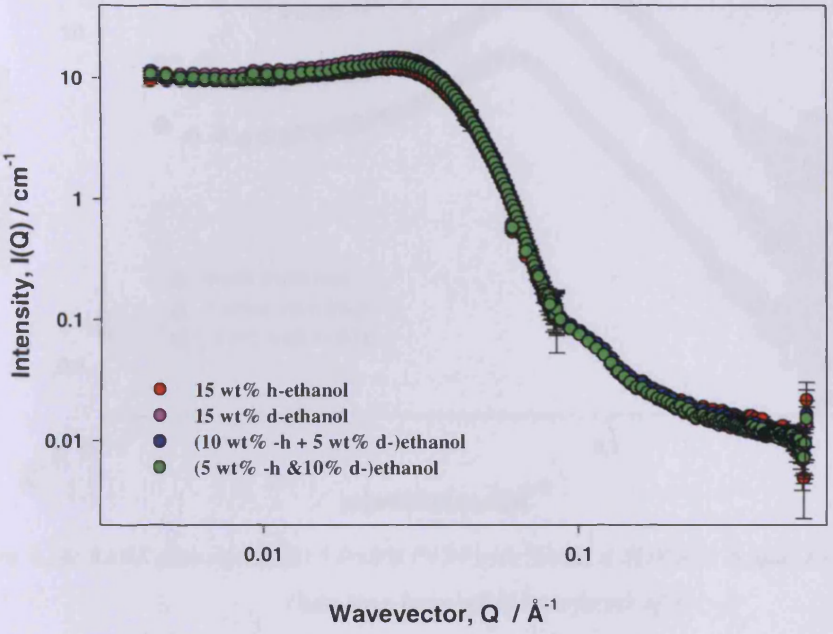

Figure 4-25: SANS data of 5.0 wt% P123 as a function of h- and d-ethanol concentration.

4.4.4. 5.0 wt% P123 with 50mM d-SDS

SANS data of 5.0 wt% P123 with 50mM d-SDS in 0, 8, and 15 wt% d-EtOH/D_2O solutions at fixed temperature, 25°C, It is shown in Figure 4-26. The SANS data not fit as was done in previous P123 systems. It can see the scattering intensity I(Q) dependence of ethanol concentration. Therefore, the addition of the ethanol leads to a higher I(Q) values, as see in this figure the peak shift to higher intensity with increases ethanol concentration especially at middle Q-value.

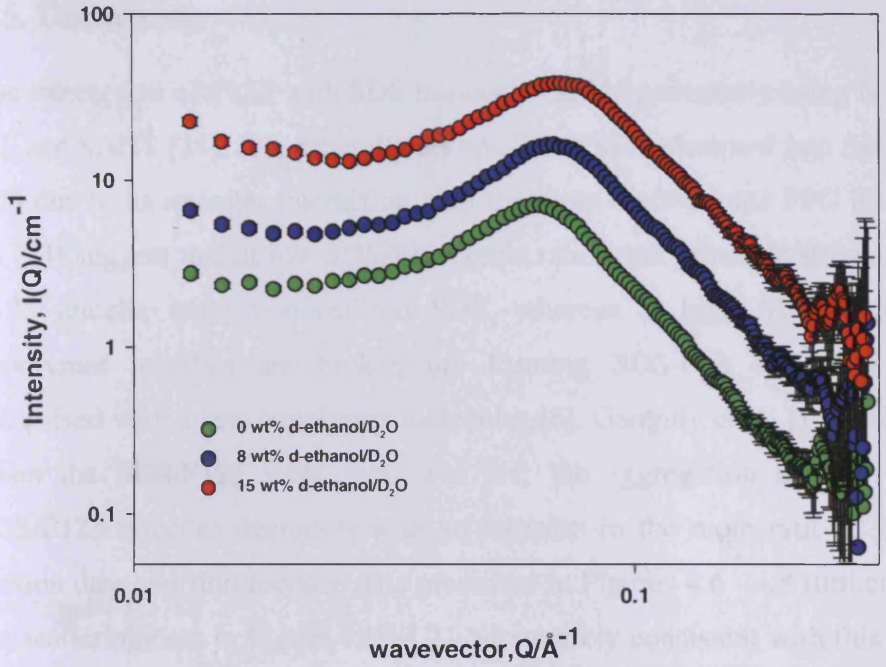

Figure 4.26: *SANS data (symbols) 5.0 wt% P123 with 50mM d-SDS in 0, 8, and 15 wt% d-EtOH/D_2O. Data have been offset by a factor of 3.*

Micellar spacing, d between two micelles for the P123-SDS is approximating given by:

$$d = 2\pi / q_{max} \qquad (4.8)$$

where; q_{max} is the scattering vector maximum, it can be see in Table 4.11, the Lamellar spacing decrease upon addition ethanol. This reduction of *d* value is accompanied by the mixing of ethanol in core and corona which leads to an increase in volume fraction of polar domain (rich in PPO) and to a decrease in water hydration of PEO blocks (PEO rich domain contains less solvent and less water molecules per PEO block) [16].

Concentration, ethanol / wt %	Q_{max} / $Å^{-1}$	d /Å
0.0	0.065	97
8.0	0.069	91
15.0	0.071	88

Table 4-11: *Micellar spacing values of 5.0 wt% P123/50mM d-SDS in various d-EtOH/D_2O concentrations at 25°C.*

4.5. Discussion

The interaction of P123 with SDS has been studied previously using NMR [23], DLS [1], and SANS [24]. It is generally accepted that SDS absorbed into the PPO core [10] [25] due to its stronger interaction with the more hydrophobic PPO block. Jansson et al. [24] suggest that at low SDS/P123 mole ratios, the principle structure resembles a P123 micelle with co-micellised SDS, whereas at high SDS/P123 mole ratios, copolymer micelles are broken up, forming SDS-rich surfactant micelles co-micellised with a few copolymer molecules [8]. Ganguly et al. [10] later showed that when the SDS/P123 mole ratio was 5:1, the aggregation number of the mixed SDS/P123 micelles decreases with an increase in the mole ratio [23]. The surface tension data and fluorescence data presented in Figures 4.6 - 4.8 further reinforced by the scattering data in Figure 4.19-4.21, are entirely consistent with this understanding within region i, SDS starts to bind to the pre-formed P123 micelle, displacing the polymer-bound fluorescence dye thereby driving it into an environment where it is less fluorescent (*i.e.* the more polar continuous phase), whilst not significantly affecting either the surface activity of P123 or the interfacial composition of the solution. At the onset of region ii, sufficient binding of SDS to P123 has occurred that the P123 micelle has "dissolved" forming a SDS-rich mixed micelles, resulting in a considerable loss of scattering intensity, and an increase in surface tension as either the material is stripped from the interface or replaced by less surface active species.

The composition of the mixed micelles extracted from the SANS analysis suggests a largely SDS character, *viz* α(SDS)=35(±5)% for [P123]=0.2 wt%/[SDS]=0.5mM (molar ratio 150). The transition from P123-rich to SDS-rich mixed micelles continues into region iii, commensurate with the regeneration of significant numbers of ionic mixed micelles (the [SDS] is too low to form pure SDS micelles) into which the fluorescent dye is now solubilised driving the increase in fluorescence intensity. Now, α(SDS) = 5(±0.5)% for [P123]=0.2wt%/[SDS]=0.5mM (molar ratio 1500).

4.6. Conclusion and further work

The effect of ethanol on P123 micellization has been studied using different complimentary techniques, including surface tension, fluorescence, viscosity, PGSE-NMR and SANS. Upon addition of ethanol to P123/water solutions, the CMC of the polymer is largely invariant. There is an increase in viscosity, but this reflects the increase observed in the background of the simple solvent. The self-diffusion coefficient of P123 decreases, somewhat contradicting the viscosity of the solvent. However, the aggregation number of the induce decreases. The surface tension and fluorescence is shown to give complimentary estimates of the various CMCs present in the P123/SDS/ethanol/water system. SANS and PGSE-NMR were used to investigated the structural aggregation features of Pluronic P123 with varying [SDS], [ethanol] and temperature. These results show the aggregation behaviour of P123 is sensitive to changes in temperature of the solution.

In the future work could go in a number of directions, the same set of techniques, such as, used the reverse kind of architecture of Pluronic with PEO as the middle block, i.e., PPO-PEO-PPO, exists and offers great new possibilities which have not been discussed in the present study, and this system would also benefit from study across a wide range of concentrations and temperatures.

4.7. References

[1] J. Jansson, K. Schillen, G. Olofsson, R. C. da Silva, W. Loh, Journal of Physical Chemistry B 108 (2004) 82-92.
[2] B. Bharatiya, G. Ghosh, P. Bahadur, J. Mata, Journal of Dispersion Science and Technology 29 (2008) 696-701.
[3] N. J. Turro, B. H. Baretz, P. L. Kuo, Macromolecules 17 (1984) 1321-1324.
[4] P.C. Griffiths, N. Hirst, A. Paul, S. M. King, R. K. Heenan, R. Farley, Langmuir 20 (2004) 6904-6913.
[5] M. A. Safarpour, A. A. Rafati, H. Gharibi, M. R. Sameti, Journal of the Chinese Chemical Society 46 (1999) 983-991.
[6] P. Alexandridis, J. F. Holzwarth, T. A. Hatton, Macromolecules 27 (1994) 2414-2425.
[7] G. Wanka, H. Hoffmann, W. Ulbricht, Macromolecules 27 (1994) 4145-4159.
[8] E. Hecht, H. Hoffmann, Langmuir 10 (1994) 86-91.
[9] D. L. Zhou, P. Alexandridis, A. Khan, Journal of Colloid and Interface Science 183 (1996) 339-350.
[10] R. Ganguly, V. A. Aswal, P. A. Hassan, I. K. Gopalakrishnan, S. K. Kulshreshtha, Journal of Physical Chemistry B 110 (2006) 9843-9849.
[11] L. Zheng, C. Guo, J. Wang, X. F. Liang, S. Chen, J. H. Ma, B. Yang, Y. Y. Jiang, H. Z. Liu, Journal of Physical Chemistry B 111 (2007) 1327-1333.
[12] K. M. Park, J. W. Bae, Y. K. Joung, J. W. Shin, K. D. Park, Colloids and Surfaces B-Biointerfaces 63 (2008) 1-6.
[13] M. M. Youssry, F. F. Asaro, L. L. Coppola, L. L. Gentile, I. I. Nicotera, Journal of Colloid and Interface Science 342 (2010) 348-353.
[14] R. C. da Silva, G. Olofsson, K. Schillen, W. Loh, Journal of Physical Chemistry B 106 (2002) 1239-1246.
[15] Zhao Yurong, Chen Xiao, Yang Chunjie, Zhang Guodong, Journal of Physical Chemistry B 111 (2007) 13937.
[16] S.S. Soni, G. Brotons, M. Bellour, T. Narayanan, A. Gibaud, Journal of Physical Chemistry B 110 (2006) 15157-15165.
[17] J.S. Pedersen, M.C. Gerstenberg, Macromolecules 29 (1996) 1363-1365.
[18] J.S. Pedersen, M.C. Gerstenberg, Colloids and Surfaces A 213 (2003) 175-187.
[19] J. Joseph, C.A. Dreiss, T. Cosgrove, J.S. Pedersen, Langmuir 23 (2007) 460-466.
[20] N. W. Aschcroft, J. Lekner, Physical Review 145 (1966) 83-90.
[21] P. Alexandridis, T.A. Hatton, Colloids and Surfaces A 96 (1995) 1-46.
[22] R. Ganguly, V.K. Aswal, P.A. Hassan, I.K. Gopalakrishnan, J.V. Yakhmi, Journal of Physical Chemistry B 109 (2005) 5653-5658.
[23] M. Almgren, J. Vanstam, C. Lindblad, P.Y. Li, P. Stilbs, P. Bahadur, Journal of Physical Chemistry 95 (1991) 5677- 5684.
[24] J. Jansson, K. Schillen, M. Nilsson, O. Soderman, G. Fritz, A. Bergmann, O. Glatter, Journal of Physical Chemistry B 109 (2005) 7073-7083.
[25] E. Hecht, K. Mortensen, M. Gradzielski, H. Hoffmann, Journal of Physical Chemistry 99 (1995) 4866-4874.

Chapter 5: Phase Behaviour of Concentrated Pluronics

5. Context

Pluronic P123 $(PEO)_{20}$-$(PPO)_{70}$-$(PEO)_{20}$ triblock copolymer is an important non-ionic surfactant that has been extensively used in numerous applications such as detergency, foam formation, dispersion stabilization, and drug delivery [1-3]. Depending on the concentration and temperature, it is capable of building different structures in water as can be seen from a typical phase diagram of P123-water system such as that determined by Wanka et al. [4]. Typically, with increasing P123 concentration, aggregates such as micelle, cubic, hexagonal, and lamellar phases are formed in aqueous solutions.

Hamley has been investigating [5] the structural properties of the P123-water system using a variety of experimental techniques including surface tension, ^{1}H-NMR spectrum, rheology, dynamic light scattering (DLS), polarizing optical microscopy (POM), small-angle neutron scattering (SANS), small-angle X-ray scattering (SAXS), and differential scanning calorimetry (DSC). Their investigations have improved the understanding of the P123 phase behaviour yet its intrinsic microphase behaviour is still ambiguous.

Recently, Zhao et al. [6] have simulated the phase behaviour of the aqueous P123 system in the mesoscopic region ($0 < [P123] < 100$) using dynamic density functional method, where molecular dynamics was used to simulate microphase separation of P123/water binary mixtures. Their results show that, with an increase in concentration of P123, a variety aggregates such as micelle, hexagonal, and lamellar phases are formed respectively at concentrations 3~30 wt% for micelle, 32~55 wt% for hexagonal, and 65~80 wt% for lamellar phase. It can be concluded that the mesoscopic simulation method is a valuable tool for the description of mesoscale morphology formation and gives an insight into the process of aggregate formation.

In a previous chapter (Chapter 4), we studied the mixed micellization of P123 and SDS in water/ethanol solutions using surface tension, fluorescence, viscosity, PGSE-NMR and SANS. In this chapter, we focus on the interaction and structures of the Pluronic at higher [P123] from 10-30 wt% as a function of both [< [ethanol] < 15 wt%] and [< [SDS] < 25 wt%] using PGSE-NMR and SANS, over that region where only micellar structures exist.

5.1. Pulsed-gradient spin-echo NMR study

PGSE-NMR experiments were carried out on the Bruker AMX360 NMR spectrometer, operating at 360 MHz using the stimulated echo-sequence as described elsewhere [7, 8] More details may be found in chapters two and three.

5.1.1. Self-diffusion coefficient

Attenuation functions describing the diffusion of P123 in ethanol/ D_2O mixtures are shown in Figures 5-1 to 5-3, for 10, 15 and 20 wt% P123 in 0, 8 and 15 wt% ethanol/D_2O mixtures respectively. The decays of all signals were non-exponential, indicating that all systems showed some slight polydispersity.

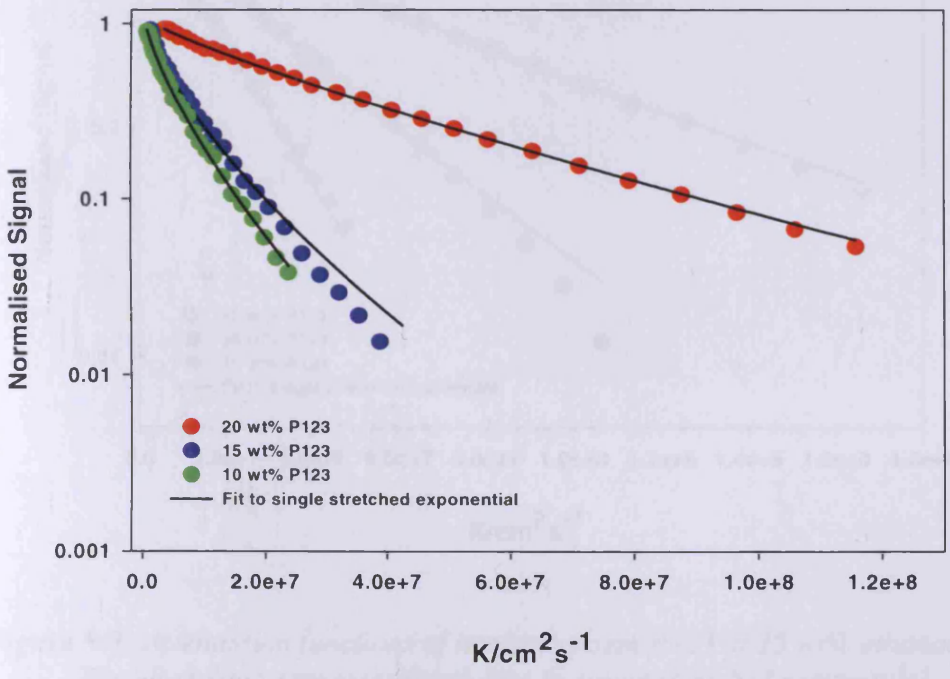

Figure 5-1: Attenuation functions of binary system P123 in D_2O. The black lines represent fitted data to single stretched exponential.

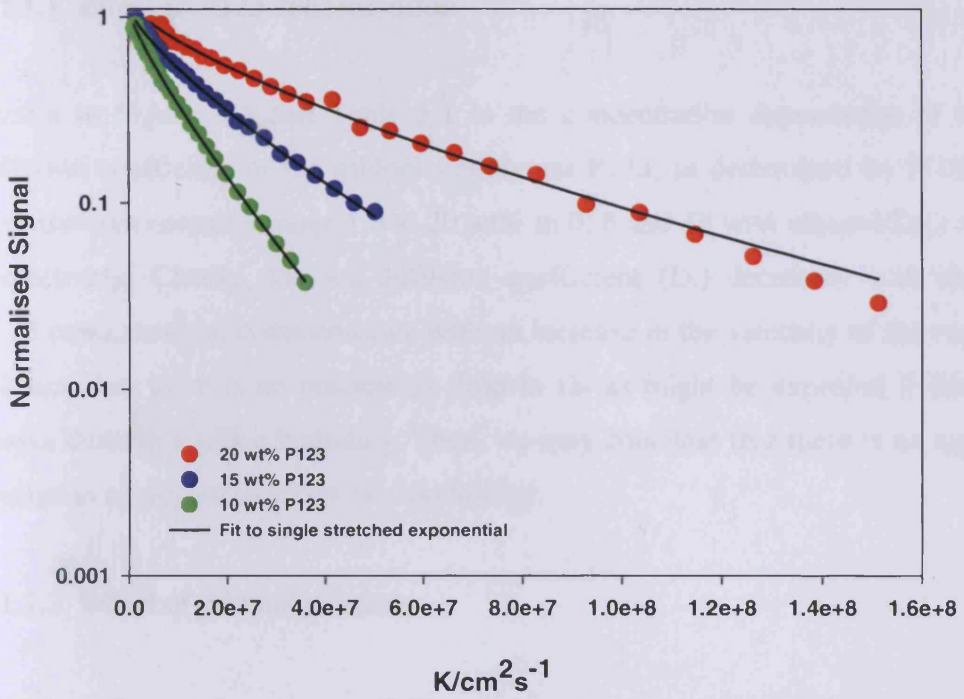

Figure 5-2: *Attenuation functions of ternary system P123 in 8.0 wt% ethanol/D_2O. The black lines represent fitted data to single stretched exponential.*

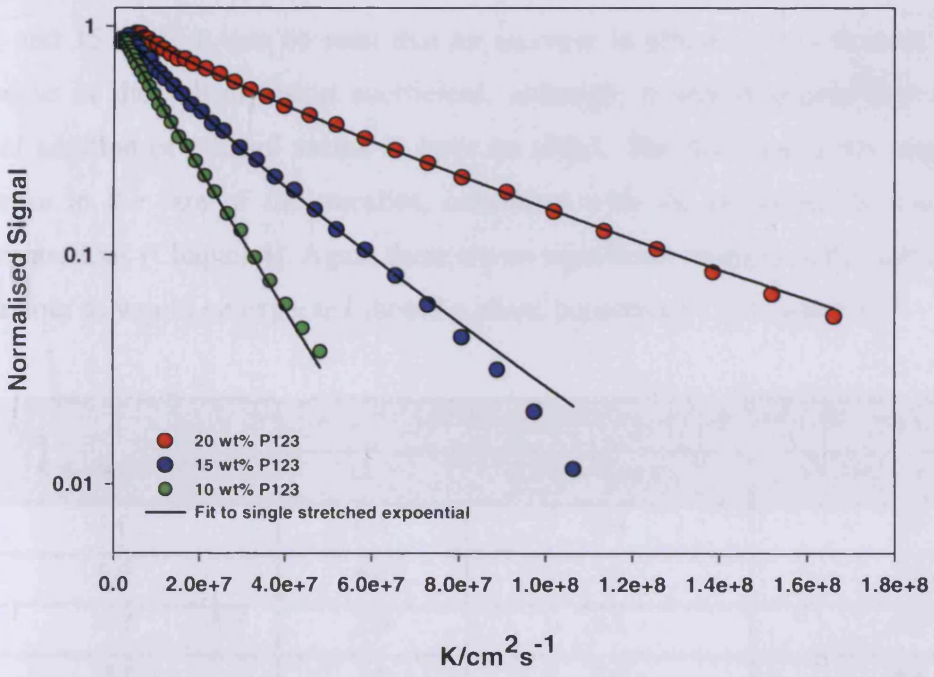

Figure 5-3: *Attenuation functions of ternary system P123 in 15 wt% ethanol/D_2O. The black lines represent fitted data to single stretched exponential.*

5.1.1.1. Effect of P123 concentration

Shown in Figure 5-4 and Table 5-1 is the concentration dependence of the self-diffusion coefficient of the triblock copolymer P123, as determined by PGSE-NMR over the concentration range 1.0 to 20 wt% in 0, 8 and 15 wt% ethanol/D_2O mixtures respectively. Clearly, the self-diffusion coefficient (D_s) decreases with increasing P123 concentration, commensurate with an increase in the viscosity of the copolymer solution, but there is no precipitous drop in Ds as might be expected if the system passes through a phase boundary. Thus, we may conclude that there is no significant change in aggregate structure or morphology.

5.1.1.2. Effect of ethanol content

Addition of ethanol to aqueous P123 solutions has a significant influence on the self-assembly behaviour of these copolymers. Ethanol is known to be a good solvent for both PEO and PPO blocks of the PEO-PPO-PEO triblock copolymer [9]. Figure 5-4 and Table 5-1 shows the effect of the ethanol on the self-diffusion coefficient for a range of P123 concentrations from 1.0 to 20 wt% at different ethanol concentrations 0, 8 and 15 wt%. It can be seen that an increase in ethanol concentration leads to decrease in the self-diffusion coefficient, although, it would appear that only the initial addition of ethanol seems to have an effect. The decrease in Ds suggests an increase in the size of the micelles, consistent with the behaviour at lower P123 concentrations (Chapter 4). Again there are no significant changes in the self diffusion behaviour as would be expected should a phase boundary be encountered.

Conc., P123/ wt%	Self-diffusion coefficient / (10^{-11} ± 5.0 %) / m^2s^{-1}		
	D_2O	8.0 wt% EtOH/D_2O	15.0 wt% EtOH/D_2O
1.0	5.1	2.4	2.2
5.0	4.0	1.6	1.5
10.0	2.0	1.1	1.0
15.0	1.4	0.6	0.4
20.0	0.4	0.3	0.2

Table 5-1: *Self-diffusion coefficient of P123 in 0, 8 and 15 wt% h-ethanol/D_2O %EtOH/D_2O solutions.*

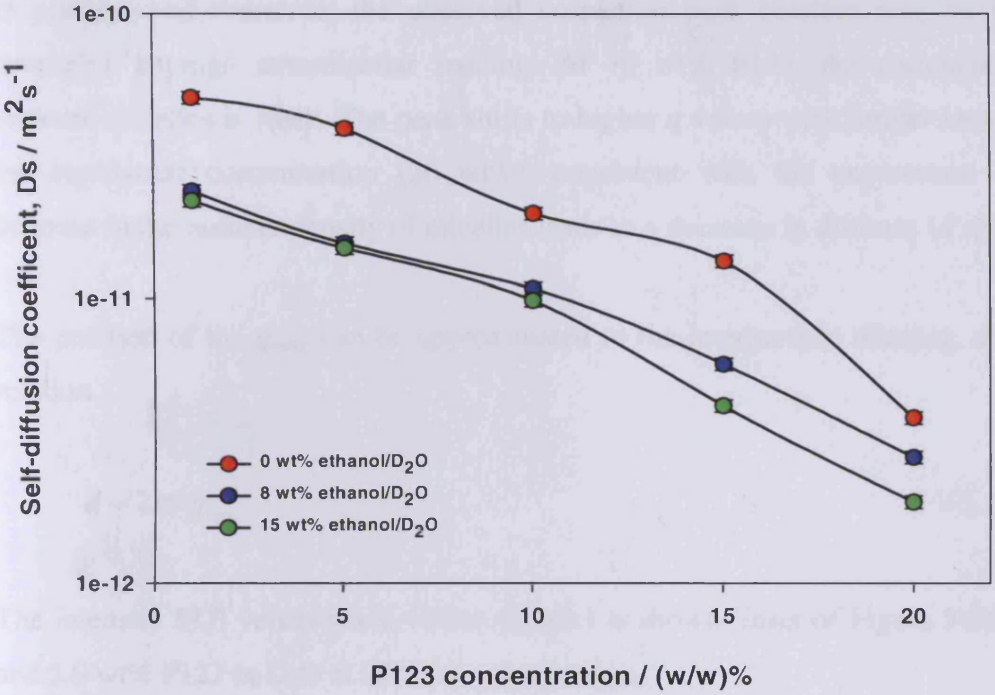

Figure 5-4: *Self-diffusion coefficient as a function of P123 in h-ethanol/D_2O mixtures. The black lines are guides to the eye.*

5.2. Small-angle neutron scattering study

Small–angle neutron scattering SANS measurements were performed as described previously [9] and more details may be found in chapter three.

5.2.1. Scattering of P123 in ethanol/ D_2O mixtures

Small-angle neutron scattering was used to characterise aqueous solutions of P123 copolymer at three different concentrations (10, 20, and 30 wt%) at 25°C and in ethanol/D_2O mixtures over the range 0 < [ethanol] < 15 wt%.

5.2.1.1. Effect of P123 concentration

Figures 5-5 to 5-7 shown representative SANS spectra. For 20 wt%, a peak emerges in the low ***q*** region of the scattering curve, indicating that the micelles are correlated

in position and therefore, the observed correction peak position may be used to determine average intermicellar spacing. At 10 wt% P123, the correlation peak between micelles is weak. The peak shifts to higher q values with further increases in the copolymer concentration (30 wt%), consistent with the expectation that an increase in the number density of micelles leads to a decrease in distance (d spacing).

The position of the q_{max} can be approximated to the interparticle distance, d, by the relation.

$$d \approx 2\pi / q_{\max} \tag{5.1}$$

The intensity I(Q) versus wave vector (Q) plot is shown (inset of Figure 5-5) for 0.2 and 5.0 wt% P123 in D_2O at 25°C, for comparison.

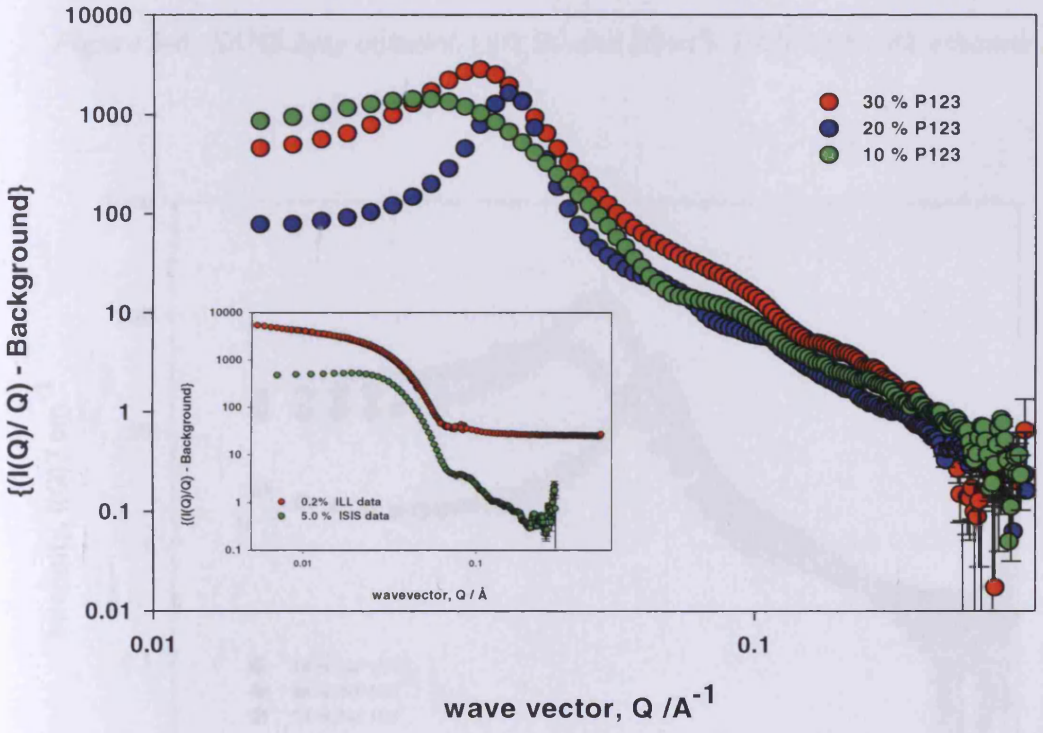

Figure 5-5: SANS data (symbols) 10, 20 and 30 wt% P123/D_2O, inset shows data for 0.2 and 5.0 wt% P123 for comparison.

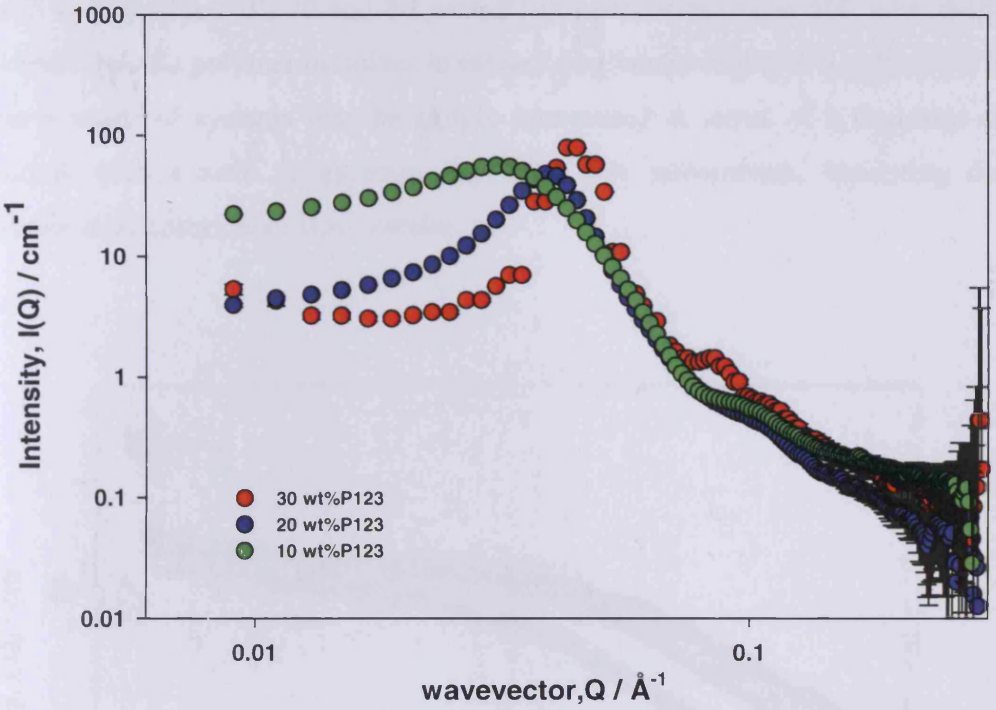

Figure 5-6: SANS data (symbols) 10, 20 and 30 wt% P123 in 8 wt% ethanol/ D_2O.

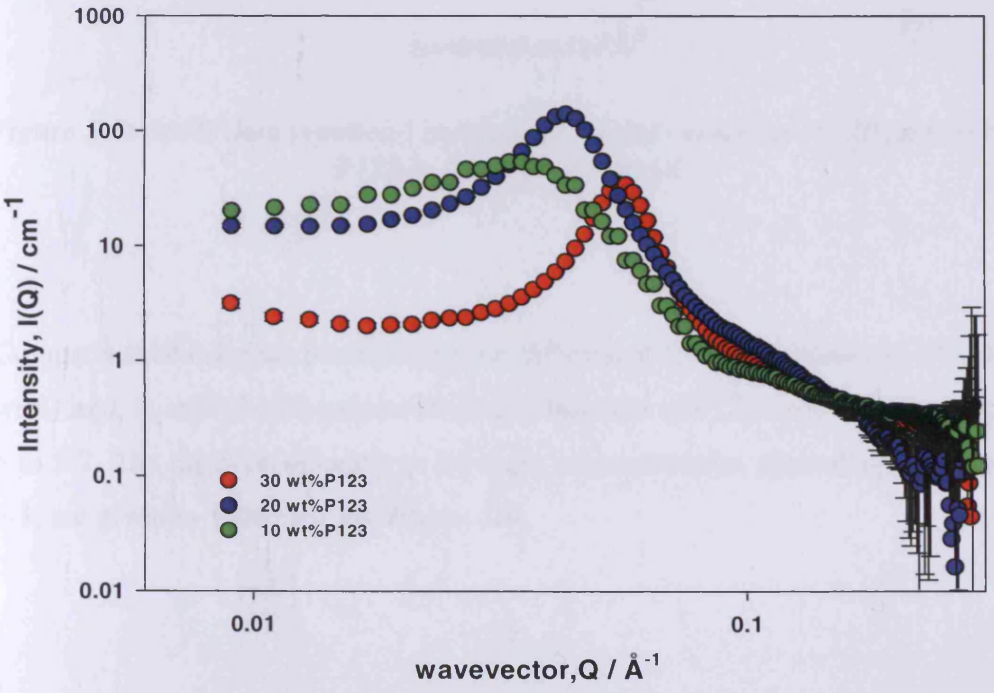

Figure 5-7: SANS data (symbols) 10, 20 and 30 wt% P123 in 15 wt% ethanol/D_2O.

The SANS data for 10, 20 and 30 wt% P123 concentrations in 100 wt% d-ethanol, evidence that the polymer dissolves in ethanol is given in Figure 5-8, where the SANS from a series of systems may be simply interpreted in terms of a Gaussian coil in solution, with a radii of gyration (R_g) of a few nanometres, indicating discrete polymer molecules rather than micelle.

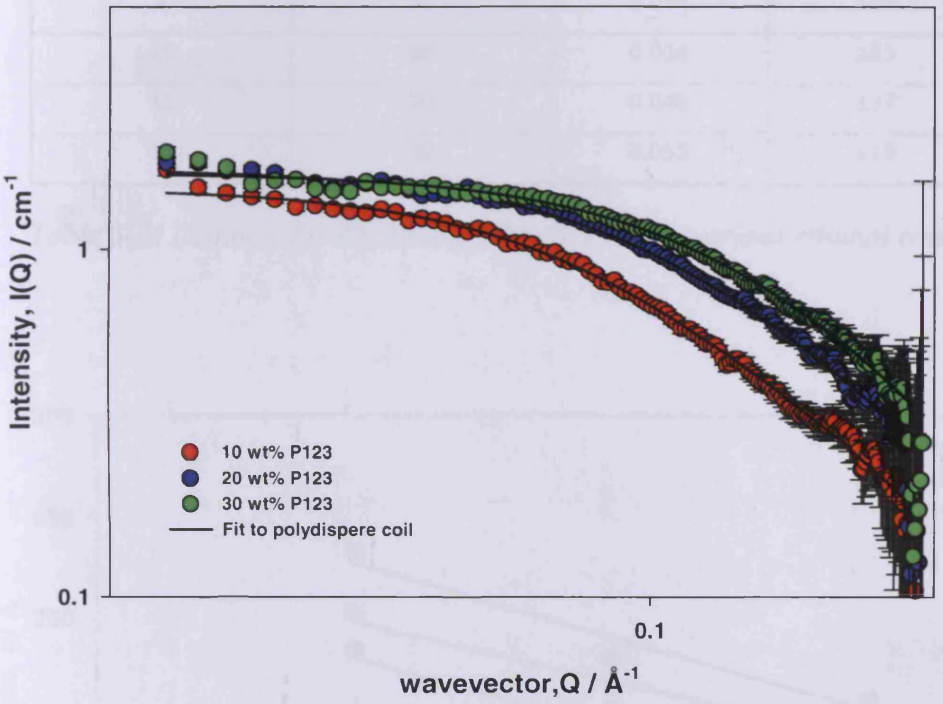

Figure 5-8: *SANS data (symbols) and data fits (solid curves) of 10, 20 and 30 wt% P123 in 100 wt% d-ethanol.*

Comparison of the peak positions for the different P123 concentrations (10, 20 and 30 wt%) in 0, 8, and 15 wt% ethanol D_2O as a function of P123 concentration, Figures 5-5 to 5-7. The micellar separations for these concentrations, according to the equation 5-1, are given in Table 5-2 and Figure 5-9.

Total concentrations, wt%		Peak Position	
Ethanol	*P123*	$q_{max}/Å^{-1}$	*d/Å*
0	10	0.027	233
0	20	0.035	180
0	30	0.039	160
8	10	0.031	203
8	20	0.039	160
8	30	0.044	145
15	10	0.034	185
15	20	0.046	137
15	30	0.055	115

Table 5-2: *Distance for 10, 20 and 30 wt% P123 in various ethanol concentrations.*

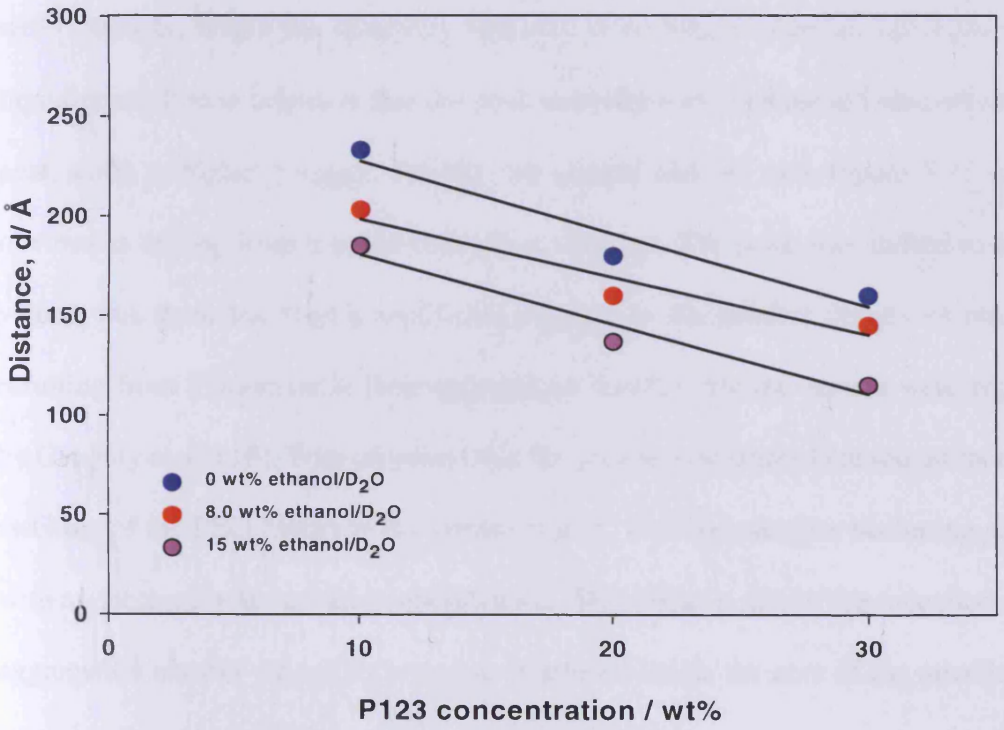

Figure 5-9: *Peak position in the SANS data of P123 as a function of [P123] in different ethanol concentrations at 25°C.*

5.2.1.2. Effect of ethanol content

Addition of ethanol has a significant effect on the self-assembly behaviour of these copolymers in solution. An increase in ethanol content in the aqueous copolymer solutions leads to an increase in CMC and CMT and a decrease in the aggregation number of the copolymer micelles [9]. Figures 5-10 to 5-12 shows the effect of ethanol on the SANS spectra of 10, 20 and 30 wt% P123 solutions in different ethanol concentrations 0, 8, and 15 wt% respectively. ***Firstly***, from Figure 5-10 it can be seen that the 10 wt% sample exhibits micelle-like scattering and the shift to higher Q-values of the correlation peak positions, suggests smaller micelles, similar to the 5.0 wt% case (Chapter 4). ***Secondly***, Figure 5-11 shows the SANS data obtained for 20 wt% solutions, where the scattering observed is no longer micellar, but more likely liquid crystalline in origin, is that the peak sharpens with increasing [ethanol] and the peak shifts to higher q values. ***Finally***, the sample with 30 wt% Figure 5-12 is very obvious as arising from a liquid crystalline structure. The peak was shifted to high q values; this there has been a significant increase in the number density of micelles, resulting from a decrease in their aggregation number. Similar results were reported by Ganguly et al. [10]. Who proposed that the presence of ethanol caused an increased swelling of the PEO blocks in the corona region, with the micelles becoming smaller with an increase in the ethanol concentration. This effect is due to the reduction of the aggregation number caused by presence of ethanol inside the core of the micelles and is concomitant with the increase in volume fraction [11].

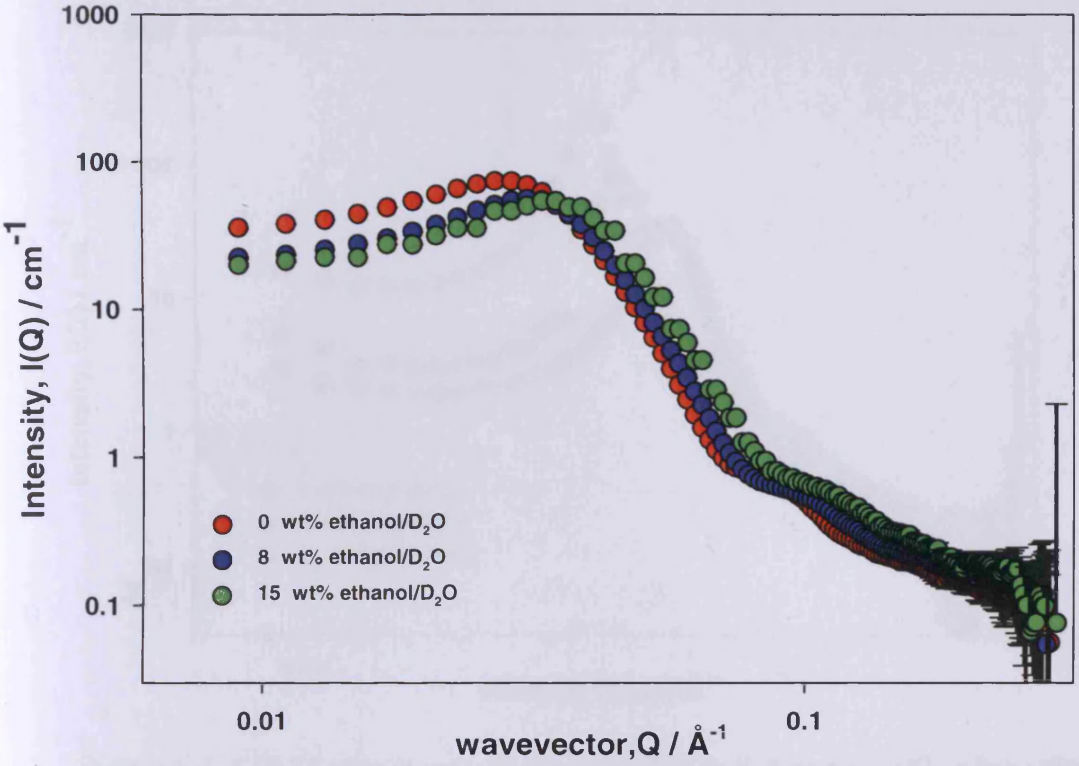

Figure 5-10: SANS data (symbols) 10 wt% P123 in 0, 8 and 15 wt% ethanol/D_2O.

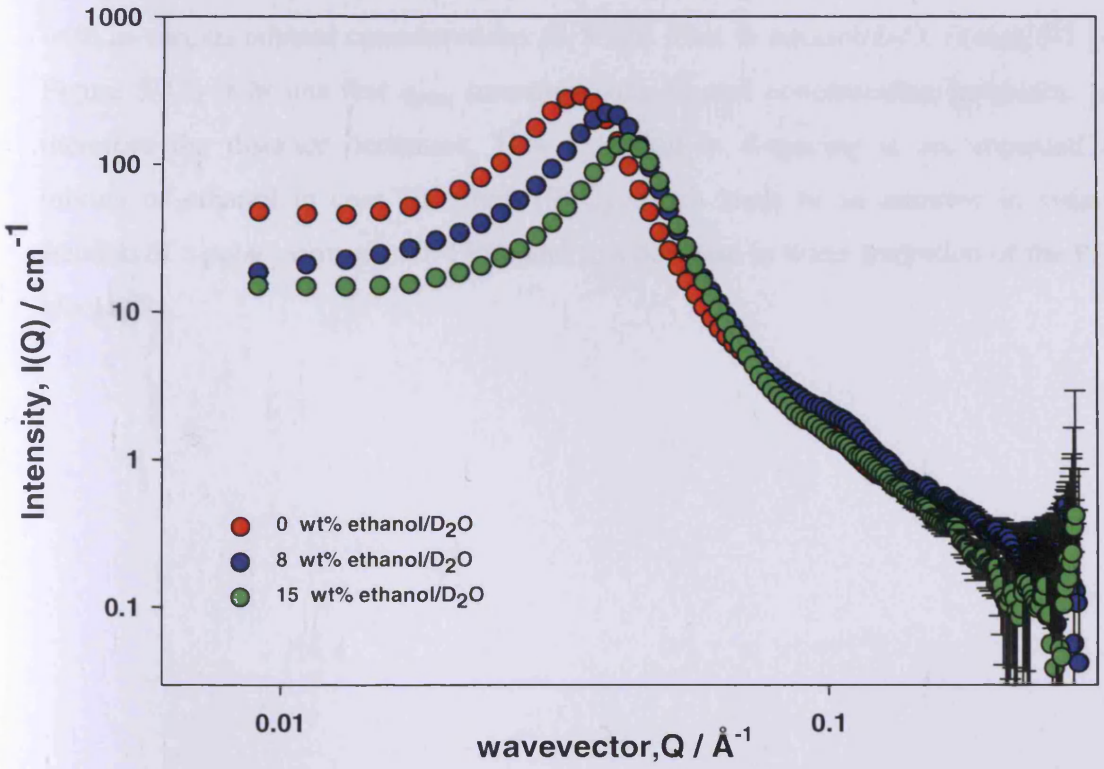

Figure 5-11: SANS data (symbols) 20 wt% P123 in 0, 8 and 15 wt% ethanol/D_2O.

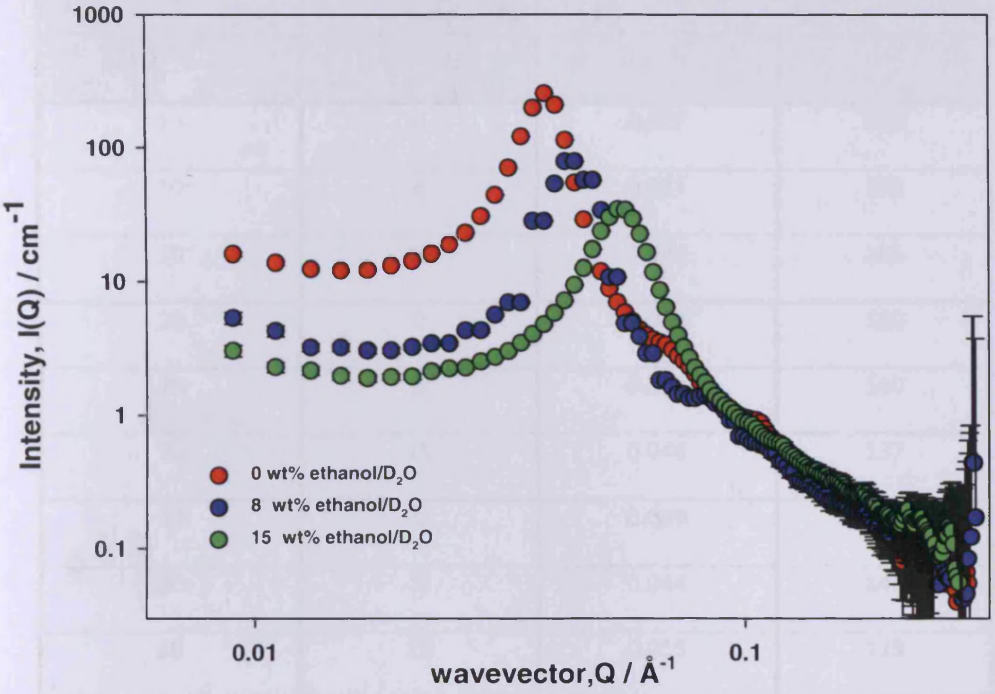

Figure 5-12: *SANS data (symbols) 30 wt% P123 in 0, 8 and 15 wt% ethanol/D_2O.*

Comparison of the peak position q_{max} and distance (d-spacing) for the 10, 20, and 30 wt% in various ethanol concentrations (0, 8 and 15wt % ethanol/D_2O, (Table 5-3 and Figure 5-13) indicates that q_{max} increases with ethanol concentration increases, and therefore the distance decreases. This reduction in d-spacing is accompanied by mixing of ethanol in core and shell (PEO) which leads to an increase in volume fraction of a polar domain (rich PPO) and to a decrease in water hydration of the PEO blocks [9].

Total concentrations, wt%		Peak Position	
P123	*Ethanol*	$q_{max}/Å^{-1}$	*d/Å*
10	0	0.027	233
10	8	0.031	203
10	15	0.034	185
20	0	0.035	180
20	8	0.039	160
20	15	0.046	137
30	0	0.039	160
30	8	0.044	145
30	15	0.055	115

Table 5-3: *Distance for 10, 20 and 30 wt% P123 in various ethanol concentrations.*

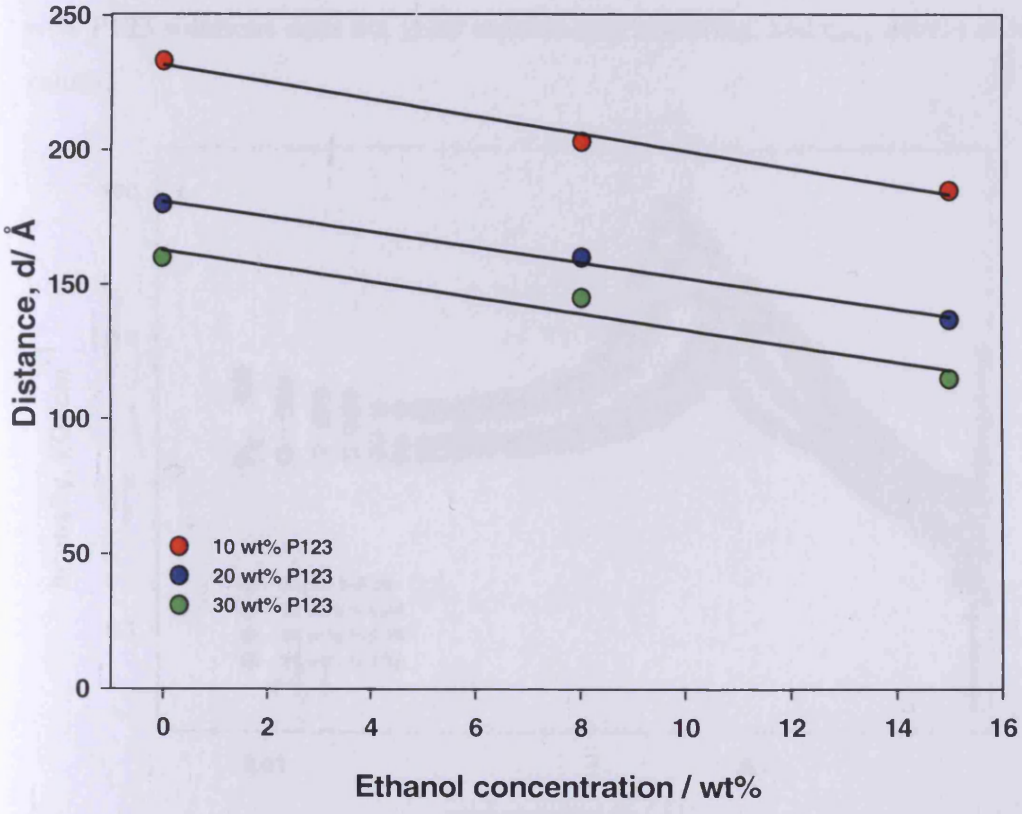

Figure 5-13: *Peak position in the SANS data of P123 as a function of [ethanol] for 10, 20 and 30 wt% P123.*

5.2.2. Scattering of P123-SDS in ethanol/D_2O mixtures

Anionic surfactants such as sodium dodecyl sulfate (SDS) are in general, known to affect aggregation behaviour of the Pluronic in the same manner as ethanol. At first, consider the series with 30 wt% P123 with SDS, where we have examined the effect of addition of SDS on the micellar size for copolymer solutions containing 0, 8 and 15 wt% ethanol.

The analysis of the structure of the mixed P123/SDS micelles assumes that the SDS molecules are dissolved in the micellar core. This assumption was made on the basis of a report that the interaction between the SDS and the PPO units is significantly stronger than that between the SDS and PEO units [12].

5.2.2.1. Effect of SDS on the P123-SDS interaction

Figure 5-14 shows the scattering pattern of 30 wt% P123 with a range of h-SDS concentrations from 5.0 to 25 wt% in D_2O. It can be seen that addition of SDS to 30 wt% P123 solutions does not yield micelle-like scattering, and q_{max} moves to higher q values.

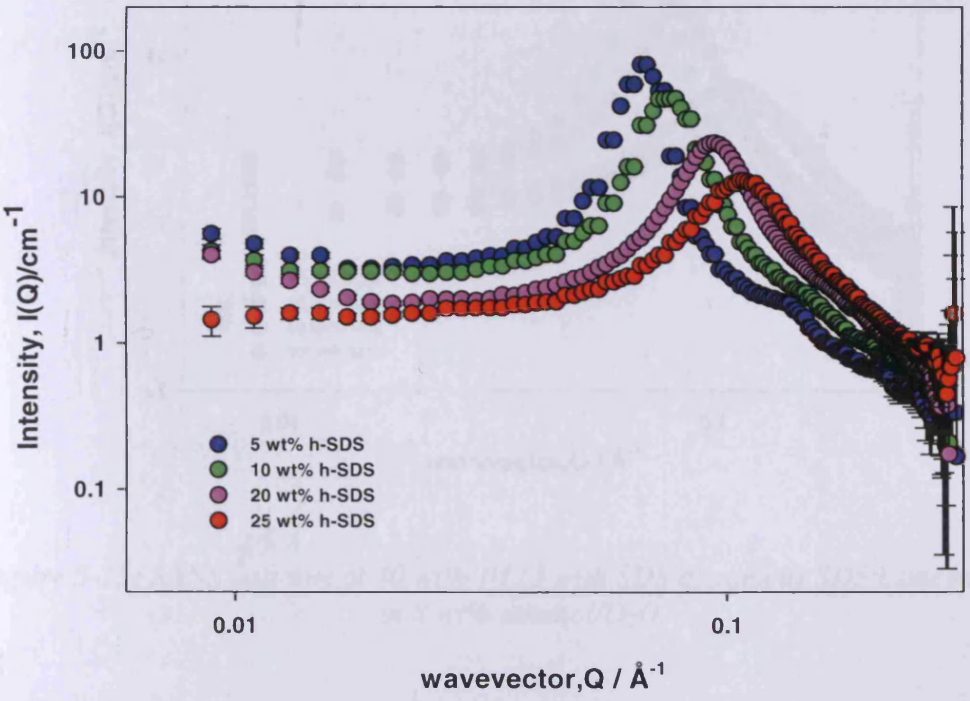

Figure 5.14: SANS patterns of 30 wt% P123 with SDS at various SDS concentrations in D_2O.

5.2.2.2. Effect of SDS on the P123-SDS-ethanol interaction

Figures 5-15 and 5-16 show the scattering from 30 wt% P123 with a range of h-SDS concentrations from 5.0 to 25 wt% in 8 and 15 wt% ethanol/D_2O mixtures respectively. It can be seen that micelle-like scattering is not observed, with peaks being much broader than in the pure water case, with q_{max} moving to higher q values, although the effect is stronger than in the pure water case, in the same time shows the scattering intensity decrease with increasing SDS concentration.

5.2.2.3. Effect of ethanol on the P123/SDS/ethanol interaction

Figures 5-15 and 6-16 shows the scattering pattern from 30 wt% P123 and the effect of ethanol. On addition of ethanol, the peak exhibited by moves to higher q-values indicating reduction in d-spacing is accompanied by mixing of the ethanol in core and shell.

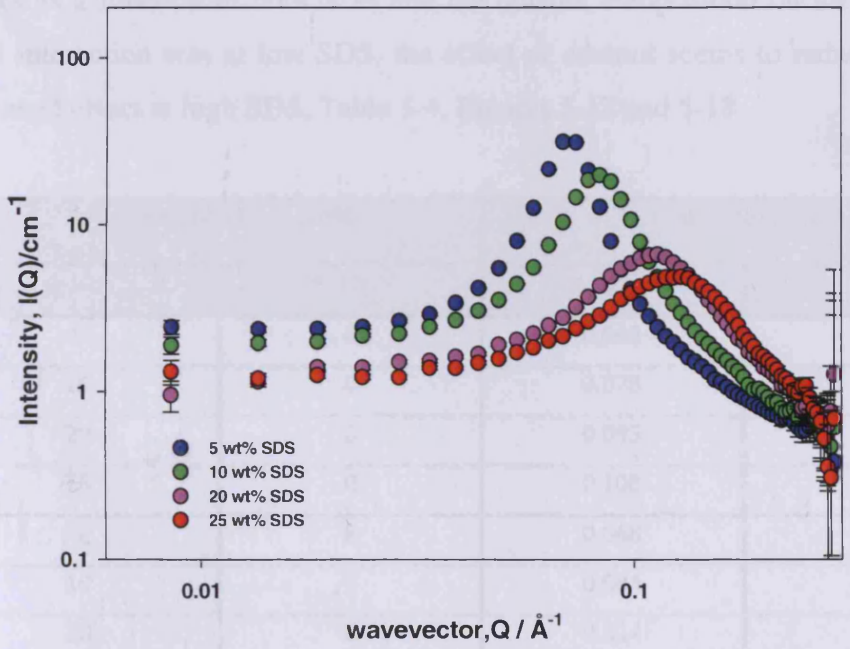

Figure 5-15: *SANS patterns of 30 wt% P123 with SDS at various SDS Concentrations in 8 wt% ethanol/D_2O.*

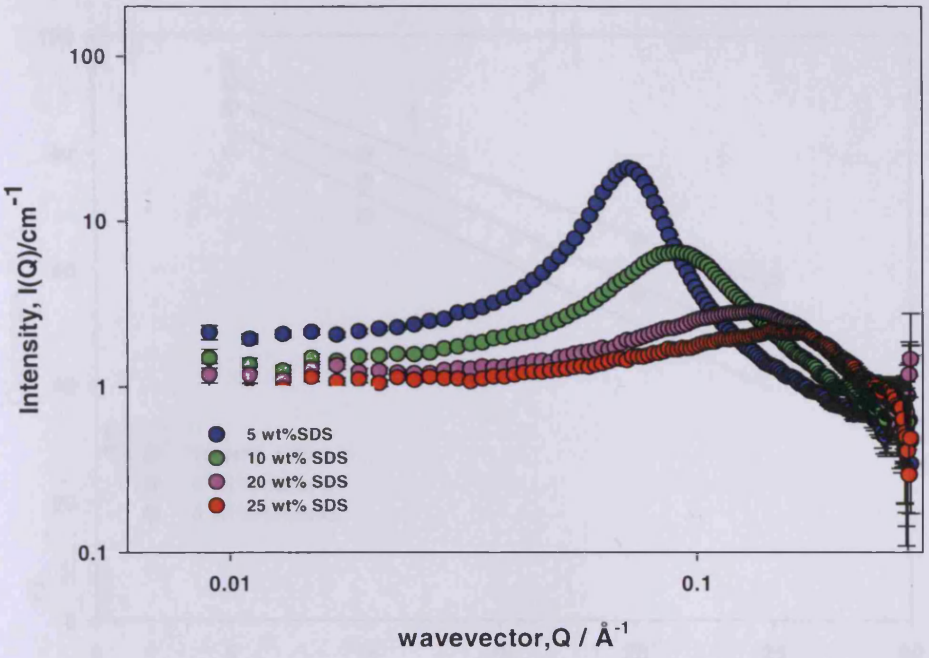

Figure 5-16: *SANS patterns of 30 wt% P123 with SDS at various SDS Concentrations in 15 wt% ethanol/D_2O.*

Comparison of the peak position (d spacing) for 30 wt% P123/h-SDS/ethanol mixtures as a function of both SDS and the ethanol composition on the P123-SDS-ethanol interaction was at low SDS, the effect of ethanol seems to reduce, whereas, pronounced effect at high SDS, Table 5-4, Figures 5-17 and 5-18.

Total concentrations ,wt%		Peak Position	
h-SDS	*Ethanol*	$q_{max}/Å^{-1}$	*d/Å*
5	0	0.068	95
10	0	0.078	80
20	0	0.095	65
25	0	0.108	58
5	8	0.068	92
10	8	0.084	75
20	8	0.114	55
25	8	0.128	49
5	15	0.071	88
10	15	0.091	69
20	15	0.134	47
25	15	0.146	43

Table 5-4: *distance for 30 wt% P123 with SDS at various SDS concentrations.*

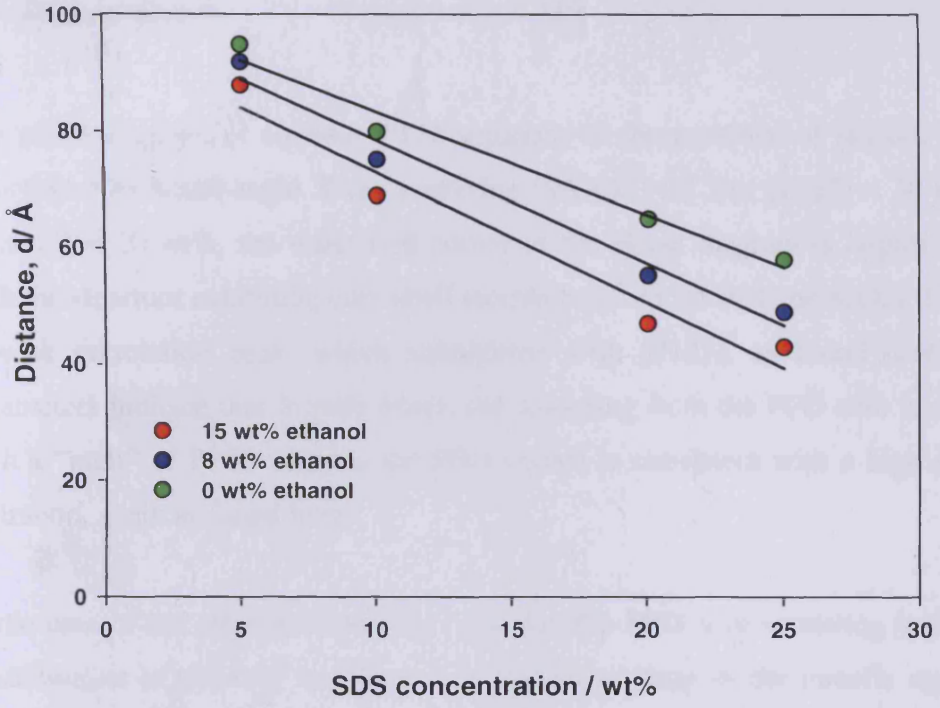

Figure 5-17: *Peak position in the SANS data of P123/SDS as a function of [SDS] of 30 wt% P123 at various ethanol concentrations.*

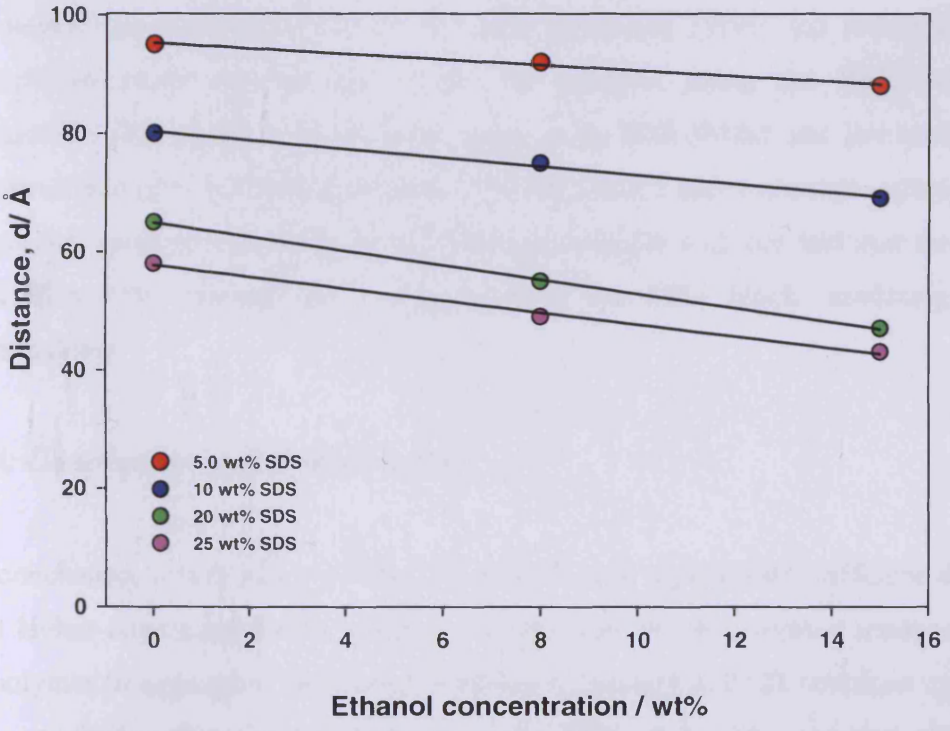

Figure 5-18: *Peak position in the SANS data of P123/SDS as a function of [ethanol] of 30 wt% P123 at various SDS concentrations.*

5.3. Discussion

The phase diagram of aqueous P123 solutions in the presence of ethanol has been determined by small-angle X-ray scattering (SAXS) [43]. For [P123] < 30 wt%, and [ethanol] < 20 wt%, the water-rich corner of the phase diagram is largely micellar, with the structure exhibiting core-shell morphology. At 20 wt% the SAXS data shows a weak correlation peak, which strengthens with [P123], as found here. The fit parameters indicate that in pure water, the scattering from the PPO core is consistent with a "melt" of PPO, whereas the PEO corona is consistent with a high degree of hydration, again as found here.

In the case of the ethanol-containing solutions, the PPO core scattering indicates the solubilisation of ethanol, and there is a significant drop in the micelle aggregation number, as with the analysis presented here. The core radius is approximately 45 Å, with a comparable shell thickness 35 Å, comparable to the insight gained here. Accordingly, the two studies report similar aggregation numbers.

At higher concentrations of P123 and with increasing [SDS] and [ethanol], strong correlation peaks emerge that render the analysis using the Pederson model intractable. The position of the peak scales with both [SDS] and [ethanol] with a characteristic ($\beta = 0.35$) that indicates both the ethanol and surfactant induce smaller structures (peak moves to higher Q values), consistent with the fact that the ethanol and SDS both interact more strongly with the PPO block, rendering it less hydrophobic.

5.4. Conclusion and Future work

In conclusion, it was observed that the behaviour is significantly different for lower and higher concentrations of both ethanol and SDS due to enhanced tendency of the copolymer to aggregate. Moreover, addition of ethanol to P123 solutions appears to have a similar effect to that addition of the SDS were more complex changes in stability and shape of the micelles were observed. Therefore, the aggregation

behaviour of Pluronic is sensitive to changes in both the SDS and the ethanol quantity.

Future work could go in a number of directions. The same set of techniques can be used P123 in the presence of other types of surfactant (e.g. cationic or non-ionic). The P123-SDS system could also be investigated at the full range of ethanol concentrations, up to 100 wt%, to determine the point at which micellization no longer occurs and the impact that ethanol rich environments have on the micellization process and interactions between polymer and surfactant. This system would also benefit from study across a wide range of temperatures.

5.5. References

[1] G. Wanka, H. Hoffmann, W. Ulbricht, Colloid and Polymer Science 268 (1990) 101-117.
[2] W. Brown, K. Schillen, M. Almgren, S. Hvidt, P. Bahadur, Journal of Physical Chemistry 95 (1991) 1850-1858.
[3] Z. Zhou, B. Chu, Macromolecules 27 (1994) 2025-2033.
[4] G. Wanka, H. Hoffmann, W. Ulbricht, Macromolecules 27 (1994) 4145-4159.
[5] Ian W. Hamley, Block Copolymers in Solution: Fundamental and Applications: John Wiley & Sons: Canada, (2005).
[6] Y.R. Zhao, X. Chen, C.J. Yang, G.D. Zhang, Journal of Physical Chemistry B 111 (2007) 13937-13942.
[7] P.C. Griffiths, A. Paul, P. Stilbs, E. Petterson, Macromolecules 38 (2005) 3539-3542.
[8] A. Paul, P.C. Griffiths, E. Pettersson, P. Stilbs, B.L. Bales, R. Zana, R.K. Heenan, Journal of Physical Chemistry B 109 (2005) 15775-15779.
[9] J. Armstrong, B. Chowdhry, J. Mitchell, A. Beezer, S. Leharne, Journal of Physical Chemistry 100 (1996) 1738-1745.
[10] R. Ganguly, V.K. Aswal, P.A. Hassan, I.K. Gopalakrishnan, J.V. Yakhmi, Journal of Physical Chemistry B 109 (2005) 5653-5658.
[11] S.S. Soni, G. Brotons, M. Bellour, T. Narayanan, A. Gibaud, Journal of Physical Chemistry B 110 (2006) 15157-15165.
[12] M. Almgren, J. Vanstam, C. Lindblad, P.Y. Li, P. Stilbs, P. Bahadur, Journal of Physical Chemistry 95 (1991) 5677-5684.

Chapter 6: Physicochemical Characterization of Responsive Polymers

6. Context

Stimuli-responsive polymers are materials which undergo dramatic conformational changes due to small changes in their environment and find application in photolithography, printing materials, non-linear optical materials and actuators. The most important systems from a biomedical point of view are temperature and pH. However, since these polymers are amphiphilic, they undergo self-organization in aqueous solution forming hydrophobic nanometre-sized domains that are able to solubilize water-insoluble organic compounds [1-4].

Temperature sensitive systems exhibit a critical solution temperature (CST) at which the phase of polymer and solution is changed in accordance with their composition. Those systems exhibiting monophasic above a certain temperature but phase separate below this temperature, have an upper critical solution temperature (UCST). On the other hand, polymer solutions that appear as monophasic below a specific temperature and biphasic above it, generally exhibit the so-called lower critical solution temperature (LCST) [5].

Alexander et al [6] have based their research on commercially available polyethylene glycol ethyl ether methacrylate (PEGMA-EE, Mn 246) and polyethylene glycol methyl ether methacrylate (PEGMA-ME, Mn 475). The co-solubility profiles of these monomers enabled aqueous solutions to be prepared at 4°C, and polymerization by atomic-transition radical polymerization ATRP) [7]. The versatility of the ATRP synthesis also allowed the preparation of "hybrid" block copolymers, named P6 and P7 here, composed of statistical sequences of PEGMA-EE246 with PEGMA-ME475, from which were grown an outer block of PEGMA-ME475, and their the characterization (Scheme 6-1 and Table 6-1). Solution properties of these polymers could be controlled by co-monomer content and addition sequence, with all the polymers containing PEGMA-EE 246 exhibiting a LCST.

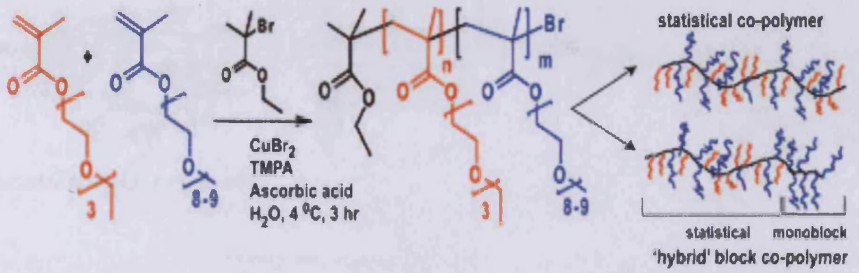

Scheme 6-1: Polymer synthesis and schematic of co-polymer structures. Figure adapted from Magnusson et al. Ref. [6]

Copolymer	Molar ratio n:m[a]	M_n[b]	M_w/M_n[b]	% m[c]	LCST,°C[d]
P6	Hybrid block g-PEGMA ME 475 ([n:m]:m) = 85:15:6	22.2	1.46	44	45
P7	Hybrid block g-PEGMA ME 475 ([n:m]:m)= 89:11:17	14.7	1.33	30	37

Table 6-1: The characterization of Hybrid P6 and P7.

where: (a) n:m = molar ratio of PEGMA-EE 246: PEGMA-ME 475; (b) From GPC (THF, poly(styrene) standards); (c) NMR integral; (d) From sharp increase in UV adsorption of solution in water at 550 nm[6].

Polymer-protein hybrids were prepared in an analogous manner. The polymerization from trypsin was carried out by adopting a previous polymerization method of "smart" PEGMA previously reported by Magnusson et al. [6], Scheme 6-2 and Table 6-2 [8]. A polymer with a targeted LCST of 37°C was initially grown from the functionalized trypsin protein to create a smart trypsin Hybrid A. The purified polymer conjugate was then used to initiate a second polymerization with PEGMA (Mn 475) to create the triblock trypsin Hybrid B.

Conjugate	M_n[a]	M_w/M_n[a]	% BCA[b]	LCST,°C[c]
Hybrid A = conjugate trypsin-P6	28,300	1.19	14.82	36
Hybrid B = conjugate trypsin-P7	45,606	1.53	9.14	36

Table 6-2: The characterization of Hybrid A and Hybrid B.

where: (a) from GPC; (b) Protein content determined by bicinchoninic and assay (BCA); and (c) UV absorption of 3mg/ml solutions in 1 x PBS at 550 nm.

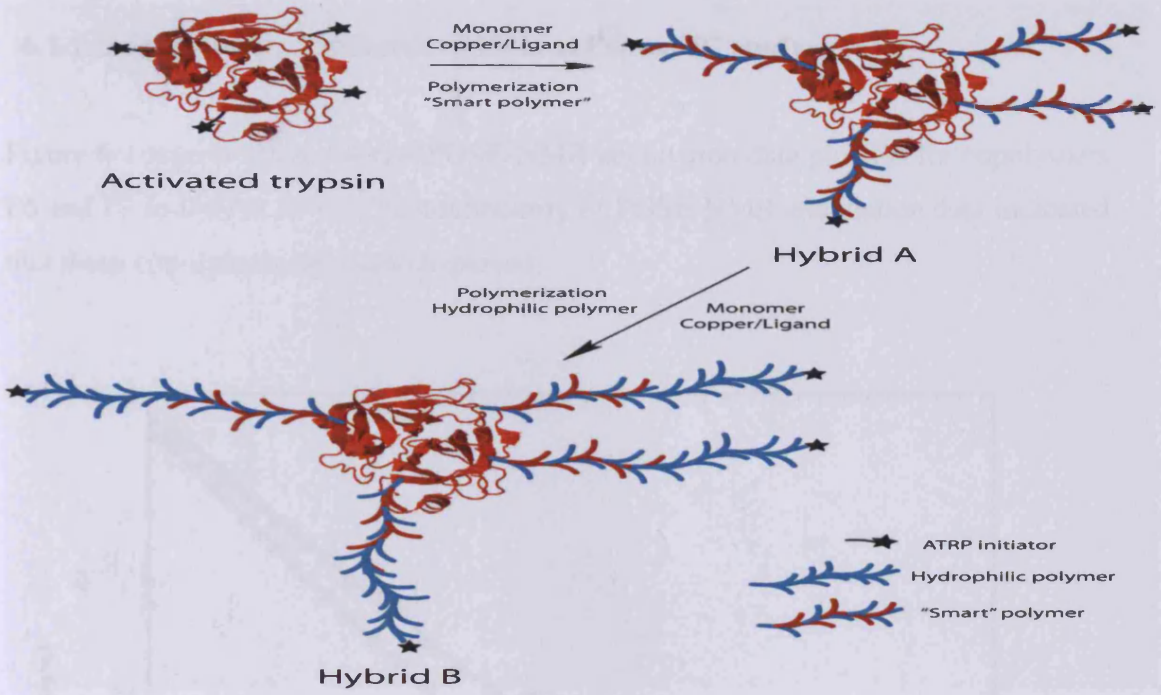

Scheme 6-2: Polymerization and schematic of trypsin conjugate to synthesize a statistical "smart" hybrid (trypsin-hybrid A) a triblock (trypsin-hybrid B). Figure adapted from Yasayan et al. Ref. [8].

The polymers studied here were kindly donated by Prof Cameron Alexander [6] and previously characterized using Transmission Electron Micrograph (TEM), Nuclear Magnetic Resonance (NMR), Dynamic Light Scattering DLS and Elcrospray ionization mass spectrometer (ESI-MS). The target of this study was to explore further the physical-chemical properties of these copolymers by using pulsed-gradient spin-echo NMR (PGSE-NMR) and small-angle neutron scattering (SANS) to provide a fundamental understanding of their solution behaviour.

6.1. Pulsed-gradient spin-echo NMR

Measurements were conducted on a Bruker AMX360 NMR spectrometer using a stimulated echo-sequence as described elsewhere [9-11], and in chapters two and three. This conformation uses a 5mm diffusion probe (Cryomagent Systems, Indianapolis) and a Bruker gradient (GRASP) spectroscopy accessory unit to deliver trapezoidal gradient pulses. All experiments were performed at range of the temperature from 20 to 45°C for P6 copolymer and 20 to 35°C for both P7 copolymer and conjugate trypsin-P6.

6.1.1. Self-diffusion coefficient of Hybrid P6 and P7 study

Figure 6-1 represent typical raw PGSE-NMR attenuation data plus fits for copolymers P6 and P7 in D_2O at 25°C. The nonlinearity of PGSE-NMR attenuation data indicated that these copolymers are monodispersed.

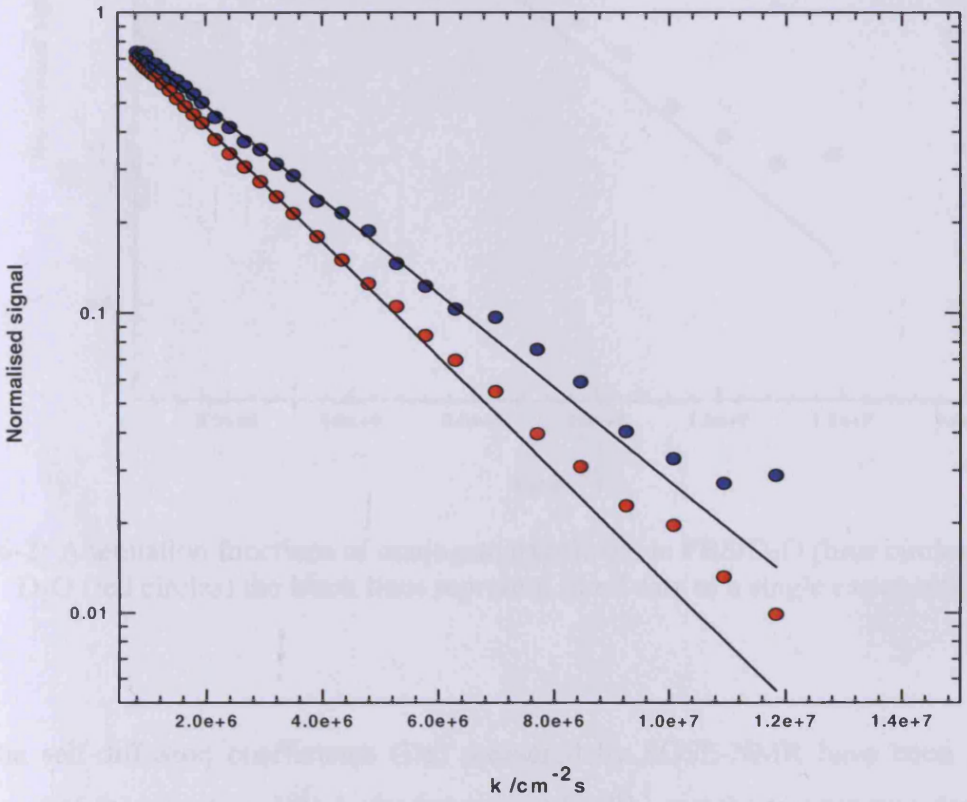

Figure 6-1: Attenuation functions P6 (blue circles), P7 (red circles) in D_2O and the black lines represent fitted data to a single exponential.

The attenuation functions for P6 with and without trypsin in PBS/ D_2O and fits at 25°C are presented in Figure 6-2. We can see in this Figure the linearity of PGSE-NMR attenuation data for P6 in D_2O also indicated that this copolymer is monodispersed, and also the linearity of PGSE-NMR for conjugate P6-trypsin indicated that is monodispersed.

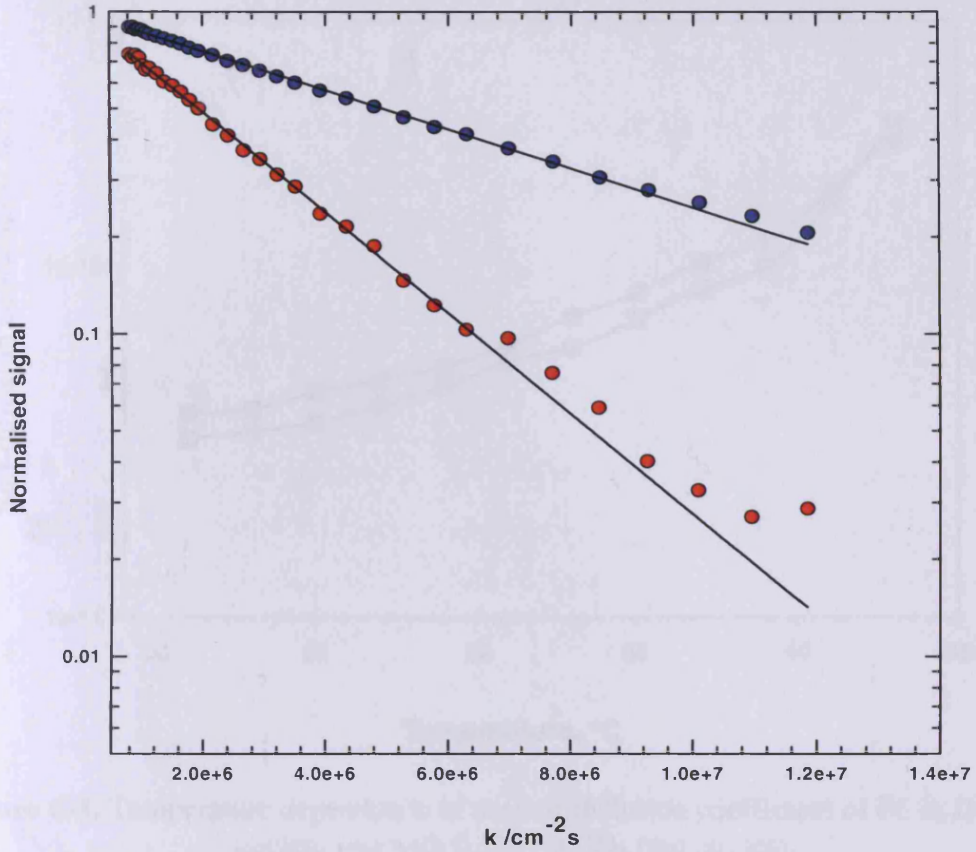

Figure 6-2: Attenuation functions of conjugate trypsin-P6 in PBS/D_2O (blue circles) and P6 in D_2O (red circles) the black lines represent fitted data to a single exponential.

The self-diffusion coefficients (Ds) measured by PGSE-NMR have been recast in terms of the corresponding hydrodynamic radii (Rh) and the temperature dependence of this estimate of the solution conformation. Diffusion of copolymers P6 and P7 are presented in Figures 6-3 and 6-4 and exhibited a similar pattern in that, with increasing temperature, the self-diffusion coefficient increased. The temperature behavior (LCST) of copolymers P6 and P7 is in excellent agreement with that observed by Cameron et al. [6], at 43°C and 35°C for P6 and P7 in D_2O respectively. Therefore, the NMR diffusion experiments were not performed at temperatures close to the LCST.

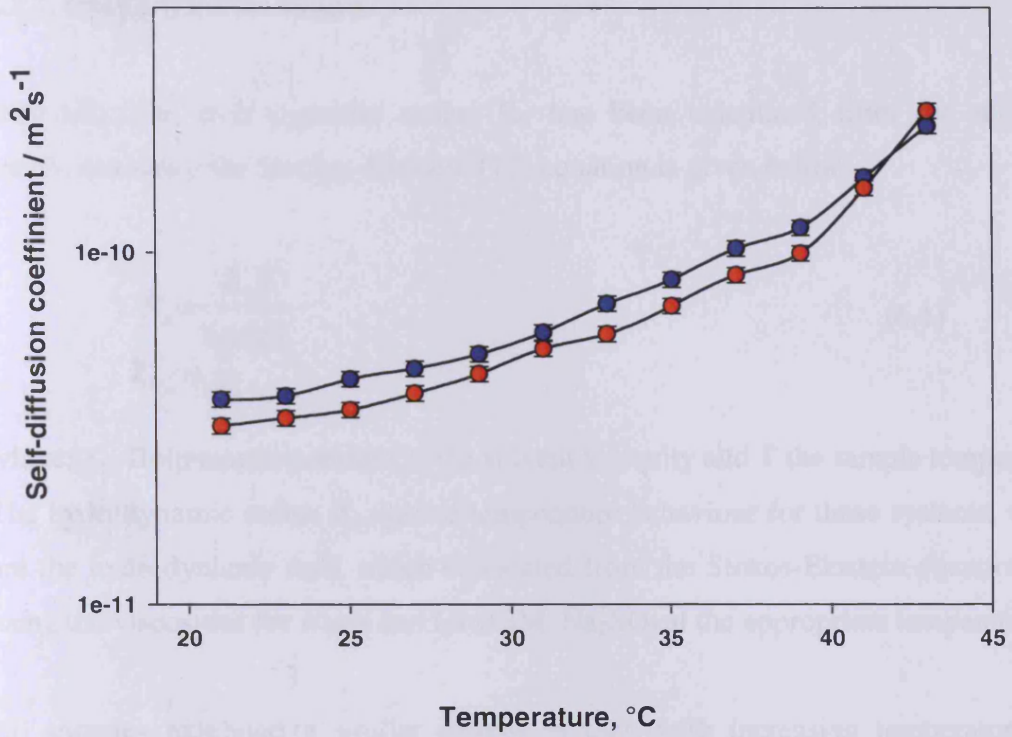

Figure 6-3: Temperature dependence of the self-diffusion coefficient of P6 in D_2O (blue circles) and with 0.3M Na_2SO_4 (red circles).

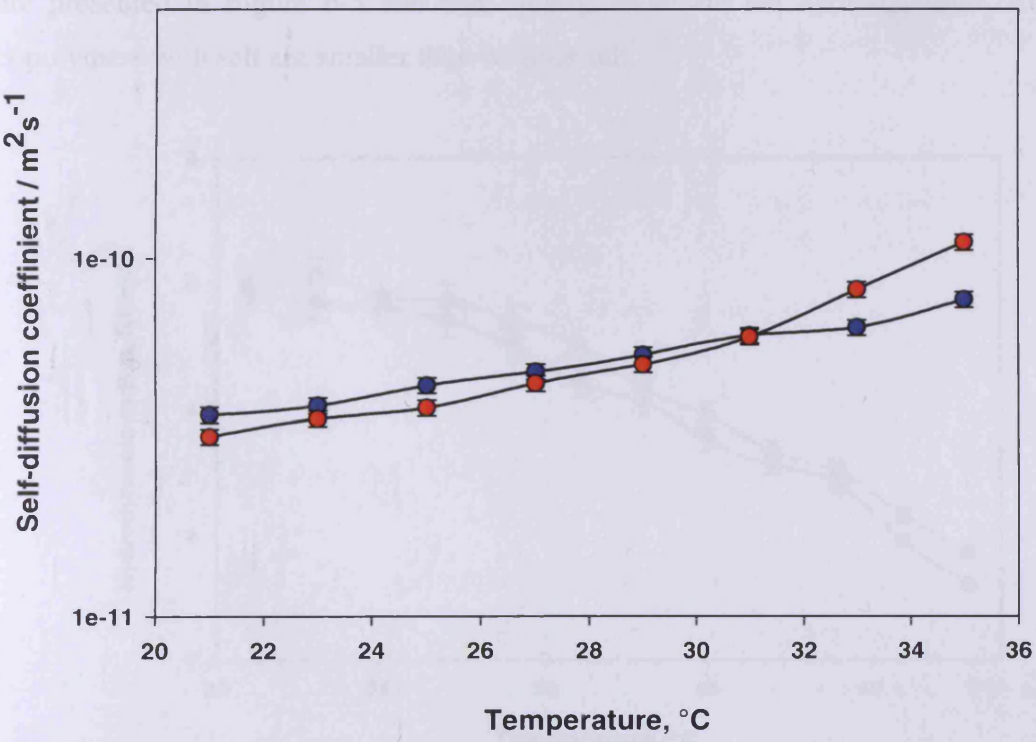

Figure 6-4: Temperature dependence of the self-diffusion coefficient of P7 in D_2O (blue circles) and with 0.3M Na_2SO_4 (red circles).

6.1.2. Hydrodynamic radius

Generally, the hydrodynamic radius R_h has been calculated from the diffusion coefficient using the Stockes-Einstein [12] equation is given below.

$$R_h = \frac{K_B T}{6\pi\eta D_s} \qquad (6.1)$$

where; K_B Boltzmanns constant, η the solvent viscosity and T the sample temperature. The hydrodynamic radius R_h against temperature behaviour for these systems, shown are the hydrodynamic radii which calculated from the Stokes-Einstein equation [12] using the viscosities for water and for 0.3M Na_2SO_4 at the appropriate temperature.

All samples exhibited a similar pattern in that, with increasing temperature, the hydrodynamic radius decrease. Indeed, the hydrodynamic radii for P6 was greater than that for P7, reflecting the different of molar ratio of PEGMA-EE-246 and PEGMA-475 in both copolymers. For comparison, the addition of salt for P6 and P7 are presented in Figure 6-5 and 6-6, clearly, there are the hydrodynamic radii of copolymers with salt are smaller than without salt.

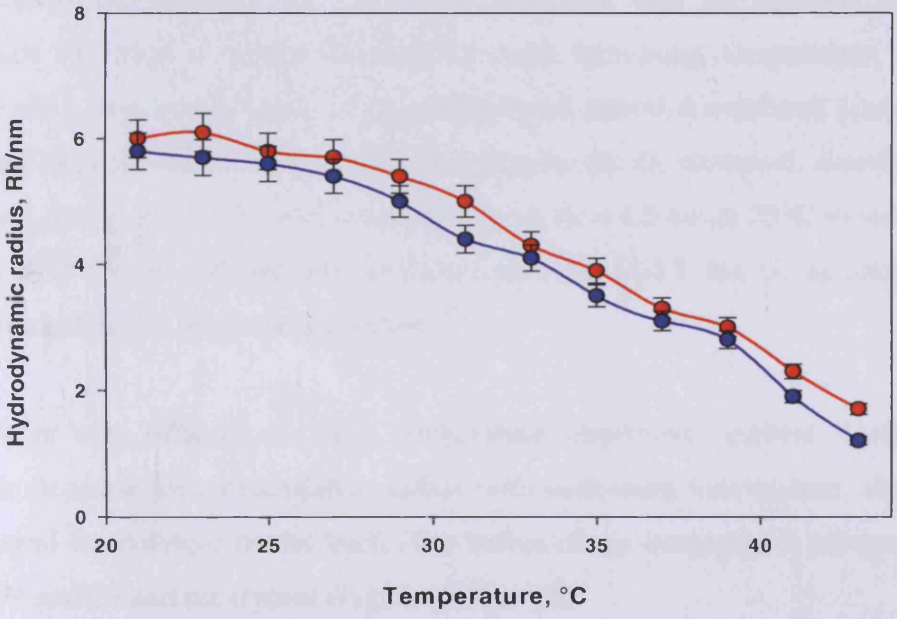

Figure 6-5: Temperature dependence of the hydrodynamic radius of P6 in D_2O (red circles) and with 0.3M Na_2SO_4 (blue circles).

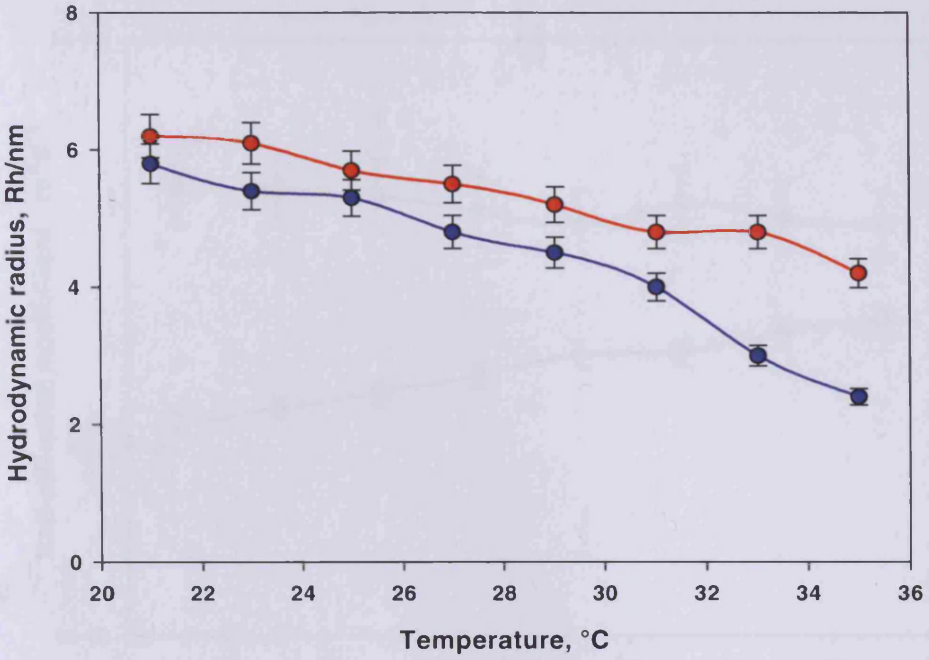

Figure 6-6: Temperature dependence of the hydrodynamic radius of P7 in D_2O (red circles) and with 0.3M Na_2SO_4 (blue circles).

6.1.3. Self-diffusion coefficient for trypsin and conjugate trypsin-P6 (hybrid A)

The self-diffusion coefficients (D_s) against temperature behaviour for trypsin and conjugate trypsin-P6 (hybrid A) are presented in Figures 6-7 and 6-8 respectively, also shown are the hydrodynamic radii (R_h) calculated from the equation 6.1. The trypsin data exhibited a weaker dependence with increasing temperature, the D_s increased and a decrease in the R_h. On the other hand, hybrid A exhibited pronounced temperature dependence with increasing temperature; the D_s increased, therefore, the R_h decrease, and it is clearly exhibits collapse from R_h = 4.5 nm at 25°C to around R_h = 3.0 nm at 35°C, this collapse stars to occur below the LCST, but all the sample are still homogeneous, i.e. no phase separation.

Hybrid A is very different in their temperature responsive. Hybrid A shows a monotonic decrease in hydrodynamic radius with increasing temperature, similar to that observed for polymer model itself. The radius of the conjugate is always grater than the P6 and P7 and the trypsin (Figures 6-7 to 6.9).

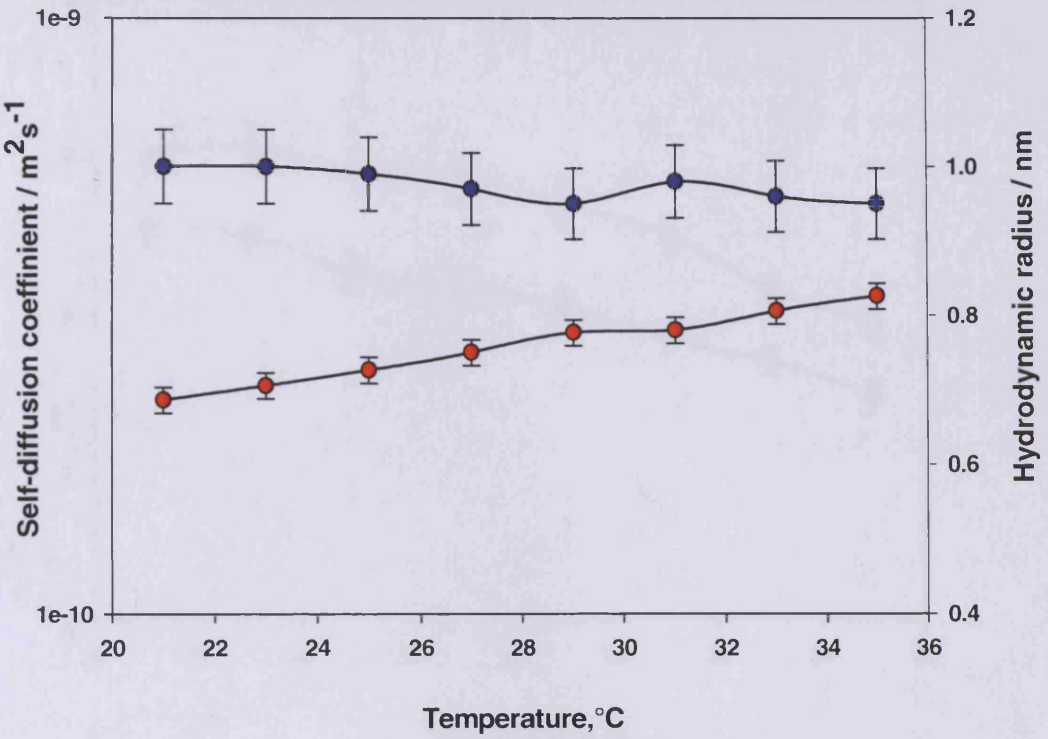

Figure 6-7: Temperature dependence of the self-diffusion coefficient (red circles) and hydrodynamic radius (blue circles) of trypsin in PBS/D_2O.

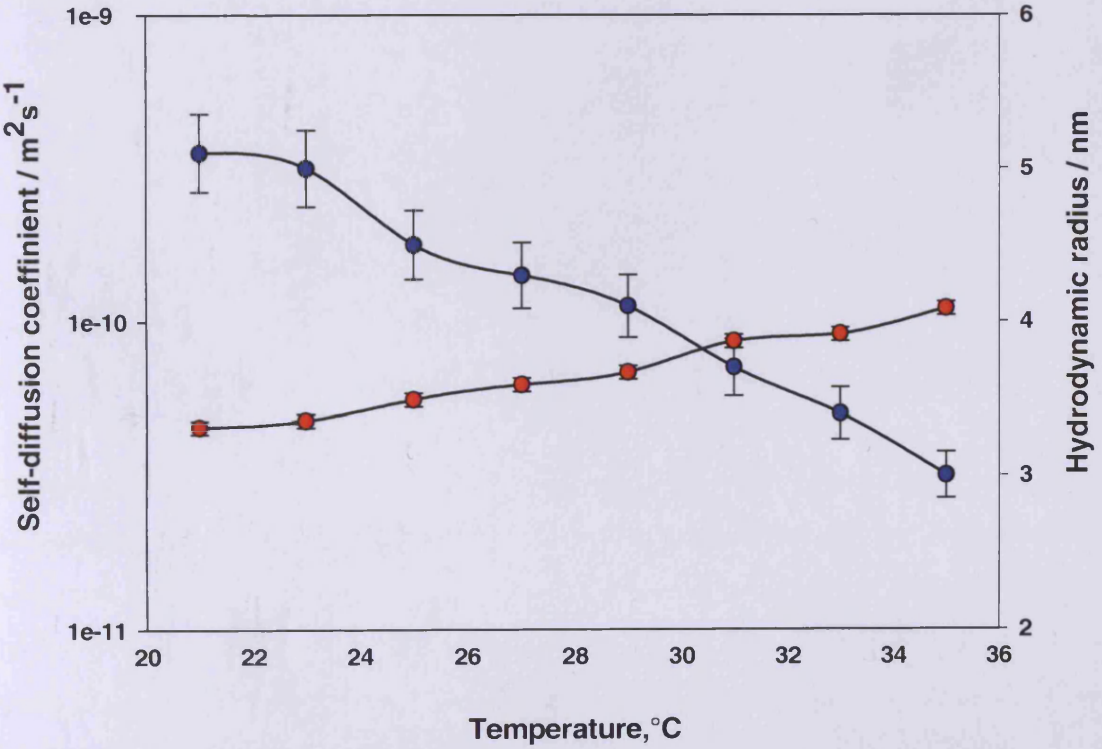

Figure 6-8: Temperature dependence of the self-diffusion coefficient (red circles) and hydrodynamic radius (blue circles) of hybrid A in PBS/D_2O.

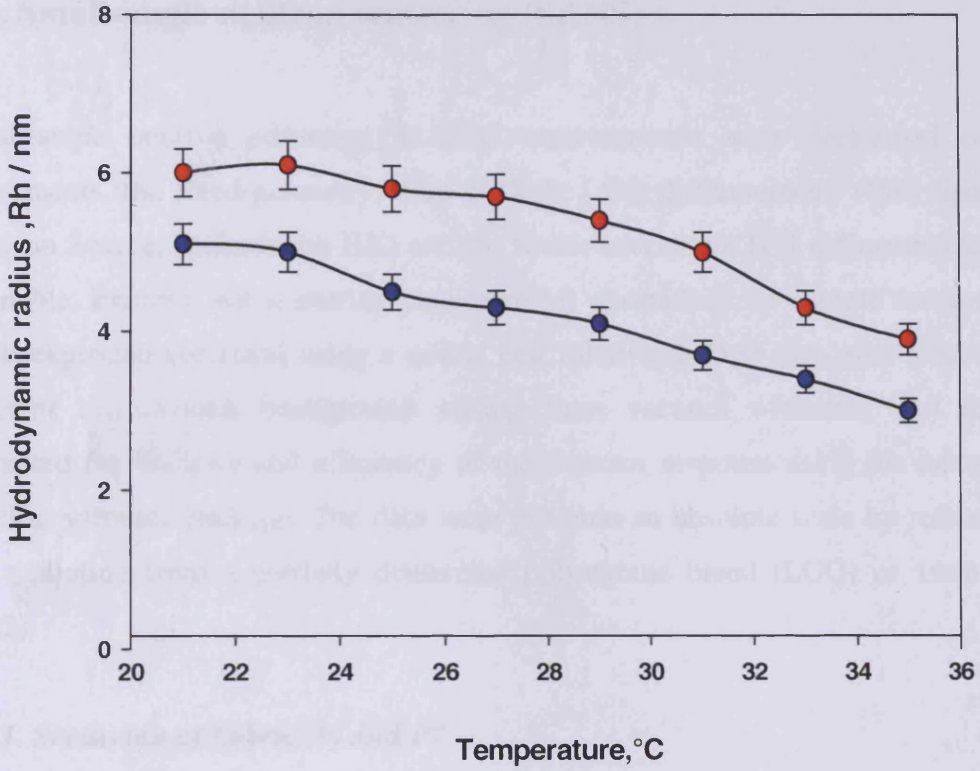

Figure 6-9: Hydrodynamic radius comparison between P6 (blue circles) and hybrid A (red circles) in PBS/D_2O.

6.2. Small-angle neutron scattering (SANS)

Small-angle neutron scattering (SANS) measurements were performed on two instruments, the fixed-geometry, time-of-flight LOQ diffractometer (ISIS Spallation Neutron Source, Oxfordshire UK) and the fixed-wavelength D11 diffractometer (ILL Grenoble, France). All scattering data were (a) normalised for sample transmission, (b) background corrected using a quartz cell filled with D_2O (this also removes the inherent instrumental background arising from vacuum windows, etc) and (c) corrected for linearity and efficiency of the detector response using the instrument-specific software package. The data were put onto an absolute scale by reference to the scattering from a partially deuterated polystyrene blend (LOQ) or 1mm water (D22).

6.2.1. Scattering of hybrid P6 and P7

Two samples from each polymer were prepared in the presence and in the absence of the salt (0.3M Na_2SO_4), and scattering pattern observed at different temperatures. According to the SANS data, both hybrid polymers P6 and P7 scattered in same way at low temperature and data were fitted to polydispersed Gaussian coil, whereas, at high temperatures were fitted to polydispersed two shell hard spheres, i.e. P6 and P7 with salt and without salt at 20°C were fitted to polydispersed Gaussian coil model, whereas rest of the data were fitted to polydispersed two shell hard sphere model. Both from SANS and PGSE-NMR data, it was shown that P6 is small compare to P7. The ratio Rh/Rg is 1.5, 1.6, 1.6, and 1.6 for P6 with and without salt, P7 with and without salt respectively, Table 6.4.

Scattering behaviour of both polymers changed at high temperature resembling conformational changes of the structure. The significant scattering at low Q-value was observed for P6 with salt at 50°C resembling some aggregated structure Figures 6-10 and 6-11. Whereas, P7 with salt at the same temperature, produced shoulder peak, implying pronounced structure factor Figures 6-12, 6-13 and Table 6-3. This could be due to micellization of the P7 at high temperature which was evident by PGSE-NMR data as well.

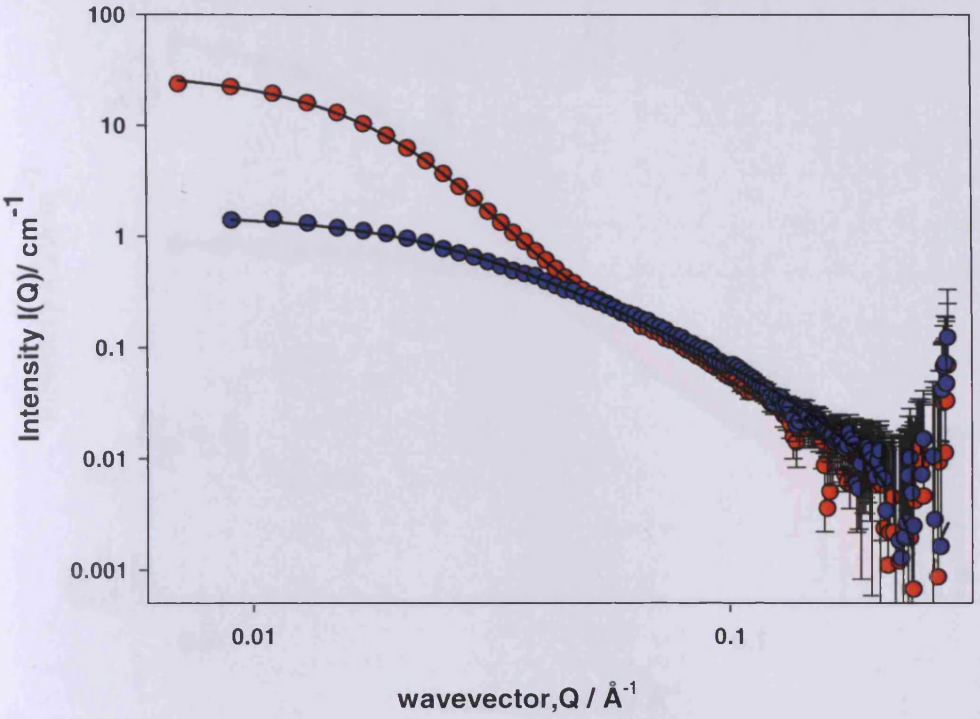

Figure 6-10: SANS data of 1.0 wt% P6 in D_2O at 20°C (blue circles), 50°C (red circles) and the black lines represent fitted data.

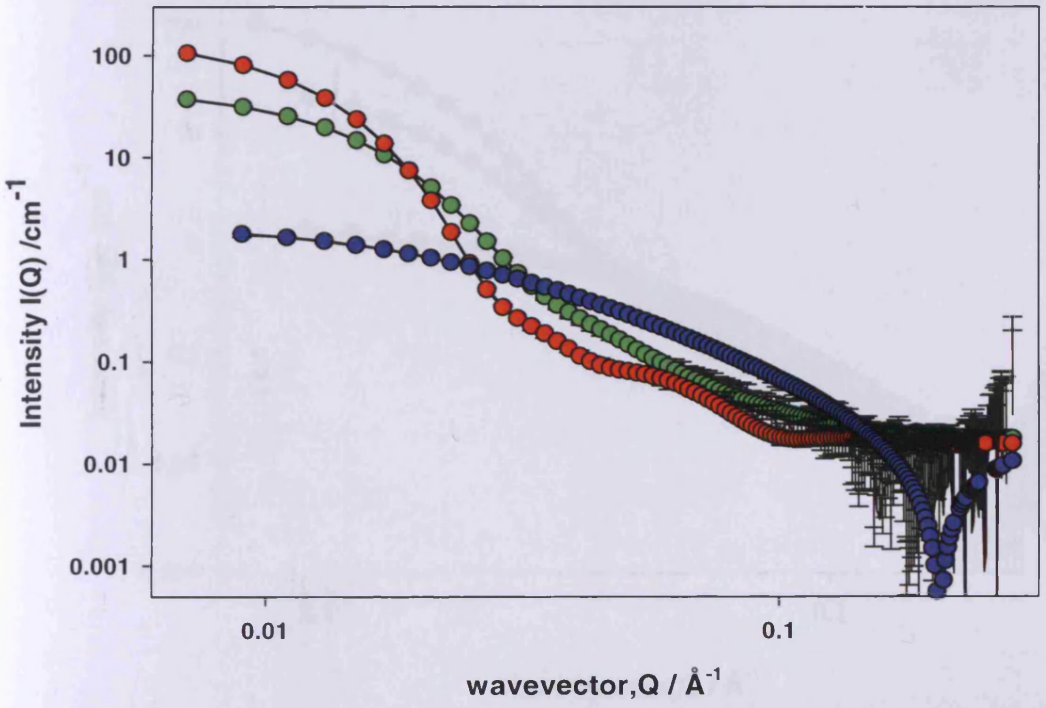

Figure 6-11: SANS data of 1.0 wt% P6 with 0.3M Na_2SO_4/D_2O at 20°C (blue circles), 35°C (green circles), at 50° (red circles) and the black lines represent fitted data.

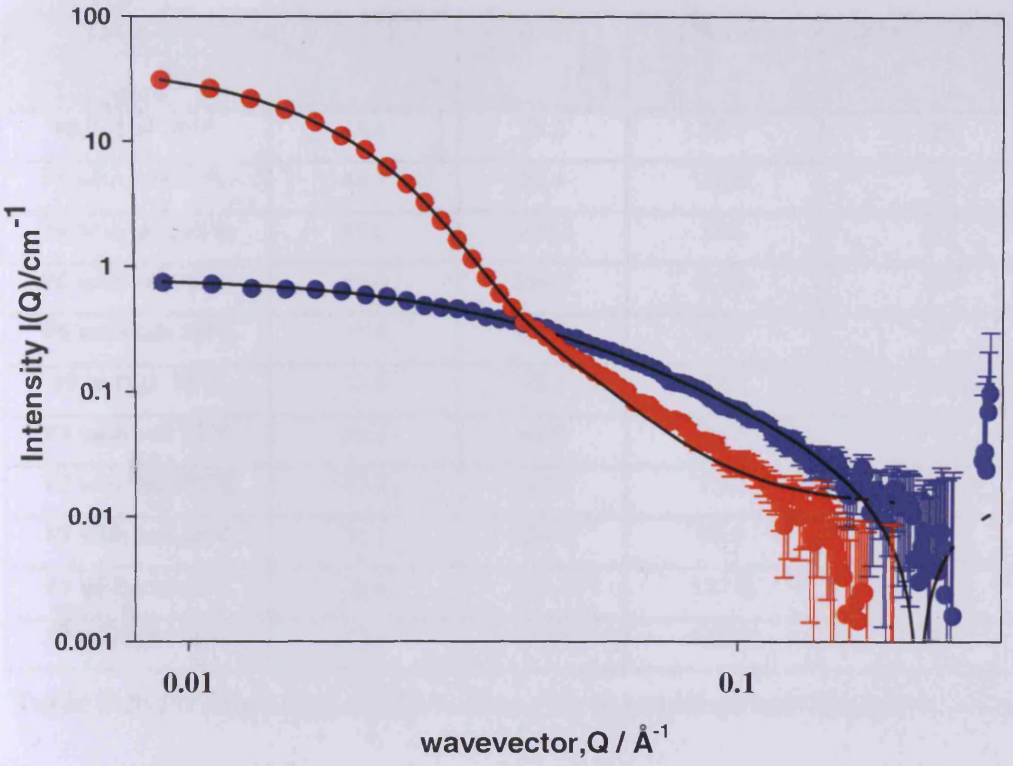

Figure 6-12: SANS data of 1.0 wt% P7 in D_2O at 20°C (blue circles), 50°C (red circles) and the black lines represent fitted data.

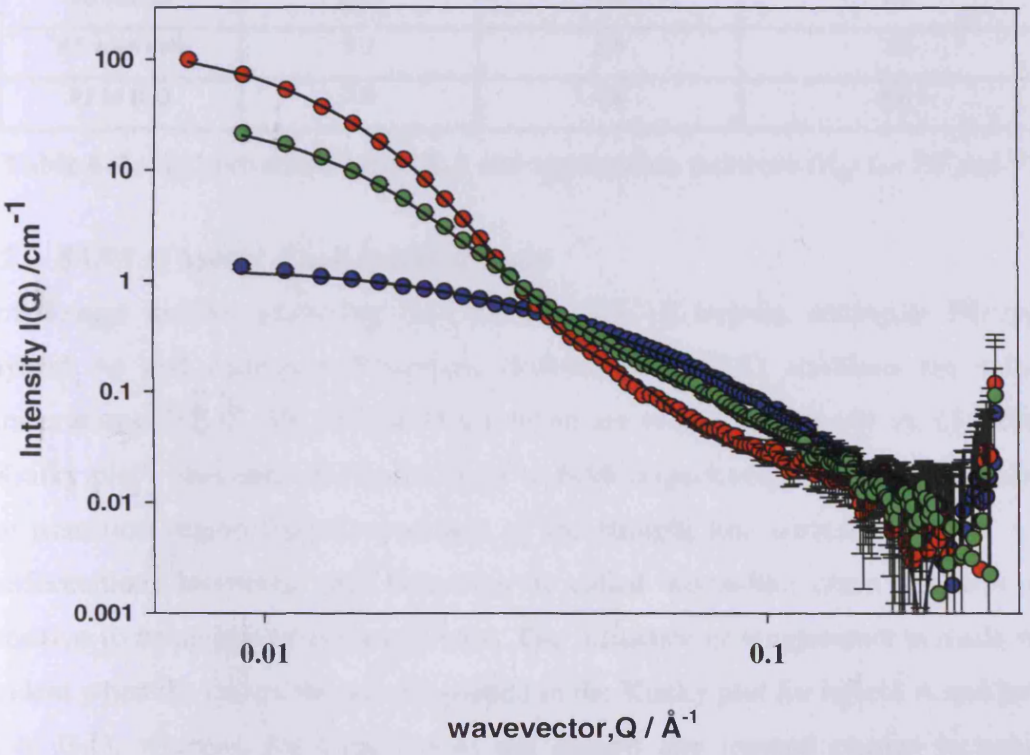

Figure 6-13: SANS data of 1.0 wt% P7 with 0.3M Na_2SO_4/D_2O at 20°C (blue circles), 27°C (green circles), at 40° (red circles) and the black lines represent fitted data.

Sample	R_1 (Å)	R_2 (Å)	Shell (Å)	Spherical Radius
P6 in D_2O 50°C	43.4	79.2	35.7	35
P6 with salt 27°C	48.7	81.4	32.6	35
P6 with salt 35°C	89.6	108.2	18.5	35
P6 with salt 40°C	46.8	134.7	87.8	35
P6 with salt 50°C	77.4	167.2	89.7	35
P7 in D_2O 50°C	63.0	95.2	32.1	35
P7 with salt 27°C	51.2	82.0	30.8	35
P7 with salt 35°C	42.8	114.5	71.7	35
P7 with salt 40°C	40.5	123.8	83.0	35
P7 with salt 43°C	36.8	164.2	127.0	35
P7 with salt 46°C	15.1	115.3	100.2	35

Table 6-3: Fit parameters obtained from fish as polydispersed Gaussian coil mode.

Sample	R_h/nm (± 0.2) from PGSE-NMR	R_g/nm (± 0.1) from SANS	R_h/R_g
P6 with salt	12.8	8.4	1.5
P6 in D_2O	12.3	7.8	1.6
P7 with salt	9.2	5.8	1.6
P7 in D_2O	7.6	4.8	1.6

Table 6-4: Hydrodynamic radii (R_h) and aggregation numbers (R_g) for P6 and P7.

6.2.2. SANS of hybrid A and hybrid B study

Small-angle neutron scattering data for 1.0 wt% of trypsin, conjugate P6-trypsin (hybrid A) and conjugate P7-trypsin (hybrid B) in D_2O solutions for selected temperatures (20, 25, 30, 32 and 34°C), when are plotted $Q^2 * I(Q)$ vs. Q, called a "Kratky plot" illustrated in Figures 6-14 to 6-16 respectively, which reveals clearly the transition region from intersection of the straight line corresponding to a rod conformation. Moreover, this behaviour is called worm-like chain and this very sensitive to behaviour of polymer chain. The influence of temperature is made more evident when the same data sets are plotted in the Kratky plot for hybrid A and hybrid B in D_2O, whereas, for trypsin does not exhibit any marked change in solution conformation over the above temperature range.

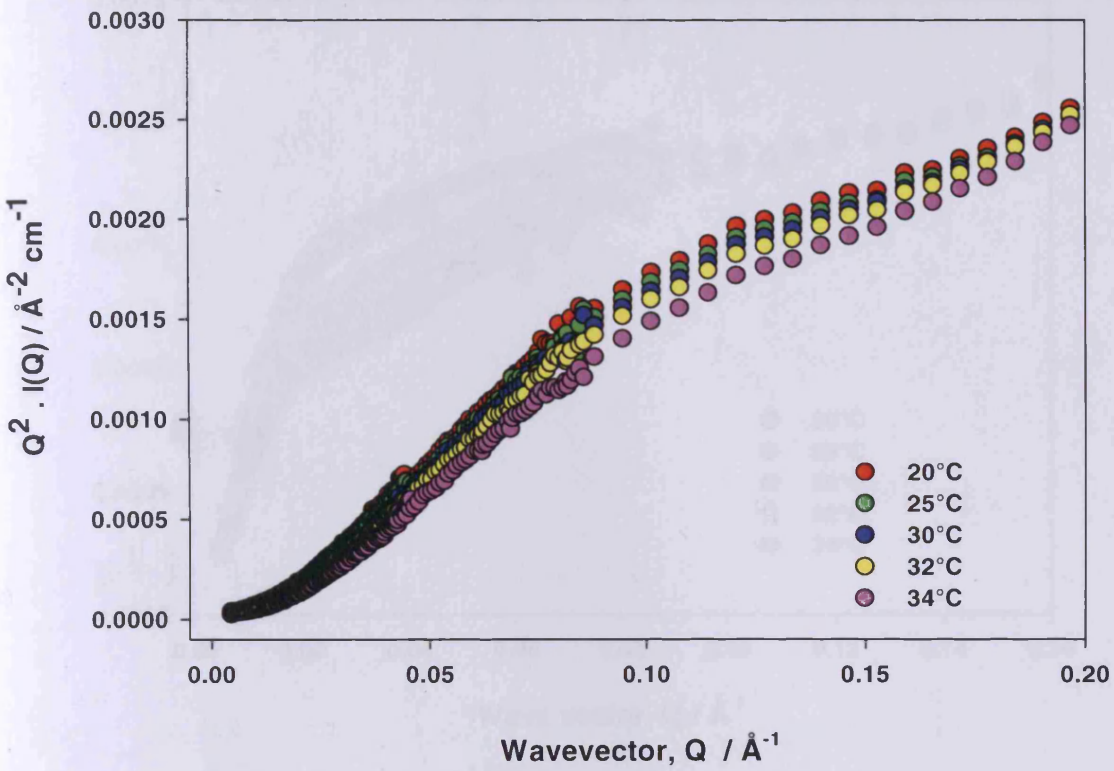

Figure 6-14: Kratky Plot of 1.0 wt% trypsin in D_2O at different temperatures.

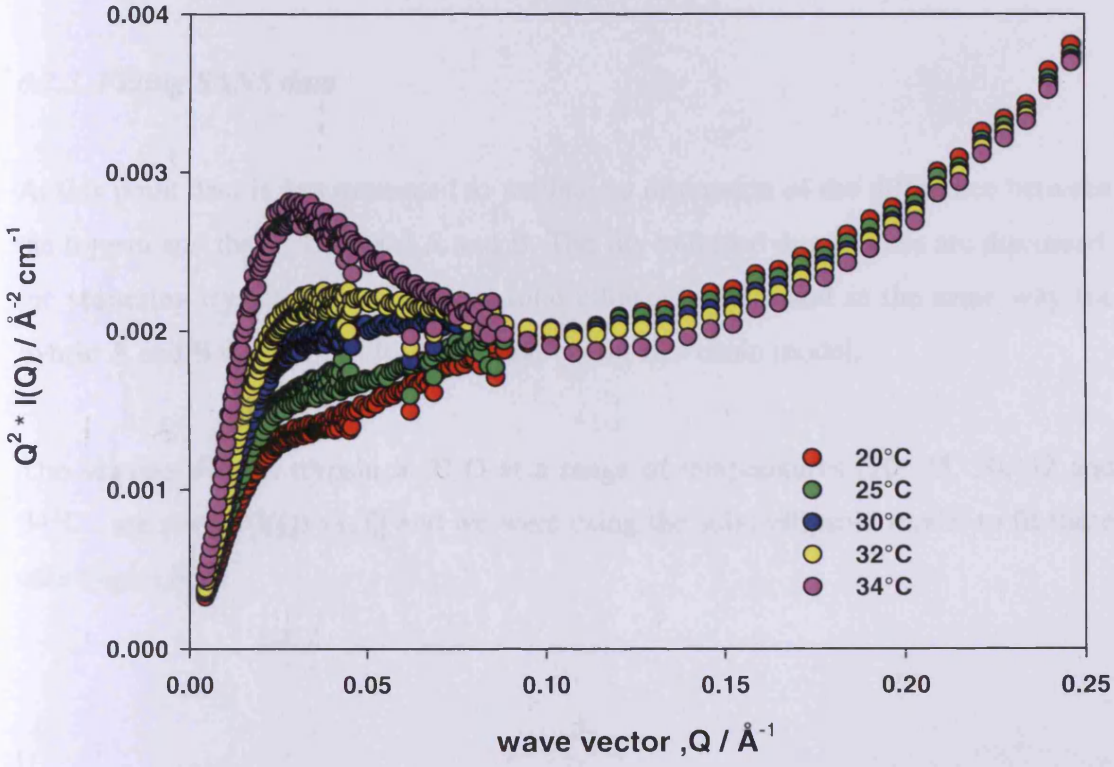

Figure 6-15: Kratky Plot of 1.0 wt% Hybrid A in D_2O at different temperatures.

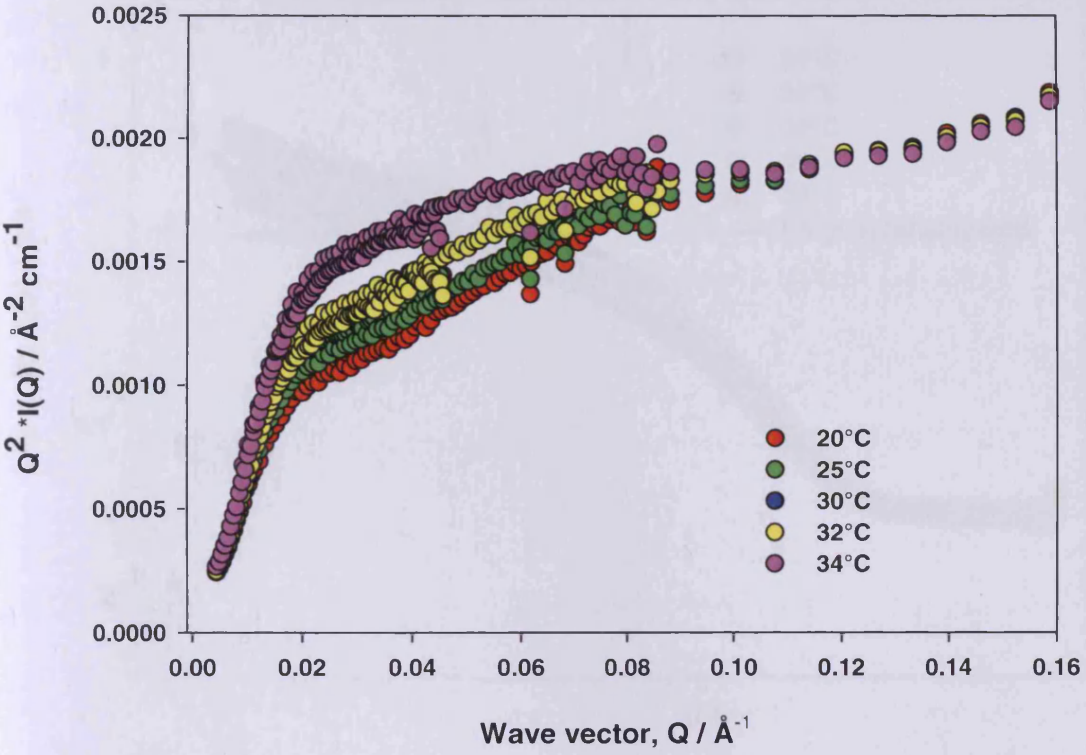

Figure 6-16: Kratky Plot of 1.0 wt% Hybrid B in D_2O at different temperatures.

6.2.3. Fitting SANS data

At this point data is just presented to facilitate a discussion of the difference between the trypsin and the both hybrid A and B. The fits to underlying models are discussed, the scattering trypsin data will fit to solid ellipsoid model and in the same way the hybrid A and B data will fit to Kholodenko worm-like chain model.

The scatting data of trypsin in D_2O at a range of temperatures (20, 25, 30, 32 and 34°C), are plotted I(Q) vs. Q and we were using the solid ellipsoid model to fit these data Figure 6-17.

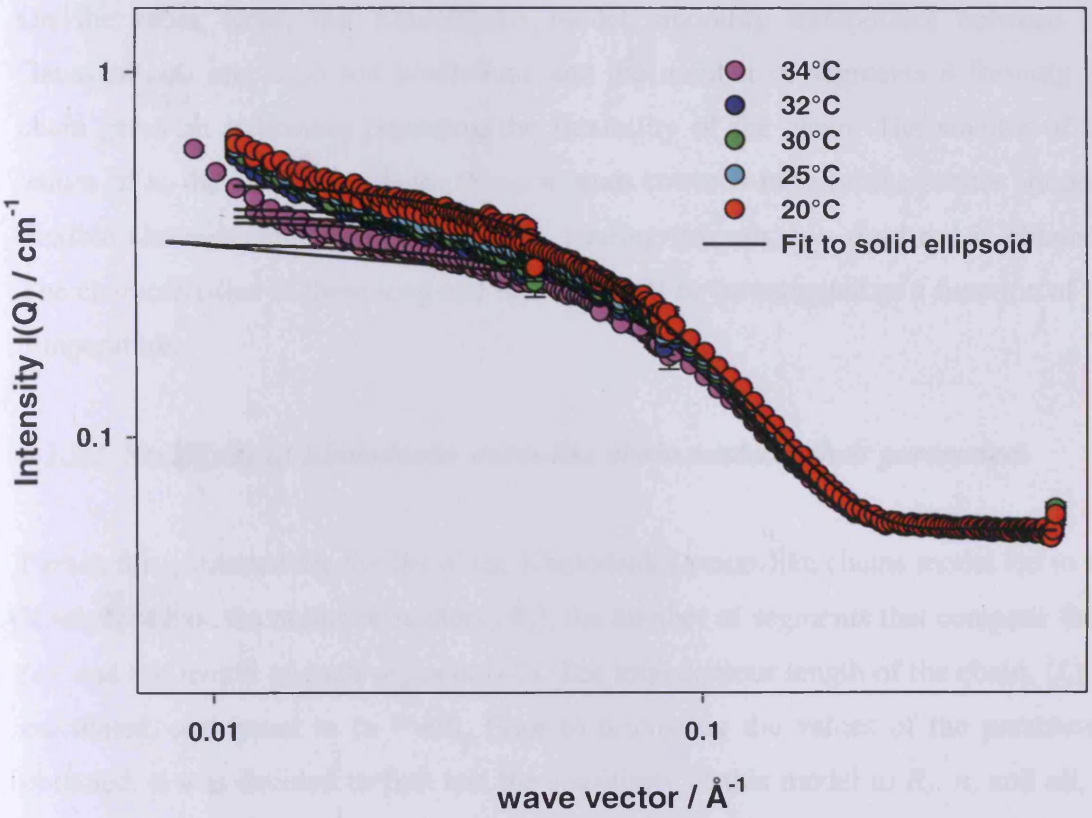

Figure 6-17: SANS data of 1.0 wt% trypsin in D_2O at different temperatures and the black lines represent fitted data.

In recent decades, the worm-like chain (WLC) has emerged as the standard model for the description of semi-flexible polymers. The defining property of a WLC is a mechanical bending stiffness that is an intrinsic material constant of the polymer [13]. Therefore, the hybrid A and B fit a model that allows fitting over the whole Q range is Kholodenko worm-like chain model, this model was tested against the bulk of the scattering data using the FISH program [14]. The Kholodenko worm-like chain model was derived from a Gaussian coil model, where long thin rods are made of a series of n cylindrical elements of statistical length *ell* and radius R_l in which n =10. The contour length of the chain, L, is equal to the product n . *ell*.

On the other hand, the Kholodenko model smoothly interpolates between the Gaussian coil and rigid rod predictions and the number of segments *n* forming the chain gives an indication regarding the flexibility of the chain. The smaller of the values of *n*, the stiffer the chain. When *n* tends towards infinity, the scatter adopts a flexible Gaussian random coil. Whereas, tending towards *1*, a rigid rod is obtained. The characteristics of these long and thin rods will be investigated as a function of the temperature.

6.2.3.1. Sensitivity of Kholodenko worm-like chain model to their parameters

Parameters extracted via the fits of the Kholodenko worm-like chains model led to the Kholodenko of the radius of scatters (R_1), the number of segments that compose them (*n*), and the length of each segment (*ell*). The total contour length of the chain, (*L*), is calculated, and equal to (*n* * *ell*). Prior to discussing the values of the parameters obtained, it was decided to first test the sensitivity of this model to R_1, *n*, and *ell*, as follows. A best fit giving physical sensible parameters was determined. Then, all parameters were kept to their optimal values, except R_1, *n*, and *ell* that were varied, each one at a time.

This study was conducted on a typical dataset, belonging to a sample composed of 1.0 wt% hybrid A in D_2O measured at 25°C as example. Figure 6-18 presents the best fit obtained while all parameters were allowed to float, and Table 6-5 the corresponding parameters values.

Hybrid A in D_2O	R_1/Å	*n*	*ell*/Å	(L = n * ell)/ Å
at 25°C	14	50	46	2300

Table 6-5: Parameters values for sample of 1.0 wt% hybrid A in D_2O, fitted with Kholodenko worm-like chain model.

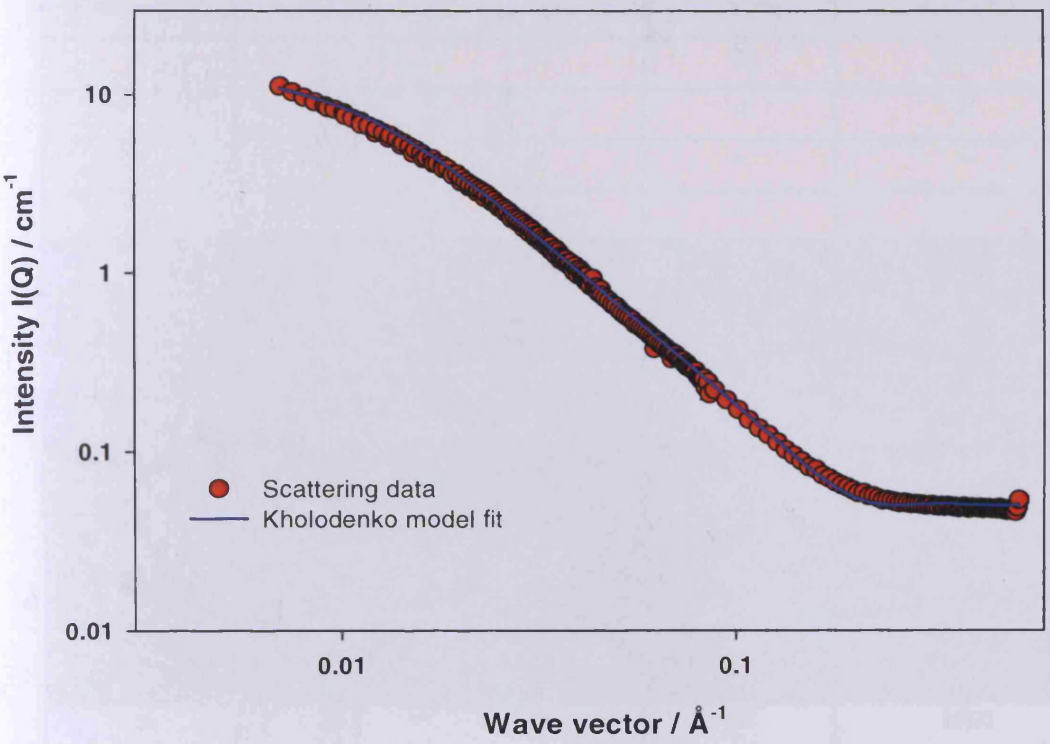

Figure 6-18: Scattering data of 1.0 wt% hybrid A in D_2O (red circles) and optimal fit (blue line) using the Kholodenko worm-like chain model.

6.2.3.2. Experimental design

The input values chosen to test the sensitivity of the radius R_l were 10, 12, 14, and 16Å, the *n* and *ell* could be kept constant chosen to test. To test the sensitivity of the chain length *ell* values were chosen as 50, 80, 100, 200, and to test the sensitivity of the number of segments *n* values were chosen as 1, 10, 50, 100 and 200Å. The total length *L* of the chain could be kept constant by varying both *n* and *ell* at the same time, as (*L= n * ell)*, and the binary systems (n & ell) chosen to test the sensitivity of *n* and *ell* were chosen as (50; 20), (1000; 10), (200; 5), and (1000; 1), leading to the experimental following design described in Table 6-6.

Experiment	R_1/ Å	n	ell/ Å	(L = n * ell)/ Å
1	10	60	45	2700
2	12	≈	≈	≈
3	14	≈	≈	≈
4	16	≈	≈	≈
5	15	60	50	3000
6	≈	≈	80	4800
7	≈	≈	100	6000
8	≈	≈	200	12000
9	15	1	45	45
10	≈	10	≈	450
11	≈	50	≈	2250
12	≈	100	≈	4500
13	≈	200	≈	9000
14	15	50	20	1000
15	≈	100	10	1000
16	≈	200	5	1000
17	≈	1000	1	1000

Table 6-6: Experimental design aimed at testing the sensitivity of the Kholodenko worm-like chain model to R_1, n and ell.

6.2.3.3. Sensitivity of R_1 (experimentals 1-4)

Figure 6-19 presents the Kholodenko model data points for experiments 1 to 4, along with the raw scattering data and the best fit. Although the entire range of radii testes (10 - 16Å) resulted in adequate fits to high Q values up to 0.11Å, the radius of 12Å was found to be the only fit over the entire Q range. The fits are very sensitive to R_1 values in the mid Q range, and it is easily conceivable that a clear distinction could be made between radii values of 12 ± 1Å.

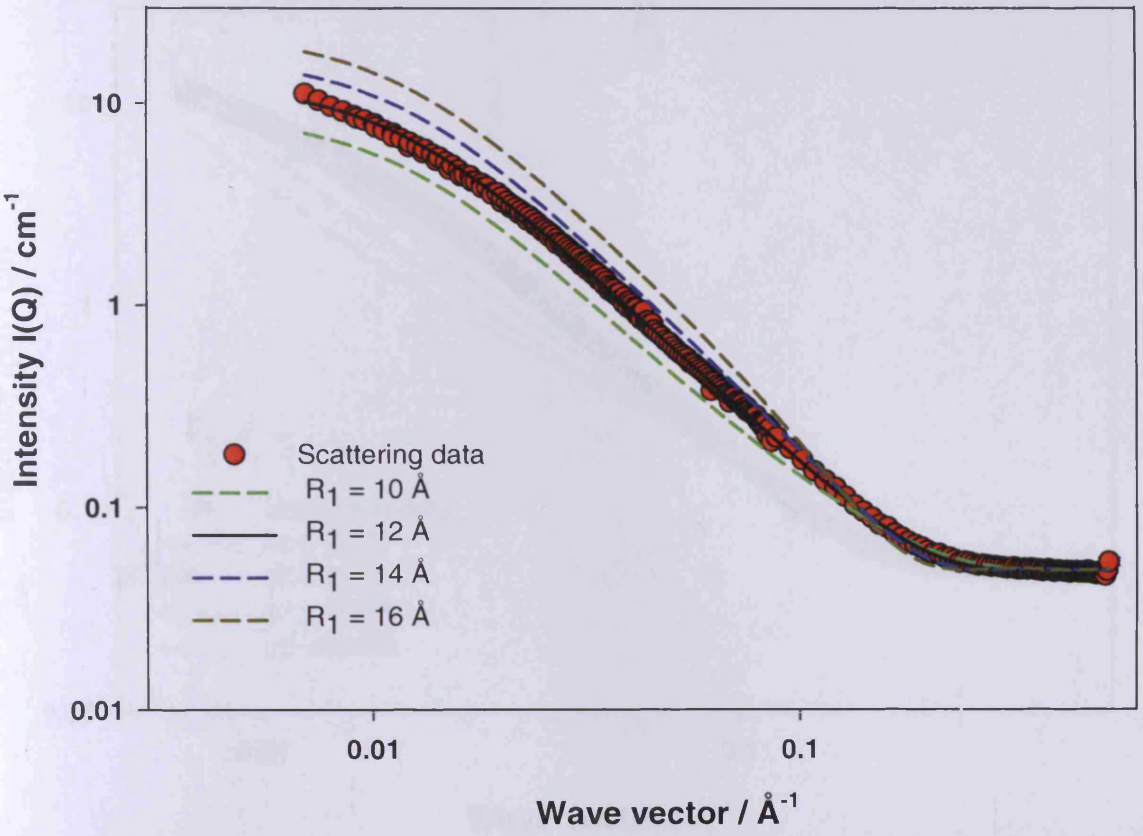

Figure 6-19: Kholodenko model data points for experiments (1- 4), along with the raw scattering data and the best fit of 1.0 wt% Hybrid A in D_2O at 25°C

6.2.3.4. Sensitivity of ell (experimentals 5-8)

Figure 6-20 presents the Kholodenko model data points for experiments 5 to 8, along with the raw scattering data and the best fit. Increasing the length of the segments above their optimal value results in a poor fit to the data (*ell* = 100, 200Å), however, for lower *ell* values (*ell* = 50, 80Å) and therefore lower chains. It should be noted that for *ell* > 50Å, the fit routine became very unstable and could not converge anymore. The model therefore seems to loss it sensitivity towards lower chain elements. The fits are very sensitive to *ell* values in the mid *Q* range, and it is easy conceivable that a clear distinction could be made between *ell* values of 50 ± 5Å.

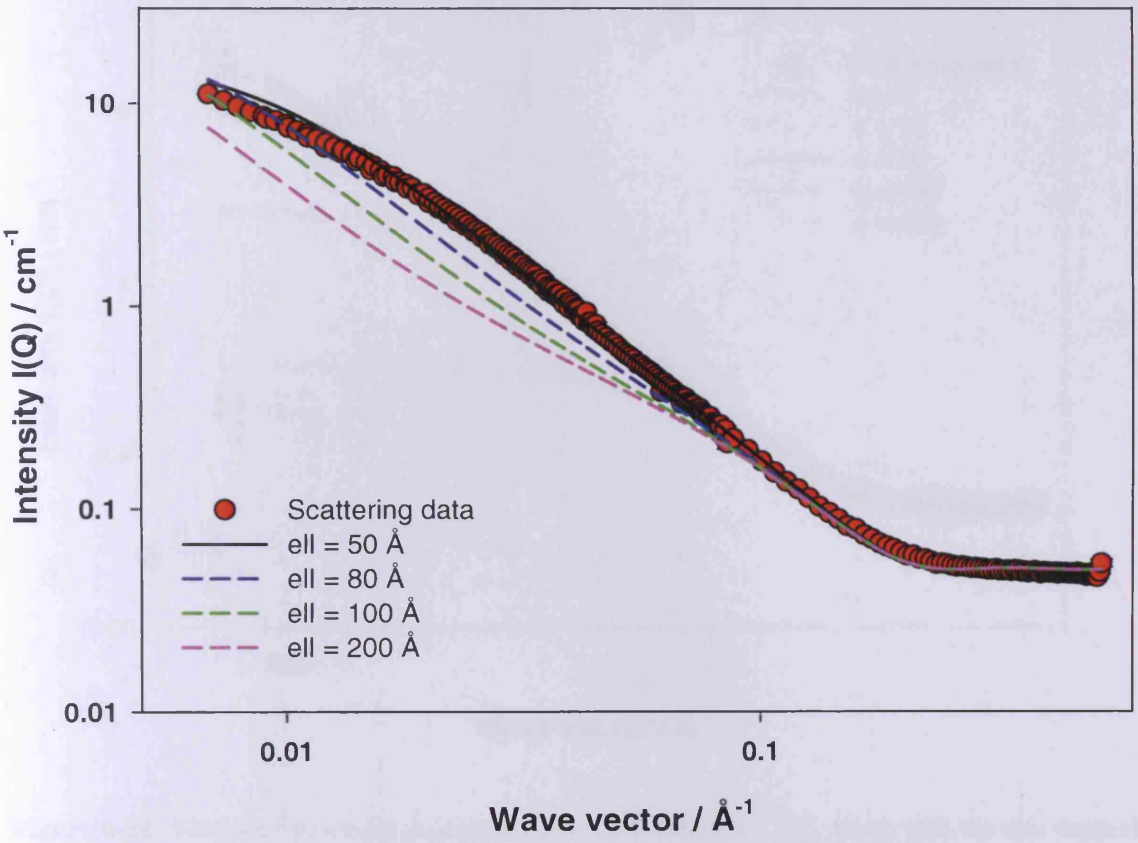

Figure 6-20: Kholodenko model data points for experiments (5- 8), along with the raw scattering data and the best fit of 1.0 wt% Hybrid A in D_2O at 25°C

6.2.3.5. Sensitivity of n (experimentals 9-13)

Figure 6.21 presents the Kholodenko model data points for experiments 9 to 13, along with the raw scattering data and the best fit. Although the entire range of the number of segment n values (1-200) resulted in adequate fits to high Q values up to 0.1Å, the number of segment of 50 was found to be the only fit over the entire Q range. The model seems to loss its sensitivity towards longer chain ($n > 50$), whereas, it very sensitive to n values (a strong deviation) is observed towards lower chain ($n < 50$), and it is easy conceivable that a clear distinction could be made between n values of 50 ± 10.

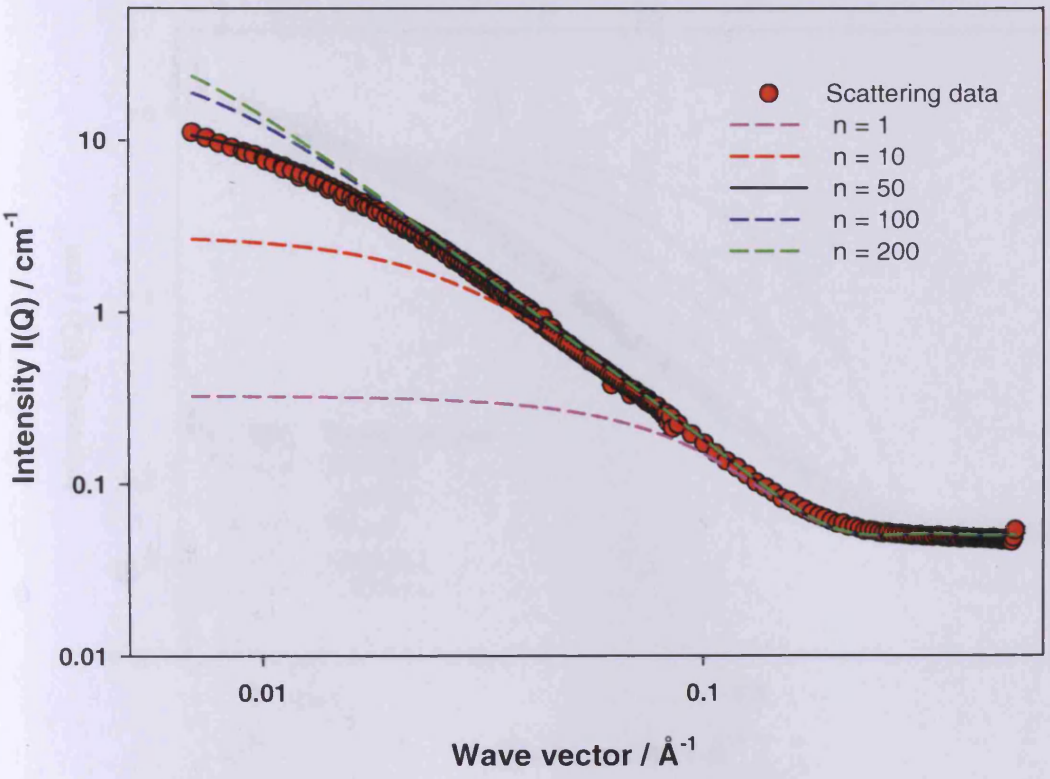

Figure 6-21: Kholodenko model data points for experiments (9 - 13), along with the raw scattering data and the best fit of 1.0 wt% Hybrid A in D_2O at 25°C

6.2.3.6. Sensitivity of (n, ell) couples for constant L (experimentals 14-17)

It was shown in Figure 6-22 above the longer chain lengths, the fitting were hardly sensitive to both the *n* and *ell*. For binary values (50, 20) and (100, 10) of *n* and *ell* respectively, the curvature of the fittings is narrowly affected. For highly different ratios of *n* and *ell*, i.e. (200, 5) and (1000, 1), a strong deviation is observed.

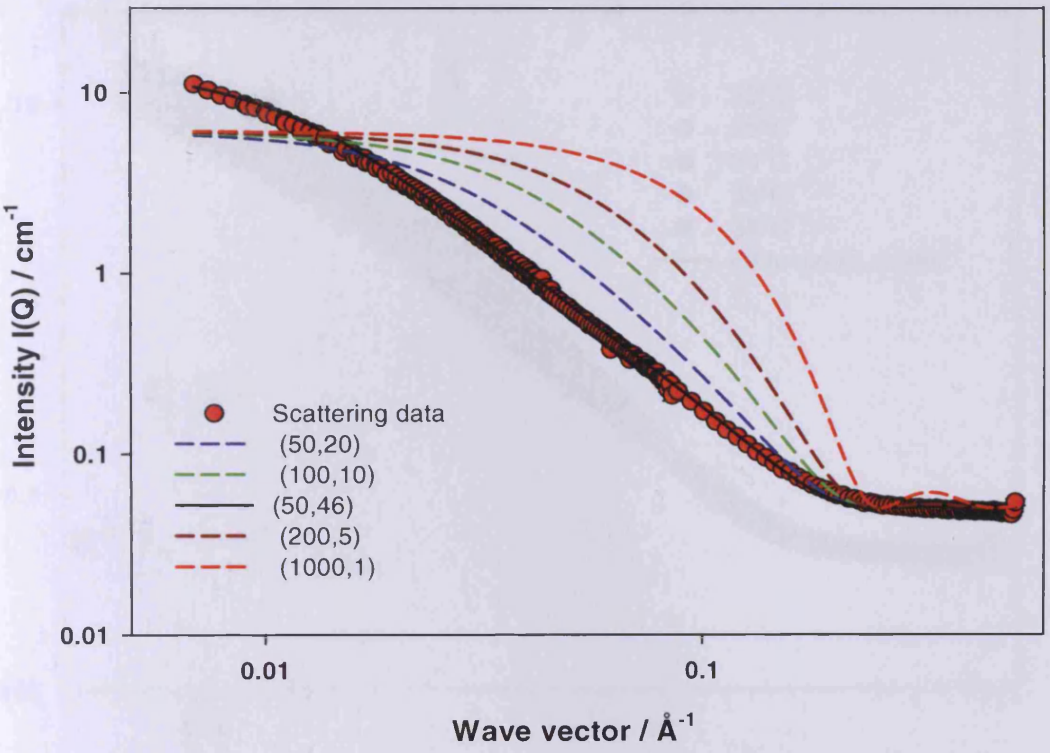

Figure 6-22: Kholodenko model data points for experiments (14 – 17), along with the raw scattering data and the best fit of 1.0 wt% Hybrid A in D_2O at 25°C

The conclusion from tested the sensitivity of the parameters of Kholodenko model. The most sensitive parameter seems to be the radius R_1, and for long chains, the fittings are much less sensitive to the number of segments *n* and their length *ell*.

The fitting were the FISH program [14],using a Gaussian coil for wormlike chains, named the Kholodenko worm-like chain model and the best fit values of the parameters describing the size and shape of particles presents in the samples. Both hybrid A and B in D_2O scattered in the same way at different temperature and their data were fitted to Kholodenko worm-like chain Figures 6-23 and 6.24 and also the parameters for these conjugates are shown in Tables 6-7 and 6-8.

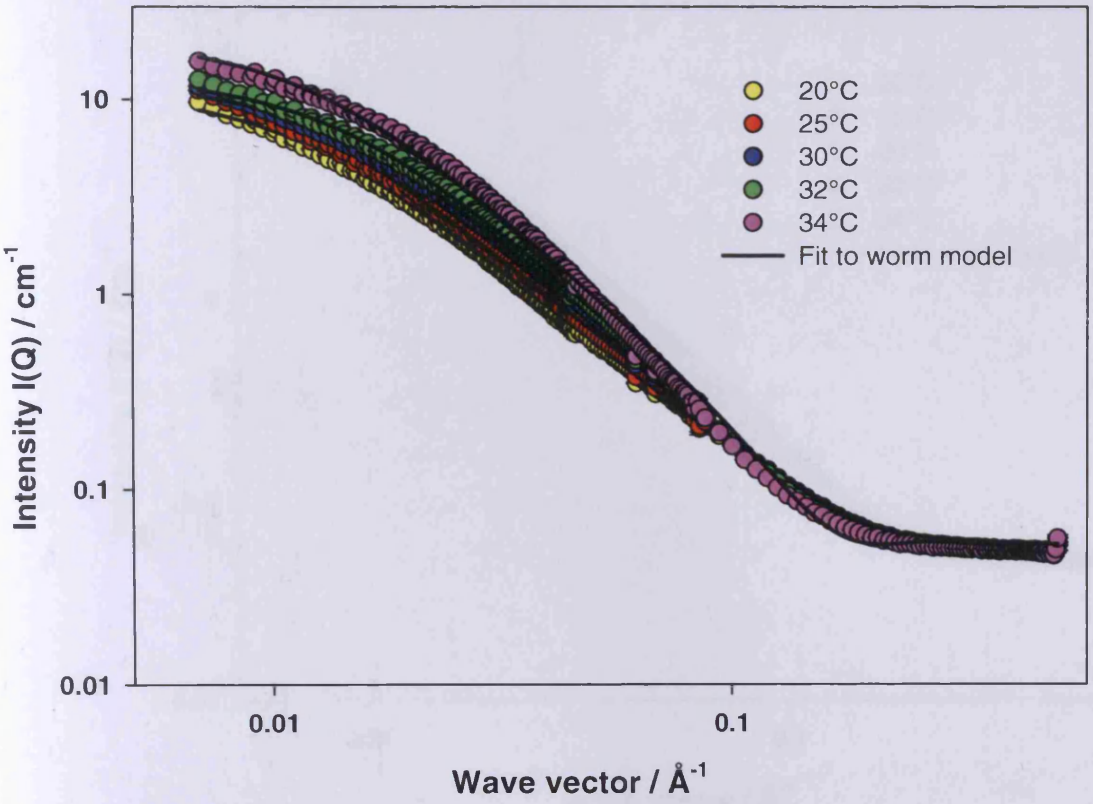

Figure 6-23: SANS data of 1.0 wt% hybrid A in D_2O at different temperatures and the black lines represent fitted data.

Temperature	R_1 /Å	n	ell/Å	(L = n * ell)/ Å
20°C	13	60	46	2760
25°C	14	60	44	2640
30°C	16	60	44	2640
32°C	16	60	42	2520
34°C	18	60	40	2400

Table 6-7: Fit parameters obtained from fish as Kholodenko worm-like chain model.

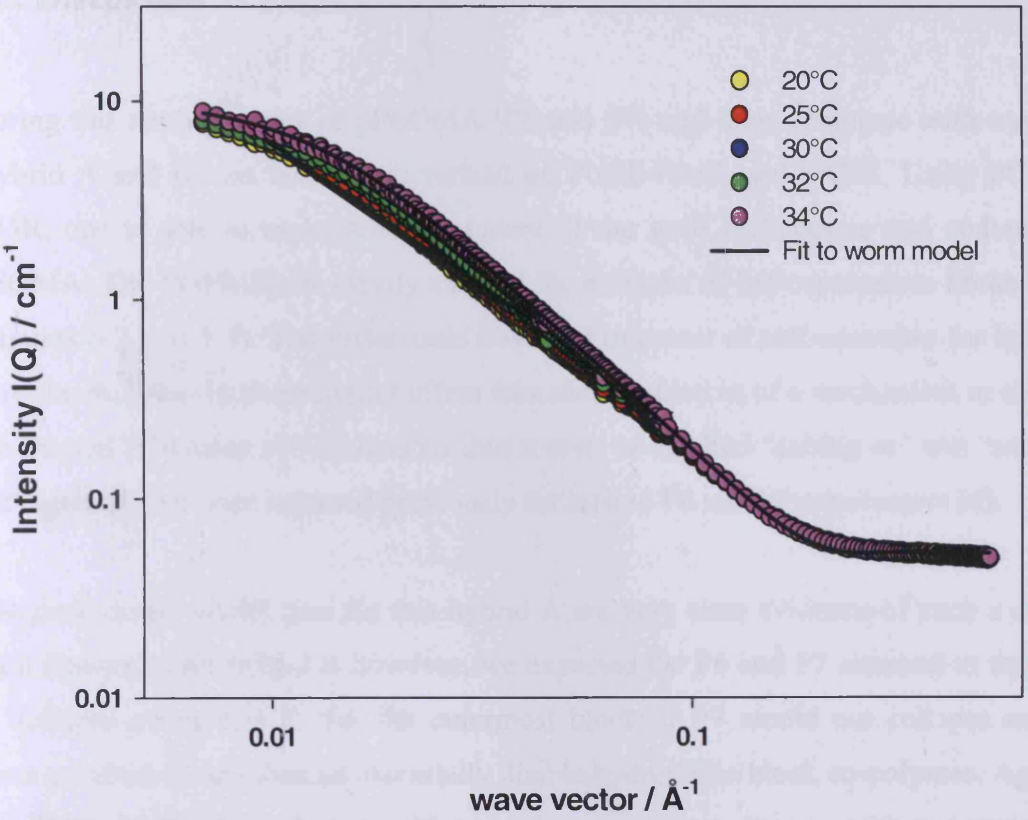

Figure 6-24: SANS data of 1.0 wt% hybrid B in D_2O at different temperatures and the black lines represent fitted data.

Temperature	R_1 /Å	n	ell/Å	(L = n * ell)/ Å
20°C	14	30	62	4860
25°C	15	30	58	1740
30°C	15	30	55	1650
32°C	14	50	42	2100
34°C	15	50	39	1950

Table 6.8: Fit parameters obtained from fish as Kholodenko worm-like chain model.

6.3. Discussion

During this study a series of pPEGMA (P6 and P7) and their conjugate with trypsin (hybrid A and B) has been characterized by PGSE-NMR and SANS. Using PGSE-NMR, one is able to understand the nature of the graft architecture and content of PEGMA. The PGPE-NMR clearly showed the collapse of the copolymers P6 and P7 (Figures 6-3 and 6-4). The differences observed in extent of self-assembly for hybrid A in the different ionic strength buffers was also suggestive of a mechanism in which the P6 and P7 chains self-associated into a core, as marked "salting in" and "salting out" effects have been reported previously for related P6 and P7 copolymers [6].

The peak in the SANS data for this hybrid A are very clear evidence of such a core-shell structure. For hybrid B however, we expected the P6 and P7 attached to trypsin to collapse above LSCT, but the outermost block of P7 would not collapse under these conditions, and thus an essentially double hydrophilic block co-polymer. Again, the PGSE-NMR show that the P6 and P7 component collapses with temperature. Although self-assembly of double-hydrophilic block co-polymers has been observed with other systems [15].

The SANS data P6, P7 and their conjugates hybrid A and B with trypsin data substantial differences in the scattering as a function of temperature. Both the intensity and the form of scattering change. All samples exhibited a similar pattern in that, with increasing temperature. Scattering data were fitted to polydispersed Gaussian coil at low temperature (20°C), while, and at high temperature were fitted to polydispersed two shell hard spheres (Figure 6-10 to 6-13). However, scattering behaviour of both polymers, P6, P7 at high temperature resembling conformational changed of the structure Figures 6-12 and 6-13 and Table 6-3. On the other hand, scattering data for trypsin, P6 and P7 conjugates (hybrid A and B) in D_2O solutions at temperatures 20-34°C, when were plotted $Q^2 * I(Q)$ against Q, which called Kratky plot (Figures 6-14 to 6-16). It can be seen from these figures the influence of temperature is more evident for hybrid A and B, while, trypsin did not much change with temperature, reflecting a denatured protein. According to the scattering data, both hybrid A and B were fitted to Kholodenko worm-like chain model, Figures 6-23

and 6-24 and fit parameters in Tables 6.7 and 6.8. While, trypsin data were fitted to solid ellipsoid model Figure 6.17.

6.4. Conclusion and future work

The solution conformation of two thermo- and ion-responsive polymers has been quantified by PGSE-NMR and SANS. With increasing temperature, the coil collapses as a consequence of the differing solubilities of the two consistent monomers. Na_2SO_4 has a more prouncned effect on the hybrid block copolymers, P6 and P7. The larger polymer when grafted to the protect trypsin (hybrid A and B), also showed a thermo-responsive behaviour. These data underline the feasibility of engineering polymers for polymer-protein conjugates that possess a unique, triggerable characteristic.

6.5. References

[1] Lgor Y. Galaev, B. Mattiasson, Tibtech August 17 (1999) 335-340.
[2] M. Aguilar, C. Evira, A. Gallardo, B. Vazquez, J. Roman, Tibtech August 3 (2007) 1-27.
[3] Kaled Al-Tahami, J. Singh, Recent Patents on Drug delivery & Formulation 1 (2007) 65-71.
[4] Eun Seok Gil, S.M. Hudson, Progress Polymer Science 29 (2004) 1173-1222.
[5] S. Fujishige, K. Ando, Journal of Physical Chemistry A, 93 (1989) 3311-3313.
[6] J. Magnusson, A. Khan, G. Pasparakis, A. Saeed, W. Wang, C. Alexander, Journal of American Chemical Society 130 (2008) 10852-10853.
[7] K. Min, H. Gao, K. Matyjaszewski, Journal of American Chemical Society 127 (2005) 3825-3830.
[8] G. Yasayan, A. O. Saeed, F. Fernandez-Trillo, S. Allen, M. C. Davies, A. Jangher, A. Paul, K. J. Thurecht, S. M. King, R. Schweins, P. C. Griffiths, J. P. Magnusson, C. Alexander., Polymer Chemistry 7 (2011) 1567-1578.
[9] P.C. Griffiths, A. Paul, P. Stilbs, E. Petterson, Macromolecules 38 (2005) 3539-3542.
[10] A. Paul, P.C. Griffiths, E. Pettersson, P. Stilbs, B.L. Bales, R. Zana, R.K. Heenan, Journal of Physical Chemistry B 109 (2005) 15775-15779.
[11] J. Davies, P. Griffiths, Journal of Physical Chemistry 95 (1991) 5677-5684.
[12] G. Stokes, Cambridge Philos.Trans.1851,9,8-106. Reprinted in Mathematical and Physical Papers, 2nd Ed.; Johnson Reprint Corp.: New York, 1996; Vol. 3, p 1.
[13] C. Heussinger, M. Bathe, E. Frey, Physical Review Letters 99 (2007).
[14] R. K. Heenan, Fish, Rutherford Appleton Laboratory, Didcot, UK.
[15] W. Agut, A. Brulet, D. Taton, S. Lecommandoux, Langmuir 23 (2007) 11526-11533.

Appendix

Published Manuscript

1. Polymeric micelle disruption by cosolvents and anionic surfactants

***Abdulhakim Jangher**, P. C. Griffiths, A. Paul, R.. Schweins, R. K. Heenan and S. M. King*

Submitted to *"Colloids and Surfaces A"*.

2. Responsive hybrid block co-polymer conjugates of portions-controlled architecture to modulate substrate specificity and solution behaviour.

G. Yasayan, A. O. Saeed, F. Fernandez-Trillo, S. Allen, M. C. Davies, ***Abdulhakim Jangher****, A. Paul, K. J. Thurecht, S. M. King, R. Schweins, P. C. Griffiths, J. P. Magnusson and C. Alexander, Polymer Chemistry 7 (2011) 1567-1578.*

Polymer Chemistry

View Online
Dynamic Article Links

Cite this: *Polym. Chem.*, 2011, **2**, 1567

www.rsc.org/polymers

PAPER

Responsive hybrid block co-polymer conjugates of proteins–controlled architecture to modulate substrate specificity and solution behaviour†

Gökçen Yaşayan,[a] Aram O. Saeed,[a] Francisco Fernández-Trillo,[a] Stephanie Allen,[a] Martyn C. Davies,[a] Abdulhakim Jangher,[e] Alison Paul,[e] Kristofer J. Thurecht,[b] Stephen M. King,[c] Ralf Schweins,[d] Peter C. Griffiths,[e] Johannes P. Magnusson*[a] and Cameron Alexander*[a]

Received 25th March 2011, Accepted 13th May 2011
DOI: 10.1039/c1py00128k

Responsive co-polymers based on polyethyleneglycol methacrylate (PEGMA) monomers have been grown by aqueous phase ATRP from a model protein, trypsin, to generate hybrid polymer-protein block conjugates. The conjugates (Hybrids **I** and **II**) both contained the same segment of grafted responsive co-polymer to afford a phase transition at 37 °C, Hybrid **II** however differed from Hybrid **I** by having a second block of hydrophilic pPEGMA monomer grown from the end of the responsive block. The resultant 'diblock' and 'triblock' hybrids were characterised in terms of their temperature-dependent behaviour in solution by dynamic light scattering, small-angle neutron scattering and pulsed-gradient spin-echo NMR, and their structures at surfaces examined by aqueous phase atomic force microscopy and cryo transmission electron microscopy. These data showed that Hybrids **I** and **II** differed in their solution behaviour with temperature, dependent on the arrangement of their grafted polymer blocks. Hybrid **I** self-assembled into higher-order structures above 37 °C before precipitating reversibly, whereas Hybrid **II** remained essentially constant in size across a similar temperature range even when its attached intermediate polymer block underwent a phase transition. The differences in polymer-protein hybrid behaviour were also manifest in enzyme activity assays with temperature-dependent hydrolysis of both peptide and protein substrates varying with hybrid architecture. Overall the data show that it is possible to grow responsive polymer-protein block co-polymers of varied structures, architectures and solution behaviour and that these can be used to control bioconjugate activity.

Introduction

Proteins and enzymes are increasingly used in biotechnology and medicine, but the utility of many is hampered by short half-life profiles in the bloodstream and limited stability *in vitro*.[1] These shortcomings can be addressed by engineering selective changes in amino acid sequences to create more stable derivatives, or by creating a protective/stabilising layer for the protein by attachment of polymers. In principle, the protective shell could be any material that is hydrophilic, stable and sterically shielding, but in practice poly(ethylene glycol) (PEG)-based polymers have been the most investigated.

The popularity of PEG polymers for bioconjugation arises from their inert chemistry once attached and their favourable toxicology profile, which has led to FDA approval.[2] However, in certain applications the inertness of PEG polymers can be disadvantageous, such as where strong cellular/membrane interactions are required, or if recycling of protein is necessary for a bioprocessing use. Moreover, attachment of non-functionalised PEG chains normally generates a permanent change in the activity of the protein, which cannot be manipulated to suit the inherently dynamic biological environment. It is thus highly desirable to devise protein conjugation strategies that enable the activity of the protein to be modulated in a controllable way.

Conjugation of responsive or 'smart' polymers offer a means by which this functional or behavioral change in a protein can be introduced and then controlled by an external stimulus. In general, responsive polymers exhibit a non-linear change in their

[a]*The School of Pharmacy, Boots Science Building, University of Nottingham, University Park, Nottingham, NG7 2RD, UK. E-mail: Johannes.magnusson@nottingham.ac.uk; cameron.alexander@nottingham.ac.uk; Fax: +44 (0) 115 951 5102; Tel: +44 (0) 846 7678*
[b]*Australian Institute for Bioengineering and Nanotechnology (AIBN), Corner College and Cooper Roads (Building 75), The University of Queensland, Brisbane, Queensland, 4072, Australia*
[c]*Science and Technology Facilities Council, Rutherford Appleton Laboratory, Harwell Science and Innovation Campus, Didcot, OX11 OQX, UK*
[d]*Institut Laue-Langevin, 6 rue Jules Horowitz, 38000 GRENOBLE, France*
[e]*School of Chemistry, Cardiff University, Main Building, Park Place, Cardiff, CF10 3AT, UK*
† Electronic supplementary information (ESI) available. See DOI: 10.1039/c1py00128k

properties following a stimulus, such as change in temperature, pH or *via* radiation.[3] Polymers of this type have been used in the bioconjugation context to aid in the recovery of proteins,[4] improve their stability,[5] or increase accumulation in a target tissue.[6] To date, the most extensively studied "smart" polymer is poly N-isopropylacrylamide (PNIPAm)[7] which exhibits a lower critical solution temperature (LCST) at 32 °C. The effect of PNIPAm on the activity of enzymes, and its application in the recovery of proteins have been widely reported.[4,8] Unfortunately, there are some concerns over potential PNIPAm cytotoxicity,[9] and as a consequence, "smart" poly(ethylene glycol methacrylate) (PEGMA) based copolymers[10] have been proposed as potential biocompatible alternatives.[11] The similarity of the PEGMA based polymers to PEG makes them promising candidates for biomedical applications.

Of particular interest is the possibility of using responsive PEGMA-type polymers as multi-faceted protein activity modifiers, wherein the variable conformations displayed by the polymer chains as they respond to stimuli invoke different functional properties of the protein. The additional advantage of PEGMA materials is their accessibility in a range of architectures through controlled polymerisation techniques. In previous papers we have described a fully aqueous route to responsive PEGMA materials,[12,13] and a number of PEGMA-protein conjugates have now been prepared.[14–18]

Here we show how PEGMA based polymers can be used to form responsive copolymer-protein conjugates by growing directly from the functionalised protein and, importantly, that the sequence and architectures of the attached co-polymers have a critical effect on the structures of the conjugates and on the activity of the conjugated protein. Thermoresponsive PNIPAm polymers have been grown from proteins previously[19–21] but to our knowledge growing a thermoresponsive PEGMA polymer from a biomacromolecule has not previously been reported. Trypsin was selected as the model protein due to its well known proteolytic activity and its importance in biotechnology applications.[22] Activity data for trypsin-polymer conjugates have also been reported previously,[23–27] and very recently a responsive PEGMA-trypsin polymer was described.[15] Through an extension of the fully aqueous atom transfer radical polymerization (ATRP) route, we have been able to prepare different polymer-protein architectures from a common trypsin ancestor, and have evaluated the solution behaviour and activity of these hybrids. We demonstrate that the architectures of the co-polymers and the structures of the two trypsin hybrid conjugates (Hybrids **I** and **II**, Scheme 1) change markedly following temperature stimuli across the phase transition temperatures, and that these structures in turn can be used to modulate the properties of the protein polymer hybrids in terms of stability and reactivity.

Materials and methods

All solvents and reagents were of analytical or HPLC grade and purchased from Sigma or Fisher Scientific unless otherwise stated. Deuterated solvents were purchased from Sigma.

Polyethylene glycol ethyl ether methacrylate (PEGMA-EE 246, M_n 246), and polyethylene glycol methyl ether methacrylate (PEGMA-ME 475, M_n 475) were purchased from Sigma Aldrich and purified before use by passing through a column filled with neutral alumina. N-α-Benzoyl-DL-arginine p-nitroanilide hydrochloride (BAPNA) (>98%), α-bromoisobutyryl bromide (98%), benzamidine hydrochloride (99%), casein (sodium salt), copper (II) bromide ($CuBr_2$, 99%), L-ascorbic acid (99%), N,N′-disuccinimidyl carbonate (DSC) (>95%) tetraethylene glycol (99%), triethylamine (99.5%), and trypsin from porcine pancreas were used as received from Sigma Aldrich. Phosphate Buffer Saline (PBS) was used as received from Fisher Scientific. 1X PBS used is equivalent to a concentration of 137 mM NaCl, 2.7 mM KCl and 10 mM phosphate buffer. Water used for the polymerisations was of ELGA grade. Tris(2-pyridyl) methylamine (TPMA) was prepared as described elsewhere.[28] Dialysis membrane (MWCO 6-8000, regenerated cellulose) was used as received from Spectrapor. Centrifugation was carried out using a Centaur II centrifuge.

For AFM studies, mica discs and specimen discs were purchased from Agar Scientific (Stansted, UK), SNL-10 (Sharp Nitride Lever-10) AFM probes were purchased from Bruker (Cambridge, UK). Syringe filters (20 nm, Anotop 10) were purchased from Whatman (Kent, UK) and 0.2 μm syringe filters were purchased from Interlab (Wellington, New Zealand).

Measurements and analysis

Gel permeation chromatography (GPC)

Molecular weights and molecular weight distributions were determined using a Varian/Polymer Laboratories GPC-50 instrument with triple detection (RI, viscometry and MALLS). Chromatograms were run at 40 °C using chloroform ($CHCl_3$) as eluent with a flowrate of 1 ml min^{-1}. The columns used were Resipore Mixed-D, detection was performed by a Refractive

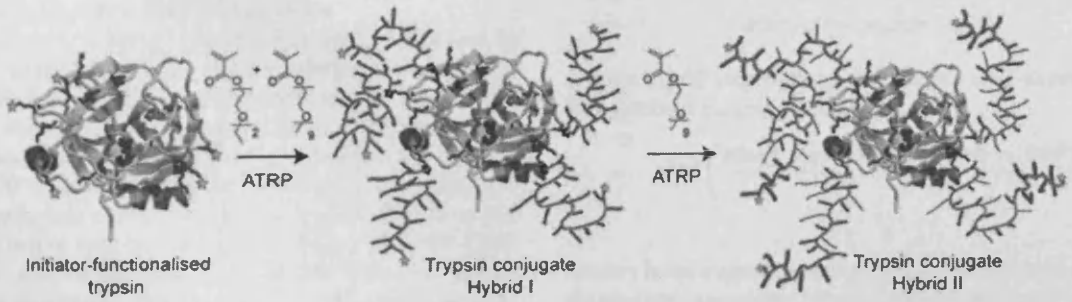

Scheme 1 Design criteria of trypsin conjugates with a statistical responsive co-polymer hybrid (trypsin–Hybrid **I**) and a triblock (trypsin Hybrid **II**).

Index detector (RI). The machine was calibrated with linear polystyrene standards.

Polymers were cleaved specifically by adapting a method from Jaquemard *et al.*[29] The protein polymer hybrid (20 mg), 10 mL of anhydrous THF and 200 μL of tetra-n-butylammonium fluoride (TBAF) were placed in a round bottom flask with a condenser and the mixture was refluxed for 6 h. The THF was evaporated and the polymer extracted into chloroform and analysed by GPC.

SDS PAGE

SDS-PAGE gel electrophoresis was carried out at 100 mV using 8% acrylamide running gel and 4% stacking gel prepared by the standard method (non denaturating conditions) and visualised by Coomassie staining.[30]

The gels were additionally stained to detect PEG using the barium/iodine method.[31]

DLS (Dynamic light scattering)

Hydrodynamic radii of the protein polymer hybrids in solution were measured *via* scattered light recorded at a 90° angle to incident radiation in a Viscotek 802 dynamic light scattering (DLS) instrument equipped with a 50 mW internal laser operating at a wavelength of 830 nm. From standard auto correlation functions, measured diffusion coefficients were related to particle hydrodynamic radius *via* the Stokes–Einstein equation

$$R_H = kT/6\pi\eta D$$

where R_H is the hydrodynamic radius, k is the Boltzmann constant, T is the temperature, and η is the viscosity of the solvent. Additionally it was assumed that particles were spherical and non-interacting.

Measurements quoted are the averages of triplicate samples of six replicates with at least 10 readings of particle size recorded at each temperature. Radii quoted are averages for samples where >75% of the scattered light in terms of particle masses was from polymers within the size range quoted unless otherwise stated.

Transmission Electron Microscopy (TEM)

Samples were prepared on carbon/formvar grids which were made hydrophilic by argon plasma cleaning (in a Fischione Model 1020 Plasma Cleaner) prior to use. Samples were spotted onto the grid with a Cryo-plunge (CP3 Gatan Inc) and were instantaneously frozen using liquid ethane, creating a frozen hydrated sample in a thin film of vitreous ice.

Solutions of each hybrid (1 mg mL^{-1}) in 0.05 M Tris and 20 mM $CaCl_2$ buffer were prepared, the solutions were filtered through a 200 nm syringe filter. Samples below the cloud point temperature were spotted onto grids without any further treatment. Samples above the cloud point temperature were heated for 5 min at 70 °C prior to the solution spotting process. In these cases the appropriate solution (5 μL) was placed directly on the Cryo-plunge before application on the chilled grid. Cryo-TEM spectroscopy was carried out on a JEOL Ltd JEM-2100F microscope with a Gatan 914 Cryo-tomography holder. Images were taken with a Gatan Orius camera.

Atomic Force Microscopy (AFM)

Topography images and particle analysis of Hybrid I and Hybrid II were acquired in liquid with AFM (MultiMode Scanning Probe Station with Nanoscope IIIa controller (Bruker, Santa Barbara, CA) operating tapping mode. Images were acquired using an E-scanner, at scan rates between 5–8 Hz.

AFM height images of trypsin were obtained in liquid at room temperature using a Multimode 8 Scanning Probe Microscopy station, operating in PeakForce Tapping™ mode. This imaging mode permitted greater control of probe-sample contact force and facilitated imaging of these samples. Images were acquired using an E-scanner, at scan rates between 1–2 Hz.

AFM studies on the hybrids were carried out at different temperatures using an external heating stage (Nanoscope, Bruker, Santa Barbara, CA). The samples were injected onto freshly cleaved mica at 30 °C and the temperature increased to 40 °C; finally the temperature was reduced to 30 °C. These experiments were designed to assess the aggregation behaviour of the protein-polymer hybrids and determine whether the aggregation was reversible.

For AFM experiments all protein and protein-polymer conjugate solutions were prepared at a concentration of 10 μg ml^{-1} with 0.05 M Tris buffer, containing 20 mM $CaCl_2$ (pH 8.2) and filtered with a 20nm syringe filter. Image data were analysed using NanoScope Analysis software (Version 1.20 (Bruker)).

MALDI TOF (Matrix-assisted laser desorption/ionisation–time of flight)

MALDI TOF analysis was carried out on a Bruker MALDI TOF Ultraflex II machine.

Samples were prepared as described elsewhere.[32] Briefly an aqueous solution of the conjugate (1.0 mg mL^{-1}) was mixed with an equal volume of matrix material (8 mg sinapic acid, 0.5 mL water and 0.5 mL MeCN). An aliquot (2 μL) of the resulting mixture was spotted on to a plate target and allowed to dry. The level of conjugation was determined by comparing the molecular weight of conjugate to native trypsin.

Pulsed-Gradient Spin-Echo NMR (PGSE-NMR)

Measurements were conducted on a Bruker AMX360 NMR spectrometer using a stimulated echo-sequence, as described elsewhere.[33] This configuration uses a 5 mm diffusion probe (Cryomagnet Systems, Indianapolis) and a Bruker gradient (GRASP) spectroscopy accessory unit to deliver trapezoidal gradient pulses.

The self-diffusion coefficient D_s was extracted by fitting the integrals for a given peak to eqn (1);

$$A(\delta,G,\Delta) = A_0\exp(-kD_s) \quad (1)$$

A is the signal amplitude in the absence (A_0) or presence of the field gradient pulses ($A(\delta,G,\Delta)$),

$$k = -\gamma^2G^2\left(\frac{30\Delta(\delta+\sigma)^2-(10\delta^3+30\sigma\delta^2+35\sigma^2\delta+14\sigma^3)}{30}\right) \quad (2)$$

where γ is the magnetogyric ratio, Δ the diffusion time (140 ms), σ the gradient ramp time (250 μs), δ the gradient pulse length (500 μs $< \delta <$ 3 ms) and G the gradient field strength (0.5 $< G <$ 3 T m^{-1}).

Small-Angle Neutron Scattering (SANS)

Small-angle neutron scattering (SANS) measurements were performed on two instruments-the fixed-geometry, time-of-flight LOQ diffractometer (ISIS Spallation Neutron Source, Oxfordshire UK) and the fixed-wavelength D11 diffractometer (ILL, Grenoble, France). On LOQ, neutron wavelengths spanning 2.2 to 10 Å were used to access a Q range ($Q = 4\pi\sin(\theta/2)/\lambda$) of approximately 0.008 to 0.25 $Å^{-1}$ (25 Hz), with a fixed sample-detector distance of 4.1m. On D11, the wavelength was set at 8 Å, and three sample-detector distances were employed to span a comparable Q range. On both cameras, the samples were contained in 2 mm path length, UV-spectrophotometer grade, quartz cuvettes (Hellma) and mounted in aluminium holders on top of an enclosed, computer-controlled, sample chamber. Sample volumes were approximately 0.4 cm^3. Temperature control was achieved through the use of a thermostated circulating bath pumping fluid through the base of the sample chamber. Under these conditions a temperature stability of better than ± 0.5 °C can be achieved. Experimental measuring times were approximately 40 min.

All scattering data were (a) normalised for the sample transmission, (b) background corrected using a quartz cell filled with D_2O (this also removes the inherent instrumental background arising from vacuum windows, *etc.*) and (c) corrected for the linearity and efficiency of the detector response using the instrument-specific software package. The data were put onto an absolute scale by reference to the scattering from a partially deuterated polystyrene blend (LOQ) or 1 mm water (D22).

BCA (Bicinchoninic acid) protein assay

Protein content quantification of protein polymer hybrids was assessed using the BCA assay of Smith *et al.*[34] In a typical assay, solutions (3.0 mg mL^{-1}) of the protein polymer hybrids were incubated with a BCA/copper solution and the absorbance read at 562 nm. This absorbance was compared to a calibration from a bovine serum albumin standard.

Cloud-point and Lower Critical Solution Temperature (LCST) determinations

A protein polymer stock solution (3.0 mg mL^{-1}) was prepared using double distilled water (DDW) and the appropriate salts. The UV absorption for each sample was measured at a wavelength of 550.0 nm over a temperature range of 20.0 °C–65.0 °C. The temperature was controlled and measured using a peltier plate heating system (Beckman) and was increased at a rate of 0.5 °C min^{-1}. We considered the cloud point to be the onset of a sharp increase in UV absorption at 550 nm in accordance with prior studies.[35] A Beckman Coultier DU 800 UV spectrophotometer with a thermostat was used for activity assays and cloud point measurements.

Trypsin activity assay and enzyme kinetics using BAPNA (N-α-Benzoyl-DL-arginine 4-nitroanilide hydrochloride)

The activity of the trypsin hybrids towards a small molecule substrate was estimated according to the method of Erlanger *et al.*[36] A fresh solution of BAPNA was made by dissolving 40 mg in 2.5 mL of DMSO and diluting to 50 mL with 0.05 M Tris HCl/20 mM $CaCl_2$ buffer—pH 8.2. 280 μL of BAPNA solution was used for each assay. The solution was equilibrated at appropriate temperature for 10 min, then 20 μL of trypsin aliquots (160 μg mL^{-1} eq. of native trypsin) were added, initial absorbance change was recorded at 410 nm. Relative activity of the hybrids was estimated by comparing the change in absorbance to that of native trypsin at 22 °C.

Michealis Menten plots were derived for the polymer hybrids and native protein at 26 °C and 40 °C respectively. 185 μL of BAPNA solution (at various concentrations) were used for each assay, the solution was incubated on a UV spectrometer with a temperature control for 10 min before adding 15 μL of protein solution (160 μg mL^{-1} eq. of native trypsin) to the cuvette. The change in absorbance at 410 nm was read immediately for each of the concentrations. All experiments were carried out in triplicate.

Trypsin protease activity towards casein

The activity of the hybrids against a macromolecular substrate was estimated according to the method of Singh and Krikorian[37] A 2.5% solution of casein in Tris buffer (0.05 M Tris HCl, 20 mM $CaCl_2$ pH 8.2) was prepared. Casein solution (1.0 mL) and Tris buffer (350 μL of 0.05 M Tris HCl; 20 mM $CaCl_2$ pH 8.2) were used for each assay. The solution was equilibrated at the appropriate temperature for 10 min after which trypsin aliquots (100 μL of 80 μg mL^{-1} of trypsin eq.) were added and incubated for 20 min. The reaction was stopped by adding 10% trichloroacetic acid (2.0 mL) to the solution, the mixture was centrifuged at 4000 rpm for 30 min and the clear supernatant collected. The absorbance of the solution was recorded at 280 nm and then compared to absorbance of a native trypsin solution to determine the relative activity. All experiments were carried out in triplicate.

Trypsin thermal stability

Native trypsin and hybrids solutions were incubated at room temperature and 37 °C over 2 days (160 μg mL^{-1} eq. of native trypsin) in 1X PBS buffer at pH 7.4. The residual activity was measured using the BAPNA assay by incubating 185 μL of BAPNA solution with 15 μL of protein solution for 10 min at room temperature. The initial change in absorbance was measured at 410 nm and compared to that of the protein solutions prior to heating.

Modification of trypsin: conjugation of ATRP initiator functionality trypsin

Linker synthesis was carried out as previously reported.[14] Trypsin (760 mg, 0.034 mmol) and benzamidine hydrochloride (48 mg, 0.30 mmol) were dissolved in 76 mL of 100 mM PBS and the pH was adjusted to 7.5. The amine reactive triethylene glycol ATRP initiator (400 mg, 0.82 mmol) was dissolved in 1.5 mL of DMSO and added dropwise, the reaction was left to react for 90 min. The mixture was dialysed with a cellulose membrane MWCO 6-8000 for 2 days at 4 °C, centrifuged at 4000 rpm, the supernatant collected and lyophilised. The total amount of modified trypsin was 760 mg.

Polymerisation of trypsin-statistical polymer Hybrid I. Trypsin (384 mg, 0.016 mmol (5 modified lysines on average)), PEGMA–EE-246 (5.0 g, 20.4 mmol), PEGMA–ME-475 (1.7 g, 3.6 mmol), $CuBr_2$ (35.7 mg, 0.16 mmol) and TPMA (46.5 mg, 0.016 mmol) were dissolved in 20 mL of 50 mM PBS pH 8.0. The mixture was placed in an ice bath at 4 °C and bubbled through with argon for 15 min, after which ascorbic acid (4.23 mg, 0.024 mmol) was added to initiate the polymerisation. The reaction was stopped after 16 h and free monomer, copper and ligand were removed by dialysis (MWCO 6-8000). The dialysis was carried out for 3 days at 4 °C in water with EDTA (4 mM) present. After lyophilisation 2.8 grams of viscous material Hybrid I were recovered.

Polymerisation of trypsin–triblock Hybrid II. Hybrid **I** (1.4 mg, 0.006 mmol), PEGMA–ME-475 (3.6 g, 7.5 mmol), $CuBr_2$ (26.8 mg, 0.12 mmol) and TPMA (34.8 mg, 0.012 mmol) were dissolved in 9 mL of 50 mM PBS pH 8.0. The mixture was placed in an ice bath at 4 °C and bubbled through with argon for 15 min, after which ascorbic acid (3.17 mg, 0.018 mmol) was added to initiate. The reaction was stopped after 16 h and free monomer, copper and ligand were removed by dialysis (MWCO 6-8000). The dialysis was carried out for 3 days at 4 °C in water with EDTA (4 mM) present. After lyophilisation 2.0 grams of viscous material Hybrid **II** were recovered.

Responsive co-polymers to match those grafted from Hybrid I and Hybrid II, *i.e.* a $(PEGMA\text{-}EE\text{-}246)_{85}$-stat-$(PEGMA\text{-}ME\text{-}475)_{15}$ (Co-Polymer 1) and a $[(PEGMA\text{-}EE\text{-}246)_{85}$-stat-$(PEGMA\text{-}ME\text{-}475)_{15}]_{92}$-*graft*-$(PEGMA\text{-}ME\text{-}475)_{50}$ (Co-Polymer 2) were prepared by our previous methods.[12]

Results

The pre-requisite for preparing responsive co-polymer conjugates with varying architectures required a method to grow statistical and block materials from the protein of choice, in this case, trypsin. Our prior routes to "smart" PEGMA copolymers[12] utilised polyethylene glycol ethyl ether (PEGMA-EE-246; M_n 246) and polyethylene glycol methyl ether (PEGMA-ME-475; M_n 475) methacrylates, with varying monomer feed and the AGET ATRP method[38] to produce co-polymers under fully aqueous conditions. These afforded polymers with LCST values across a wide temperature range. Accordingly, we needed ATRP initiator sites on the protein, and thus synthesised a hetero-bifunctional linker with an amino-reactive terminus and a radical generating center (Scheme 2). The linker was synthesised from a tetraethylene glycol (TEG) precursor *via* a published route.[14]

The initiator was conjugated to accessible lysine residues on the protein through a succinimidyl succinate reactive group, in phosphate buffered saline (PBS) with an excess of the ATRP initiator and benzamidine hydrochloride present. This generated the 'core' functionalised trypsin (Scheme 2 and Fig. 1a) used in subsequent polymerisation experiments. Benzamidine was used to protect the active sites of trypsin from potential conjugations and to prevent autocatalysis since it is a known inhibitor of the enzyme.[39]

The polymerisation from trypsin was carried out at low temperature (4 °C) under aqueous conditions. A polymer with a targeted LCST of 37 °C was initially grown from the functionalised trypsin protein to create co-polymer trypsin Hybrid **I**

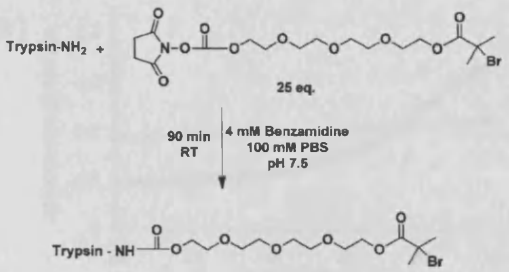

Scheme 2 Conjugation of initiator-functionalised trypsin.

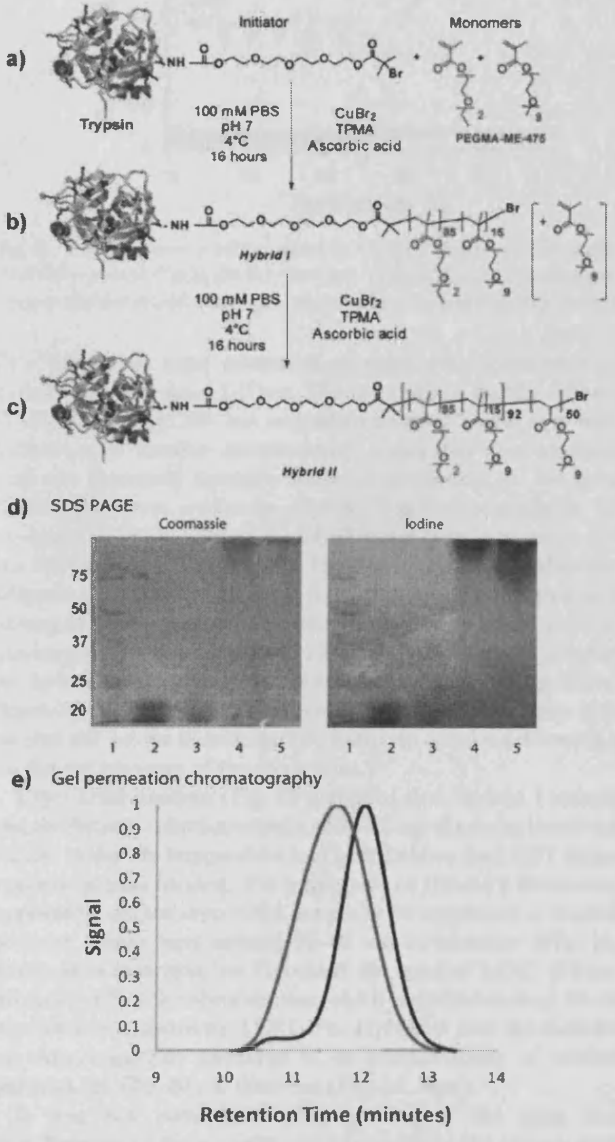

Fig. 1 Synthetic scheme for initiator-functionalised trypsin (a), Hybrid I (b) and Hybrid II (c). SDS PAGE (d) for Hybrid I and II with stains for protein (Coomassie) and PEG (iodine) indicate success of polymer growth from trypsin (Lane 1: Marker; Lane 2: Native Trypsin; Lane 3: Initiator-functionalised Trypsin; Lane 4: Hybrid I, Lane 5: Hybrid II). e) Gel permeation traces of polymer after cleavage from protein. (Black trace–Hybrid I, Green Trace–Hybrid II).

(Table 1, Fig. 1b). The purified polymer conjugate was then split into portions, of which one was used to initiate a second polymerisation with PEGMA-ME-475 to create the triblock trypsin Hybrid II. (Table 1, Fig. 1c).

Electrophoresis (SDS PAGE, Fig. 1d) revealed that all of the activated trypsin had polymerised to form Hybrid I *i.e.* no native or initator-functionalised trypsin was observed in the SDS PAGE gel after polymerisation. An additional low molecular weight band was observed in the gel for the native trypsin and to a less extent for the initiator functionalised trypsin, which stems from its autocatalysis. This was not observed for the polymerised trypsin as the polymer chains decreased autocatalytic breakdown, most likely due to increased steric hindrance. Neither hybrid penetrated the gel to a great extent due to their bulkiness. Characterisation (Fig. 1e) of the polymer species grown from the proteins was achieved by treatment of the conjugates with tetrabutylammonium fluoride to cleave the polymer-protein links. GPC analysis indicated that the polymer cleaved from Hybrid I was mostly of narrow polydispersity although a small tail was observed towards the high molecular weight range; the calculated polydispersity for the main peak was 1.19. The polymers from Hybrid II exhibited broader molecular weight distribution (PDI 1.53) than their precursors but the peak observed was symmetrical. Comparison of the two chromatographs clearly showed that Hybrid I had efficiently initiated the polymerisation of PEGMA-ME-475 to form Hybrid II.

The solution properties of Hybrids I and II were examined by means of dynamic light scattering (DLS, ESI†) and UV turbidity as a function of temperature. Both conjugates were shown to exhibit temperature-dependent solution behaviour, but the specific effects were different for each polymer, and strongly dependent on the ionic environment of the solution. (Fig. 2)

In isotonic phosphate-buffered saline (PBS) solution, both hybrids exhibited increases in turbidity at raised temperature, although the increase was much smaller for Hybrid II than Hybrid I. In Tris buffer, Hybrid I showed a large increase in turbidity above the LCST, indicating aggregation or assembly to larger objects. Conversely, Hybrid II exhibited a slight decrease in turbidity at the onset of LCST, implying that above the LCST the aggregation state or size of objects present in solution decreased. DLS experiments (ESI†) recorded in Tris buffer showed that in all cases, mixed populations of species were present in suspensions, indicating some heterogeneity in the conjugates across the temperature ranges. Particle size distributions based on scattered light intensity were dominated by the larger species, but estimated sizes based on number distributions suggested that for both Hybrid I and II in Tris buffer, non-aggregated particles were the majority species. For Hybrid II in Tris buffer, the most numerous particles were those with an average R_H of around 5–7 nm. The size was not greatly affected by the onset of LCST but seemed to decrease slightly (in both intensity and number distributions), which was in accordance with the decreased turbidity observed previously. In the same buffer, the most numerous Hybrid I particles exhibited an average R_H of 5 nm below the LCST but a large increase to 150 nm above the LCST (see ESI†). The different solution behaviour between the two buffers stems from their different salting out/salting in properties, we have previously demonstrated that the thermoresponsive behaviour of PEGMA is significantly affected by the ionic environment.[12] In order to evaluate the temperature-dependent behaviour further, cryo-TEM and AFM analysis were carried out on the hybrids in Tris buffer to acquire information on the morphology of the conjugates.

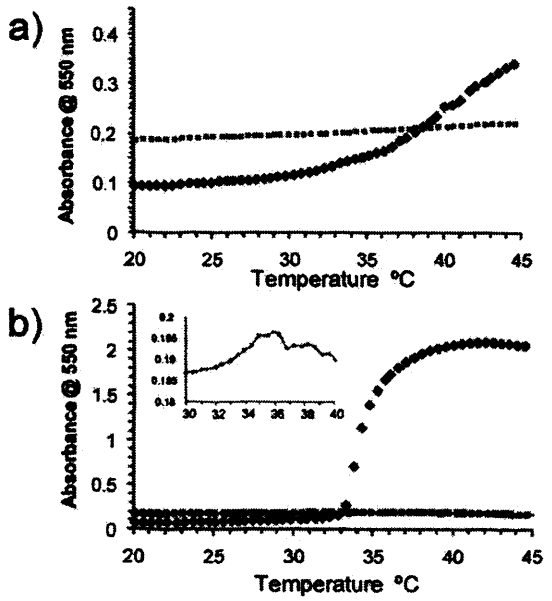

Fig. 2 Temperature-turbidity curves in 1X PBS (top) and Tris buffer (0.05 M + 20 mM $CaCl_2$ pH 8.2, bottom). Trypsin Hybrid I (blue trace). Trypsin Hybrid II (red trace). (Expanded area—Hybrid II in Tris buffer).

Cryo-TEM analysis (Fig. 3) suggested that Hybrid I formed mainly discrete spherical objects of 70–80 nm diameter below the LCST. When the temperature was raised above the LCST larger aggregates were formed. The aggregates of Hybrid I themselves appeared from the cryo-TEM images to be composed of smaller particles which were around 30–40 nm in diameter (Fig. 3b, inset). In comparison, for Hybrid II the onset of LCST did not markedly affect the observed size, which remained around 20–50 nm below and above the LCST. For Hybrid II also the particles on close inspection appeared to be conglomerates of smaller particles, of ~10–20 nm diameter (Fig. 3d, inset).

It was not possible to discern whether the sizes and morphologies of the particles and aggregates in the images were inherent or influenced by dehydration/flash-freezing artefacts by TEM alone. Accordingly, we investigated the morphologies of the protein-polymer conjugates by AFM of particles in aqueous suspension. The images obtained showed that under all conditions the conjugates were approximately spherical, although there was a size range of particles across all the samples (Fig. 4).

Table 1

Hybrid	Initiators[a]	M_n[b]	M_w/M_n[b]	LCST[c]	BCA[d]
I	5.1	28300	1.19	36 °C	14.82%
II	5.1	45606	1.53	36 °C	9.14%

[a] Average number of initiating sites as determined with MALDI TOF. [b] From GPC—length of each polymer chain. [c] Cloud point measured by UV absorption of 3 mg mL^{-1} solutions in 1X PBS at 550 nm. [d] Protein content determined by bicinchoninic acid assay (BCA).

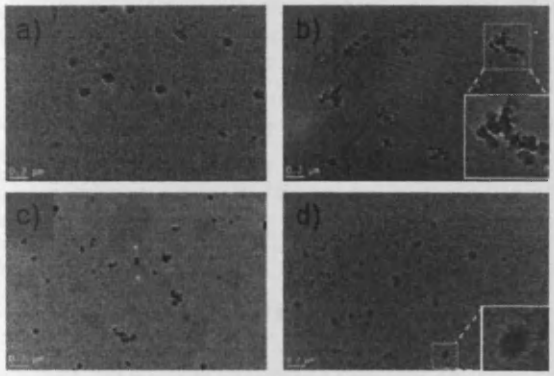

Fig. 3 Cryo-TEM imaging of trypsin conjugates in 0.05 M Tris and 20 mM $CaCl_2$ buffer. a) Hybrid **I** flash-frozen from solution at temperatures below the LCST, b) Hybrid **I** flash-frozen from solution at temperatures above the LCST, c) Hybrid **II** frozen from below the LCST, d) Hybrid **II** frozen from above the LCST (scale bars 0.2 μm). Insets to (b) and (d) show particles at higher magnification.

To probe their self-assembly behaviour, a heating stage was utilised, *in situ*, and samples were imaged at 30 °C before increasing the temperature to 40 °C. Following imaging at this increased temperature, samples were cooled to 30 °C and then imaged again. Samples were left for at least 30 min following temperature increases/decreases, to allow samples to equilibrate prior to resuming imaging.

Grain size analysis of the features observed in AFM at each temperature showed that the mean diameter of the Hybrid **II** remained between 7–11 nm at all temperatures, while the mean diameter of Hybrid **I** increased from 7 nm (at 30 °C) to ~ 24 nm (at 40 °C), with the maximum size at this temperature of 58 nm (Table 2). The mean particle size of Hybrid **I** returned to ~ 11 nm when the system was cooled down to 30 °C, possibly reflecting that full dissociation of the aggregates was hindered by the presence of underlying mica surface.

Further characterisation of the solution conformation of the hybrids, and their PEGMA analogues, was carried out by pulsed-gradient spin-echo NMR (PGSE-NMR) and small-angle neutron scattering (SANS). The self-diffusion coefficients measured by PGSE-NMR were recast in terms of the corresponding hydrodynamic radii and the temperature dependence of this estimate of the solution conformations are presented in the ESI.† From this data trypsin was shown not to display any marked change in solution conformation over the temperature range 20–35 °C. The PEGMA polymers—here used as models for the thermoresponsive grafts grown from the trypsin core—did show the expected monotonic decrease in hydrodynamic radii over the same temperature range. However, the NMR diffusion experiments were performed at temperatures below the LCSTs owing to the difficulties in interpreting signal broadening of the polymers alone as they precipitated at the LCST.

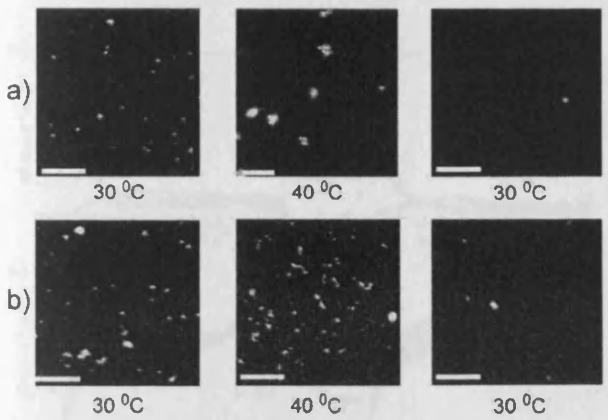

Fig. 4 Selected AFM topography images of a) Hybrid **I** and b) Hybrid **II**. The system was heated to 30 °C (left hand panel), then to 40 °C (middle panel) before being cooled to 30 °C (right hand panel). Scale bars are 100 nm. Vertical scale is 8 nm for Hybrid **I** at 40 °C and 2 nm for the other images.

For the polymer-trypsin conjugates, *i.e.* Hybrid **I** and **II**, rather different temperature responses were observed compared to each other and compared to the native enzyme and the non-conjugated polymers. Hybrid **I** showed a monotonic decrease in hydrodynamic radius with increasing temperature, similar to that observed for the polymer model itself. The radius of the conjugate was always greater than that of the free PEGMA polymer and the trypsin. Hybrid **II** on the other hand displayed a different temperature profile, showing a pronounced decrease in size around 28 °C, with the size at the higher temperature approaching that of the trypsin core. The collapse of the triblock grafts thus appeared to give rise to a changed architecture of the conjugate relative to polymer collapse in the diblock conjugate, with both qualitative and quantitative agreement with the behaviour observed in the AFM studies.

Additional insight was gained by considering the solution neutron scattering. Data are presented in two formats—as a conventional (raw data) plot ($I(Q)$ *vs.* Q) in the ESI,† and in the form of a Kratky plot ($Q^2I(Q)$ *vs.* Q, which emphasises the departure from Gaussian statistics of the polymer conformation) which yielded information on the differences in the two conjugate structures and their variation with temperature. The conventional plot indicated that with increasing temperature, Hybrid **I** (diblock) and Hybrid **II** (triblock) polymers showed an increase in scattering. At low temperatures the monotonically decaying data were well-described by a simple polydisperse Gaussian coil model, with radii of gyration of few nanometres, consistent with the AFM and NMR estimates of the solution conformation. At higher temperatures, points of inflexion were evident in these exemplar data, indicating that the structures present possessed delineated or phase separated regions with different scattering length densities, *i.e.* core–shell structures. Indeed, such a model fitted the data well, with core radii of a few nanometres and a slightly thicker shell, although these quantities should not be over interpreted in the absence of other confirmatory techniques.

The Kratky representation emphasised these differences rather more markedly. The scattering from a typical Gaussian coil, which varies as $I(Q) \sim Q^{-2}$ would be expected to increase to a plateau, attaining a horizontal asymptote. A compact or globular structure would exhibit a maximum at a Q value corresponding to some characteristic length scale, *e.g.* a radius of gyration or correlation length.

As may be seen and as expanded in the ESI,† the PEGMA diblock (Fig. 5a) and triblock (Fig. 5b) polymers at low

Table 2 Analysis of the sizes of features observed in AFM images of trypsin, Hybrid **I** and Hybrid **II**. The system was heated to 30 °C (i), then subsequently to 40 °C. (ii), and afterwards cooled down to 30 °C. (iii). Image data were analysed using NanoScope Analysis software

	Total particle count	Mean diameter (nm)	Minimum diameter (nm)	Maximum diameter (nm)
Trypsin	87	4.3	3.3	8.1
Hybrid I at 30 °C (i)	99	6.8	3.7	14.2
Hybrid I at 40 °C (ii)	101	23.7	10.3	58.3
Hybrid I at 30 °C (iii)	8	11.2	7.6	15,8
Hybrid II at 30 °C (i)	98	7.4	3.7	14.9
Hybrid II at 40 °C(ii)	122	7	3.4	17.5
Hybrid I at 30 °C (iii)	50	10.6	3.4	19.1

temperature exhibited the behaviour expected for a Gaussian coil, but showed pronounced peaks as the temperature approached that at which the polymer phase separated. No macroscopic phase separation was observed in these samples. Again, Hybrid **I** and **II** were easily distinguished by their temperature profiles—Hybrid **I** (Fig. 5c) showed a pronounced peak at $Q = 0.025$ Å^{-1}, corresponding to $R = 25$ nm, whereas Hybrid **II** (Fig. 5d) showed only a change in slope at this Q value. This suggests that Hybrid **I** possessed a much more compact structure, or associated into a higher order structure with a characteristic dimension somewhat larger than the single bio-conjugate molecule precursor, but Hybrid **II** did not self-assemble in the same way.

Having shown the variation of polymer architecture on the assembly of Hybrid **I** and **II**, we investigated the effect on trypsin stability and activity. Initial experiments focused on trypsin-mediated hydrolysis of N-α-benzoyl-DL-arginine p-nitroanilide hydrochloride (BAPNA). Assays were carried out using native trypsin and the Hybrid **I** and **II** conjugates with different concentration of BAPNA and at temperatures below and above the LCST (Fig. 6). The data showed that modification of the protein increased stability over time towards BAPNA hydrolysis (Fig. 6a) but decreased the turnover rate of the enzyme and its affinity for the peptide substrate (Fig. 6b and c). There was however a significant difference between the two hybrids with temperature change. Below the LCST of the attached polymers (Fig. 6b) both hybrids exhibited similar turnover rate and affinity for the low molar mass BAPNA substrate. Above the LCST (Fig. 6c), Hybrid **I** exhibited higher turnover than Hybrid **II** but significantly lower affinity for the substrate.

In assays to probe whether variations in polymer-enzyme conjugate self-assembly were responsible for the differences in Hybrid **I** and Hybrid **II**, we examined the activities of the conjugates towards substrates of different size. The activities of the hybrids were studied, again using the model peptide BAPNA, but compared with a protein (casein) to assess hydrolysis of a higher molar mass substrate. The activities were mapped across

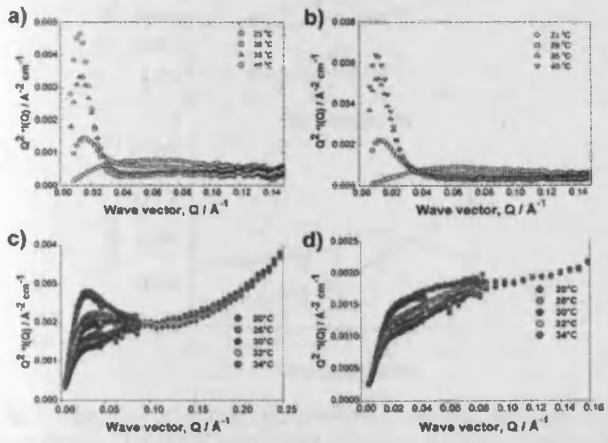

Fig. 5 Temperature dependence of the small-angle neutron scattering from the co-polymer analogues **1** and **2** (a,b) and their trypsin hybrids (bottom) in PBS/D_2O for Hybrid **I** (c) and Hybrid **II** (d).

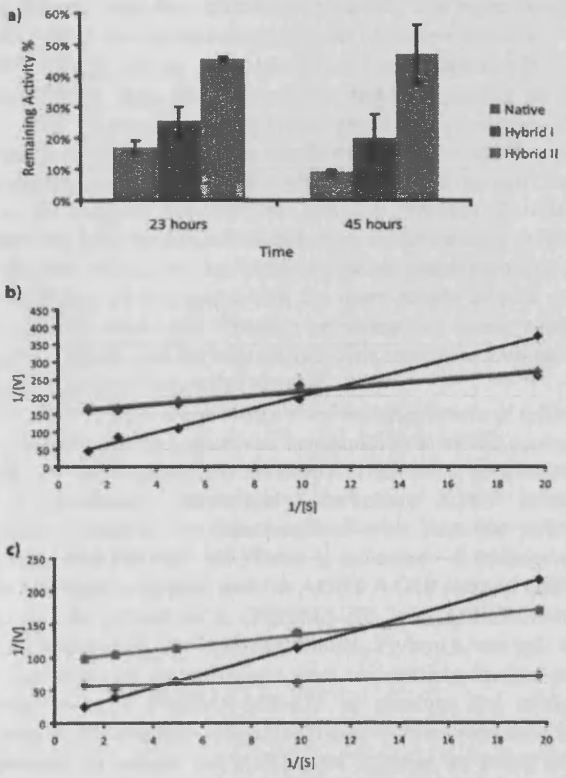

Fig. 6 Enzyme kinetics and thermal stability of hybrids. a) Thermal stability of hybrids at 37 °C in 1X PBS pH 7.4 as a function of time. (Native—grey trace, Hybrid **I**—blue trace, Hybrid **II**—red trace). Line-weaver–Burk plots for BAPNA substrate below LCST b) 26 °C and above LCST c) 40 °C. (Native—black trace, Hybrid **I**—blue trace, Hybrid **II**—red trace).

a range of temperatures around the LCST of the conjugates and compared to the activity of native trypsin (Fig. 7).

In terms of overall activity, both hybrids exhibited a reduced ability to hydrolyse the substrates, as expected owing to increased steric hindrance on the surface of the conjugates and their larger hydrodynamic volume. However, in accord with the kinetics assays, a notable difference in activity between the two hybrids was apparent. When compared in terms of activity against the small peptide substrate, Hybrid I caused a greater extent of hydrolysis than Hybrid II across the whole temperature range. For the casein substrate the activity of Hybrid I was initially higher than Hybrid II, but as the temperature reached the LCST, the activity reached a maximum and then decreased to an extent lower than the activity of Hybrid II. Casein is known to form nanoclusters and higher-order structures ("casein micelles") in solution,[40] and thus the different activities of the hybrids towards casein hydrolysis were likely to be a function of the different self-assembly modes of the conjugates at the varying temperatures.

Discussion

The starting point for this investigation was the desire to produce 'active' bioconjugates with functionalities that could be controlled by a responsive synthetic polymer. We also aimed to do this using chemistry that would be amenable to a variety of delicate biomolecules, and which would allow a range of polymer architectures to be assembled easily. Although there have been a large number of reports of responsive polymer-protein conjugates, the full possibilities for preparing these conjugates in multicomponent architectures have only recently begun to be explored.[41–45] In addition, while the richness of block co-polymer structures has been opened up enormously by controlled radical techniques, the ability to synthesise as well as characterise polymer-biopolymer conjugates as block co-polymers is relatively new. We therefore set out to prepare responsive polymer-protein conjugates as hybrid block co-polymers, and to compare a 'conventional' polymer-protein "di-block" conjugate with a novel "tri-block" architecture consisting of a responsive polymer in between an enzyme block and a non-responsive hydrophilic block.[46] The strategy behind the work was informed by the contrasting practical advantages and disadvantages of protein conjugation. In general, attachment of polymers such as PEG improves the stability of proteins to non-specific absorption and/or degradation in the bloodstream by creating a steric shield on the protein's surface. However, polymer conjugation can at the same time generally have detrimental effects on the activity of the protein by decreasing the accessibility towards substrates and receptors.[47] The effect is dependent on the nature and length of both the linker and polymer, and the extent of conjugation.[48,49] Deactivation of the protein can be alleviated by attachment of polymers to sites away from the catalytic centres, but this is not possible in all cases even though a number of very elegant strategies have been developed for site-specific conjugation.[38,50,51] A possible solution to this problem is the use of a polymer that can shield the protein under one set of conditions, but collapse to expose the active site under another set of conditions. Pioneering work by the Hoffman group established this concept, using thermoresponsive poly(NIPAm).[52,53] The drawback to this procedure is that collapse of a thermosensitive polymer attached to a protein in effect leads to the formation of an amphiphilic block co-polymer. In turn this may exhibit self-assembly into more complex architectures that confound predictions of protein activity.

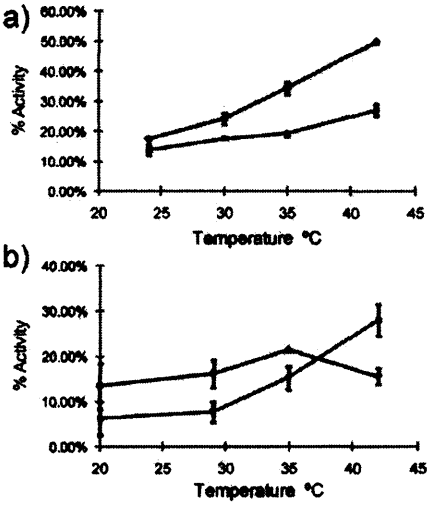

Fig. 7 Reactivity of hybrids towards different substrates as a function of temperature. a) BAPNA assay (small substrate) b) Casein assay (large substrate). Hybrid I (blue trace), Hybrid II (red trace). The activity of native trypsin at 22 °C (BAPNA) and 20 °C (Casein) was set in each case as the reference activity (*i.e.* 100% activity at the start time).

Accordingly, we set out to grow responsive polymers from an active protein, with the simultaneous aim of exploring whether "di- and tri-block" architectures could be prepared from a protein under fully aqueous conditions, and also whether these architectures could be used to control enzyme activity in different ways. A related goal was to establish whether a triblock responsive polymer-protein architecture could be used to confer 'switchable' behaviour but without causing phase separation of the conjugate as can occur with the more simple diblock polymer-protein structures. Finally, we aimed to assess whether enzyme stability and activity altered with conjugate architecture in comparison to the native enzyme.

The first steps in the protocol involved attachment of initiator functionality, in the presence of benzamidine to inhibit proteolysis during the coupling step. As shown in Scheme 2, generation of an α,ω-functional succinimidyl carbonate ATRP initiator enabled trypsin to be functionalised with sites for polymer growth. MALDI-TOF MS (Table 1) indicated ~5 initiator sites were attached to trypsin, and the AGET ATRP method enabled the smooth growth of a $(PEGMA\text{-}EE\text{-}246)_{85}$:$(PEGMA\text{-}ME\text{-}475)_{15}$ co-polymer. The resulting diblock, Hybrid I, was split into two batches, one of which was used to reinitiate further polymerisation with PEGMA-ME-475 to produce the triblock, Hybrid II. The conditions used for these reactions were especially important to ensure the stability of trypsin, as using lower temperature decreases the rate of autocatalysis and prevents aggregation. The choice of monomers was also critical,[12] as ATRP in water by this route would not have been possible with other thermoresponsive PEGMA based copolymers which have been previously reported,[10] owing to their lower solubilities in water compared to PEGMA-EE-246 and PEGMA-ME-475.

Confirmation of polymer growth, hybrid block formation, and reinitiation of polymerisation from Hybrid I to form Hybrid II was obtained by SDS-PAGE, and by GPC analysis of polymers cleaved from the conjugates by ammonium fluoride hydrolysis (Fig. 1d and e). Clear shifts in protein bands were observed *via* Coomassie staining of SDS-PAGE gels following polymer growth from trypsin. Subsequent staining by iodine revealed the PEG components of the broader bands of the PEGMA-trypsin conjugates. Lower molar mass fragments were not observed, indicating that under the polymerisation conditions fragmentation of the protein *via* autocatalytic breakdown of trypsin or through radical-mediated scission did not occur. Further evidence of the controlled polymerisation was that successful reinitiation from the chain-end of the poly(PEGMA-EE-246: PEGMA-ME-475) co-polymer in Hybrid I to form the polymer component of Hybrid II was possible. This was apparent in the GPC traces of polymers cleaved from each hybrid, with a higher molar mass of the mixed copolymer of poly(PEGMA-EE-246-stat-PEGMA-ME-475)-*g*-poly(PEGMA-ME-475) clearly observable (Fig. 1e).

These particular co-monomer compositions for the polymer parts of Hybrid I and II had been chosen based on our previous reports of statistical and block co-polymers prepared by AGET ATRP.[12] We therefore expected the polymer components of the conjugates to exhibit thermoresponsive behaviour, but, as apparent from Fig. 2 the effects were different for each hybrid, and varied also with the solvation properties of buffer used. Under the high-ionic concentrations of PBS at pH 7.4, Hybrid I exhibited a slightly non-linear change in turbidity with temperature between ~30–45 °C at concentrations of 3 mg mL^{-1}, and a 3-fold increase in turbidity overall across this temperature range. By contrast Hybrid II showed no significant changes in turbidity across the same temperature range and at the same concentration. In the reduced ionic strength of the conventional trypsin proteolysis buffer (0.05M Tris, pH 8.2, and containing 20mM $CaCl_2$) Hybrid I showed a sharp LCST at 34 °C (*i.e.* just below the LCST of the polymer after cleavage from trypsin as reported in Table 1) and a ~20-fold increase in turbidity between 34–37 °C. Hybrid II behaved very differently, showing a very small reduction in turbidity across the same temperature range in Tris buffer (Fig. 2b). These variations in temperature-responsive behaviour were strongly suggestive of differences in block behaviour in the different conjugates. Hybrid I was expected to become an amphiphilic di-block co-polymer above the LCST of the attached poly(PEGMA-EE-246-stat-PEGMA-ME-475); the assembly into higher order structures above LCST was a likely result assuming appropriate packing of the poly(PEGMA) chains into a 'core'. DLS data (ESI†) was supportive of this interpretation, as ~ 10 nm diameter species were observed in Tris buffer at 30 °C (below polymer LCST), but strongly scattering particles of ~300 nm diameter were predominant at 45 °C (above polymer LCST). PGSE-NMR provided supporting evidence for the collapse of the poly(PEGMA-EE-246-stat-PEGMA-ME-475) chains. The differences observed in extent of self-assembly for Hybrid I in the different ionic strength buffers was also suggestive of a mechanism in which the pPEGMA chains self-associated into a core, as marked salting in and salting out effects have been reported previously for related poly(PEGMA-EE-246-stat-PEGMA-ME-475) co-polymers.[12] The peak in the SANS data for this hybrid are very clear evidence of such a core-shell structure.

For Hybrid II however, we expected the poly(PEGMA-EE-246-stat-PEGMA-ME-475) attached to trypsin to collapse above LCST, but the outermost block of poly(PEGMA-ME475) would not collapse under these conditions, and thus an essentially double-hydrophilic block co-polymer was anticipated irrespective of whether the temperature was above or below the LCST of the middle block. Again, the PGSE-NMR show that the poly(PEGMA-EE-246-stat-PEGMA-ME-475) component collapses with temperature. Although self-assembly of double-hydrophilic block co-polymers has been observed with other systems,[54,55] the turbidimetry and DLS data suggested that for Hybrid II under the conditions described (PBS or Tris buffer, 20–45 °C), higher order structures were not formed, confirmed by the absence of the peak in the Kratky plot for this hybrid.

Cryo-TEM (Fig. 3) yielded further data that indicated differences in self-assembly modes of the hybrid bioconjugates. Although drying artefacts cannot be excluded from cryo-TEM, the apparent clusters of particles in micrographs of Hybrid I flash-frozen from above polymer LCST were suggestive of self-association. These particle clusters were visually different from particles of Hybrid I below LCST, and of Hybrid II below or above LCST. The size ranges observed in TEM (2–50 nm for Hybrid II, 50–400 nm for Hybrid I) were more indicative of clusters of clusters rather than individual polymer-trypsin particles, and in all cases were larger than those observed in DLS. However, the larger particles in a polydisperse sample would have been more likely to settle fast on a cryo-TEM grid, and thus absolute size ranges would not be expected to match those in DLS exactly. Nevertheless, the distinct appearance of Hybrid I structures from above LCST compared to all the other samples implied a different assembly mode for this polymer above LCST.

Due to the limitations of cryo-TEM, imaging of samples was carried out using AFM in dilute buffer at variable temperatures (Fig. 4 and Table 2). As apparent from Fig. 4a, an increase in temperature from 30 °C to 40 °C resulted in an increase in size of Hybrid I, and a subsequent decrease in size of particles as the sample was cooled back to 30 °C. By contrast, Hybrid II (Fig. 4b and Table 2) did not self-assemble into larger structures to any significant degree over the same temperature profiles. Grain size analysis (Table 2) indicated some dispersity in particle sizes across both polymer hybrids, thus we cannot rule out completely any self-assembly for Hybrid II, but as apparent from Fig. 4, there were clearly more, and much larger, particulate species for Hybrid I at 40 °C than for Hybrid II under the same conditions. The sizes of the Hybrid II particles measured by AFM at all temperature ranges, and for Hybrid I recorded at 30 °C (before and after heating), were slightly broader than the dimensions observed in DLS experiments before aggregation. This broadening can be attributed to the finite size of the apex of the AFM probe, which frequently results in the broadening of image features.[56] However, in general AFM results were in good agreement with DLS, except for Hybrid I at elevated temperatures. Both techniques showed that aggregation occurred at 40 °C, but absolute values ranged from 10–58 nm in size as reported by AFM studies but 150 nm in DLS studies. This discrepancy may have been as a result of the swelling of the polymer chains of the conjugates in buffer in DLS studies and a hindered aggregation process in AFM studies due to the surface association of the conjugates with the mica surface; however, it may simply also

have reflected the different sampling nature of AFM (individual measurements) and DLS (averaged scatter).

The possible changes in trypsin structure and the likely differences in enzyme accessibility due to self-assembly modes of the hybrids were probed by activity assays. We used the well-known small peptide analogue, BAPNA, and the protein casein, which itself is known to self-assemble into complex higher-order structures.

Native trypsin loses its integrity at raised temperature,[57] the scope of which is also affected by the pH and ion environment.[58] As can be observed from Fig. 6a, both Hybrid I and Hybrid II were more stable compared to native trypsin, as measured by their ability to hydrolyse BAPNA over time. Hybrid II was much more stable, which we attribute to the fact that it did not precipitate from solution over time, remained better hydrated[8] and likely presented a more persistent steric shield against attack from adjacent trypsin hybrids in solution than would have been the case for native trypsin. However, both hybrids displayed lower affinities for the small molecule substrate and lower turn-over rates. These data were not unanticipated, as extensive conjugation of polymer chains (~ 5 attached to each trypsin for both hybrids in this case) and higher molecular weight of the polymers[57] is known to reduce access of substrates more to binding sites in comparison to lower levels of conjugation and smaller polymers. Activities of the conjugates varied with temperature, with a greater change for Hybrid I compared to Hybrid II across the LCST. Intriguingly, for the higher molar mass substrate, casein, there was a sharp decrease in hydrolysis using Hybrid I around its LCST, but an increase in the activity of Hybrid II over the same range. We attribute this to the decreased accessibility of the larger, self-assembled Hybrid I systems above LCST compared to Hybrid II. Recent data suggests that casein micelles possess an internal structure composed of a bicontinuous system of water channels and, in the presence of calcium phosphate, strands formed of calcium phosphate/casein nanoclusters.[40] Such a structure is known to be permeable to trypsin, and should allow acccess to the non-associated Hybrid II structures, but would exclude superstructures/assemblies of Hybrid I above LCST.

When considered together, the data from turbidimetry, DLS, TEM, AFM and enzyme activity suggest a model for the polymer-trypsin hybrids and their differing behaviours below and above the LCSTs of their attached polymer chains (Scheme 3).

We suggest that Hybrid I self-assembled and eventually aggregated above LCST due to collapse of the responsive polymer segment and the generation of exposed hydrophobic regions. It is probable that the high level of water associated with the PEGMA side chains drove the self assembly,[12] where the collapse of the polymer led to high loss of water and a large change of the packing parameter. Lowering the temperature below the LCST rehydrated the polymer again allowing the protein hybrid to disassemble. It is likely then that the reduced trypsin activity of Hybrid I above the LCST arose from the aggregation and precipitation which made the enzyme less accessible than Hybrid II at the higher temperatures. By contrast, for Hybrid II the presence of the outermost block of hydrophilic PEGMA-ME-475 created a steric shield which remained chain-extended even after collapse of the intermediate block, thus disrupting hydrophobic interactions and subsequent aggregation. However, this

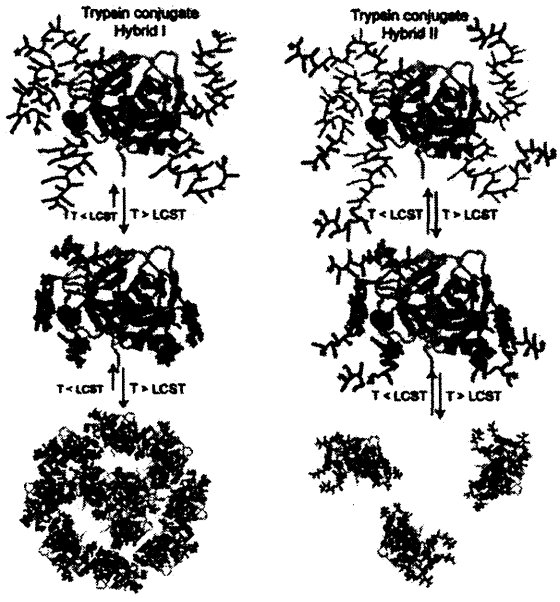

Scheme 3 Cartoon representation of the solution behaviour of Hybrid I (left) and Hybrid II (right).

hydrophilic outer block also rendered Hybrid II more bulky and sterically hindered access to the attached trypsin at temperatures below and above LCST. Accordingly, while Hybrid II was more stable to autocatalytic degradation it did not display temperature dependent hydrolytic activity, except for activity against casein micelles/nanoclusters where the accessibility of the substrate itself was likely to have been size-critical. The large size of the casein micelle (~100 nm) most likely allowed access of Hybrid II, which although larger than Hybrid I below LCST, was likely to be smaller than Hybrid I above LCST as it remained unimeric, whereas the aggregation of Hybrid I into large clusters above the LCST led to a decreased accessibility of the protease towards the casein substrate. This behaviour was not observed with the small peptide substrate since the diffusion of the small peptide into the aggregate network was less likely to be as sterically hindered.

Conclusions

In conclusion, we have demonstrated the successful synthesis of "smart" PEGMA trypsin conjugates using the "growing from" approach. The polymerisations were carried out in fully aqueous solution at 4 °C using conditions mild enough to be applicable to many other sensitive proteins and biopolymers. By adopting the ATRP AGET polymerisation method to grow from the protein different polymers, two different morphologies were attainable. The morphology of the polymer was shown to affect the solution behaviour of the protein and subsequently its activity. In addition, the substrate specificity could be modified as a function of the polymer architecture. For practical applications, polymer bioconjugates need to be more active than the native protein/biopolymer, or more stable. Here we have shown that hybrid bioconjugates can be more stable, and also substrate selective, dependent on architecture, but with the penalty of reduced proteolytic activity. Accordingly, the methodology we have developed could have potential applications in the field of mass

spectroscopy, drug delivery and for catalysis. In particular, these responsive hybrid conjugates could be used to target different receptors/substrates through changes in polymer architecture and external stimulus, thus enabling switchable specificity of protein activity as required.

Acknowledgements

We thank the Engineering and Physical Sciences Research Council (EPSRC for grants EP/C013220/1, EP/H005625/1 and EP/G042462/1), STFC for the provision of neutron beam time, the Turkish Government (Scholarship to GY), the Australian Research Council (DP1094205, DP0880032) and the University of Nottingham for financial support. We also thank Drs George Pasparakis and Wenxin Wang for many helpful discussions, Christine Grainger-Boultby for technical support and Dr Michael Fay and Dr Christopher Parmenter for assisting with the Cryo-TEM experiments.

Notes and references

1 S. Frokjaer and D. E. Otzen, *Nat. Rev. Drug Discovery*, 2005, **4**, 298–306.
2 F. M. Veronese and G. Pasut, *Drug Discovery Today*, 2005, **10**, 1451–1458.
3 P. S. S. Allan and S. Hoffman, *Macromol. Symp.*, 2004, **207**, 139–152.
4 Z. L. Ding, G. H. Chen and A. S. Hoffman, *J. Biomed. Mater. Res.*, 1998, **39**, 498–505.
5 C. Ó. F. A. Murphy, *Biotechnol. Bioeng.*, 1998, **58**, 366–373.
6 A. Chilkoti, M. R. Dreher and D. E. Meyer, *Adv. Drug Delivery Rev.*, 2002, **54**, 1093–1111.
7 M. Heskins and J. E. Guillet, *J. Macromol. Sci., Part A: Pure Appl. Chem.*, 1968, **2**, 1441–1455.
8 H. Lee and T. G. Park, *Biotechnol. Prog.*, 1998, **14**, 508–516.
9 H. Vihola, A. Laukkanen, L. Valtola, H. Tenhu and J. Hirvonen, *Biomaterials*, 2005, **26**, 3055–3064.
10 J. F. Lutz and A. Hoth, *Macromolecules*, 2006, **39**, 893–896.
11 J.-F. Lutz, O. Akdemir and A. Hoth, *J. Am. Chem. Soc.*, 2006, **128**, 13046–13047.
12 J. P. Magnusson, A. Khan, G. Pasparakis, A. O. Saeed, W. Wang and C. Alexander, *J. Am. Chem. Soc.*, 2008, **130**, 10852–10853.
13 S. R. Abulateefeh, A. O. Saeed, J. W. Aylott, W. C. Chan, M. C. Garnett, B. R. Saunders and C. Alexander, *Chem. Commun.*, 2009, 6068–6070.
14 J. P. Magnusson, S. Bersani, S. Salmaso, C. Alexander and P. Caliceti, *Bioconjugate Chem.*, 2010, **21**, 671–678.
15 Z. Zarafshani, T. Obata and J.-F. o. Lutz, *Biomacromolecules*, 2010, **11**, 2130–2135.
16 S. M. Ryan, X. X. Wang, G. Mantovani, C. T. Sayers, D. M. Haddleton and D. J. Brayden, *J. Controlled Release*, 2009, **135**, 51–59.
17 W. Gao, W. Liu, J. A. Mackay, M. R. Zalutsky, E. J. Toone and A. Chilkoti, *Proc. Natl. Acad. Sci. U. S. A.*, 2009, **106**, 15231–15236.
18 J.-F. Lutz, *Adv. Mater.*, 2011, **23**, 2237.
19 K. L. Heredia, D. Bontempo, T. Ly, J. T. Byers, S. Halstenberg and H. D. Maynard, *J. Am. Chem. Soc.*, 2005, **127**, 16955–16960.
20 C. Boyer, V. Bulmus, J. Liu, T. P. Davis, M. H. Stenzel and C. Barner-Kowollik, *J. Am. Chem. Soc.*, 2007, **129**, 7145–7154.
21 P. De, M. Li, S. R. Gondi and B. S. Sumerlin, *J. Am. Chem. Soc.*, 2008, **130**, 11288–11289.
22 J. V. Olsen, S.-E. Ong and M. Mann, *Mol. Cell. Proteomics*, 2004, **3**, 608–614.
23 M. A. Gauthier and H. A. Klok, *Polym. Chem.*, 2010, **1**, 1352–1373.
24 A. Mero, G. Pasut, L. D. Via, M. W. M. Fijten, U. S. Schubert, R. Hoogenboom and F. M. Veronese, *J. Controlled Release*, 2008, **125**, 87–95.
25 M. Yan, J. Ge, W. G. Dong, Z. Liu and P. Ouyang, *Biochem. Eng. J.*, 2006, **30**, 48–54.
26 K. L. Heredia, D. Bontempo, T. Ly, J. T. Byers, S. Halstenberg and H. D. Maynard, *J. Am. Chem. Soc.*, 2005, **127**, 16955–16960.
27 Y. Hao, M. Andersson, C. Virto, I. Y. Galaev, B. Mattiasson and R. Hatti-Kaul, *Biocatal. Biotransform.*, 2001, **19**, 341–359.
28 Z. Tyeklar, R. R. Jacobson, N. Wei, N. N. Murthy, J. Zubieta and K. D. Karlin, *J. Am. Chem. Soc.*, 1993, **115**, 2677–2689.
29 U. Jacquemard, V. Bénéteau, M. Lefoix, S. Routier, J.-Y. Mérour and G. Coudert, *Tetrahedron*, 2004, **60**, 10039–10047.
30 F. M. B. Ausubel, R. Kingston, R. E. Moore, D. D. Seidman, J. G. Smith, J. A. Struhl, and K, *Short Protocols in Molecular Biology*, 5th edn, Wiley, 2002.
31 M. M. Kurfürst, *Anal. Biochem.*, 1992, **200**, 244–248.
32 B. S. Lele, H. Murata, K. Matyjaszewski and A. J. Russell, *Biomacromolecules*, 2005, **6**, 3380–3387.
33 J. A. Davies and P. C. Griffiths, *Macromolecules*, 2003, **36**, 950–952.
34 P. K. Smith, R. I. Krohn, G. T. Hermanson, A. K. Mallia, F. H. Gartner, M. D. Provenzano, E. K. Fujimoto, N. M. Goeke, B. J. Olson and D. C. Klenk, *Anal. Biochem.*, 1985, **150**, 76–85.
35 D. Cunliffe, C. de las Heras Alarcon, V. Peters, J. R. Smith and C. Alexander, *Langmuir*, 2003, **19**, 2888–2899.
36 B. F. Erlanger, N. Kokowsky and W. Cohen, *Arch. Biochem. Biophys.*, 1961, **95**, 271–278.
37 M. Singh and A. D. Krikorian, *J. Agric. Food Chem.*, 1982, **30**, 799–800.
38 S. Shaunak, A. Godwin, J. W. Choi, S. Balan, E. Pedone, D. Vijayarangam, S. Heidelberger, I. Teo, M. Zloh and S. Brocchini, *Nat. Chem. Biol.*, 2006, **2**, 312–313.
39 V. Arasaratnam, I. Y. Galaev and B. Mattiasson, *Enzyme Microb. Technol.*, 2000, **27**, 254–263.
40 D. G. Dalgleish, *Soft Matter*, 2011, **7**, 2265–2272.
41 H. M. Li, A. P. Bapat, M. Li and B. S. Sumerlin, *Polym. Chem.*, 2011, **2**, 323–327.
42 M. Li, H. M. Li, P. De and B. S. Sumerlin, *Macromol. Rapid Commun.*, 2011, **32**, 354–359.
43 D. Roy, J. N. Cambre and B. S. Sumerlin, *Prog. Polym. Sci.*, 2010, **35**, 278–301.
44 L. A. Canalle, D. Lowik and J. C. M. van Hest, *Chem. Soc. Rev.*, 2010, **39**, 329–353.
45 D. Lowik, E. H. P. Leunissen, M. van den Heuvel, M. B. Hansen and J. C. M. van Hest, *Chem. Soc. Rev.*, 2010, **39**, 3394–3412.
46 The terms "di-block" and "tri-block" are in quotation marks becauseon average 5 polymer chains were attached to each trypsin molecule, however, as the properties of each polymer chain grown from the trypsin anchor were expected to be similar, it is more convenient to refer to "di-block" than "oligo-di-block".
47 A. S. Hoffman, *Clin. Chem.*, 2000, **46**, 1478–1486.
48 B. Treetharnmathurot, L. Dieudonne, E. L. Ferguson, D. Schmaljohann, R. Duncan and R. Wiwattanapatapee, *Int. J. Pharm.*, 2009, **373**, 68–76.
49 M. Matsukata, T. Aoki, K. Sanui, N. Ogata, A. Kikuchi, Y. Sakurai and T. Okano, *Bioconjugate Chem.*, 1996, **7**, 96–101.
50 S. Balan, J. W. Choi, A. Godwin, I. Teo, C. M. Laborde, S. Heidelberger, M. Zloh, S. Shaunak and S. Brocchini, *Bioconjugate Chem.*, 2007, **18**, 61–76.
51 K. L. Christman, R. M. Broyer, Z. P. Tolstyka and H. D. Maynard, *J. Mater. Chem.*, 2007, **17**, 2021–2027.
52 G. H. Chen and A. S. Hoffman, *Bioconjugate Chem.*, 1993, **4**, 509–514.
53 A. S. Hoffman and P. S. Stayton, *Prog. Polym. Sci.*, 2007, **32**, 922–932.
54 G. Pasparakis and C. Alexander, *Angew. Chem., Int. Ed.*, 2008, **47**, 4847–4850.
55 W. Agut, A. Brulet, D. Taton and S. Lecommandoux, *Langmuir*, 2007, **23**, 11526–11533.
56 D. Ricci and P. C. Braga, in *Atomic Force Microscopy: Biomedical Methods and Applications*, ed. D. Ricci and P. C. Braga, Humana Press Inc., Totowa, NJ, 2004, pp. 25–37.
57 B. Treethammathurot, C. Ovartlarnporn, J. Wungsintaweekul, R. Duncan and R. Wiwattanapatapee, *Int. J. Pharm.*, 2008, **357**, 252–259.
58 M. L. Simon, K. Laszlo, M. Kotorman and B. Szajani, *Acta Biol. (Szeged)*, 2001, **45**, 43–49.